frontiers | Research Topics

Emerging learnings in cell therapy: Novel binding domains, universal CAR-T cells, and more

Edited by
Anand Rotte, Matthew John Frigault, Binod Dhakal and Christopher Heery

Published in
Frontiers in Immunology
Frontiers in Oncology

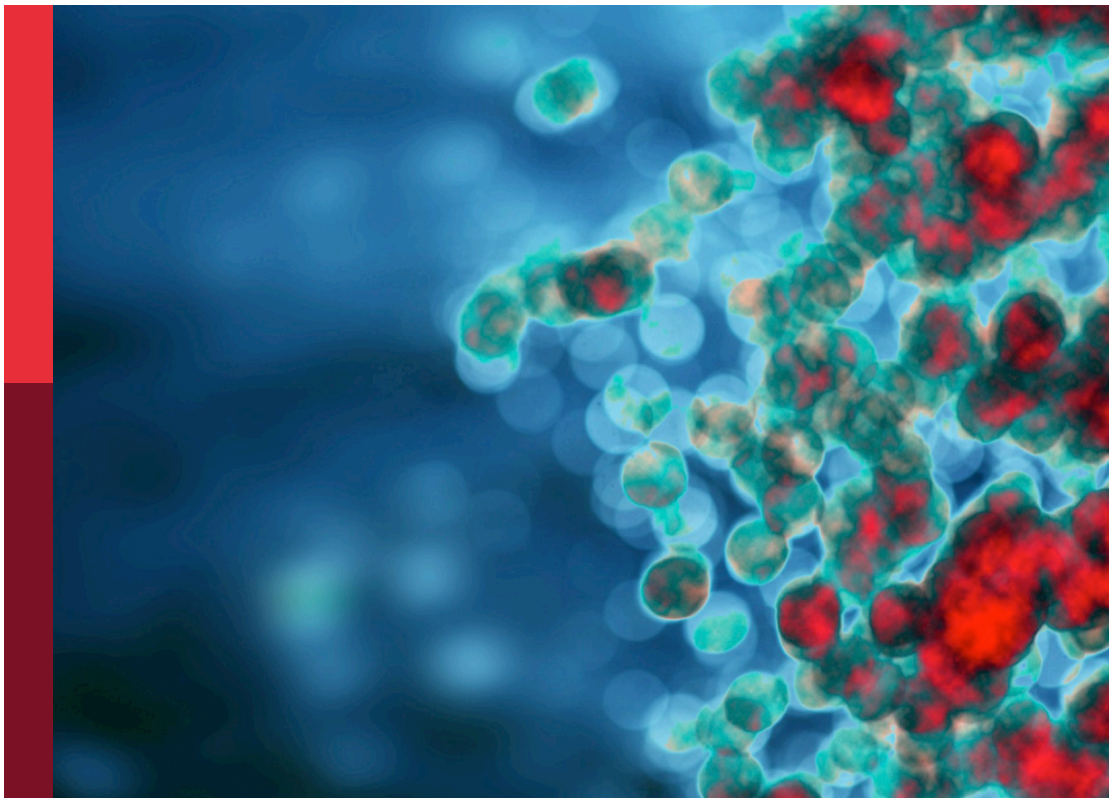

FRONTIERS EBOOK COPYRIGHT STATEMENT

The copyright in the text of individual articles in this ebook is the property of their respective authors or their respective institutions or funders. The copyright in graphics and images within each article may be subject to copyright of other parties. In both cases this is subject to a license granted to Frontiers.

The compilation of articles constituting this ebook is the property of Frontiers.

Each article within this ebook, and the ebook itself, are published under the most recent version of the Creative Commons CC-BY licence. The version current at the date of publication of this ebook is CC-BY 4.0. If the CC-BY licence is updated, the licence granted by Frontiers is automatically updated to the new version.

When exercising any right under the CC-BY licence, Frontiers must be attributed as the original publisher of the article or ebook, as applicable.

Authors have the responsibility of ensuring that any graphics or other materials which are the property of others may be included in the CC-BY licence, but this should be checked before relying on the CC-BY licence to reproduce those materials. Any copyright notices relating to those materials must be complied with.

Copyright and source acknowledgement notices may not be removed and must be displayed in any copy, derivative work or partial copy which includes the elements in question.

All copyright, and all rights therein, are protected by national and international copyright laws. The above represents a summary only. For further information please read Frontiers' Conditions for Website Use and Copyright Statement, and the applicable CC-BY licence.

ISSN 1664-8714
ISBN 978-2-8325-4832-5
DOI 10.3389/978-2-8325-4832-5

About Frontiers

Frontiers is more than just an open access publisher of scholarly articles: it is a pioneering approach to the world of academia, radically improving the way scholarly research is managed. The grand vision of Frontiers is a world where all people have an equal opportunity to seek, share and generate knowledge. Frontiers provides immediate and permanent online open access to all its publications, but this alone is not enough to realize our grand goals.

Frontiers journal series

The Frontiers journal series is a multi-tier and interdisciplinary set of open-access, online journals, promising a paradigm shift from the current review, selection and dissemination processes in academic publishing. All Frontiers journals are driven by researchers for researchers; therefore, they constitute a service to the scholarly community. At the same time, the *Frontiers journal series* operates on a revolutionary invention, the tiered publishing system, initially addressing specific communities of scholars, and gradually climbing up to broader public understanding, thus serving the interests of the lay society, too.

Dedication to quality

Each Frontiers article is a landmark of the highest quality, thanks to genuinely collaborative interactions between authors and review editors, who include some of the world's best academicians. Research must be certified by peers before entering a stream of knowledge that may eventually reach the public - and shape society; therefore, Frontiers only applies the most rigorous and unbiased reviews. Frontiers revolutionizes research publishing by freely delivering the most outstanding research, evaluated with no bias from both the academic and social point of view. By applying the most advanced information technologies, Frontiers is catapulting scholarly publishing into a new generation.

What are Frontiers Research Topics?

Frontiers Research Topics are very popular trademarks of the *Frontiers journals series*: they are collections of at least ten articles, all centered on a particular subject. With their unique mix of varied contributions from Original Research to Review Articles, Frontiers Research Topics unify the most influential researchers, the latest key findings and historical advances in a hot research area.

Find out more on how to host your own Frontiers Research Topic or contribute to one as an author by contacting the Frontiers editorial office: frontiersin.org/about/contact

Emerging learnings in cell therapy: Novel binding domains, universal CAR-T cells, and more

Topic editors

Anand Rotte – Arcellx Inc, United States

Matthew John Frigault – Massachusetts General Hospital Cancer Center, United States

Binod Dhakal – Medical College of Wisconsin, United States

Christopher Heery – Arcellx, United States

Citation

Rotte, A., Frigault, M. J., Dhakal, B., Heery, C., eds. (2024). *Emerging learnings in cell therapy: Novel binding domains, universal CAR-T cells, and more*. Lausanne: Frontiers Media SA. doi: 10.3389/978-2-8325-4832-5

Table of contents

frontiers | Frontiers in Oncology

TYPE Editorial
PUBLISHED 15 April 2024
DOI 10.3389/fonc.2024.1404376

Check for updates

OPEN ACCESS

EDITED AND REVIEWED BY
Vassiliki A. Boussiotis,
Beth Israel Deaconess Medical Center and Harvard Medical School, United States

*CORRESPONDENCE
Anand Rotte
arotte@arcellx.com

RECEIVED 20 March 2024
ACCEPTED 29 March 2024
PUBLISHED 15 April 2024

CITATION
Rotte A (2024) Editorial: Emerging learnings in cell therapy: novel binding domains, universal CAR-T cells, and more.
Front. Oncol. 14:1404376.
doi: 10.3389/fonc.2024.1404376

COPYRIGHT
© 2024 Rotte. This is an open-access article distributed under the terms of the Creative Commons Attribution License (CC BY). The use, distribution or reproduction in other forums is permitted, provided the original author(s) and the copyright owner(s) are credited and that the original publication in this journal is cited, in accordance with accepted academic practice. No use, distribution or reproduction is permitted which does not comply with these terms.

Editorial: Emerging learnings in cell therapy: novel binding domains, universal CAR-T cells, and more

Anand Rotte*

Department of Clinical and Regulatory Affairs, Arcellx Inc, Redwood City, CA, United States

KEYWORDS

CAR-T cells, D-Domains, protein aggregation, Tonic signaling, cell therapy (CT)

Editorial on the Research Topic

Emerging learnings in cell therapy: novel binding domains, universal CAR-T cells, and more

This recent decade has seen a dramatic improvement in the potential of immunotherapy and cell therapy as options for the treatment of cancer (1–6). Research interest in cell therapy has increased significantly over the past few years, with a focus on improving efficacy and addressing challenges (7) that has resulted in the introduction of novel target binding domains, dual intracellular signaling domains, T cells redirected for universal cytokine-mediated killing (TRUCKs), and allogeneic cell therapies (8). The current Research Topic, "*Emerging learnings in cell therapy: novel binding domains, universal CAR-T cells, and more*" aimed to attract new innovative research on cell therapy for cancer. Articles published in the Research Topic include two review articles, five preclinical studies, two studies reporting findings from real-world use of CAR-T cells, and one study reporting findings on atypical T-cell receptor (TCR)-T cells.

The review article by Zhang et al. provided a summary of recent developments in CAR-T cell therapy for solid tumors. The authors mainly discussed the strategies developed to increase the efficacy of CAR-T cells in solid tumors through the use of dual-targets, receptor switches, and CARs that are designed to resist the inhibitory signaling molecules in the TME. The second review article by Liu et al. summarized the latest advances and updates from the ASH 2022 annual meeting on anti-CD7 CAR-T cells and their application for treatment of acute myeloid leukemia and T-Lymphocyte Leukemia and Lymphoma.

The importance of intracellular costimulatory domain (4-1-BB) in activating non-canonical NF-κB pathways and thereby reducing T-cell exhaustion and improving T-cell survival has been demonstrated previously (9). Julamanee and colleagues extended the knowledge of intracellular costimulatory domains further and showed in their study that a novel B-cell signaling moiety, CD79A/CD40-based CAR, can stimulate both canonical and non-canonical signaling pathways inside the cell and improve the CAR-T cell function (10). In their current study, Ung et al. further explored the downstream mechanisms in CD79A/CD40 based CAR-T cells. The authors reported enrichment of genes known to be associated with T-cell proliferation, interferon signaling, and memory-cell signatures,

upregulation of genes related to glycolysis and fatty acid metabolism, and downregulation of T-cell exhaustion in CD79A/CD40 CAR-T cells.

Zhang et al. advanced the research on targeting gp350, an envelope protein of Epstein Barr Virus (EBV) detected in 25% of biopsies from nasopharyngeal carcinoma (NPC) and developed gp350.CAR-T cells. The authors reported preclinical characterization of gp350.CAR-T cells that were produced under good manufacturing practices and noted the applicability of the product for NPC. In another study, Swan et al. aimed to address multiple challenges of CAR-T cells including improving CAR-T cell persistence, tumor penetration, tumor heterogeneity, and possible inhibition of the endogenous immune system due to lymphodepletion by chemotherapy or radiation. The authors developed CAR-T cells that secreted IL7, a cytokine well known to promote T-cell survival and proliferation alone or along with Fms-like tyrosine kinase receptor 3 ligand (Flt3L), a cytokine known to promote DC differentiation, expansion, and survival. They also characterized the activity of the CAR-T cells in a glioblastoma model.

Potez et al. aimed to address the recurrence or relapse of glioblastoma multiforme (GBM) attributed to glioma stem cells (GSCs) and reported the characterization of CAR-T cells targeting GSMs. In their study, researchers combined two previously identified (11), 7-amino acid length peptides that specifically bind to GSCs using *in vitro* and *in vivo* phage display, biopanning through a flexible linker peptide to develop CAR-T cells targeting GSCs. The combined peptide with 29 amino acids was used in place of scFv as an antigen binding domain in the study. Authors reported that the peptide-based CAR-T cells (E-28t28z-tCD34) had significantly higher IFN-ϒ secretion when co-cultured with GSCs compared to differentiated glioma cells and showed that N-cadherin was the likely ligand on tumor cells that bound to the CAR.

Solid tumors are considered resistant to CAR-T cells due to the immunosuppressive tumor microenvironment that favors the expression of inhibitory immune checkpoints on effector T-cells such as T cell immunoreceptor with immunoglobulin and ITIM domain (TIGIT) (12). Yang et al. aimed to address the expression of inhibitory immune checkpoints through anti-mesothelin CAR-T cells that constitutively produce TIGIT-blocking single-chain variable fragments. In their article, authors characterized the activity of anti-mesothelin CAR-T cells that produced anti-TIGIT scFvs constitutively using *in vitro* and *in vivo* experiments and reported that the self-delivery of anti-TIGIT scFvs resulted in enhanced infiltration and activity of CAR-T cells in the TME.

Treatment-related adverse events and subsequent hospitalizations are a concern for CAR-T cell therapy. The retrospective observational cohort study by Lipe et al. analyzed the emergency department (ED) visits of patients after receiving CAR-T cell therapy and the association with survival outcomes. Authors reported that patients with ED visits within 14 days of CAR-T cell treatment had significantly better survival outcomes compared to patients with ED visits after 14 days of CAR-T cell treatment; they explained that earlier ED visits were mainly due to an inflammatory response to CAR-T cell therapy possibly resulting in better survival outcomes and the later ED visits were likely due to disease progression resulting in worse survival. In the case report and literature review study by Nogués-Castell et al., authors presented the case history of a patient with plasma cell leukemia (PCL) who achieved complete response after CAR-T cell therapy and later developed orbital tumors consistent with plasmacytoma in both eyes.

Adoptive cell therapy using T-cells expressing transgenic T-cell receptors (TCR-T cells) is an alternative to CAR-T cell therapy and is believed to have advantages over CAR-T cells for solid tumors due to their ability to target intracellular antigens in an MHC-dependent manner. Mercier-Letondal et al. studied engineered TCR-T cells and characterized the phenotype and functional features of atypical TCR-T cells by generating mismatched MHC II-restricted TCR/CD8-expressing T cells and cytotoxic CD4+ T cells against HPV16-derived epitope.

In summary, the articles published as part of the Research Topic covered broad areas of research in cell therapy, ranging from binding domains and intracellular signaling domains and insights into TCR-T cell engineering to real-world outcomes of CAR-T cells. Additional follow-up studies in animal models as well as phase 1 clinical studies may confirm the safety and efficacy of newly developed cell therapies.

Author contributions

AR: Writing – original draft, Writing – review & editing.

Conflict of interest

AR is employed at Arcellx Inc, a biotech company developing CAR T-cell therapies for the treatment of cancer. However, other than the regular employment benefits, author did not receive any additional salary or benefits for drafting this manuscript. Arcellx was not involved in the drafting and did not influence the contents of the manuscript.

Publisher's note

All claims expressed in this article are solely those of the authors and do not necessarily represent those of their affiliated organizations, or those of the publisher, the editors and the reviewers. Any product that may be evaluated in this article, or claim that may be made by its manufacturer, is not guaranteed or endorsed by the publisher.

References

1. Pan K, Farrukh H, Chittepu V, Xu H, Pan CX, Zhu Z. CAR race to cancer immunotherapy: from CAR T, CAR NK to CAR macrophage therapy. *J Exp Clin Cancer Res*. (2022) 41:119. doi: 10.1186/s13046-022-02327-z

2. Lemaire V, Shemesh CS, Rotte A. Pharmacology-based ranking of anti-cancer drugs to guide clinical development of cancer immunotherapy combinations. *J Exp Clin Cancer Res*. (2021) 40:311. doi: 10.1186/s13046-021-02111-5

3. Rotte A. Predictive models for response and survival in patients treated with anti-PD-1 monotherapy or with anti-PD-1 and ipilimumab combination: editorial commentary. *Ann Trans Med*. (2023) 11:227. doi: 10.21037/atm-22-6564

4. Rotte A, Frigault MJ, Ansari A, Gliner B, Heery C, Shah B. Dose-response correlation for CAR-T cells: a systematic review of clinical studies. *J Immunother Cancer*. (2022) 10(12):e005678. doi: 10.1136/jitc-2022-005678

5. Zmievskaya E, Valiullina A, Ganeeva I, Petukhov A, Rizvanov A, Bulatov E. Application of CAR-T cell therapy beyond oncology: autoimmune diseases and viral infections. *Biomedicines*. (2021) 9(1):59. doi: 10.3390/biomedicines9010059

6. Asmamaw Dejenie T, Tiruneh GMM, Dessie Terefe G, Tadele Admasu F, Wale Tesega W, Chekol Abebe E. Current updates on generations, approvals, and clinical trials of CAR T-cell therapy. *Hum Vaccin Immunother*. (2022) 18:2114254. doi: 10.1080/21645515.2022.2114254

7. Kandra P, Nandigama R, Eul B, Huber M, Kobold S, Seeger W, et al. Utility and drawbacks of chimeric antigen receptor T cell (CAR-T) therapy in lung cancer. *Front Immunol*. (2022) 13:903562. doi: 10.3389/fimmu.2022.903562

8. Tomasik J, Jasinski M, Basak GW. Next generations of CAR-T cells - new therapeutic opportunities in hematology? *Front Immunol*. (2022) 13:1034707. doi: 10.3389/fimmu.2022.1034707

9. Long AH, Haso WM, Shern JF, Wanhainen KM, Murgai M, Ingaramo M, et al. 4-1BB costimulation ameliorates T cell exhaustion induced by tonic signaling of chimeric antigen receptors. *Nat Med*. (2015) 21:581–90. doi: 10.1038/nm.3838

10. Julamanee J, Terakura S, Umemura K, Adachi Y, Miyao K, Okuno S, et al. Composite CD79A/CD40 co-stimulatory endodomain enhances CD19CAR-T cell proliferation and survival. *Mol Ther*. (2021) 29:2677–90. doi: 10.1016/j.ymthe.2021.04.038

11. Kim J, She C, Potez M, Huang P, Wu Q, Prager BC, et al. Phage display targeting identifies EYA1 as a regulator of glioblastoma stem cell maintenance and proliferation. *Stem Cells*. (2021) 39:853–65. doi: 10.1002/stem.3355

12. Rotte A, Sahasranaman S, Budha N. Targeting TIGIT for immunotherapy of cancer: update on clinical development. *Biomedicines*. (2021) 9(9):1277. doi: 10.3390/biomedicines9091277

frontiers | Frontiers in Immunology

TYPE Original Research
PUBLISHED 24 November 2022
DOI 10.3389/fimmu.2022.1064339

Check for updates

OPEN ACCESS

EDITED BY
Anand Rotte,
Arcellx Inc., United States

REVIEWED BY
Haopeng Wang,
ShanghaiTech University, China
Kailin Xu,
Xuzhou Medical University, China

*CORRESPONDENCE
Jakrawadee Julamanee
jjakrawadee@gmail.com;
jakrawadee.j@psu.ac.th

SPECIALTY SECTION
This article was submitted to Cancer Immunity and Immunotherapy, a section of the journal Frontiers in Immunology

RECEIVED 08 October 2022
ACCEPTED 11 November 2022
PUBLISHED 24 November 2022

CITATION
Ung S, Choochuen P, Khopanlert W, Maneechai K, Sangkhathat S, Terakura S and Julamanee J (2022) Enrichment of T-cell proliferation and memory gene signatures of CD79A/CD40 costimulatory domain potentiates CD19CAR-T cell functions. *Front. Immunol.* 13:1064339. doi: 10.3389/fimmu.2022.1064339

COPYRIGHT
© 2022 Ung, Choochuen, Khopanlert, Maneechai, Sangkhathat, Terakura and Julamanee. This is an open-access article distributed under the terms of the Creative Commons Attribution License (CC BY). The use, distribution or reproduction in other forums is permitted, provided the original author(s) and the copyright owner(s) are credited and that the original publication in this journal is cited, in accordance with accepted academic practice. No use, distribution or reproduction is permitted which does not comply with these terms.

Enrichment of T-cell proliferation and memory gene signatures of CD79A/CD40 costimulatory domain potentiates CD19CAR-T cell functions

Socheatraksmey Ung[1,2], Pongsakorn Choochuen[2,3], Wannakorn Khopanlert[1,2], Kajornkiat Maneechai[1,2], Surasak Sangkhathat[2,3], Seitaro Terakura[4] and Jakrawadee Julamanee[1]*

[1]Stem Cell Laboratory, Hematology Unit, Division of Internal Medicine, Faculty of Medicine, Prince of Songkla University, Hat Yai, Songkhla, Thailand, [2]Department of Biomedical Sciences and Biomedical Engineering, Faculty of Medicine, Prince of Songkla University, Hat Yai, Songkhla, Thailand, [3]Translational Medicine Research Center, Faculty of Medicine, Prince of Songkla University, Hat Yai, Songkhla, Thailand, [4]Department of Hematology and Oncology, Nagoya University Graduate School of Medicine, Nagoya, Japan

CD19 chimeric antigen receptor (CAR) T-cells have demonstrated remarkable outcomes in B-cell malignancies. Recently, the novel CD19CAR-T cells incorporated with B-cell costimulatory molecules of CD79A/CD40 demonstrated superior antitumor activity in the B-cell lymphoma model compared with CD28 or 4-1BB. Here, we investigated the intrinsic transcriptional gene underlying the functional advantage of CD19.79A.40z CAR-T cells following CD19 antigen exposure using transcriptome analysis compared to CD28 or 4-1BB. Notably, CD19.79A.40z CAR-T cells up-regulated genes involved in T-cell activation, T-cell proliferation, and NF-κB signaling, whereas down-regulated genes associated with T-cell exhaustion and apoptosis. Interestingly, CD19.79A.40z CAR- and CD19.BBz CAR-T cells were enriched in almost similar pathways. Furthermore, gene set enrichment analysis demonstrated the enrichment of genes, which were previously identified to correlate with T-cell proliferation, interferon signaling pathway, and naïve and memory T-cell signatures, and down-regulated T-cell exhaustion genes in CD79A/CD40, compared with the T-cell costimulatory domain. The CD19.79A.40z CAR-T cells also up-regulated genes related to glycolysis and fatty acid metabolism, which are necessary to drive T-cell

proliferation and differentiation compared with conventional CD19CAR-T cells. Our study provides a comprehensive insight into the understanding of gene signatures that potentiates the superior antitumor functions by CD19CAR-T cells incorporated with the CD79A/CD40 costimulatory domain.

KEYWORDS

gene expression profiling, CAR-T cell, CD79A/CD40, costimulatory domain, CD19

Introduction

Chimeric antigen receptor (CAR) is a synthetic receptor that targets antigens and reprograms T-cell specificity, function, and persistence (1). Engineered anti-CD19CAR-T cells demonstrate remarkable clinical efficacy against various hematologic malignancies, especially in B-cell acute lymphoblastic leukemia (B-ALL) and B-cell non-Hodgkin lymphoma (B-NHL) (2, 3). However, the loss of CAR-T cell engraftment or escape variants of leukemia blasts leads to disease relapses in almost half of the patients (4). Thus, the persistence of CAR-T cells plays a crucial role in exhibiting the success of this adoptive cell treatment approach.

Previous studies demonstrated that CD19CAR incorporated with the 4-1BB enhanced CAR-T cell persistence more than incorporating the CD28 costimulatory domain (5, 6). The mechanisms by which CD28 or 4-1BB costimulated CD19CAR-T cells mediated this phenomenon have been widely investigated. Long and colleagues identified the molecular pathways that contributed to the ameliorating effect of the 4-1BB signal on CAR-T cell exhaustion (6). Another factor is distinct endogenous T-cell signaling in which CD28 mainly activates the PI3K-Akt pathway that contributes to the increment of glucose metabolism and glycolysis (7). In contrast, recent studies illustrated that the non-canonical NF-κB activated by 4-1BB costimulatory domain accelerated the CAR-T cell survival function (8, 9). In addition, 4-1BB in CAR-T promoted $CD8^+$ central memory T-cells that enhanced respiratory capacity, fatty acid oxidation, and mitochondrial biogenesis (10).

Besides the T-cell costimulatory domain, B-cell-derived signaling domains have been studied to enhance CAR-T cell functions. CAR-T cell that incorporated the MyD88/CD40 costimulatory domain demonstrated greater T-cell proliferation and antitumor activity in a preclinical model (11). The additional transcriptomic analysis revealed that MyD88/CD40 promoted the expression of transcription factors associated with a less differentiated state of T-cell compared with T-cell-derived costimulatory domains (12). Recently, a study by Julamanee and colleagues developed an innovative CD19CAR structure using a novel composite of B-cell signaling moiety, CD79A/CD40 (CD19.79A.40z), to enhance both canonical and non-canonical NF-κB signaling to synergize with T-cell signaling and improve CAR-T cell function. CD19.79A.40z CAR-T cells enhanced NF-κB and nuclear factor of activated T-cell (NFAT) signaling after being stimulated with CD19 antigen. Moreover, CD19.79A.40z CAR-T cells exhibited superior antitumor activity and CAR-T cell proliferation in both B-ALL and B-NHL murine models compared with CD19CAR-T cells incorporated with either CD28 or 4-1BB (13).

To extend the knowledge of the intrinsic transcriptional gene underlying the B-cell-derived costimulatory domain, CD79A/CD40 of CD19CAR-T cell response, we investigated the differentially expressed genes (DEGs) using transcriptome analysis compared to the conventional CD28 or 4-1BB costimulated CD19CAR-T cell. Pathway enrichment analysis illustrated that CD19.79A.40z CAR-T cells up-regulated genes correlated with T-cell activation, proliferation, positive regulation of interferon production, and the NF-κB signaling pathway, and down-regulated genes mediating apoptosis and programmed cell death. Notably, a gene set enrichment analysis (GSEA) revealed that CD19.79A.40z CAR-T cells were enriched in glycolysis, fatty acid metabolism, and naïve and memory-related genes compared with conventional CAR-T cells.

Methods

Cell lines

The Nalm6, K562, and K562 cell lines that are genetically engineered to express CD19 (CD19-K562) are maintained in our laboratory and were used for CAR-T cell functional assays. Nalm6 cells tagged with firefly luciferase (FFluc) and enhanced with green fluorescent protein, which was established elsewhere (13), were used for the cytotoxic assay. The $CD19^+$ EBV-transformed lymphoblastoid cell line (EBV-LCL) was used as a source of feeder cells for T-cell culture (14). Cell lines were cultured and maintained in RPMI-1640 containing 10% fetal

bovine serum, 1% penicillin/streptomycin, and 1% L-glutamine, and incubated at 37°C in a humidified atmosphere containing 5% CO_2.

Human subjects

The research protocols were approved by the Human Research Ethics Committee of the Faculty of Medicine, Prince of Songkla University, Thailand (REC.64-415-14-1). Peripheral blood mononuclear cells (PBMCs) were obtained from healthy volunteer donors. Written informed consent was obtained from each donor in accordance with the Declaration of Helsinki.

CD19CAR structures and viral vector construction

The third-generation CD19CAR structure that included the anti-CD19 single chain variable fragment (scFv)-IgG4/hinge-CD28 transmembrane domain (TM)-CD79A/CD40 intracellular domain (IC)-CD3ζ IC followed by the self-cleaving T2A sequence and a truncated version of epidermal growth factor receptor (tEGFR), which was previously established (13), was used as a template to generate a second-generation CD19CAR structure. The construct was designed to include a transduction and selection marker downstream of a T2A sequence that consisted of a truncated version of the tEGFR lacking the EGF binding and intracellular signaling domains. The T-cell costimulatory receptors CD28 and 4-1BB were generated by overlap polymerase chain reaction and assembled using NEBuider® HIFi DNA Assembly Cloning Kit (New England BioLabs, Ipswich, MA, USA) to delete or insert the pre-designed costimulatory gene into the CD19CAR structure backbone. The CAR genes were then ligated into the LZRS-pBMN-Z vector and further verified by direct sequencing. Next, the CAR genes were transfected into the Phoenix-Ampho (Orbigen, San Diego, CA, USA) retroviral packaging cells to make gamma retroviral supernatants.

Generation, expansion, and selection of CD19CAR-T cells

PBMCs were isolated from the whole blood of healthy volunteers using Lymphoprep™ (StemCell Technologies Inc., Canada) density-gradient centrifugation. $CD3^+$ cells were purified with immunomagnetic beads (Miltenyi Biotec, Bergisch Gladbach, Germany) and activated using anti-CD3/CD28 beads (Invitrogen, Carlsbad, CA, USA). $CD3^+$ cells were then cultured in RPMI-1640 medium containing 10% human serum, 0.8mM L-glutamine, 1% penicillin/streptomycin, and 0.5 μM 2-mercaptoethanol (cytotoxic T-cell medium; CTL), which was supplemented with 50 IU/ml of recombinant human interleukin-2 (IL-2). The activated $CD3^+$ cells are retrovirally transduced on day 3 using recombinant human retronectin fragment-coated plates (Retronectin, Takara Bio, Otsu, Japan) and centrifuged at 2100 rpm for 1 h at 32°C. On day 7, CAR^+ T-cells were purified using biotin-conjugated anti-EGFR monoclonal antibody and counterstained with anti-biotin beads (Miltenyi Biotec). The enriched CAR^+ T-cells were further expanded by culturing with γ-irradiated EBV-LCL feeder cells at a responder:stimulator ratio of 1:7 for 10 days until a sufficient number of cells for downstream experiments was obtained (14).

CAR-T cell proliferation assay

Untransduced- or CD19CAR-T cells were stimulated once with the γ-irradiated CD19-K562 cell line at an target to target (E:T) ratio of 1:1 and cultured in medium with or without exogenous IL-2 supplementation for 10 days. T-cell proliferation was measured by counting viable cells using trypan blue at indicated time points.

Prolonged co-culture assay

Untransduced- or CD19CAR-T cells were co-cultured with Nalm6-FFluc at various E:T ratios (1:1, 1:8, 1:16) without IL-2 supplementation. The percentage of residual target cells was assessed using the flow cytometry technique at various time points up to nine days.

Cytokine secretion assay

Untransduced- or CD19CAR-T cells were stimulated with the γ-irradiated CD19-K562 cell line at an E:T ratio of 1:1 and cultured in medium without IL-2 supplementation for 16 hours. The cell culture supernatants were collected, and the IL-2, interferon-γ (IFN-γ), and tumor necrosis factor-α (TNF-α) concentrations were measured using sandwich ELISA (BD Biosciences, San Jose, CA, USA).

CAR-T cell immunophenotypes

Untransduced- or CD19CAR-T cells were cultured with the γ-irradiated CD19-K562 cell line in a 1:1 ratio for seven days without IL-2 supplementation. The T-cells were stained with monoclonal antibodies conjugated with fluorophores: CD3, CD8, CD45RA, CD62L (BD Biosciences), PD-1, LAG-3, CTLA-4, and TIM-3 (BioLegend, San Diego, CA, USA). The $tEGFR^+$ cells were stained with biotinylated anti-EGFR antibody

(R&D Systems, Bio-Techne, MN, USA) and counterstained with streptavidin-phycoerythrin (BD Biosciences). All samples were analyzed by a CytoFlex S flow cytometer machine (Beckman Coulter Inc, CA, USA) and data were analyzed using FlowJo software (Tree Star).

RNA extraction and RNA sequencing

mRNA was extracted from cells using RNA Blood Mini Kit (QIAGEN, Germany) according to the manufacturer's instructions. RNA concentration and purity were measured by a NanoDrop™ spectrophotometer (Thermo Fisher Scientific). The RNA integrity number (RIN) was assessed using the Agilent Technologies 2100 Bioanalyzer. Total RNA 100–200 ng was used to undergo polyA selection and TruSeq RNA library preparation according to the manufacturer's instructions (TruSeq Stranded mRNA LT Kit; Illumina). The samples were barcoded and run on a Hiseq 4000 (Illumina).

Differential gene expression analysis

A summary of the RNA analysis pipeline used in this study is shown in Figure S2A. A total of nine RNA samples (RIN score above 7) from three healthy donors were RNA-seq. The quality control of raw sequence read data in the FASTQ file from RNA-seq was assessed using the FastQC tool before further analysis to avoid inaccurate results. The Trimmomatic tool was used to trim the adapter sequences or other contaminating sequences. Short sequence reads were mapped to the reference genome from GENCODE (GRCh38) to identify their genomics position using HISAT2. The expression levels of each gene were estimated by counting the number of reads aligned to each full-length transcript. The expression count matrix was then computed from the mapped reads using HTSeq. The EdgeR program, a Bioconductor package, was used to perform the DEG analysis between the three groups: CD19.79A.40z vs. CD19.28z, CD19.79A.40z vs. CD19.BBz, and CD19.28z vs. CD19.BBz. The false discovery rate (FDR) was calculated using the Benjamini-Hochberg method to adjust the p-value. The DEGs were selected at FDR ≤ 0.05 and fold change ≥ 1.5-fold difference. Volcano plots and heatmaps of the DEGs were generated using the EnhancedVolcano package and Pheatmap package, respectively, in R version 4.1.2.

Pathway enrichment analysis

To identify regulation of functionally related gene ontology (GO) terms and enriched pathways, we performed both ranked gene list analyses on the whole gene expression level using GSEA software version 4.2.3 (15) and the DEG list was separately analyzed for up- and down-regulated genes using g:Profiler version e105_eg52_p16_e84549f (16). The input of GSEA was a ranked list of all available genes with normalized counts generated in EdgeR without using a cut-off in each comparison group. The reference gene sets used from the Molecular Signatures Database (MsigDB) were h.all.v7.5.1.symbols (hallmark), c2.cp.reactome.v7.5.1.symbols (curated), c5.all.v7.5.1.symbols (gene ontology), and c7.all.v7.5.1.symbols (immunologic signature).

GSEA assesses genes from the top to the bottom of the ranked list to produce an enrichment score (ES) for a pathway, which increases the ES if a gene is part of the pathway and decreases the score otherwise. Enrichment in the top and bottom ranking genes is amplified, whereas enrichment in genes with more moderate ranks is not amplified. The normalized enrichment score (NES) reflects the enrichment of the pathway in the list and is derived as the maximum value of the running sum normalized relative to pathway size. Enrichment at the top and bottom of the list is represented by positive and negative NES values, respectively. A nominal p-value ≤ 0.05 and FDR q-value ≤ 0.25 were considered statistically significant in the enrichment plots (15).

The functional enrichment analysis of DEGs in g:Profiler was performed using the function g:Gost functional profiling to map the input genes list and identify the statistically significant enriched terms on gene ontology-biological process (GO-BP) and REACTOME databases. The significance threshold of 0.05 was applied using the g:SCS multiple testing correction method.

Statistical analysis

Statistical analyses of *in-vitro* experiments were performed using GraphPad Prism version 9.4.0 (GraphPad Software, La Jolla, CA, USA). All of the experimental data are presented as mean ± SEM. The differences among results were evaluated with one-way ANOVA or two-way ANOVA with Bonferroni's or Tukey's post-test correction when appropriate. Differences were considered statistically significant when $p \leq 0.05$.

Results

CD79A/CD40 enhanced CD19CAR-T cell proliferation after CD19 antigen stimulation

To confirm whether each CAR-T cell structure contained proper functions, we developed a CD19CAR structure that incorporated either the CD28, 4-1BB, or CD79A/CD40 gene (Figure 1A). CD19CAR-T cells were successfully generated and expanded with feeder cells before an *in vitro* assay (Figures 1B, S1A). We first examined T-cell proliferation after stimulation

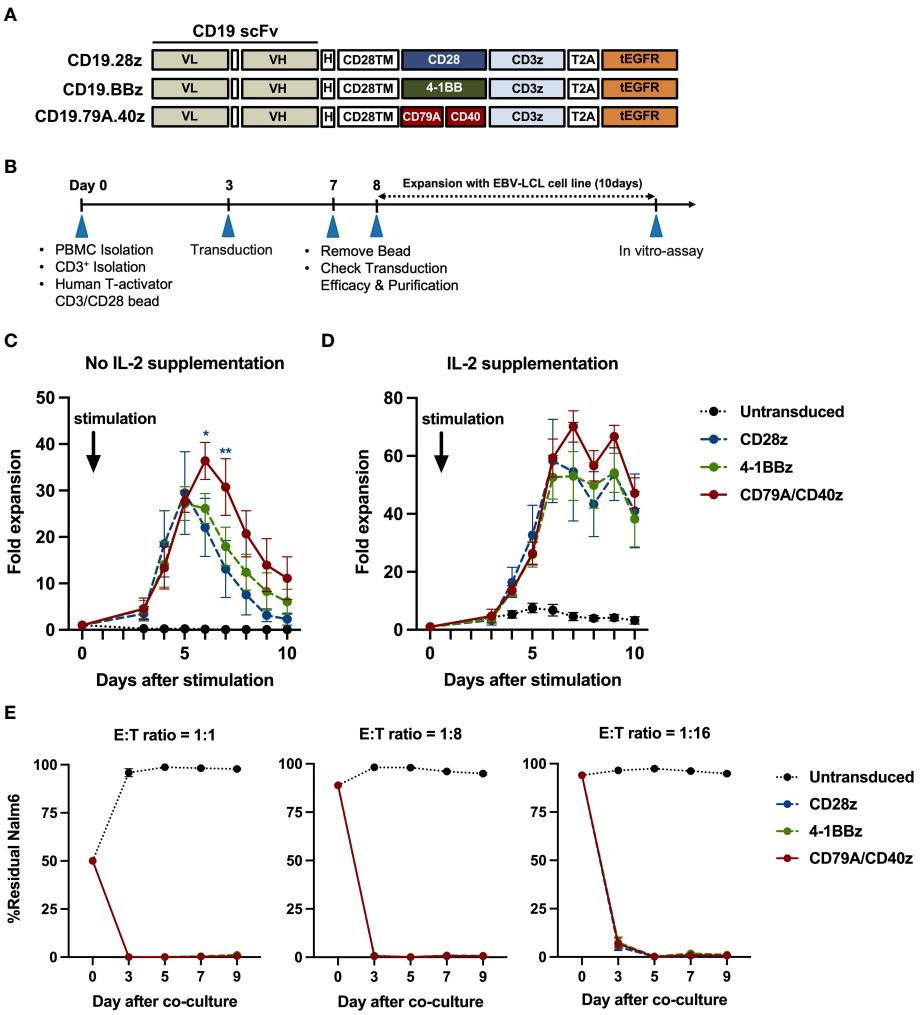

FIGURE 1
CD19CAR-T cell structure and CD19CAR-T cell response upon CD19$^+$ target cell stimulation in an *in vitro* assay. **(A)** Schematic of CD19CAR-T cell structures. Each costimulatory domain either CD28 (CD28z), 4-1BB (BBz), or CD79A/CD40 (CD79A.40z) was fused into anti-CD19 scFv-H-CD28TM followed by CD3ζ and tEGFR. scFv, single chain variable fragment; VL, light-chain variable fragment; VH, heavy chain variable fragment; H, short 12 amino acid of IgG4 Fc-derived spacer of hinge; TM, transmembrane domain; tEGFR, truncated EGFR. **(B)** Experimental schematic of CD19CAR-T cell generation and functional analysis. EBV-LCL, EBV-transformed lymphoblastoid cell line. **(C, D)** T-cell proliferation assay. Untransduced or CD19CAR-T cells were stimulated with γ-irradiated CD19-K562 cell line in 1:1 ratio for 10 days and cultured without **(C)** IL-2 supplementation or with **(D)** IL-2 supplementation (50 IU/ml). T-cell proliferation were measured by counting viable cells. Arrows mark the day of CD19-K562 cell stimulation. **(E)** Prolonged co-culture assay. Untransduced or CD19CAR-T cells were co-cultured with Nalm6-FFluc at E:T ratios of 1:1 (left), 1:8 (middle), and 1:16 (right) for a total of nine days without exogenous IL-2. The remaining Nalm6-FF were assessed by flow cytometry at the indicated time points. All data were pooled from three different donors and are presented as mean ± SEM. 2-way ANOVA for **(C, D)**; *p < 0.05, **p < 0.01 (CD19.79A.40zCAR- vs. CD19.28z CAR-T cells); One-way ANOVA for **(E)**.

with the CD19 antigen. The CD19.79A.40z CAR-T cells exhibited superior CAR-T cell proliferation regardless of IL-2 supplementation (Figures 1C, D). To assess cytotoxicity, we performed a prolonged co-culture assay. The T-cells were cultured with CD19$^+$ target cells at various effector to target cell ratios without IL-2 supplementation. After three days of culture, all CD19CAR-T cells could suppress tumor cell growth until the last day of the co-culture assay (Figure 1E). In terms of cytokine secretion, we observed similar amounts of IFN-γ, IL-2, and TNF-α in the culture medium after stimulation with target cells in the ratio of 1:1 for 16 hours (Figure S1B). To investigate the T-cell immunophenotype and the intrinsic transcriptional gene following target antigen exposure, we stimulated CAR-T cells with CD19 antigen and cultured them for seven days without exogenous IL-2. The T-cells were assessed for T-cell expansion and immunophenotypes for T-cell subsets and exhaustion markers before and after stimulation (Figure 2A). Higher T-cell proliferation was again observed in CD19.79A.40z CAR-T cells compared with CD19.28z CAR-T cells (Figure S1C). Regarding T-cell subsets, CAR-T cells predominantly

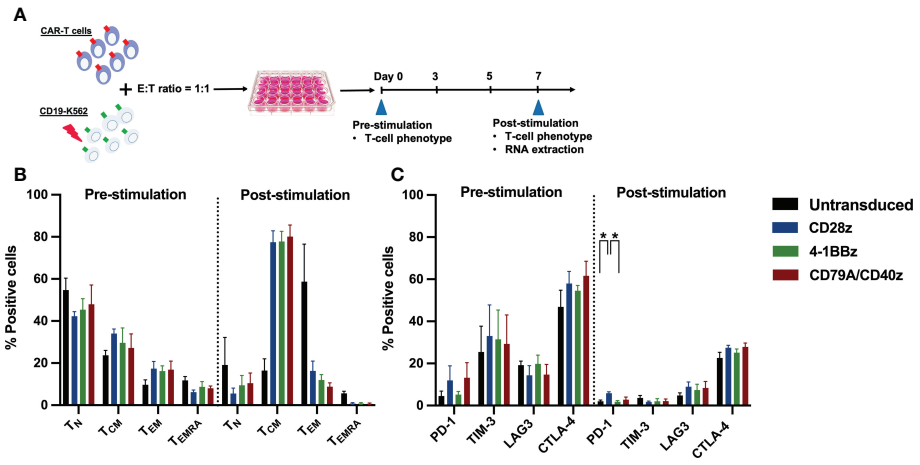

FIGURE 2
CAR-T cell immunophenotype assays. **(A)** Experimental schematic of antigen stimulation and CD19CAR-T cell phenotype assays. CD19CAR-T cells were stimulated with γ-irradiated CD19-K562 cell line in a 1:1 ratio for seven days and cultured without IL-2 supplementation. Then, the CD19CAR-T cell proliferation, T-cell differentiation, and exhaustion phenotypes were assessed before and after stimulation on day 0 and day 7, respectively. The remaining CD19CAR-T cells 3–6 x 10^6 cells were harvested at post stimulation on day 7 and extracted for RNA for further RNA sequencing. **(B)** The percentages of T-cell differentiation subsets were determined by $CD62L^+$ $CD45RA^+$ naïve T (T_N), $CD62L^+$ $CD45RA^-$ central memory T (T_{CM}), $CD62L^-$ $CD45RA^-$ effector memory T (T_{EM}), and $CD62L^-$ $CD45RA^+$ effector memory re-expressing CD45RA T (T_{EMRA}) cells before and after stimulation. **(C)** The percentage of T-cell exhaustion was determined by exhausted T-cell markers $PD\text{-}1^+$, $TIM\text{-}3^+$, $LAG\text{-}3^+$, and $CTLA\text{-}4^+$ before and after stimulation. Data were pooled from three different donors and are shown as mean ± SEM; One-way ANOVA for **(B, C)**; *p < 0.05.

expressed naïve and central memory phenotypes at pre-stimulation and mostly differentiated into central memory T-cells after stimulation without any differences among the CAR constructs (Figure 2B). Higher expressions of the T-cell exhaustion phenotypes, which included PD-1, TIM-3, LAG-3, and CTLA-4, were observed at pre-stimulation compared with the post-stimulation phase among the CD19CAR constructs. It was observed that only CD19.28z CAR-T cells highly expressed PD-1 after stimulation compared with the others (Figure 2C). In addition, similar overexpressions of TIM-3 and CTLA-4 were observed among the CAR structures at baseline and only CTLA-4 after stimulation. From these results, we confirmed a higher CAR-T cell proliferation of CD19CAR that incorporated the CD79A/CD40 costimulatory domain compared with the T-cell-derived costimulatory domain.

Distinctive gene expressions of CD19.79A.40z CAR-T cells after stimulation with target cells

To further investigate the transcriptomic differences among CAR structures, RNA was extracted from the CD19CAR-T cells after stimulation with target cells for seven days (Figure 2A). The DEGs of the three groups were assessed and compared: CD19.79A.40z CAR-T cells vs. CD19.28z CAR-T cells; CD19.79A.40z CAR-T cells vs. CD19.BBz CAR-T cells; and CD19.28z CAR-T cells vs. CD19.BBz CAR-T cells. The distributions of all DEGs obtained from each comparison and the gene names of the most significant and highest expression changes from the DEG list are shown in volcano plots (Figures 3A, B) with statistical significance of DEG data (adjusted p-value) versus the magnitude of the expression change (log2 fold change). According to the DEG analysis using EdgeR, the CD19.79A.40z CAR-T cells resulted in significant changes in the expression of 374 genes compared with the CD19.28z CAR-T cells: 232 genes were up-regulated and 142 genes were down-regulated (Figures 3A, C). Notably, we observed the up-regulation of T-cell activation genes included major histocompatibility complex class II genes (*HLA-DP, HLA-DR*, and *HLA-DM*), *CCR7, TFRC, LEF1, MYB, ZP3, CD74*, and *MAP3K8*, while down-regulation of T-cell exhaustion and apoptosis genes included *ID3*, *PDCD1*, and *EOMES* in CD19.79A.40z CAR-T cells (Figure 3A). Surprisingly, only one up-regulated gene, CD40, was identified among the CD19.79A.40z CAR- and CD19.BBz CAR-T cells (Figure S2B). Moreover, 104 DEGs were observed among the CD19.28z CAR- and CD19.BBz CAR-T cells, in which 32 DEGs were up-regulated and 72 DEGs were down-regulated in CD19.28z CAR-T cells (Figures 3B, C). From the DEG analysis, CD19.79A.40z CAR-T cells exhibited markedly up- and down-regulated genes compared with CD19.28z CAR-T cells after antigen stimulation. Nonetheless, we identified similar gene expression profiling among the CD19.79A.40z CAR- and CD19.BBz CAR-T cells, which was correlated to greater proliferative capacity in these two co-stimulatory domains.

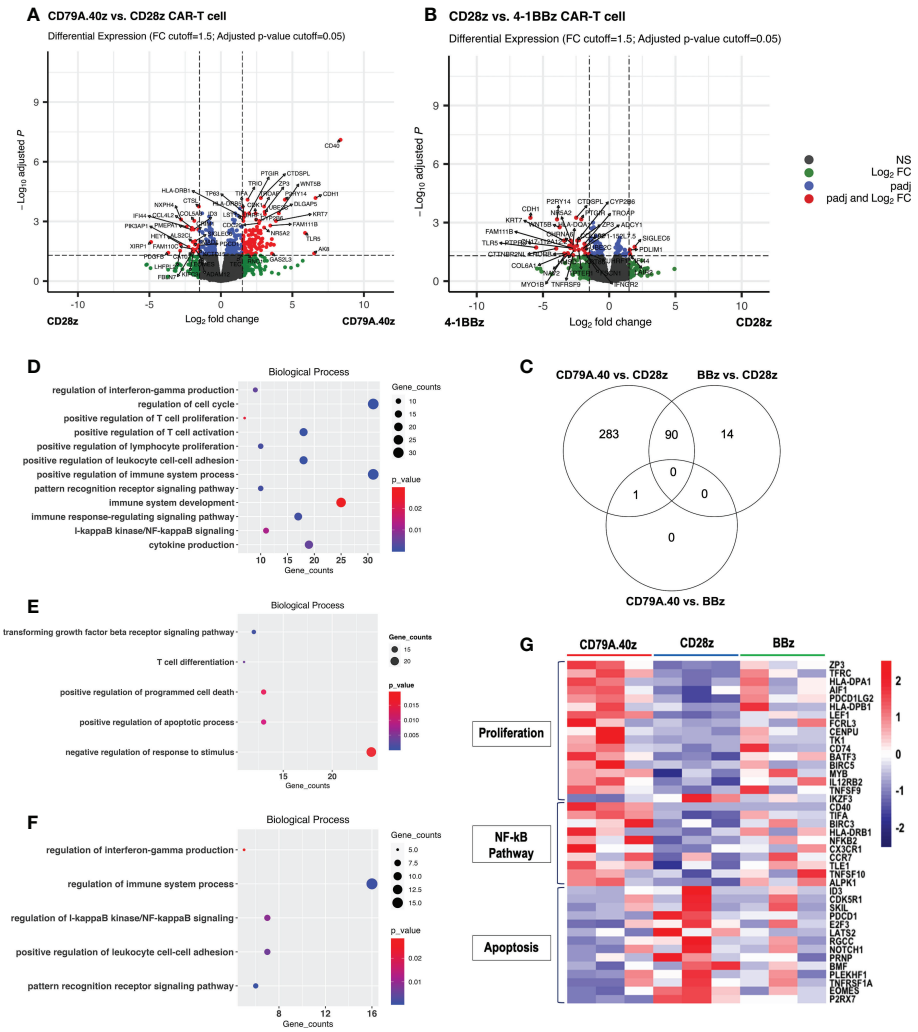

FIGURE 3
Differential gene expression profiling analysis of CD19CAR-T cell. **(A, B)** Volcano plots of DEGs between **(A)** CD19.28z CAR-T cells vs. CD19.79A.40z CAR-T cells and **(B)**, CD19.BBz CAR-T cells vs. CD19.28z CAR-T cells. Visualization of DEGs in volcano plots. Up-regulated- and down-regulated genes with FDR < 0.05 are marked in red. DEGs were selected with thresholds of false discovery rates (FDR) ≤ 0.05 and ≥ 1.5-fold difference. **(C)** Venn diagram illustrating the number of overlapped DEGs between each comparison: CD19.79A.40z CAR-T cells vs. CD19.28z CAR-T cells, CD19.79A.40z CAR-T cells vs. CD19.BBz CAR-T cells, and CD19.BBz CAR-T cells vs. CD19.28z CAR-T cells. **(D–F)** Gene ontology-biological processes (GO-BP) of up- **(D)** and down-regulated DEGs **(E)** in CD19.79A.40z CAR-T cell compared to CD19.28z CAR-T cells. **(F)** The up-regulated DEGs in CD19.BBz CAR-T cells compared to CD19.28z CAR-T cells. **(G)**. Heatmap of normalized counts, under the indicated CD19CAR-T cells in three major categories related to proliferation genes, NF-κB pathway genes, and apoptosis genes. Gene names are listed on the right side and each CAR structure is marked at the top of the colored map. The color bar indicates the normalized counts values.

Advantage of CD19.79A.40z CAR-T cell proliferation and persistence related to various biological pathways

We next sought to define the molecular pathways contributing to the greater CAR-T cell functions. The DEGs were analyzed separately for up- and down-regulated genes in terms of gene ontology categories and enriched biological pathways. The findings obtained from the DEG data of CD19.79A.40z CAR-T cells vs. CD19.28z CAR-T cells using the g:Profiler software indicated significant categories of pathway enrichment according to the gene ontology-biological process (GO-BP) database (Figures 3D, E). The up-regulated DEGs in the CD19.79A.40z CAR-T cells revealed that the most significant enriched pathways were those related to positive regulation of T-cell proliferation, T-cell activation, cell-cell adhesion, IFN-γ production, cytokine production, and I-κB kinase/NF-κB signaling (Figure 3D). In contrast, the enriched

GO-BP of down-regulated DEGs in CD19.79A.40z CAR-T cells were transforming growth factor beta receptor signaling pathway, positive regulation of apoptotic process, and programmed cell death (Figure 3E).

Furthermore, only up-regulated DEGs in CD19.BBz CAR-T cells compared with CD19.28z CAR-T cells were significantly enriched in GO-BP and similar to those in CD19.79A.40z CAR-T cells (Figure 3F). Of note, since only one DEG was identified among CD19.79A.40z CAR-T cells vs. CD19.BBz CAR-T cells, no enrichment results were obtained from the analysis. The three major DEG pathways related to T-cell proliferation, NF-κB signaling, and apoptosis are shown in the heatmap (Figure 3G). Significant up-regulation of key transcriptional regulators of T-cell proliferation, such as *ZP3*, *TFRC*, *HLA-DPA1*, *AIF1*, *HLA-DPB1*, *TNFSF9*, *BATF3*, *CD74*, *IL12RB2*, and *MYB* as well as NK-κB related genes including *CD40*, *BIRC3*, *NFKB2*, *CCR7*, and *TNFSF10*, was observed in CD19.79A.40z CAR-T cells compared with the others. On the other hand, CD19.79A.40z CAR-T cells also down-regulated apoptosis-related genes including *ID3*, *PDCD1*, *NOTCH1*, and *EOMES*. To conclude, the pathway enrichment analysis demonstrated that CD19.79A.40z CAR-T cells significantly up-regulated genes regulated T-cell proliferation, T-cell activation, and NF-κB signaling, whereas down-regulated genes related to apoptotic process and programmed cell death, which potentiated CAR-T cell proliferation.

CD19.79A.40z CAR-T cells enriched in genes related to T-cell proliferation, memory signatures, and less expressed genes regulated T-cell exhaustion

To interpret the genome-wide transcriptional profiles related to T-cell function, differentiation, and exhaustion of CD19CAR-T cells after antigen stimulation, we further characterized the molecular pathway using GSEA. A comparison of the top 50 gene markers of CD19.79A.40z CAR-T cells vs. CD19.28z CAR-T cells is shown in Figure 4A. *CD79A*, *CD40*, *IL2*, *IFNGR2*, *ZP3*, and *BATF3* were in the top 25 genes most correlated with the CD19.79A.40z CAR-T cell phenotype. In contrast, *CXCR6*, *P2RX7*, *EOMES*, *CD28*, and *PDCD1* were in the top 25 genes most correlated with CD19.28z CAR-T cells, in which higher PD-1 expression was observed in CD19.28z CAR-T cells following CD19 antigen stimulation compared with the other constructs (Figure 2C). The top 25 genes most correlated with the CD19.79A.40z CAR-T cell phenotype versus the top 25 genes most correlated with the CD19.BBz CAR-T cell phenotype are also illustrated in Figure 4B.

The GSEA demonstrated that the CD19.79A.40z CAR-T cells enriched in genes previously identified to correlate with T-cell proliferation, compared with either CD19.CD28z CAR- or CD19.BBz CAR-T cells, included *IL-2*, *ZP3*, *TFRC*, and *CD70* (Figure 4C). Moreover, we further examined the enrichment of ranked gene lists in interferon signaling pathway using the REACTOME database. Significant up-regulation of the gene set associated with interferon signaling was found in CD19.79A.40z CAR-T cells, such as *IFNGR2* (type II IFN-γ), *HLA-DOB2*, *GBP6*, *OAS3*, *HERC5*, *FLNB*, and *IRF1*, compared with CD19.28z CAR-T cells (Figure 4D). Compared with CD19.BBz CAR-T cells, CD19.79A.40z CAR-T cells down-regulated the exhausted-related genes of CD8 T-cells (Figure 4E). In contrast, the enrichment in gene sets associated with memory and naïve CD8 T-cell were predominantly observed in CD19.79A.40z CAR-T cells (Figures 4F, G).

Furthermore, we analyzed other GSEA gene sets using the hallmark collection. The CD19.79A.40z CAR-T cells were strongly related to various pathways compared with the CD19.28z CAR- or CD19.BBz CAR-T cells such as E2F target genes, Mtorc1 signaling, Myc target v1, and oxidative phosphorylation (Figures S3A–H). Regarding CAR-T cell metabolism, CD19.79A.40z CAR-T cells demonstrated an enrichment in genes related to both fatty acid and glycolysis metabolism compared with the others (Figures S3I–K). Our data suggested that CD19.79A.40z CAR-T cells responded to target cell stimulation by up-regulating genes related to T-cell activation, interferon signaling, memory-related signatures, fatty acid and glycolysis metabolism, as well as down-regulating the exhausted gene signatures.

Discussion

The costimulatory domain significantly impacts the functions of CAR-T cells. To date, the most extensively employed costimulatory domains within CD19-targeted CARs have been CD28 and 4-1BB (17). The 4-1BB-costimulated CAR-T cells have substantially slower kinetics but have higher persistence. On the other hand, CD28-costimulated CAR-T cells are linked to more rapid T-cell proliferation and tumor eradication (18). In this study, we constructed three CD19CAR structures with different costimulatory domains (CD28, 4-1BB, or CD79A/CD40) and assessed their functions in an *in vitro* assay. CD19.79A.40z CAR-T cells showed higher proliferative capacity than CD19.28z CAR- or CD19.BBz CAR-T cells, which was consistent with a previous report (13). The strong NF-κB, NFAT, and p38 nuclear-translocating signals generated by the CD79A/CD40 costimulatory domain following CD19 antigen stimulation were proposed as the contributing factors for greater CAR-T cell proliferation and persistence. From RNA sequencing analysis, we provided informative data on gene expression profiling of CD19CAR-T cells incorporated with a B-cell costimulatory domain in response to short-term antigen stimulation. The pathway enrichment analysis suggested up-regulated DEGs in T-cell proliferation, T-cell activation, cell cycle regulation, regulation of interferon production, and NF-κB

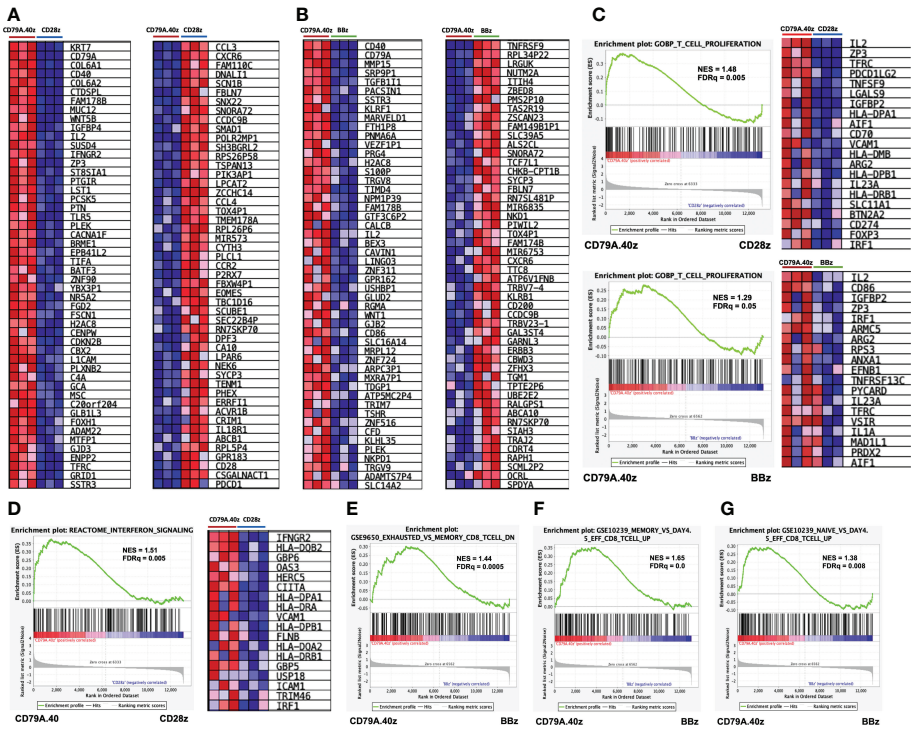

FIGURE 4
Gene set enrichment analysis of CD19.79A.40z CAR-T cells following antigen stimulation. **(A, B)** Heatmap of the top 50 up- (left) or down- (right) regulated genes differentially expressed by either **(A)** CD19.79A.40z CAR-T cells vs. CD19.28z CAR-T cells or **(B)** CD19.79A.40z CAR-T cells vs. CD19.BBz CAR-T cells. The colors reflect expression values of normalized counts, which range from red (high expression), pink (moderate expression), light blue (low expression), to dark blue (lowest expression). **(C)** Representative GSEA results of enriched GO-BP T-cell proliferation in CD79A.40z CAR-T cells vs. CD19.28z CAR-T cells (upper) and CD79A.40z CAR-T cells vs. CD19.BBz CAR-T cells (lower) with heatmap of the top up-regulated genes (right). **(D)** GSEA of significantly enriched in interferon signaling pathway of CD79A.40z CAR-T cells vs. CD19.28z CAR-T cells, using the REACTOME database with heatmap of the top up-regulated genes (right). **(E)** GSEA enriched in down-regulation of exhausted-relative to memory CD8 T-cell related gene in CD19.79A.40z CAR-T cells vs. CD19.BBz CAR-T cells. **(F, G)** GSEA up-regulated in **(F)** memory-relative to effector-related genes and **(G)** naïve-relative to effector-related genes of CD19.79A.40z CAR-T cells vs. CD19.BBz CAR-T cells. The upper part of each GSEA plot displays the enrichment score, whereas the lower part displays the ranked list metric of the gene set. The ranked gene list is shown in the middle: red indicates up-regulation; blue indicates down-regulation; and the black vertical line indicates the gene set. FDR q-value cutoff ≤ 0.25, Nominal p-value ≤ 0.05.

pathway in CD19.79A.40z CAR-T cells compared with CD19.28z CAR-T cells. Interestingly, we found that CD19.79A.40z CAR- and CD19.BBz CAR-T cells were enriched in almost similar pathways, which translated into a similar advantage in T-cell proliferation and persistence of these costimulatory structures.

T-cell differentiation subsets of all CAR-T constructs predominantly expressed naïve and central memory phenotypes at pre-stimulation and most differentiated into central memory T-cells after stimulation according to their self-renewal capacity compared with effector T-cells that were undetectable at the end of culture. Higher T-cell exhaustion was demonstrated by higher PD-1 expression in CD19.28z CAR-T cells following CD19 antigen stimulation compared with the other constructs which correlated with the up-regulated *PDCD1* gene in CD19.28z CAR-T cells from RNA sequencing analysis.

The previous study by Long and colleagues investigated the molecular pathways contributing to the ameliorating effect of the 4-1BB signal on CAR-T cell exhaustion compared to CD28. They did not demonstrate any differences in transcription factors associated with memory generation between 4-1BB and CD28 in the CD19CAR-T cell model; however, differences appeared in the GD2CAR-T cell model. The GD2.28z CAR-T cells showed higher expression of genes encoded by inhibitory receptors or transcription factors such as *LAG-3*, *TIM-3*, *TBX21*, and *EOMES*. On the other hand, GD2.BBz CAR-T cells highly expressed genes encoded by transcription factors associated with memory such as *KLF6*, *JUN*, and *JUNB* (6). In this study, CD19.79A.40z CAR-T cells enriched in genes associated with T-cell proliferation, NK-κB signaling, and naïve and memory signatures such as *ZP3*, *IFNGR2*, *BATF3*, *TNFSF9*, *BATF3*, *CD74*, *IL12RB2*, *MYBBIRC3*, *NFKB2*, *CCR7*, and *TNFSF10*. Furthermore, less expressed genes related to apoptosis and T-

cell exhaustion included *CXCR6*, *P2RX7*, *ID3*, *NOTCH1*, *EOMES*, and *PDCD1*. Similar results from a previous study by Prinzing et al. reported a transcriptomic analysis of B-cell costimulation of MyD88/CD40 in CAR-T cells in solid tumor models. Higher levels of *MYB* and *FOXM1*, the key cell regulators, and low levels of *TBET* and *BLIMP1* were identified, which promoted terminal T-cell differentiation compared with CD28- or 4-1BB-endowed CAR-T cells. They concluded that MyD88/CD40 costimulation is a less differentiated CAR-T phenotype, which translates into greater proliferative capacity and persistence (12). These findings highlighted the less-differentiated T-cell subsets and memory characteristics of the CAR-T cells that incorporated the B-cell-derived costimulatory domain, which translated into better T-cell persistence and enhanced antitumor activity (12, 13, 19, 20).

Among the DEGs, we discovered an up-regulation of the *BATF3* gene in CD79A/CD40 over the others, which enhanced T-cell proliferative capacity and memory phenotypes. A recent study by Ataide et al. demonstrated that long-lasting *BATF3* expression in T-cells promoted survival and transition to a memory T-cell phenotype. *BATF3* also regulated T-cell apoptosis and longevity *via* the pro-apoptotic factor *BIM* (21). In addition, CD79A/CD40 also significantly down-regulated the Ikaros Family Zinc Finger Protein 3, *IKZF3* gene. Immune cell development and cytokine signaling are two main functions of the IKZF family members that have been thoroughly established (22). A recent study indicated that the knock-out *IKZF3* gene (*IKZF3* KO) enhanced proliferation and could potentiate the killing effect of CAR-T cells in solid tumor cells *in vitro* and xenograft models by increasing the expression of genes mediating cytokine signaling and cytotoxicity (23).

Concomitantly, GSEA also demonstrated the enrichment genes in Mtorc1 signaling and Myc target v1, which are the pathways involved in cell cycle, proliferation, differentiation, and survival (24, 25). The metabolic pathway of the CD19.79A.40z CAR-T cells was demonstrated by enrichment of both glycolysis and fatty acid metabolism compared with the others, which correlated with the high NF-κB and NFAT signaling following CD19 antigen stimulation in the recent study (13). Previous studies demonstrated that CD28-costimulated CD19CAR-T cells enhanced glycolytic metabolism and induced an effector memory phenotype. In contrast, 4-1BB-based CD19CAR-T cells were found to depend on fatty acid metabolism and induced a central memory phenotype (10, 26). The underlying metabolic pathway is closely linked to T-cell activation and proliferation (27). The activation of T-cells requires metabolic programming to support the proliferation and differentiation of naïve T-cells upon antigen recognition (7, 28). Following T-cell activation, the expression of glycolysis and glutaminolysis-related genes are up-regulated to produce extracellular nutrients including glucose, glutamine, and amino acids (28–30). Fatty acid synthesis then proceeds to support T-cell proliferation (27).

Besides CD19CAR-T cells, we tested CD79A/CD40 costimulatory domain in other CAR models: CD20CAR-T and CD37CAR-T cells. CD20CAR incorporated with CD79A/CD40 or 4-1BB costimulatory domain showed higher proliferative capacity compared with CD28 after stimulation with CD20-K562 cells. In contrast, we did not observe any difference in CAR-T cell proliferation among costimulatory domains in CD37CAR-T cells after stimulation with CD37 positive antigen. There was no significant difference among the costimulatory domains in both CAR-T cell models regarding cytokine secretion and cytotoxicity. The inconsistent results of CD79A/CD40 costimulatory domain among CD19CAR-T cell and 20CAR-T or CD37CAR-T cell models were possibly caused from multifactorial factors including the differences in antigen binding affinity, the flexibility, and extracellular protein folding of antiCD20 or antiCD37 scFv compared with antiCD19scFv (FMC63 clone). Further studies are needed to confirm the efficacy of the novel B-cell signaling molecules in other types of CAR-T cells. Regarding limitation of study, we did not assess the protein expressions to confirm the RNA sequencing results, which was out of our scope and the further studies may be needed.

In conclusion, this study provided comprehensive gene expression profiling of CD19CAR-T cells incorporated with the B-cell-derived costimulatory domain, CD79A/CD40, which significantly up-regulated genes related to T-cell activation, proliferation, interferon production, NF-κB signaling, memory signatures, and down-regulated apoptotic and T-cell exhaustion genes compared with CD28 or 4-1BB. In addition, both glycolysis and fatty acid metabolism pathways, which are necessary to drive T-cell proliferation and differentiation, were also highly enriched in CD79A/CD40 compared with conventional costimulatory domains.

Data availability statement

The datasets presented in this study can be found in online repositories. The names of the repository/repositories and accession number(s) can be found below: NCBI under accession ID: PRJNA896859.

Ethics statement

The studies involving human participants were reviewed and approved by The Human Research Ethics Committee of the Faculty of Medicine, Prince of Songkla University, Thailand

(REC.64-415-14-1). The patients/participants provided their written informed consent to participate in this study.

Author contributions

Conception and design; SU, ST, and JJ. Development of methodology; SU, PC, and JJ. Acquisition of data; SU, PC, WK, KM, SS, ST, and JJ. Analysis and interpretation of data (e.g., statistical analysis, computational analysis); SU, PC, and JJ. Writing, review, and/or revision of the manuscript; SU, PC, WK, KM, SS, ST, and JJ. Administrative, technical, or material support (e.g., reporting or organizing data, constructing databases); SU, PC, and JJ. Study supervision; SS, ST, and JJ. All authors contributed to the article and approved the submitted version.

Funding

This work was supported by the National Science, Research and Innovation Fund (NSRF) and Prince of Songkla University (Grant No. MED6505092S to JJ), the Higher Education Research Promotion, and the Thailand Scholarships of the Higher Education Commission (Grant No.1272/2552 to SU).

Acknowledgments

The authors would like to thank the Stem Cell Laboratory, Department of Biomedical Science and Bioengineering, and Translational Medicine Research Center, Faculty of Medicine, Prince of Songkla University for the technical assistance.

Conflict of interest

The authors declare that the research was conducted in the absence of any commercial or financial relationships that could be construed as a potential conflict of interest.

Publisher's note

All claims expressed in this article are solely those of the authors and do not necessarily represent those of their affiliated organizations, or those of the publisher, the editors and the reviewers. Any product that may be evaluated in this article, or claim that may be made by its manufacturer, is not guaranteed or endorsed by the publisher.

Supplementary material

The Supplementary Material for this article can be found online at: https://www.frontiersin.org/articles/10.3389/fimmu.2022.1064339/full#supplementary-material

SUPPLEMENTARY FIGURE 1
(A) Transduction efficacy and purification of CD19CAR-T cells. **(B)** Concentration of IFN-γ, IL-2, and TNF-α secretion. T-cells were stimulated with γ-irradiated CD19-K562 cell line in a 1:1 ratio for 16 hours, and culture supernatants were analyzed using an ELISA. **(C)** Fold expansion of T-cells following γ-irradiated CD19-K562 cell line stimulation in a 1:1 ratio for seven days and cultured without IL-2 supplementation. Arrows mark the day of CD19-K562 cell stimulation. All data were pooled from three different donors and are shown as mean ± SEM. One-way ANOVA for **(A)** and **(B)**; 2-way ANOVA for **(C)**; ***p < 0.001 (CD19.79A.40zCAR- vs. CD19.28z CAR-T cells).

SUPPLEMENTARY FIGURE 2
(A) RNA-analysis pipeline. **(B)** Volcano plots of DEGs between CD19.79A.40z CAR-T cells vs. CD19.BBz CAR-T cells. Visualization of DEGs in volcano plots. Up-regulated- and down-regulated genes with FDR < 0.05 are marked in red. DEGs were selected with thresholds of false discovery rate (FDR) ≤ 0.05 and ≥ 1.5-fold difference.

SUPPLEMENTARY FIGURE 3
(A–D, K) GSEA indicated the gene enrichments in CD19.79A.40z CAR-T cells vs. CD19.28z CAR-T cells in the following hallmarks; **(A)** E2F target, **(B)** Mtorc1 signaling, **(C)** Myc target v1, **(D)** oxidative phosphorylation, and **(K)** glycolysis. **(E–J)** GSEA indicated gene enrichment in CD19.79A.40z CAR-T cells vs. CD19.BBz CAR-T cells in the following hallmarks; **(E)** E2F target, **(F)** Mtorc1 signaling, **(G)** Myc target v1, **(H)** oxidative phosphorylation, **(I)** fatty acid metabolism, and **(J)** glycolysis. The upper part of each plot displays the enrichment score, whereas the lower part displays the ranked list metric of the gene set. The ranked gene list is shown in the middle: red indicates up-regulation; blue indicates down-regulation; and the black vertical line indicates the gene set. FDR q-value cutoff ≤ 0.25, nominal p-value ≤ 0.05.

References

1. Sadelain M, Rivière I, Riddell S. Therapeutic T cell engineering. *Nature* (2017) 545(7655):423–31. doi: 10.1038/nature22395

2. Feins S, Kong W, Williams EF, Milone MC, Fraietta JA. An introduction to chimeric antigen receptor (CAR) T-cell immunotherapy for human cancer. *Am J Hematol* (2019) 94(S1):S3–9. doi: 10.1002/ajh.25418

3. Schuster SJ, Svoboda J, Chong EA, Nasta SD, Mato AR, Anak Ö, et al. Chimeric antigen receptor T cells in refractory b-cell lymphomas. *N Engl J Med* (2017) 377(26):2545–54. doi: 10.1056/NEJMoa1708566

4. O'Leary MC, Lu X, Huang Y, Lin X, Mahmood I, Przepiorka D, et al. FDA Approval summary: Tisagenlecleucel for treatment of patients with relapsed or refractory b-cell precursor acute lymphoblastic leukemia. *Clin Cancer Res* (2019) 25 (4):1142–6. doi: 10.1158/1078-0432.CCR-18-2035

5. Zhong Q, Zhu YM, Zheng LL, Shen HJ, Ou RM, Liu Z, et al. Chimeric antigen receptor-T cells with 4-1BB Co-stimulatory domain present a superior treatment outcome than those with CD28 domain based on bioinformatics. *Acta Haematol* (2018) 140(3):131–40. doi: 10.1159/000492146

6. Long AH, Haso WM, Shern JF, Wanhainen KM, Murgai M, Ingaramo M, et al. 4-1BB costimulation ameliorates T cell exhaustion induced by tonic signaling of chimeric antigen receptors. *Nat Med* (2015) 21(6):581–90. doi: 10.1038/nm.3838

7. Frauwirth KA, Riley JL, Harris MH, Parry RV, Rathmell JC, Plas DR, et al. The CD28 signaling pathway regulates glucose metabolism. *Immunity* (2002) 16 (6):769–77. doi: 10.1016/S1074-7613(02)00323-0

8. Li G, Boucher JC, Kotani H, Park K, Zhang Y, Shrestha B, et al. 4-1BB enhancement of CAR T function requires NF-κB and TRAFs. *JCI Insight* (2018) 3 (18):e121322. doi: 10.1172/jci.insight.121322

9. Philipson BI, O'Connor RS, May MJ, June CH, Albelda SM, Milone MC. 4-1BB costimulation promotes CAR T cell survival through noncanonical NF-κB signaling. *Sci Signal* (2020) 13(625):eaay8248. doi: 10.1126/scisignal.aay8248

10. Kawalekar OU, O' Connor RS, Fraietta JA, Guo L, McGettigan SE, Posey AD, et al. Distinct signaling of coreceptors regulates specific metabolism pathways and impacts memory development in CAR T cells. *Immunity* (2016) 44(3):712. doi: 10.1016/j.immuni.2016.02.023

11. Collinson-Pautz MR, Chang WC, Lu A, Khalil M, Crisostomo JW, Lin PY, et al. Constitutively active MyD88/CD40 costimulation enhances expansion and efficacy of chimeric antigen receptor T cells targeting hematological malignancies. *Leukemia* (2019) 33(9):2195–207. doi: 10.1038/s41375-019-0417-9

12. Prinzing B, Schreiner P, Bell M, Fan Y, Krenciute G, Gottschalk S. MyD88/CD40 signaling retains CAR T cells in a less differentiated state. *JCI Insight* (2020) 5 (21):e136093. doi: 10.1172/jci.insight.136093

13. Julamanee J, Terakura S, Umemura K, Adachi Y, Miyao K, Okuno S, et al. Composite CD79A/CD40 co-stimulatory endodomain enhances CD19CAR-T cell proliferation and survival. *Mol Ther* (2021) 29(9):2677–90. doi: 10.1016/j.ymthe.2021.04.038

14. Terakura S, Yamamoto TN, Gardner RA, Turtle CJ, Jensen MC, Riddell SR. Generation of CD19-chimeric antigen receptor modified CD8+ T cells derived from virus-specific central memory T cells. *Blood* (2012) 119(1):72–82. doi: 10.1182/blood-2011-07-366419

15. Subramanian A, Tamayo P, Mootha VK, Mukherjee S, Ebert BL, Gillette MA, et al. Gene set enrichment analysis: a knowledge-based approach for interpreting genome-wide expression profiles. *Proc Natl Acad Sci U S A*. (2005) 102(43):15545–50. doi: 10.1073/pnas.0506580102

16. Raudvere U, Kolberg L, Kuzmin I, Arak T, Adler P, Peterson H, et al. g:Profiler: a web server for functional enrichment analysis and conversions of gene lists (2019 update). *Nucleic Acids Res* (2019) 47(W1):W191–W8. doi: 10.1093/nar/gkz369

17. van der Stegen SJ, Hamieh M, Sadelain M. The pharmacology of second-generation chimeric antigen receptors. *Nat Rev Drug Discovery* (2015) 14(7):499–509. doi: 10.1038/nrd4597

18. Zhao Z, Condomines M, van der Stegen SJC, Perna F, Kloss CC, Gunset G, et al. Structural design of engineered costimulation determines tumor rejection kinetics and persistence of CAR T cells. *Cancer Cell* (2015) 28(4):415–28. doi: 10.1016/j.ccell.2015.09.004

19. Sommermeyer D, Hudecek M, Kosasih PL, Gogishvili T, Maloney DG, Turtle CJ, et al. Chimeric antigen receptor-modified T cells derived from defined CD8+ and CD4+ subsets confer superior antitumor reactivity *in vivo*. *Leukemia* (2016) 30(2):492–500. doi: 10.1038/leu.2015.247

20. Fraietta JA, Lacey SF, Orlando EJ, Pruteanu-Malinici I, Gohil M, Lundh S, et al. Determinants of response and resistance to CD19 chimeric antigen receptor (CAR) T cell therapy of chronic lymphocytic leukemia. *Nat Med* (2018) 24(5):563–71. doi: 10.1038/s41591-018-0010-1

21. Ataide MA, Komander K, Knöpper K, Peters AE, Wu H, Eickhoff S, et al. BATF3 programs CD8. *Nat Immunol* (2020) 21(11):1397–407. doi: 10.1038/s41590-020-0786-2

22. Powell MD, Read KA, Sreekumar BK, Oestreich KJ. Ikaros zinc finger transcription factors: Regulators of cytokine signaling pathways and CD4. *Front Immunol* (2019) 10:1299. doi: 10.3389/fimmu.2019.01299

23. Zou Y, Liu B, Li L, Yin Q, Tang J, Jing Z, et al. IKZF3 deficiency potentiates chimeric antigen receptor T cells targeting solid tumors. *Cancer Lett* (2022) 524:121–30. doi: 10.1016/j.canlet.2021.10.016

24. Dang CV. C-myc target genes involved in cell growth, apoptosis, and metabolism. *Mol Cell Biol* (1999) 19(1):1–11. doi: 10.1128/MCB.19.1.1

25. Laplante M, Sabatini DM. mTOR signaling in growth control and disease. *Cell* (2012) 149(2):274–93. doi: 10.1016/j.cell.2012.03.017

26. Boroughs AC, Larson RC, Marjanovic ND, Gosik K, Castano AP, Porter CBM, et al. A distinct transcriptional program in human CAR T cells bearing the 4-1BB signaling domain revealed by scRNA-seq. *Mol Ther* (2020) 28(12):2577–92. doi: 10.1016/j.ymthe.2020.07.023

27. Almeida L, Lochner M, Berod L, Sparwasser T. Metabolic pathways in T cell activation and lineage differentiation. *Semin Immunol* (2016) 28(5):514–24. doi: 10.1016/j.smim.2016.10.009

28. Wang R, Dillon CP, Shi LZ, Milasta S, Carter R, Finkelstein D, et al. The transcription factor myc controls metabolic reprogramming upon T lymphocyte activation. *Immunity* (2011) 35(6):871–82. doi: 10.1016/j.immuni.2011.09.021

29. Sinclair LV, Rolf J, Emslie E, Shi YB, Taylor PM, Cantrell DA. Control of amino-acid transport by antigen receptors coordinates the metabolic reprogramming essential for T cell differentiation. *Nat Immunol* (2013) 14 (5):500–8. doi: 10.1038/ni.2556

30. Macintyre AN, Gerriets VA, Nichols AG, Michalek RD, Rudolph MC, Deoliveira D, et al. The glucose transporter Glut1 is selectively essential for CD4 T cell activation and effector function. *Cell Metab* (2014) 20(1):61–72. doi: 10.1016/j.cmet.2014.05.004

frontiers | Frontiers in Immunology

TYPE Review
PUBLISHED 24 January 2023
DOI 10.3389/fimmu.2023.1045024

Check for updates

OPEN ACCESS

EDITED BY
Anand Rotte,
Arcellx Inc., United States

REVIEWED BY
Yaya Chu,
New York Medical College, United States
Justin Edwards,
Arcellx, United States

*CORRESPONDENCE
Yi Li
liyi3443@hotmail.com

SPECIALTY SECTION
This article was submitted to Cancer Immunity and Immunotherapy, a section of the journal Frontiers in Immunology

RECEIVED 15 September 2022
ACCEPTED 04 January 2023
PUBLISHED 24 January 2023

CITATION
Zhang K, Chen H, Li F, Huang S, Chen F and Li Y (2023) Bright future or blind alley? CAR-T cell therapy for solid tumors. *Front. Immunol.* 14:1045024. doi: 10.3389/fimmu.2023.1045024

COPYRIGHT
© 2023 Zhang, Chen, Li, Huang, Chen and Li. This is an open-access article distributed under the terms of the Creative Commons Attribution License (CC BY). The use, distribution or reproduction in other forums is permitted, provided the original author(s) and the copyright owner(s) are credited and that the original publication in this journal is cited, in accordance with accepted academic practice. No use, distribution or reproduction is permitted which does not comply with these terms.

Bright future or blind alley? CAR-T cell therapy for solid tumors

Kai Zhang[1,2], Hong Chen[1], Fuqiang Li[3], Sheng Huang[4], Fei Chen[5] and Yi Li[1,2]*

[1]Department of Oncology, 920th Hospital of Joint Logistics Support Force, Kunming, Yunnan, China, [2]Graduate School, Kunming Medical University, Kunming, Yunnan, China, [3]Department of Traditional Chinese Medicine, 920th Hospital of Joint Logistics Support Force, Kunming, Yunnan, China, [4]Department of Breast Surgery, Breast Cancer Center of the Third Affiliated Hospital of Kunming Medical University, Yunnan Cancer Hospital, Kunming, Yunnan, China, [5]Department of Medical Oncology, The Second Affiliated Hospital of Kunming Medical University, Kunming, Yunnan, China

Chimeric antigen receptor (CAR) T cells therapy has emerged as a significant breakthrough in adoptive immunotherapy for hematological malignancies with FDA approval. However, the application of CAR-T cell therapy in solid tumors remains challenging, mostly due to lack of suitable CAR-T target antigens, insufficient trafficking and extravasation to tumor sites, and limited CAR-T survival in the hostile tumor microenvironment (TME). Herein, we reviewed the development of CARs and the clinical trials in solid tumors. Meanwhile, a "key-and-lock" relationship was used to describe the recognition of tumor antigen via CAR T cells. Some strategies, including dual-targets and receptor system switches or filter, have been explored to help CAR T cells matching targets specifically and to minimize on-target/off-tumor toxicities in normal tissues. Furthermore, the complex TME restricts CAT T cells activity through dense extracellular matrix, suppressive immune cells and cytokines. Recent innovations in engineered CARs to shield the inhibitory signaling molecules were also discussed, which efficiently promote CAR T functions in terms of expansion and survival to overcome the hurdles in the TME of solid tumors.

KEYWORDS

CAR-T cells, solid tumor, adoptive immunotherapy, tumor microenvironment, cytokine release syndrome, tumor infiltration, immune evasion

1 Introduction

Chimeric antigen receptor (CAR) T-cell therapy represents a significant breakthrough in adoptive T-cell therapies for cancer. CAR is engineered synthetic receptors that redirects T cells to recognize the corresponding antigens in a major histocompatibility complex (MHC)-independent manner, thus activating anti-tumor responses. To date, CAR-T cell therapy has achieved tremendous successes in hematological malignancies (1). The CAR-T cell targeting the pan-B-cell marker CD19, which became the first gene-therapy product approved by US Food and Drug Administration (FDA), had achieved largely advance in patients with relapsed or refractory acute lymphoblastic leukemia and diffuse large B-cell lymphoma, with complete remission rates of up to 90%. However, despite extensive research, CAR-T cell

therapy for solid tumors have shown limited antitumor activity in early phase clinical trial, where the unique challenges must be addressed as lack of suitable CAR-T target antigens, insufficient trafficking to tumor sites, and limited CAR-T survival in the immunosuppressive tumor microenvironment (TME), and life-threatening CAR-T cells-associated toxicities. Tumor cells can construct conditions conducive to their own survival by stimulating new blood vessels, while also recruiting and stimulating immunosuppressive cells to aggregate in the TME, thus employing their secreted inhibitory cytokines and extracellular matrix (ECM) to create an environment that facilitates immune escape (2). Actually, CAR-T cells, like tumor-infiltrating T cells, are subject to physical, chemical, and cellular barriers in the TME. Furthermore, excessive activation of CAR-T cells may increase the risk of immune-related adverse events and on-target/off-tumor effects. Importantly, identifying mechanisms underlying these hurdles is vital to improve CAR T function with promising safety. Currently, many strategies to engineer more powerful CAR T cells have been proposed to mitigate antigen heterogeneity, to augment CAR T cells infiltration, to overcome immunosuppressive signaling within the TME, and to reduce toxicities (3). Herein, we describe the development of CARs and the clinical trials of CAR-T therapy for solid tumor. We next discuss the challenges posed by tumor antigens and hostile TME as well as the toxic effects associated with CAR T therapy, and present recent innovations to overcome these obstacles in solid tumors.

2 Development of CARs

The original intention of CARs is to avoid the restrictions of major histocompatibility complex (MHC) by specific immune cells. A CAR, an artificial fusion protein, is made of four key segments. The extracellular domain, typically derived from the single-chain variable fragment (scFv) of an antibody, is responsible for tumor antigen recognition (4). The hinge portion, located between scFv and transmembrane (TM) domain, provide flexibility to overcome steric hindrance, which is needed to allow the antigen domain to access the targeted epitope (5). Importantly, the hinge region with different length and composition can affect flexibility, CAR expression, signaling, and epitope recognition (6).The TM domain, along with the hinge region, anchors the CAR to cell membrane, which affects a downstream signaling cascade of T-cell activation. The intracellular signaling domain most commonly consists of a single CD3ζ domain and some co-stimulatory molecules. With a fast-paced journey to tackling the obstacles of CAR T therapy, five generations of CARs have been developed (Figure 1). The first generation CARs with only CD3ζ molecule in the intracellular signaling domain showed little therapeutic effects in early clinical trials (7). After that, co-stimulatory molecules, which enhance CAR T cell activity, were introduced into CARs, such as CD28 and CD137 (4-1BB). Depending on the number of co-stimulatory molecules, second (one domain) and third (two domains) generation CARs are designed, respectively (8). And most clinical trials are dominated by 2G and 3G CAR-T cells (9). However, the benefit of 3G CARs with two co-stimulatory molecules is model-dependent. Ramello reported that PSCA-specific second-generation CARs containing the CD28 transmembrane and co-stimulatory domains can induce additional sources of downstream signaling via the expression of a constitutively phosphorylated form of CD3ζ, suggesting that second-generation CARs could activate more intense signaling and superior antitumor efficacy as compared to third-generation CARs (10). To further optimize CAR function, some modifications of the intracellular domain were introduced based on

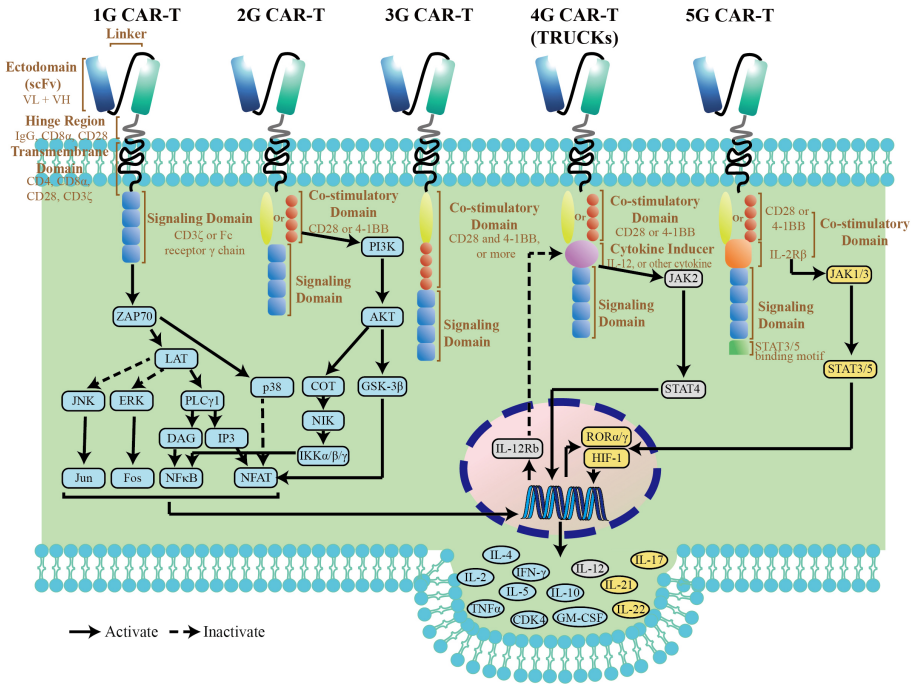

FIGURE 1
Structure diagram and simple pathway map of CAR-T cells. The pathway map is referenced from KEGG (https://www.genome.jp/kegg/).

the backbone of 2G CARs. The fourth generation CARs, also known as armored CARs or TRUCKS (T cells redirected for universal cytokine-mediated killing), are designated with a nuclear factor of activated T cells (NFAT) response element-driven cytokines, such as interleukin(IL)-12, IL-15, and granulocyte-macrophage colony-stimulating factor. Such TRUCKs, T cells redirected for universal cytokine-mediated killing have more improvement in anti-tumor efficacy and persistence than 2G CAR-T cells, which endows them with the potential to break through the immune suppressive microenvironment (11). The so-called fifth-generation (5G) CAR currently has been developed with an intracellular fragment of cytokine receptor (for instance, IL-2Rβ) and a STAT3-binding YXXQ motif. This new generation of CARs was capable of inducing cytokine signaling after triggering JAK-STAT3/5 pathway, which provided the T cells with superior cytolytic activity even after repeated antigen exposures (12).

3 Phase I/II clinical trials of CAR-T cell therapy against solid tumors

CAR T cell therapy has impressive achievements in the arena of hematological malignancies, in which seven CAR T products have been approved by the FDA (13), starting from the first CAR-T drug Kymriah® (tisagenlecleucel, Novartis) in August 2017 for acute B lymphocytic leukemia (14) to most recently CARVYKTI™ (ciltacabtagene autoleucel, Legend Biotech) for CD19-positive relapsed or refractory diffuse large B-cell lymphoma in February 2022 (15). With the success of CAR T cells in hematologic malignancies, a growing number of clinical trials are underway focusing on translating this therapy to solid tumors. Up to date, 249 clinical trials of CAR T in solid tumors have been registered in the National Institutes of Health (NIH) database. All studies are phase I/II trails, and more than 50 potential targets have been investigated, including glypican-3 (GPC3; NCT02395250, NCT03146234), GD2 (NCT02761915), epidermal growth factor receptor (EGFR; NCT01869166), mesothelin (MSLN, NCT03054298, NCT03323944), mucin 1 (MUC-1, CD227; NCT02587689), human epidermal growth factor receptor-2 (HER2; NCT01935843), prostate-specific membrane antigen (PSMA; NCT03089203), carcinoembryonic antigen (CEA; NCT02349724), and claudin18.2 (CLDN18.2; NCT03874897). The outcomes data have been summarized in Figure 2 and Table 1.

4 Challenges and strategies of CAR-T cell therapy against solid tumors

In contrast to CAR T cell therapies for hematological malignancies, much less success has been achieved in solid tumor. There are several known hallmarks that contribute to the limited therapeutic efficacy in solid tumors. First, it is hard to choice an ideal target antigen, which is a major determinant of both safety and efficacy in adoptive T cell therapy (28). Second, tumor cells are surrounded by the hostile TMEs with composed with stromal cells, cytokines, and immune cells, which not only prevent T cell homing into tumor sites but also drive T cell exhaustion and dysfunction. Third, the life-threatening side effects induced by CAR T cells also present an obstacle for solid cancer treatment. Here, we discuss the above challenges in detail, as well as the current strategies to improve the therapeutic efficacy.

4.1 Tumor antigens fundamentally affects treatment

The antigen recognition by immune cells has been identified as "lock-and-key" relationship. The selection of target antigen is a major determinant of safety and efficacy for CAR-T cell therapy. In general, tumor-specific antigens (TSAs) that are highly and homogeneously expressed within tumors are "idea" CAR targets. However, the majority of current targets are tumor-associated antigens (TAAs), which are not only enriched on tumors, but also share expression on normal tissues, albeit at a lower level. Lack of antigen specificity carries the risk of "on target/off tumor" toxicity, which could cause chronic damages to target-expressing tissues (29). Therefore, investigators have embarked on "using specific keys to open the lock". Recently, with the development of genomic and proteomic approaches, some neoantigens with tumor specificity have been discovered (Figure 3A). For example, CLDN18.2 has emerged as a promising TAAs given its stable and high expression in digestive system tumors, especially gastric cancer (27). Moreover, the alternatively spliced isoforms of some oncogenes have been selected as attractive CAR targets, due that their tumor-restricted expression patterns limit "on target/off tumor" toxicity. EGFRvIII, a tumor-specific oncogenic mutation, is the most common variant of the EGFR in human cancers. An *in vivo* study demonstrated that CAR-T cells specific for EGFRvIII had efficient antitumor activity against lung cancer cells, indicating that it could be a potential therapeutic strategy to prevent recurrence and metastasis of lung cancer (30). Similarly, in a glioblastoma model, EGFRvIII-directed CAR T cells also successfully killed tumor cells *in vitro* and *in vivo* (31). Furthermore, its clinical translation in recurrent glioblastoma patients displayed potentially effective and safe that no cross-reactivity of wild-type EGFR was observed (32). Recently, a preclinical study also highlighted that CD44v6, the isoform variant 6 of CD44, could be used for CAR redirection in human lung adenocarcinoma and ovarian cancer (33). In addition to target tumor antigens directly, targeting the antigens selectively expressed in tumor vasculature is an alternative approach for CAR T therapy. As compared with healthy tissues, the glycoprotein CLEC14A selectively overexpressed on the surface of tumor vascular endothelial cells, which has been identified as a highly promising target of CAR T therapy with favorable safety profiles in the solid tumor models (34).

Solid tumors present a large degree of heterogeneity, which is a common mechanism of therapeutic resistance (35). Target-antigen expression is dynamically regulated by cancer cells in response to treatment, such that tumor cell subpopulations could escape CAR-T cell surveillance when a single targeted antigen was downregulated or completely lost. Therefore, the strategies of "using multiple keys to open the lock" are being pursued, and dual-target CARs have been designed, which either assemble two ScFvs on extracellular segment of a single CAR or express two different CARs in T cells (Figure 3B) (36). Recently, a CAR with antigen recognition domain of CD70 and B7-

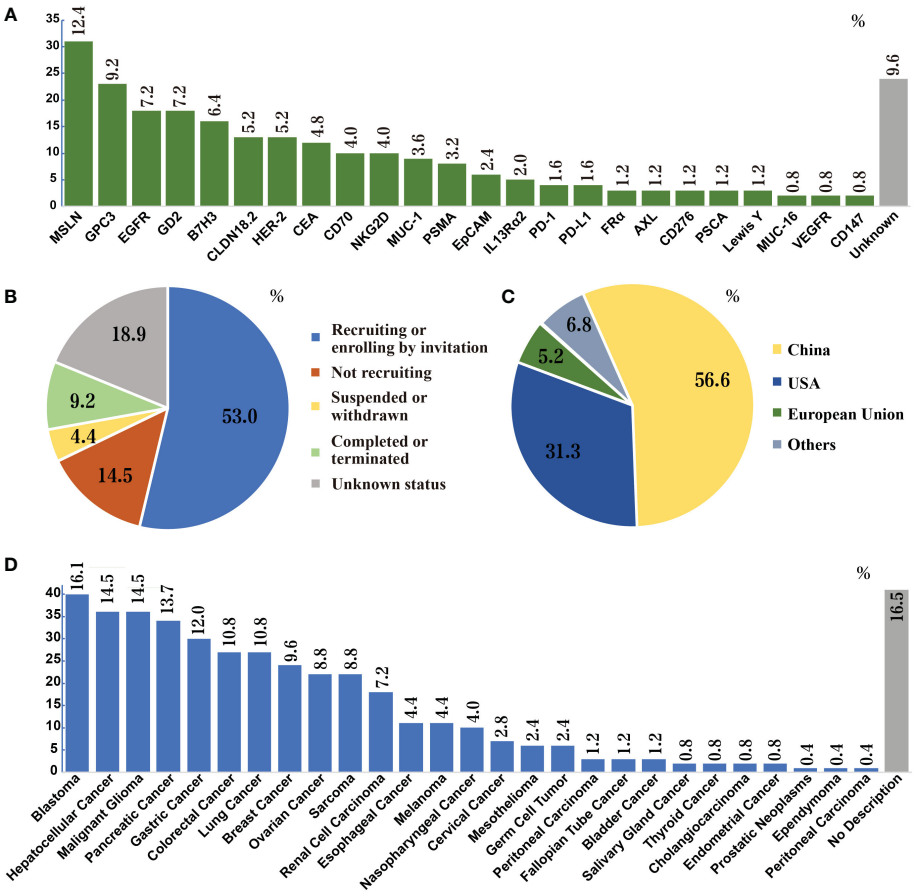

FIGURE 2
Search results of CAR-T cell therapies for solid tumors in NIH Clinical Trials Database (as of November 21, 2022). **(A)** Research frequencies of every target. **(B)** Status of clinical trials; over 60% of trials are ongoing. A total of 53 targets appeared in these clinical trials. The figure does not list the targets that appear only once (0.4%), which are: CD20, EphA2, CLDN6, CD40, TM4SF1, EpCAM, Nectin4/FAP, AFP, B4T2-001, ROR2, U87, ALPP, CD52, CD22, IL17Rα, CAIX, IM83, E2, IM92, CD171, IM96, ROR1, KKLC1, TAG72, CD56, CD33, MMP2, ICAM1 and gp100. **(C)** Countries or regions where the trials are located. The most clinical trials of CAR-T cell therapies for solid tumors are conducted in China, followed by the U.S. **(D)** Species of solid tumors studied in the clinical trials. Liver cancer, pancreatic cancer, breast cancer, sarcoma, and lung cancer are the five most studied solid tumors in clinical trials.

H3 in a linear fashion (also named Tandem CAR-T) had promising *in vitro* and *in vivo* results in models of lung cancer and melanoma (37). Similarly, in breast cancer model, superior antitumor responses were also observed in the engineered T cells armed with 2 CAR molecules specific for HER2 and MUC1 when compared to single targeted therapy (38). Although the clinical experience with these approaches is still limited, these data have highlighted that dual targeting may be a potential approach that not only enhance T-cell effector functions but also offset antigen escape in solid tumor.

As an artificially installed receptor on T cells, recognition of tumor expressing antigens depends on the affinity of distinct Fab fragments as well as on the density of targeted epitope, which is crucial for CAR T cell activation (39). Investigators have therefore explored "using the optimal key to open the lock". Modulating the stability and exposure of scFvs influences CAR affinity (Figure 3C). ScFv optimization studies have highlighted that higher affinity is not necessarily better. In order for high levels of CAR T activation, decreasing the affinity would result in an increased requirement for higher antigen density on cells. Therefore, reduced affinity enables CAR T cell to discriminate healthy tissues with a relative low antigen expression from tumor, which could minimize CAR T therapy-related toxicities (40). Recently, with safety concerns, an antibody-based switchable CAR T system was developed, which could strictly control the activity and antigen specificity of CAR T cells by the formation of a switch-dependent immunological synapse (41). The preclinical results showed that switchable CAR-T cells against HER2 was efficacious against difficult-to-treat, patient-derived advanced pancreatic tumors, which also offered potential for safety due that CAR T activity can be modulated by switch administration (42). Additionally, in a model of NSCLC, bi-specific switch-control CAR T cells demonstrated the excellent *in vitro* efficacy and safety, which displayed antigen-specific and folate-FITC dependent reactivity against both tumor and the tumor microenvironment (43). Furthermore, another strategy to ultrasensitively discriminate antigen density is implemented by utilizing a low-affinity synthetic Notch (synNotch) receptor system, which could restrict CAR activity in tumor sites and reduce toxic cross-reaction with normal tissues. The SynNotch receptors consist of an extracellular ligand-binding domain, a transmembrane domain, and an orthogonal transcription factor (such as the transcription-activating fusion protein Gal4-VP64). After binding to its cognate ligand, the SynNotch receptor acting as a filter releases its transcription factor to induce

10.3389/fimmu.2023.1045024

TABLE 1 Clinical trials of CAR-T cell therapies for solid tumors.

Target	Research Type	NCT Number	Tumor	Patients	Curative Effect*	Safety**	Research Institute	Reference
Glypcan-3	Clinical phase I trial	NCT02395250 NCT03146234	Hepatocellular carcinoma	13	OS at 3 years: 10.5% OS at 1 years: 42.0% OS at 6 months: 50.3%	CRS: 1 (Grade 5) ICANS: 0	Renji Hospital of Shanghai Jiaotong University, China	(16)
GD2	Clinical phase I trial	NCT02761915	Neuroblastoma	12	Not mentioned	CRS: 1 (Grade 3) ICANS: 0	Great Ormond Street Hospital for Children, UK	(17)
EGFR	Clinical phase I trial	NCT01869166	Cholangiocarcinoma and pancreatic cancer	16	Cholangiocarcinoma PFS (Median): 4 months Pancreatic Tumor PFS (Median): 3 months OS (Median): 4.9 months	CRS: 0 ICANS: 0	General Hospital of PLA, China	(18) (19)
MSLN	Clinical phase I trial	NCT03054298 NCT03323944	Malignant pleural mesothelioma, ovarian cancer, and pancreatic ductal adenocarcinoma	21	Pancreatic ductal carcinoma (6 patients) PFS: 1-5.4 months Other carcinoma (5 patients each) PFS (Median): 2.1 months SD at 28 days: 11 patients SD at 2-3 months: 3 patients	Pancreatic ductal carcinoma Not mentioned Other carcinoma CRS & ICANS: Not mentioned Death: 1 (due to liver necrosis and acute kidney injury, in 64 days)	University of Pennsylvania, USA	(20) (21)
MUC-1	Clinical phase I trial	NCT02587689	Adenocarcinoma of seminal vesicle	1	Not mentioned	Not mentioned	Soochow University, China	(22)
Her-2	Clinical phase I trial	NCT01935843	Biliary tract cancer and pancreatic cancer	11	PFS (Median): 4.8 months (1.5~8.3 months)	CRS: 1(Grade 3) ICANS: 0	General Hospital of PLA, China	(23)
PSMA	Clinical phase I trial	Not mentioned	Prostate cancer	5	PR: 2 patients	CRS: 0 ICANS: 0	Boston University School of Medicine, USA	(24)
PSMA	Clinical phase I trial	NCT03089203	Prostate cancer	13	Not mentioned	CRS: 5 (1 death with sepsis)	Perelman School of Medicine, University of Pennsylvania, USA	(25)
CEA	Clinical phase I trial	NCT02349724	Colorectal Cancer	10	Low dose CAR-T in 4 weeks: PD: 2 patients; SD: 2 patients. High dose CAR-T in 4 weeks: NE: 1 patients; SD: 5 patients.	CRS: 0 ICANS: 0	Third Military Medical University, China	(26)
Claudin18.2	Clinical phase I trial	NCT03874897	Gastric Cancer	37	OS at 6 months: 81.2% ORR at 6 months: 48.6%	CRS: 0 ICANS: 0	Peking University Cancer Hospital and Institute, China	(27)

*Short-term and long-term clinical evaluations are included in this table. OS, Overall Survival; PFS, Progress Free Survival; SD, Stable Disease; PR, Partial Responses; PD, Progressive Disease; ORR, overall response rate; NE, Not Evaluable. **CAR-T cell therapy-related adverse events beyond grade 2. Only CRS and ICANS are involved in this table. Numbers represent the number of patients unless otherwise noted.

transcription of CAR (Figure 3D) (44). Hernandez et al. engineered T cells with a synNotch receptor for HER2 that controlled the expression of a CAR for the same antigen, which functioned well both *in vitro* and *in vivo* with sharp discrimination between cancer cells and normal cells on the basis of HER2 expression. The results suggest that these two-step synNotch-to-CAR circuits could be a useful tool to widen the therapeutic window of engineered T cells against solid tumor (45). In another study, Tseng et al. used Logic-

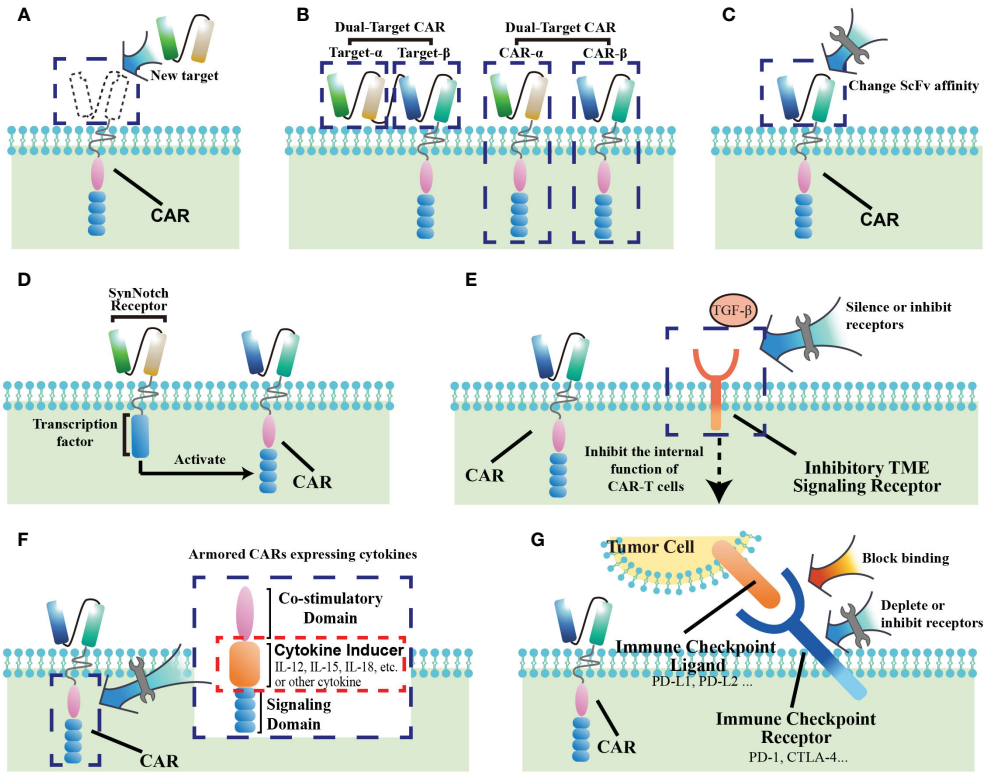

FIGURE 3
Methods of improving CAR-T cell therapy for solid tumors. **(A)** Find new targets with better specificity. **(B)** Construct dual-target CARs. **(C)** Change the affinity of the extracellular ScFv segment of CAR. **(D)** Construct SynNotch-receptor switch. **(E)** Block receptors of the inhibitory signaling from the tumor microenvironment (TME). **(F)** Armored CARs with cytokines. **(G)** Prevent CAR-T cell exhaustion through immune checkpoints.

gated(Log) GPC3-synNotch-inducible CD147-CAR to target liver cancer cells. This CAR not only used the SynNotch receptor as a switch for tumor antigen recognition, but also had dual-target recognition specificity for GPC3 and CD147, which further limited CAR to selectively recognize $GPC3^{+}CD147^{+}$ liver cancer cells. Notably, this study also demonstrated the clinical feasibility of using SynNotch receptors to regulate CAR recognition (46).

4.2 Multiple components in solid tumors create immunosuppressive microenvironment

Solid tumor cells exist in a complex tumor microenvironment, which participate in tumor progression throughout all stages of tumorigenesis (47). The TME has extensively characterized as hostile for T cells. Within the TME, the immunosuppressive cell types such as regulatory T cells (Tregs), tumor-associated macrophages (TAMs), myeloid-derived suppressor cells (MDSCs), and cancer-associated fibroblasts (CAFs) can contribute to immune evasion by inhibiting effective antitumor response of effector cells. Infiltration or polarization of these cells in human tumors has been associated with poor prognosis (48). These cells and tumor cells drive the production of tumor facilitating cytokines such as TGF-β, IL-10, and IL-4, which also promote T-cell and CAR T-cell exhaustion. The non-cellular extracellular matrix (ECM) further propagate the TME, which act as physical barriers to effectively prevent T cell infiltration. In addition, the abnormalities of the newly formed vessels have also been identified in solid tumors, which is usually leakier than normal vasculature and is therefore unable to support efficient trafficking of cytotoxic immune cells to the tumor. In general, solid tumor is considered as a special organ, which build a relatively independent system "microenvironment" to support themselves (49). Thus, the TME has a notable impact on the outcome of anticancer therapeutics. Currently, several strategies have been equipped to CAR T cells to overcome these obstacles posed by solid tumors (Figure 4).

4.2.1 TME inhibits CAR-T activity

TAMs represent one of the main tumor-infiltrating immune cell types, which are generally categorized into classical activated M1 macrophages and alternatively activated M2 macrophages. They are two functionally contrasting subtypes and can be converted into each other upon tumor microenvironment changes. M2 type macrophage (M2) could promote IL-8 secreted by Tregs, which in turn drives the production of TGF-β, thus forming an immunosuppressive microenvironment (50). A clinical study found that increased infiltration of M2 macrophage was negatively associated with CAR T cell efficacy, which also significantly inhibited proliferation of $CD4^{+}$ and $CD8^{+}$ T cells (51). M-MDSCs (monocyte-related myeloid-derived suppressor cells) are currently known as a main precursor of TAMs, which are induced into TAMs by various chemokines. MDSCs are widely present in solid tumors and are characterized by their ability to suppress both innate and adaptive immune responses (52). MDSCs commonly accumulate in TME by various cytokines

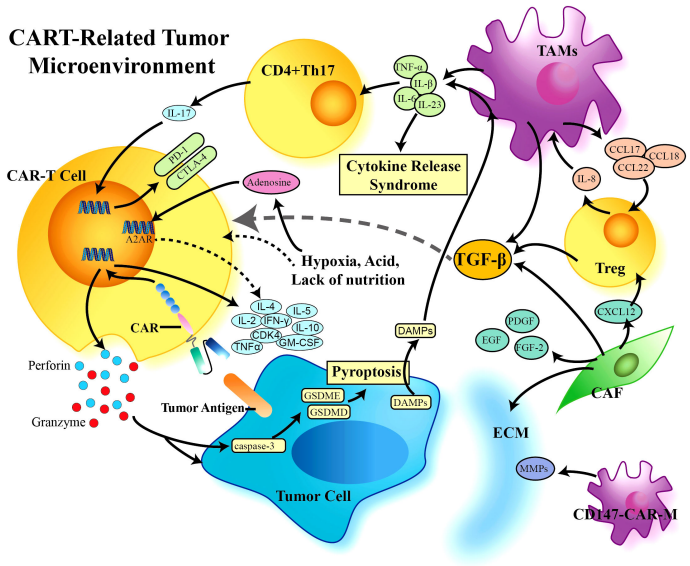

FIGURE 4
CAR-T cell-related tumor microenvironment (TME). A variety of cells participate in the formation of the tumor suppressive immune microenvironment, which limits the effect of CAR-T cells in solid tumors. TGF-β plays a central role in the TME, is produced by a variety of immunosuppressive cells, and can further negatively regulate the proliferation, differentiation, and activation of immune cells through downstream proteins and other factors. CAR, Chimeric Antigen Receptor; TGF-β, Transforming Growth Factor-β; TAMs, Tumor Associated Macrophages; Treg, Regulor T-cell; CAF, Cancer Associated Fibroblasts; ECM, Extracellular Matrix; MMPs, Matrixmetalloproteinases; DAMPs, Damage Associated Molecular Patterns.

and chemokines, including CD47 and IL-17. Studies have shown that depleting MDSCs enhanced CAR therapy efficacy in a xenograft sarcoma when treated with CAR T cells targeting GD2 (53). Burga el al. demonstrated tumor-derived GM-CSF upregulated programmed cell death ligand 1 (PD-L1) on MDSCs in a model of liver cancer, leading to CAR T cell suppression via direct engagement of programmed cell death protein 1 (PD-1) on CAR T cells. They further found GM-CSF neutralization, MDSCs eradication or PD-L1 blockade could rescue CAR T cell function (54). Tregs are a subset of $CD4^+$ T cells, which can be prohibitive of immune-mediated antitumor response. Modification of CAR T cells have specific effects on their interaction with Tregs, that CAR T cells containing both CD28 and CD3 co-stimulatory domains had superior resistance to Trges (55). In addition, immune checkpoint pathways also limit antitumor response. TAMs induce expansion of IL-17-producing $CD4^+$Th17 cells to inhibit anti-tumor immunity by upregulation of PD-1, T-lymphocyte-associated protein 4 (CTLA-4), and glucocorticoid-induced TNF receptor family-related protein (GITR) (56). Activation of CAR T cells was also compromised by TAMs, which contribute to Treg activity through secretion of IL-10 as well as PD-L1 expression, suggesting that the combination of checkpoint blockage with CAR-T cells could be necessary to combat the immunosuppressive signaling in TME.

In particular, the TME is characterized by markedly elevated levels of multiple inhibitory cytokines, including TGF-β, which directly improves the function of Tregs and TAMs (Figure 3E). TGF-β promotes stromal cells to form a stromal phenotype, which also contributes to immune evasion by downregulated chemokine receptors. CCL22, a downstream molecule of TGF-β, is mainly produced by TAMs, which could promote Tregs recruitment, and further induce TAMs to produce TGF-β via IL-8. This positive feedback loop exacerbates the formation of inhibitory TME (57). More recently, investigators have focused on developing CARs with TGF-β signaling blockage. One of TGF-β-resistant CAR T cells was engineered via CRISPR/Cas9-mediated knockout of TGF-β receptor II, which efficiently inhibited Treg transformation, and greatly improving the function of CAR-T cells in the TGF-β-enriched TME (58). Another strategy to block TGF-β signaling is to overexpress a dominant-negative TGFβRII (TGFβRDN) in CAR T cells. Interestingly, the results of a phase I trial showed PSMA-directed CAR T cells engineered with a TGFβRDN significantly enhanced antitumor immunity in patients with castration-resistant prostate cancer (CRPC). Besides safety and feasibility in clinic, the inclusion of a TGFβRDN attenuates a common immunosuppressive barrier in the TME, with effector cytokine elaboration and CAR cell persistence, which could be a useful approach against the TME to improve outcomes (25).

In addition to the above-mentioned TAMs and Tregs, CAFs, the most prominent stromal components, have been recognized as key players in the tumor microenvironment. CAFs could induce angiogenesis, improve the oxygen and nutrient supply, and provide immunosuppressive cytokines to cancer cells, including TGF-β, epidermal growth factor (EGF), platelet-derived growth factor (PDGF), and fibroblast growth factor-2 (FGF-2) (59). CAFs heterogeneity has been identified in human breast cancer. Among the four subsets, CAF-S1 promotes immunosuppressive environment, which enhances the regulatory T cell capacity to inhibit T effector proliferation (60). More recently, fibroblast activation protein (FAP), a membrane protease, has become an attractive immunotherapeutic target, due that FAP is highly expressed on CAFs in a majority of malignant solid tumors but rarely on fibroblasts in normal tissues. The CAR T cells targeting FAP have shown potent antitumor activity in preclinical models, opening up the possibility to launch an attack on CAF-mediated immunosuppression (61).

Recent evidence has suggested that armored CARs to inducibly or constitutively secrete active cytokines or express ligands is an attractive option to create an immune-supporting milieu in the TME (Figure 3F) (62). IL-12, a potent inflammatory cytokine, enhances the cytotoxic ability and leads to increased secretion of IFN-γ, TNF-α and GM-CSF. In the model of hepatocellular carcinoma, CAR T cells engineered with IL-12 expression demonstrated superior antitumor efficacy with less potential side effects and decreased Treg infiltration (63). Consistently, the enhanced antitumor immune response of IL-12 armored CAR T cells was also observed in ovarian cancer (64). Another approach to overcome immunosuppressive signaling in the TME is to engineer CARs to express CD40L, with the hypothesis that CD40L mediates $CD8^+$ T-cell immunity via secretion of inflammatory cytokines IL-12 and IFN-γ. CD40L-expressing CAR T-cells showed increased in vitro cytotoxicity compared to CAR T-cells alone. Furthermore, these CAR T-cells resulted in a significant survival benefit in mouse model (65). More recently, CAR T-cells engineered with IL-15 have also been developed. IL-15 is crucial for the memory differentiation and proliferation of T-cells and NK cells. Xu et al. found that coexpression of IL-15 with a CAR enhanced the *in vivo* persistence and therapeutic efficacy of CAR-NKTs (66). Due to the promising preclinical results, these armored CAR T-cells are under consideration for clinical trials. However, these cytokine-altering therapies may paradoxically potentiate some of the adverse events associated with CAR T-cells, which warrant further attention during clinical translation.

4.2.2 TME restricts CAR-T cell infiltration

The hostile TME also limits the migration of CAR T cells. Efficiently trafficking into tumor tissue is a precondition to exert anti-tumor activity, which requires the interaction between chemokine secreted by tumor cell and chemokine receptor on T cells. CCR4 is the receptor of chemokine Mcp-1 and expressed on activated T cells at low levels, which plays an important role in Tregs recruitment. Currently, CCR4 antagonist has been used to treat T-cell lymphoma, demonstrating that blocking its binding enhanced CAR T cells migration to overcome the hurdles in the TME. Furthermore, the consistent results were also observed in CAR T cells specific for tumor antigen mesothelin (Msln) with co-expression of chemokine receptors CCR4 in NSCLC. As shown in a NSCLC CDX model, Msln-CCR4-CAR T cells enhanced infiltration and migration into tumor tissue, along with superior anti-tumor function and high levels of proinflammatory cytokines, including IL-2, IFN-γ, and TNF-α, suggesting that CAR T cells modified with chemokine receptor could be a potential strategy to promote T cell entry (67).

Tumor stroma, as physical barriers, also effectively prevent infiltration of CAR-T cells. Stroma, mostly composed of ECM, is more complex and denser in solid tumor than in hematological malignancy (68). The ECM is produced by all of cell types within TME, which is altered in tumor by the imbalance between ECM synthesis and secretion and changes in the levels of matrix-remodeling enzymes (69). Stroma of solid tumor inhibits CAR T cell infiltration mainly through interstitial fibrosis and high interstitial pressure. High-density ECM significantly reduced migration of immune cells and blunted cytotoxicity of lymphocytes (70). Furthermore, high-density ECM decreased the density of vessels, resulting in vessel embedding into the matrix, which are also critical for T-cell trafficking and activation (71). Therefore, many clinic trials have identified that the number of CAR T cells in tumor sites was often lower than that in peripheral blood. Thus, to overcome insufficient infiltration of CAR T cells, regional CAR T cell administration has been explored. A preclinical study with CAR-PSCA T cells on gastric cancer showed that administration pattern of CAR T cells crucially influenced their antitumor activities, in which more efficient tumor control was observed when CAR-PSCA were infused peritumorally as compared with intravenous injection, raising the concern that, besides CAR T cells themselves, some other parameters, such as administration pattern, should be considered to maximum CAR-T effector functions in clinical application (72).

Matrix metalloproteinases (MMPs), a family of calcium and zinc-dependent proteolytic enzymes, can degrade almost all components of ECM. Macrophages are an important source of MMPs. From clinical data, macrophage transplantation has been confirmed to be safe and well tolerated (73). CD147, also known as ECM metalloproteinase inducer, is essential for ECM remodeling via MMPs expression. A study in breast cancer showed that CAR-CD147 targeting HER2 macrophages, which were activated after HER2 recognition to trigger the internal signaling of CD147 and increase the expression of MMPs, did not affect proliferation of tumor cells in vitro. Interestingly, the infusion of these macrophages significantly inhibited tumor growth with HER2-positive expression in vivo, along with degrading the matrix and promoting T-cell infiltration into tumors, highlighting that targeting the ECM by engineered macrophages could be an effective strategy to augment CAR T cell infiltration into solid tumors (74). In addition to MMPs, heparanase is an enzyme to degrade heparin sulfate proteoglycan (HSPG), which is the primary component of ECM. The study verified that CAR-T cells expressing heparinase also enhanced tumor infiltration with increased antitumor activity (75). In the future, the efficacy and safety of these microenvironment-targeted therapeutic strategies remains to be further demonstrated in patients.

4.2.3 TME leads to premature exhaustion of CAR-T cells

Immunosuppression in the tumor microenvironment is often based on the mutual metabolic requirements of tumor cells and immune cells. Solid tumor cells primarily use glycolysis for glucose metabolism, and this metabolic alteration renders the TME with hypoxia, acidic, deprived nutrients, and prone to oxidative stress. On the other side, activation of immune cells leads to an increased demand for glucose. This metabolic competition often limits the proliferation and effector functions of tumor-specific immune cells (76). In particular, hypoxic environment is a common mechanism to therapeutic resistance. Therefore, investigators are being explored strategies to improve CAR T cell function in low-oxygen conditions. Recently, a considerable increase of adenosine, mainly produced by endothelial cells, has been identified in hypoxic tissues. Adenosine is an important immunosuppressive factor, which has been shown to controls immune response, inflammatory tissue damage, and antitumor immunity via activation of the adenosine A_{2A} receptor ($A_{2A}R$) in some solid tumors. A study showed that CRISPR/Cas9-mediated deletion of $A_{2A}R$ in CAR T cells significantly abrogated the immunosuppressive effects of adenosine and enhanced its *in-vivo*

antitumor efficacy, with enhanced production of cytokines including IFN-γ and TNF. Importantly, no deleterious effect on memory phenotype or persistence of CAR T cells was observed (77). Another approach was to develop oxygen-sensitive CAR T cells by fusing the oxygen sensitive domain of HIF1α to CAR scaffold, which enabled very low CAR expression at normal oxygen level, but highly increased levels of CAR expression together with HIF1α in hypoxic conditions.

T cell exhaustion is a common feature of cancers. Exhausted $CD8^+$ T cells (T_{EX}) in cancer have limited effector function, which are characterized by the loss of cytokine production (IL-2, TNF, IFN-γ), high inhibitory receptor co-expression (PD-1, LAG3, TIGIT), altered metabolism, exhausted transcriptional profiles, and impaired proliferative potential and survival (78). T_{EX} are important clinical targets of immunotherapies. Understanding the transcriptional profiles of exhausted or exhausting T cells could promote the production of more functional CAR T cells. HMG-box transcription factor TOX has been identified as a central regulator of T_{EX}, and robust TOX expression results in commitment to T_{EX} (79). Besides TOX, TOX2 as well as NR4A are also critical for the transcriptional program of $CD8^+$ T cell exhaustion, all of which are targets of the calcium/calcineurin-regulated transcription factor NFAT. Within the TME, CAR T cells become exhausted and exhibit diminished ability to control the tumors. Previous study showed NR4A-deficient CAR T cells had superior efficacy at suppressing tumor growth. Another study using a CAR T cell model demonstrated that TOX and TOX2 are necessary to impose CAR T exhaustion, which were highly induced in exhausted CAR^+ tumor-infiltrating lymphocytes (CAR TILs). Interestingly, CAR TILs deficient in both TOX and TOX2 showed increased effector functions and prolonged survival of tumor-bearing mice, and their exhausted features were obviously attenuated (80). In addition, reactive oxygen species (ROS) also function to modulate the tumor environment, affecting the various stromal cells that provide metabolic support, a blood supply and immune responses to the tumor. ROS dysregulation impairs antitumor activity of T cells (81). To render CAR T cells more resilient toward ROS, Ligtenberg et al. constructed CAR-T cells expressing catalase to improve their antioxidant capacity by metabolizing H_2O_2 (CAR-CAT). Compared with traditional CAR-T cells, CAR-CAT cells had a lower oxidation state with less ROS accumulation in both basal and activated states, while maintained stronger anti-tumor activity even at high H_2O_2 levels. These results showed that protecting CAR-T cells from exhaustion mediated by tumor-associated oxidative stress could significantly improve their efficacy (82). To date, ICB targeting PD-1 and programmed cell death ligand 1 (PD-L1) have achieved clinical success for solid tumors (83). PD-L1 is up-regulated in multiple solid tumors, which serves as a ligand for PD1 on T cells to protect tumor cells from immune control (84). The ablation of PD-1 improves T cell persistence in patients with solid tumors. Thus, blockade of the PD-1/PD-L1 axis is one of the most popular strategies to combat T cell exhaustion and restore anti-tumor immune responses mediated by CAR T cells (Figure 3G) (85). Besides antibody-based checkpoint blockade, several groups have explored the strategies to modify the CAR T cells with a PD1 switching receptor and a CD28 intracellular domain. Studies showed that these CAR T cells converted PD1-mediated inhibitory signals into CD28 co-stimulatory signals, which significantly augmented the efficacy of CAR T cells in solid tumors (86).To further improve the efficacy, Le et al. designed CARPD-L1z, which contained a high-affinity scFv against human PD-L1, the intracellular structure, including 4-1BB and TLR2 co-stimulatory domains, and the CD3ζ signaling domain. As compared with the forthmentioned CARs targeting PD-1 without CD 3ζ signaling domain, CARPD-L1z efficiently lysed PD-L1 positive tumor cells with enhanced cytokine secretion in vitro, which further eliminated multiple types of tumors in xenograft (87). Additionally, to reduce immune escape and increase the target specificity concomitantly, some studies developed a novel tandem CAR T cells with PD1 and an anti-MUC1 scFv, which showed more potent antitumor activity in vivo and significantly prolonged the survival time of tumor bearing mice (88), suggesting that combination checkpoint blockade-CAR-T cell therapy is likely a new immunotherapy option in solid tumor.

4.3 Excessive activation of CAR T cells leads to adverse events

Severe toxicities following CAR T cell administration have posed a challenge to more widespread adoption in solid tumors. Massive CAR T cell activation and severe cytokine release result in the common toxicities, including cytokine release syndrome (CRS) and neurotoxicity (89). The onset of CRS coincides near the peak of CAR T expansion and cytokine production, typically occurring during the first week after CAR T administration. After infusion, CAR T cells come into contact with target cells and release a large amount of cytokines, such as TNF-α, IL-2, IL-6, IL-8, IFN-γ, and C-reactive protein, which in turn recruit immune cells and trigger a positive feedback loop, thus consequently cause a dangerous serum concentrations of cytokines in a short period. CRS leads to ensuing systemic inflammation, capillary leakage, and coagulation cascade, which causes organ damage and is ultimately life threatening. Thus several predictive biomarkers of CRS have been identified: high tumor burden, high CAR T dose, and high peak CAR T blood counts (90). For high-risk patients, preemptive treatment could reduce the incidence of subsequent severe (Grade 3+) CRS, which indicates poor prognosis (91). Neurotoxicity, also referred immune effector cell-associated neurotoxicity syndrome (ICANS), is another unique toxicity following CAR T therapy, which usually occurs within one or 3 weeks after CAR T cell infusion. Taraseviciut et al. found that ICANS development was not only correlated with a marked accumulation of both CAR T and endogenous T cells in the cerebrospinal fluid and brain parenchyma, but also associated with pro-inflammatory cytokines and T-cell encephalitis (Figure 5) (94).

Mechanisms behind CAR-T-related toxicities (CARTOX) are complicated. Accumulated evidences have identified inflammatory cytokines contribute to the development of CARTOX (95), yet the source of these cytokines still remain unclear. More recently, studies highlight the importance of monocyte/macrophage in CARTOX (96), which was not related to cytokines secreted by CAR T cells themselves (97). Modulaion of macrophage function alleviated CRS severity. Direct interactions between CAR T cells and host myeloid cells – primarily macrophages – was required to produce IL-6. Moreover, Single-cell RNA-sequencing data showed that monocytes were the main source of IL-6. in patients experiencing CRS, IL-6 was found to be highly elevated, which bas been believed to primarily mediate CRS onset (98). Another study demonstrated that monocytes produced IL-

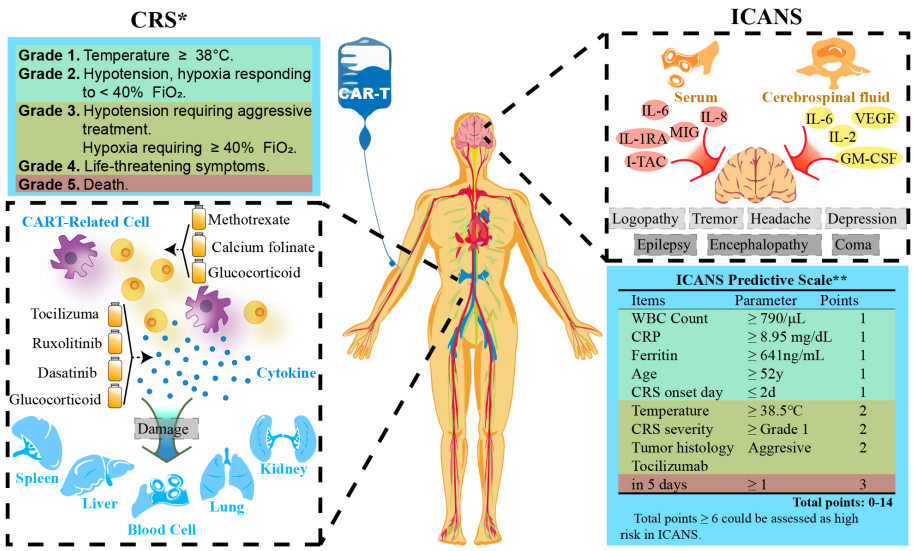

FIGURE 5
CAR-T cell therapy-related adverse events. *Grading is quoted from ASTCT (2018) (92). **Scale is referred from a study by Harvard Medical School (93). WBC, White Blood Cells; CRS, Cytokine Release Syndrome; CRP, C-reactive Protein; FiO_2, Fraction of Inspiration O_2.

1 earlier than IL-6 when cocultured with CAR T cells, suggesting that IL-1 is also linked to CRS. Recently, animal models have shown a correlation between perforin and CRS development, that perforin-deficient CAR T cells produced higher amounts of proinflammatory cytokines upon CAR-mediated in vitro activation. Additionally, cell pyroptosis, a form of inflammatory programmed cell death, has also been recognized as a major contributor to toxicity during CAR T cell therapy. Liu et al. found that CAR T cells rapidly released granzyme B in tumor cells to activate caspase 3, causing the subsequent gasdermin E (GSDME) cleavage and the release of cytokines, thus inducing CRS (99). The data further suggest GSDME as a new potential biomarker to predict the severity of CRS. Additionally, pyroptotic cells also release large amounts of DAMPs (damage-associated molecular patterns), which are endogenous immunogenic molecules released in "dangerous" situations such as tissue damage or cellular stress (100). According to the location, DAMPs have been divided into two categories, from the extracellular matrix or intracellular compartments (101). During CAR T therapy, DAMPs leakage by pyroptotic tumor cells activate macrophages and induce the release of IL-1β and IL-6, triggering CRS, highlighting the involvement of pyroptosis-DAMPs axis in CARTOX. Furthermore, some elements within the TME have been identified to correlate with CARTOX. Vascular endothelial cells appear to play an important role in CRS as reports have shown that increased levels of angiopoietin-2 and von Willebrand factor released by vascular endothelial cells were significantly associated with the severity of CRS, rendering them as biomarkers to predict prognosis of CRS (90).

Elucidating the mechanisms of CARTOX has facilitated the development of more effective treatment approaches. Current CRS management after CAR T therapy mainly relies on the blocking IL-6 with tocilizumab (recombinant humanized anti-human IL-6 receptor monoclonal antibody), which is FDA approved to treat CRS. Tocilizumab often resolves CRS symptoms within hours while the therapeutic efficacy of CAR T cells in patients was preserved. Unfortunately, tocilizumab failed to prevent neurotoxicity associated with CAR T therapy. Another way to limit toxicity of CAR T cells is to inhibit T cell receptor signal transduction via small molecule inhibitors, such as dasatinib (102). Administration of dasatinib significantly decreased levels of cytokines and protected mice from fatal CRS, which can also directly inhibit tumor-associated myeloid cells (103). Besides the forthmentioned drugs, some T-cell killing drugs, such as methotrexate and calcium folinate, have also been used to treat CRS (104). However, the toxicity on patient survival need to be careful considered because these cytokine drugs irreversibly reduce the amount of CAR T cells (105). Currently, another interesting approach is to endow CAR T cells with anti-CRS activity, which can neutralize IL-6 in the TME. Tan et al. showed that CAR T cells with a membrane bound scFv targeting IL-6 not only abrogated the symptom of CRS without compromising anti-tumor efficacy, but it had the potential to simultaneously limit the effect of TAMs (106).

5 Conclusions and outlook

In the latest decade, the use of cutting-edge genetic engineering techniques (especially CRISPR/Cas9) and/or combining with other modalities obviously improved the efficacy and safety of CAR T therapy for solid tumor, and raises the concerns that the landscape of CAR T in solid tumors is bright. In future research, the primary task of CAR-T cell therapy for solid tumors will be to obtain more precise and specific targets. At present, not many targets have been identified for solid tumors. Taking NSCLC as an example, most current clinical studies continue to focus on common targets such as EGFR, HER2, and their mutations. New targets may bring breakthroughs in solid tumor recognition for CAR-T cell therapy. In addition, by improving the affinity of the extracellular ScFv segment of CAR, the construction of a controllable CAR switch will further strengthen the target recognition

specificity of CAR-T cells and avoid the occurrence of on-target/off-tumor effects. Moreover, the development of sequencing technology and bioinformatics will enable cells to be divided into different subtypes with similar pathological behaviors and characteristics, providing more information for the design of CAR-T targets (107). Unlike hematological tumors, the denser and more complex internal environment of solid tumors remains as barrier that must be crossed. The presence of TAMs, Tregs, CAFs, and inhibitory cytokines such as IL-10, IL-4, and TGF-β in the TME severely impacts CAR-T infiltration and survival. At the same time, the complex activation mechanism of CAR-T cells can lead to tumor immune escape and adverse events during treatment (108). Better understanding of the signaling pathways between T cells and other TME cell components, as well as the intracellular cascades associated with CAR-T cell activation and depletion, will enable greater success in the treatment of solid tumors with CAR-T cell therapy. In addition, research investigating immune cells other than T cells may lead to breakthroughs. Besides the use of CAR-M cells to break through the tumor ECM, NK cells have their own unique capabilities and are not restricted by MHC-I antigen recognition. Furthermore, CAR-NK cells can be generated from allogeneic donors (109), thus providing theoretical support for mass production of CAR cells and enabling more patients with solid tumors to benefit from CAR cell therapy. With the continuous development of oncology, the treatment of solid tumors is no longer solely based on pathological and histological type or clinical stages. More emphasis is being placed on individualized and precise treatment. Although many obstacles in the treatment of solid tumors with CAR-T cell therapy remain to be addressed, we believe that CAR-T cell therapy will become an important treatment approach for solid tumors, prolonging the survival of patients and bringing tumor treatment into a new era of precision immunotherapy.

Author contributions

KZ and YL conceptualized, wrote, and edited the manuscript. The figures and charts were designed by YL and created by KZ. HC and FL reviewed references. SH and FC translated and edited the manuscript. All authors contributed to the article and approved the submitted version.

Funding

Supported by National Natural Science Foundation of China (Grant No. 81960551), Yunnan Fundamental Research Projects (Grant No. 202101AS070056) and Yunnan Fundamental Research Projects (Grant No. 202201AV070009).

Conflict of interest

The authors declare that the research was conducted in the absence of any commercial or financial relationships that could be construed as a potential conflict of interest.

Publisher's note

All claims expressed in this article are solely those of the authors and do not necessarily represent those of their affiliated organizations, or those of the publisher, the editors and the reviewers. Any product that may be evaluated in this article, or claim that may be made by its manufacturer, is not guaranteed or endorsed by the publisher.

References

1. Shah NN, Fry TJ. Mechanisms of resistance to CAR T cell therapy. *Nat Rev Clin Oncol* (2019) 16:372–85. doi: 10.1038/s41571-019-0184-6

2. Díaz-Montero CM, Rini BI, Finke JH. The immunology of renal cell carcinoma. *Nat Rev Nephrol* (2020) 16:721–35. doi: 10.1038/s41581-020-0316-3

3. Propper DJ, Balkwill FR. Harnessing cytokines and chemokines for cancer therapy. *Nat Rev Clin Oncol* (2022) 19:237–53. doi: 10.1038/s41571-021-00588-9

4. Albinger N, Hartmann J, Ullrich E. Current status and perspective of CAR-T and CAR-NK cell therapy trials in Germany. *Gene Ther* (2021) 28:513–27. doi: 10.1038/s41434-021-00246-w

5. Brudno JN, Lam N, Vanasse D, Shen Y-W, Rose JJ, Rossi J, et al. Safety and feasibility of anti-CD19 CAR T cells with fully human binding domains in patients with b-cell lymphoma. *Nat Med* (2020) 26:270–80. doi: 10.1038/s41591-019-0737-3

6. Sterner RC, Sterner RM. CAR-T cell therapy: current limitations and potential strategies. *Blood Cancer J* (2021) 11:69. doi: 10.1038/s41408-021-00459-7

7. Chen Y, E CY, Gong Z-W, Liu S, Wang Z-X, Yang Y-S, et al. Chimeric antigen receptor-engineered T-cell therapy for liver cancer. *Hepatobiliary Pancreat Dis Int* (2018) 17:301–9. doi: 10.1016/j.hbpd.2018.05.005

8. Wagner J, Wickman E, DeRenzo C, Gottschalk S. CAR T cell therapy for solid tumors: Bright future or dark reality? *Mol Ther* (2020) 28:2320–39. doi: 10.1016/j.ymthe.2020.09.015

9. Patel U, Abernathy J, Savani BN, Oluwole O, Sengsayadeth S, Dholaria B. CAR T cell therapy in solid tumors: A review of current clinical trials. *EJHaem* (2022) 3:24–31. doi: 10.1002/jha2.356

10. Ramello MC, Benzaïd I, Kuenzi BM, Lienlaf-Moreno M, Kandell WM, Santiago DN, et al. An immunoproteomic approach to characterize the CAR interactome and signalosome. *Sci Signal* (2019) 12:eaap9777. doi: 10.1126/scisignal.aap9777

11. Pietrobon V, Todd LA, Goswami A, Stefanson O, Yang Z, Marincola F. Improving CAR T-cell persistence. *Int J Mol Sci* (2021) 22:10828. doi: 10.3390/ijms221910828

12. Kagoya Y, Tanaka S, Guo T, Anczurowski M, Wang C-H, Saso K, et al. A novel chimeric antigen receptor containing a JAK-STAT signaling domain mediates superior antitumor effects. *Nat Med* (2018) 24:352–9. doi: 10.1038/nm.4478

13. Abramson JS, Palomba ML, Gordon LI, Lunning MA, Wang M, Arnason J, et al. Lisocabtagene maraleucel for patients with relapsed or refractory large b-cell lymphomas (TRANSCEND NHL 001): a multicentre seamless design study. *Lancet* (2020) 396:839–52. doi: 10.1016/S0140-6736(20)31366-0

14. Le RQ, Li L, Yuan W, Shord SS, Nie L, Habtemariam BA, et al. FDA Approval summary: Tocilizumab for treatment of chimeric antigen receptor T cell-induced severe or life-threatening cytokine release syndrome. *Oncologist* (2018) 23:943–7. doi: 10.1634/theoncologist.2018-0028

15. Watanabe N, Mo F, McKenna MK. Impact of manufacturing procedures on CAR T cell functionality. *Front Immunol* (2022) 13:876339. doi: 10.3389/fimmu.2022.876339

16. Shi D, Shi Y, Kaseb AO, Qi X, Zhang Y, Chi J, et al. Chimeric antigen receptor-Glypican-3 T-cell therapy for advanced hepatocellular carcinoma: Results of phase I trials. *Clin Cancer Res* (2020) 26:3979–89. doi: 10.1158/1078-0432.CCR-19-3259

17. Straathof K, Flutter B, Wallace R, Jain N, Loka T, Depani S, et al. Antitumor activity without on-target off-tumor toxicity of GD2-chimeric antigen receptor T cells in patients with neuroblastoma. *Sci Transl Med* (2020) 12:eabd6169. doi: 10.1126/scitranslmed.abd6169

18. Martinez M, Moon EK. CAR T cells for solid tumors: New strategies for finding, infiltrating, and surviving in the tumor microenvironment. *Front Immunol* (2019) 10:128. doi: 10.3389/fimmu.2019.00128

19. Guo Y, Feng K, Liu Y, Wu Z, Dai H, Yang Q, et al. Phase I study of chimeric antigen receptor-modified T cells in patients with EGFR-positive advanced biliary tract cancers. *Clin Cancer Res* (2018) 24:1277–86. doi: 10.1158/1078-0432.CCR-17-0432

20. Beatty GL, O'Hara MH, Lacey SF, Torigian DA, Nazimuddin F, Chen F, et al. Activity of mesothelin-specific chimeric antigen receptor T cells against pancreatic

carcinoma metastases in a phase 1 trial. *Gastroenterology* (2018) 155:29–32. doi: 10.1053/j.gastro.2018.03.029

21. Haas AR, Tanyi JL, O'Hara MH, Gladney WL, Lacey SF, Torigian DA, et al. Phase I study of lentiviral-transduced chimeric antigen receptor-modified T cells recognizing mesothelin in advanced solid cancers. *Mol Ther* (2019) 27:1919–29. doi: 10.1016/j.ymthe.2019.07.015

22. You F, Jiang L, Zhang B, Lu Q, Zhou Q, Liao X, et al. Phase 1 clinical trial demonstrated that MUC1 positive metastatic seminal vesicle cancer can be effectively eradicated by modified anti-MUC1 chimeric antigen receptor transduced T cells. *Sci China Life Sci* (2016) 59:386–97. doi: 10.1007/s11427-016-5024-7

23. Feng K, Liu Y, Guo Y, Qiu J, Wu Z, Dai H, et al. Phase I study of chimeric antigen receptor modified T cells in treating HER2-positive advanced biliary tract cancers and pancreatic cancers. *Protein Cell* (2018) 9:838–47. doi: 10.1007/s13238-017-0440-4

24. Junghans RP, Ma Q, Rathore R, Gomes EM, Bais AJ, Lo AS, et al. Phase I trial of anti-PSMA designer CAR-T cells in prostate cancer: Possible role for interacting interleukin 2-T cell pharmacodynamics as a determinant of clinical response. *Prostate* (2016) 76:1257–70. doi: 10.1002/pros.23214

25. Narayan V, Barber-Rotenberg JS, Jung I-Y, Lacey SF, Rech AJ, Davis MM, et al. PSMA-targeting TGFβ-insensitive armored CAR T cells in metastatic castration-resistant prostate cancer: a phase 1 trial. *Nat Med* (2022) 28:724–34. doi: 10.1038/s41591-022-01726-1

26. Zhang C, Wang Z, Yang Z, Wang M, Li S, Li Y, et al. Phase I escalating-dose trial of CAR-T therapy targeting CEA+ metastatic colorectal cancers. *Mol Ther* (2017) 25:1248–58. doi: 10.1016/j.ymthe.2017.03.010

27. Qi C, Gong J, Li J, Liu D, Qin Y, Ge S, et al. Claudin18.2-specific CAR T cells in gastrointestinal cancers: phase 1 trial interim results. *Nat Med* (2022) 28:1189–98. doi: 10.1038/s41591-022-01800-8

28. Heng G, Jia J, Li S, Fu G, Wang M, Qin D, et al. Sustained therapeutic efficacy of humanized anti-CD19 chimeric antigen receptor T cells in Relapsed/Refractory acute lymphoblastic leukemia. *Clin Cancer Res* (2020) 26:1606–15. doi: 10.1158/1078-0432.CCR-19-1339

29. Neelapu SS, Tummala S, Kebriaei P, Wierda W, Gutierrez C, Locke FL, et al. Chimeric antigen receptor T-cell therapy - assessment and management of toxicities. *Nat Rev Clin Oncol* (2018) 15:47–62. doi: 10.1038/nrclinonc.2017.148

30. Zhang Z, Jiang J, Wu X, Zhang M, Luo D, Zhang R, et al. Chimeric antigen receptor T cell targeting EGFRvIII for metastatic lung cancer therapy. *Front Med* (2019) 13:57–68. doi: 10.1007/s11684-019-0683-y

31. O'Rourke DM, Nasrallah MP, Desai A, Melenhorst JJ, Mansfield K, Morrissette JJ, et al. A single dose of peripherally infused EGFRvIII-directed CAR T cells mediates antigen loss and induces adaptive resistance in patients with recurrent glioblastoma. *Sci Transl Med* (2017) 9:eaaa0984. doi: 10.1126/scitranslmed.aaa0984

32. Johnson LA, Scholler J, Ohkuri T, Kosaka A, Patel PR, McGettigan SE, et al. Rational development and characterization of humanized anti-EGFR variant III chimeric antigen receptor T cells for glioblastoma. *Sci Transl Med* (2015) 7:275ra22. doi: 10.1126/scitranslmed.aaa4963

33. Porcellini S, Asperti C, Corna S, Cicoria E, Valtolina V, Stornaiuolo A, et al. CAR T cells redirected to CD44v6 control tumor growth in lung and ovary adenocarcinoma bearing mice. *Front Immunol* (2020) 11:99. doi: 10.3389/fimmu.2020.00099

34. Zhuang X, Maione F, Robinson J, Bentley M, Kaul B, Whitworth K, et al. CAR T cells targeting tumor endothelial marker CLEC14A inhibit tumor growth. *JCI Insight* (2020) 5:e138808. doi: 10.1172/jci.insight.138808

35. Larson RC, Maus MV. Recent advances and discoveries in the mechanisms and functions of CAR T cells. *Nat Rev Cancer* (2021) 21:145–61. doi: 10.1038/s41568-020-00323-z

36. Kreitman RJ, Dearden C, Zinzani PL, Delgado J, Robak T, Le Coutre PD, et al. Moxetumomab pasudotox in heavily pre-treated patients with relapsed/refractory hairy cell leukemia (HCL): long-term follow-up from the pivotal trial. *J Hematol Oncol* (2021) 14:35. doi: 10.1186/s13045-020-01004-y

37. Yang M, Tang X, Zhang Z, Gu L, Wei H, Zhao S, et al. Tandem CAR-T cells targeting CD70 and B7-H3 exhibit potent preclinical activity against multiple solid tumors. *Theranostics* (2020) 10:7622–34. doi: 10.7150/thno.43991

38. Wilkie S, van Schalkwyk MC, Hobbs S, Davies DM, van der Stegen SJ, Pereira AC, et al. Dual targeting of ErbB2 and MUC1 in breast cancer using chimeric antigen receptors engineered to provide complementary signaling. *J Clin Immunol* (2012) 32:1059–70. doi: 10.1007/s10875-012-9689-9

39. Lindo L, Wilkinson LH, Hay KA. Befriending the hostile tumor microenvironment in CAR T-cell therapy. *Front Immunol* (2020) 11:618387. doi: 10.3389/fimmu.2020.618387

40. Liu X, Jiang S, Fang C, Yang S, Olalere D, Pequignot EC, et al. Affinity-tuned ErbB2 or EGFR chimeric antigen receptor T cells exhibit an increased therapeutic index against tumors in mice. *Cancer Res* (2015) 75:3596–607. doi: 10.1158/0008-5472.CAN-15-0159

41. Chilton CH, Crowther GS, Śpiewak K, Brindell M, Singh G, Wilcox MH, et al. Potential of lactoferrin to prevent antibiotic-induced clostridium difficile infection. *J Antimicrob Chemother* (2016) 71:975–85. doi: 10.1093/jac/dkv452

42. Raj D, Yang M-H, Rodgers D, Hampton EN, Begum J, Mustafa A, et al. Switchable CAR-T cells mediate remission in metastatic pancreatic ductal adenocarcinoma. *Gut* (2019) 68:1052–64. doi: 10.1136/gutjnl-2018-316595

43. Chu W, Zhou Y, Tang Q, Wang M, Ji Y, Yan J, et al. Bi-specific ligand-controlled chimeric antigen receptor T-cell therapy for non-small cell lung cancer. *Biosci Trends* (2018) 12:298–308. doi: 10.5582/bst.2018.01048

44. Duan Y, Chen R, Huang Y, Meng X, Chen J, Liao C, et al. Tuning the ignition of CAR: optimizing the affinity of scFv to improve CAR-T therapy. *Cell Mol Life Sci* (2021) 79:14. doi: 10.1007/s00018-021-04089-x

45. Hernandez-Lopez RA, Yu W, Cabral KA, Creasey OA, Del Lopez Pazmino MP, Tonai Y, et al. T Cell circuits that sense antigen density with an ultrasensitive threshold. *Science* (2021) 371:1166–71. doi: 10.1126/science.abc1855

46. Tseng H-C, Xiong W, Badeti S, Yang Y, Ma M, Liu T, et al. Efficacy of anti-CD147 chimeric antigen receptors targeting hepatocellular carcinoma. *Nat Commun* (2020) 11:4810. doi: 10.1038/s41467-020-18444-2

47. Oliver AJ, Lau PK, Unsworth AS, Loi S, Darcy PK, Kershaw MH, et al. Tissue-dependent tumor microenvironments and their impact on immunotherapy responses. *Front Immunol* (2018) 9:70. doi: 10.3389/fimmu.2018.00070

48. Gobert M, Treilleux I, Bendriss-Vermare N, Bachelot T, Goddard-Leon S, Arfi V, et al. Regulatory T cells recruited through CCL22/CCR4 are selectively activated in lymphoid infiltrates surrounding primary breast tumors and lead to an adverse clinical outcome. *Cancer Res* (2009) 69:2000–9. doi: 10.1158/0008-5472.CAN-08-2360

49. Balakrishnan PB, Sweeney EE. Nanoparticles for enhanced adoptive T cell therapies and future perspectives for CNS tumors. *Front Immunol* (2021) 12:600659. doi: 10.3389/fimmu.2021.600659

50. Jamieson L, Forster MD, Zaki K, Mithra S, Alli H, O'Connor A, et al. Immunotherapy and associated immune-related adverse events at a large UK centre: a mixed methods study. *BMC Cancer* (2020) 20:743. doi: 10.1186/s12885-020-07215-3

51. Yan Z-X, Li L, Wang W, OuYang B-S, Cheng S, Wang L, et al. Clinical efficacy and tumor microenvironment influence in a dose-escalation study of anti-CD19 chimeric antigen receptor T cells in refractory b-cell non-hodgkin's lymphoma. *Clin Cancer Res* (2019) 25:6995–7003. doi: 10.1158/1078-0432.CCR-19-0101

52. Tesi RJ. MDSC; the most important cell you have never heard of. *Trends Pharmacol Sci* (2019) 40:4–7. doi: 10.1016/j.tips.2018.10.008

53. Long AH, Highfill SL, Cui Y, Smith JP, Walker AJ, Ramakrishna S, et al. Reduction of MDSCs with all-trans retinoic acid improves CAR therapy efficacy for sarcomas. *Cancer Immunol Res* (2016) 4:869–80. doi: 10.1158/2326-6066.CIR-15-0230

54. Burga RA, Thorn M, Point GR, Guha P, Nguyen CT, Licata LA, et al. Liver myeloid-derived suppressor cells expand in response to liver metastases in mice and inhibit the anti-tumor efficacy of anti-CEA CAR-T. *Cancer Immunol Immunother* (2015) 64:817–29. doi: 10.1007/s00262-015-1692-6

55. Loskog A, Giandomenico V, Rossig C, Pule M, Dotti G, Brenner MK. Addition of the CD28 signaling domain to chimeric T-cell receptors enhances chimeric T-cell resistance to T regulatory cells. *Leukemia* (2006) 20:1819–28. doi: 10.1038/sj.leu.2404366

56. Oura K, Morishita A, Tani J, Masaki T. Tumor immune microenvironment and immunosuppressive therapy in hepatocellular carcinoma: A review. *Int J Mol Sci* (2021) 22:5801. doi: 10.3390/ijms22115801

57. Wang D, Yang L, Yue D, Cao L, Li L, Wang D, et al. Macrophage-derived CCL22 promotes an immunosuppressive tumor microenvironment *via* IL-8 in malignant pleural effusion. *Cancer Lett* (2019) 452:244–53. doi: 10.1016/j.canlet.2019.03.040

58. Tang N, Cheng C, Zhang X, Qiao M, Li N, Mu W, et al. TGF-β inhibition *via* CRISPR promotes the long-term efficacy of CAR T cells against solid tumors. *JCI Insight* (2020) 5:e133977. doi: 10.1172/jci.insight.133977

59. Rodriguez-Garcia A, Palazon A, Noguera-Ortega E, Powell DJ, Guedan S. CAR-T cells hit the tumor microenvironment: Strategies to overcome tumor escape. *Front Immunol* (2020) 11:1109. doi: 10.3389/fimmu.2020.01109

60. Costa A, Kieffer Y, Scholer-Dahirel A, Pelon F, Bourachot B, Cardon M, et al. Fibroblast heterogeneity and immunosuppressive environment in human breast cancer. *Cancer Cell* (2018) 33:463–479.e10. doi: 10.1016/j.ccell.2018.01.011

61. Wang L-CS, Lo A, Scholler J, Sun J, Majumdar RS, Kapoor V, et al. Targeting fibroblast activation protein in tumor stroma with chimeric antigen receptor T cells can inhibit tumor growth and augment host immunity without severe toxicity. *Cancer Immunol Res* (2014) 2:154–66. doi: 10.1158/2326-6066.CIR-13-0027

62. Yeku OO, Brentjens RJ. Armored CAR T-cells: utilizing cytokines and pro-inflammatory ligands to enhance CAR T-cell anti-tumour efficacy. *Biochem Soc Trans* (2016) 44:412–8. doi: 10.1042/BST20150291

63. Liu Y, Di S, Shi B, Zhang H, Wang Y, Wu X, et al. Armored inducible expression of IL-12 enhances antitumor activity of glypican-3-Targeted chimeric antigen receptor-engineered T cells in hepatocellular carcinoma. *J Immunol* (2019) 203:198–207. doi: 10.4049/jimmunol.1800033

64. Koneru M, Purdon TJ, Spriggs D, Koneru S, Brentjens RJ. IL-12 secreting tumor-targeted chimeric antigen receptor T cells eradicate ovarian tumors in vivo. *Oncoimmunology* (2015) 4:e994446. doi: 10.4161/2162402X.2014.994446

65. Curran KJ, Seinstra BA, Nikhamin Y, Yeh R, Usachenko Y, van Leeuwen DG, et al. Enhancing antitumor efficacy of chimeric antigen receptor T cells through constitutive CD40L expression. *Mol Ther* (2015) 23:769–78. doi: 10.1038/mt.2015.4

66. Xu X, Huang W, Heczey A, Liu D, Guo L, Wood M, et al. NKT cells coexpressing a GD2-specific chimeric antigen receptor and IL15 show enhanced *In vivo* persistence and antitumor activity against neuroblastoma. *Clin Cancer Res* (2019) 25:7126–38. doi: 10.1158/1078-0432.CCR-19-0421

67. Wang Y, Wang J, Yang X, Yang J, Lu P, Zhao L, et al. Chemokine receptor CCR2b enhanced anti-tumor function of chimeric antigen receptor T cells targeting mesothelin in a non-small-cell lung carcinoma model. *Front Immunol* (2021) 12:628906. doi: 10.3389/fimmu.2021.628906

68. Wu T, Dai Y. Tumor microenvironment and therapeutic response. *Cancer Lett* (2017) 387:61–8. doi: 10.1016/j.canlet.2016.01.043

69. Cox TR, Erler JT. Remodeling and homeostasis of the extracellular matrix: implications for fibrotic diseases and cancer. *Dis Model Mech* (2011) 4:165–78. doi: 10.1242/dmm.004077

70. Park D, Son K, Hwang Y, Ko J, Lee Y, Doh J, et al. High-throughput microfluidic 3D cytotoxicity assay for cancer immunotherapy (CACI-IMPACT platform). *Front Immunol* (2019) 10:1133. doi: 10.3389/fimmu.2019.01133

71. Valkenburg KC, de Groot AE, Pienta KJ. Targeting the tumour stroma to improve cancer therapy. *Nat Rev Clin Oncol* (2018) 15:366–81. doi: 10.1038/s41571-018-0007-1

72. Wu D, Lv J, Zhao R, Wu Z, Zheng D, Shi J, et al. PSCA is a target of chimeric antigen receptor T cells in gastric cancer. *biomark Res* (2020) 8:3. doi: 10.1186/s40364-020-0183-x

73. Doerschuk CM. Pulmonary alveolar proteinosis and macrophage transplantation. *N Engl J Med* (2015) 372:1762–4. doi: 10.1056/NEJMcibr1413035

74. Zhang W, Liu L, Su H, Liu Q, Shen J, Dai H, et al. Chimeric antigen receptor macrophage therapy for breast tumours mediated by targeting the tumour extracellular matrix. *Br J Cancer* (2019) 121:837–45. doi: 10.1038/s41416-019-0578-3

75. Caruana I, Savoldo B, Hoyos V, Weber G, Liu H, Kim ES, et al. Heparanase promotes tumor infiltration and antitumor activity of CAR-redirected T lymphocytes. *Nat Med* (2015) 21:524–9. doi: 10.1038/nm.3833

76. Dal Bo M, de Mattia E, Baboci L, Mezzalira S, Cecchin E, Assaraf YG, et al. New insights into the pharmacological, immunological, and CAR-t-cell approaches in the treatment of hepatocellular carcinoma. *Drug Resist Update* (2020) 51:100702. doi: 10.1016/j.drup.2020.100702

77. Giuffrida L, Sek K, Henderson MA, Lai J, Chen AX, Meyran D, et al. CRISPR/Cas9 mediated deletion of the adenosine A2A receptor enhances CAR T cell efficacy. *Nat Commun* (2021) 12:3236. doi: 10.1038/s41467-021-23331-5

78. Zhang L, Zhao Y, Dai Y, Cheng J-N, Gong Z, Feng Y, et al. Immune landscape of colorectal cancer tumor microenvironment from different primary tumor location. *Front Immunol* (2018) 9:1578. doi: 10.3389/fimmu.2018.01578

79. Khan O, Giles JR, McDonald S, Manne S, Ngiow SF, Patel KP, et al. TOX transcriptionally and epigenetically programs CD8+ T cell exhaustion. *Nature* (2019) 571:211–8. doi: 10.1038/s41586-019-1325-x

80. Seo H, Chen J, González-Avalos E, Samaniego-Castruita D, Das A, Wang YH, et al. TOX and TOX2 transcription factors cooperate with NR4A transcription factors to impose CD8+ T cell exhaustion. *Proc Natl Acad Sci U.S.A.* (2019) 116:12410–5. doi: 10.1073/pnas.1905675116

81. Cheung EC, Vousden KH. The role of ROS in tumour development and progression. *Nat Rev Cancer* (2022) 22:280–97. doi: 10.1038/s41568-021-00435-0

82. Ligtenberg MA, Mougiakakos D, Mukhopadhyay M, Witt K, Lladser A, Chmielewski M, et al. Coexpressed catalase protects chimeric antigen receptor-redirected T cells as well as bystander cells from oxidative stress-induced loss of antitumor activity. *J Immunol* (2016) 196:759–66. doi: 10.4049/jimmunol.1401710

83. Gong J, Chehrazi-Raffle A, Reddi S, Salgia R. Development of PD-1 and PD-L1 inhibitors as a form of cancer immunotherapy: a comprehensive review of registration trials and future considerations. *J Immunother Cancer* (2018) 6:8. doi: 10.1186/s40425-018-0316-z

84. Qian Y, Gong Y, Fan Z, Luo G, Huang Q, Deng S, et al. Molecular alterations and targeted therapy in pancreatic ductal adenocarcinoma. *J Hematol Oncol* (2020) 13:130. doi: 10.1186/s13045-020-00958-3

85. Xie W, Medeiros LJ, Li S, Yin CC, Khoury JD, Xu J. PD-1/PD-L1 pathway and its blockade in patients with classic Hodgkin lymphoma and non-Hodgkin Large-cell lymphomas. *Curr Hematol Malig Rep* (2020) 15:372–81. doi: 10.1007/s11899-020-00589-y

86. Schlenker R, Olguín-Contreras LF, Leisegang M, Schnappinger J, Disovic A, Rühland S, et al. Chimeric PD-1:28 receptor upgrades low-avidity T cells and restores effector function of tumor-infiltrating lymphocytes for adoptive cell therapy. *Cancer Res* (2017) 77:3577–90. doi: 10.1158/0008-5472.CAN-16-1922

87. Qin L, Zhao R, Chen D, Wei X, Wu Q, Long Y, et al. Chimeric antigen receptor T cells targeting PD-L1 suppress tumor growth. *biomark Res* (2020) 8:19. doi: 10.1186/s40364-020-00198-0

88. Li T, Wang J. Therapeutic effect of dual CAR-T targeting PDL1 and MUC16 antigens on ovarian cancer cells in mice. *BMC Cancer* (2020) 20:678. doi: 10.1186/s12885-020-07180-x

89. Siegler EL, Kenderian SS. Neurotoxicity and cytokine release syndrome after chimeric antigen receptor T cell therapy: Insights into mechanisms and novel therapies. *Front Immunol* (2020) 11:1973. doi: 10.3389/fimmu.2020.01973

90. Hay KA, Hanafi L-A, Li D, Gust J, Liles WC, Wurfel MM, et al. Kinetics and biomarkers of severe cytokine release syndrome after CD19 chimeric antigen receptor-modified T-cell therapy. *Blood* (2017) 130:2295–306. doi: 10.1182/blood-2017-06-793141

91. Roex G, Timmers M, Wouters K, Campillo-Davo D, Flumens D, Schroyens W, et al. Safety and clinical efficacy of BCMA CAR-t-cell therapy in multiple myeloma. *J Hematol Oncol* (2020) 13:164. doi: 10.1186/s13045-020-01001-1

92. Lee DW, Santomasso BD, Locke FL, Ghobadi A, Turtle CJ, Brudno JN, et al. ASTCT consensus grading for cytokine release syndrome and neurologic toxicity associated with immune effector cells. *Biol Blood Marrow Transplant* (2019) 25:625–38. doi: 10.1016/j.bbmt.2018.12.758

93. Rubin DB, Al Jarrah A, Li K, LaRose S, Monk AD, Ali AB, et al. Clinical predictors of neurotoxicity after chimeric antigen receptor T-cell therapy. *JAMA Neurol* (2020) 77:1536–42. doi: 10.1001/jamaneurol.2020.2703

94. Taraseviciute A, Tkachev V, Ponce R, Turtle CJ, Snyder JM, Liggitt HD, et al. Chimeric antigen receptor T cell-mediated neurotoxicity in nonhuman primates. *Cancer Discovery* (2018) 8:750–63. doi: 10.1158/2159-8290.CD-17-1368

95. Deng T, Tang C, Zhang G, Wan X. DAMPs released by pyroptotic cells as major contributors and therapeutic targets for CAR-t-related toxicities. *Cell Death Dis* (2021) 12:129. doi: 10.1038/s41419-021-03428-x

96. Norelli M, Camisa B, Barbiera G, Falcone L, Purevdorj A, Genua M, et al. Monocyte-derived IL-1 and IL-6 are differentially required for cytokine-release syndrome and neurotoxicity due to CAR T cells. *Nat Med* (2018) 24:739–48. doi: 10.1038/s41591-018-0036-4

97. Giavridis T, van der Stegen SJ, Eyquem J, Hamieh M, Piersigilli A, Sadelain M. CAR T cell-induced cytokine release syndrome is mediated by macrophages and abated by IL-1 blockade. *Nat Med* (2018) 24:731–8. doi: 10.1038/s41591-018-0041-7

98. Turtle CJ, Hanafi L-A, Berger C, Hudecek M, Pender B, Robinson E, et al. Immunotherapy of non-hodgkin's lymphoma with a defined ratio of CD8+ and CD4+ CD19-specific chimeric antigen receptor-modified T cells. *Sci Transl Med* (2016) 8:355ra116. doi: 10.1126/scitranslmed.aaf8621

99. Liu Y, Fang Y, Chen X, Wang Z, Liang X, Zhang T, et al. Gasdermin e-mediated target cell pyroptosis by CAR T cells triggers cytokine release syndrome. *Sci Immunol* (2020) 5:eaax7969. doi: 10.1126/sciimmunol.aax7969

100. Zhang J, Wu H, Yao X, Zhang D, Zhou Y, Fu B, et al. Pyroptotic macrophages stimulate the SARS-CoV-2-associated cytokine storm. *Cell Mol Immunol* (2021) 18:1305–7. doi: 10.1038/s41423-021-00665-0

101. Roh JS, Sohn DH. Damage-associated molecular patterns in inflammatory diseases. *Immune Netw* (2018) 18:e27. doi: 10.4110/in.2018.18.e27

102. Belin C, Devic P, Ayrignac X, Dos Santos A, Paix A, Sirven-Villaros L, et al. Description of neurotoxicity in a series of patients treated with CAR T-cell therapy. *Sci Rep* (2020) 10:18997. doi: 10.1038/s41598-020-76055-9

103. Liang W, Kujawski M, Wu J, Lu J, Herrmann A, Loera S, et al. Antitumor activity of targeting SRC kinases in endothelial and myeloid cell compartments of the tumor microenvironment. *Clin Cancer Res* (2010) 16:924–35. doi: 10.1158/1078-0432.CCR-09-1486

104. Cao J-X, Wang H, Gao W-J, You J, Wu L-H, Wang Z-X. The incidence of cytokine release syndrome and neurotoxicity of CD19 chimeric antigen receptor-T cell therapy in the patient with acute lymphoblastic leukemia and lymphoma. *Cytotherapy* (2020) 22:214–26. doi: 10.1016/j.jcyt.2020.01.015

105. Cobb DA, Lee DW. Cytokine release syndrome biology and management. *Cancer J* (2021) 27:119–25. doi: 10.1097/PPO.0000000000000515

106. Tan AH, Vinanica N, Campana D. Chimeric antigen receptor-T cells with cytokine neutralizing capacity. *Blood Adv* (2020) 4:1419–31. doi: 10.1182/bloodadvances.2019001287

107. Safarzadeh Kozani P, Safarzadeh Kozani P, Ahmadi Najafabadi M, Yousefi F, Mirarefin SM, Rahbarizadeh F. Recent advances in solid tumor CAR-T cell therapy: Driving tumor cells from hero to zero? *Front Immunol* (2022) 13:795164. doi: 10.3389/fimmu.2022.795164

108. Klichinsky M, Ruella M, Shestova O, Lu XM, Best A, Zeeman M, et al. Human chimeric antigen receptor macrophages for cancer immunotherapy. *Nat Biotechnol* (2020) 38:947–53. doi: 10.1038/s41587-020-0462-y

109. Pockley AG, Vaupel P, Multhoff G. NK cell-based therapeutics for lung cancer. *Expert Opin Biol Ther* (2020) 20:23–33. doi: 10.1080/14712598.2020.1688298

frontiers | Frontiers in Immunology

TYPE Original Research
PUBLISHED 02 February 2023
DOI 10.3389/fimmu.2023.1103695

Check for updates

OPEN ACCESS

EDITED BY
Anand Rotte,
Arcellx Inc., United States

REVIEWED BY
Xi Zhang,
Xinqiao Hospital, China
Jeffrey J. Pu,
University of Arizona, United States

*CORRESPONDENCE
Xi Zhang
xi.zhang@biosg.com
Renata Stripecke
renata.stripecke@uk-koeln.de

SPECIALTY SECTION
This article was submitted to Cancer Immunity and Immunotherapy, a section of the journal Frontiers in Immunology

RECEIVED 20 November 2022
ACCEPTED 12 January 2023
PUBLISHED 02 February 2023

CITATION
Zhang X, Wang T, Zhu X, Lu Y, Li M, Huang Z, Han D, Zhang L, Wu Y, Li L, Klawonn F and Stripecke R (2023) GMP development and preclinical validation of CAR-T cells targeting a lytic EBV antigen for therapy of EBV-associated malignancies.
Front. Immunol. 14:1103695.
doi: 10.3389/fimmu.2023.1103695

COPYRIGHT
© 2023 Zhang, Wang, Zhu, Lu, Li, Huang, Han, Zhang, Wu, Li, Klawonn and Stripecke. This is an open-access article distributed under the terms of the Creative Commons Attribution License (CC BY). The use, distribution or reproduction in other forums is permitted, provided the original author(s) and the copyright owner(s) are credited and that the original publication in this journal is cited, in accordance with accepted academic practice. No use, distribution or reproduction is permitted which does not comply with these terms.

GMP development and preclinical validation of CAR-T cells targeting a lytic EBV antigen for therapy of EBV-associated malignancies

Xi Zhang[1]*, Tiaoxia Wang[1], Xiaona Zhu[1], Yong Lu[1], Mingpeng Li[1], Zhihong Huang[1], Deping Han[1], Longzhen Zhang[2], Yang Wu[2], Liantao Li[2], Frank Klawonn[3,4,5] and Renata Stripecke[5,6,7,8]*

[1]Biosyngen/Zelltechs Pte. Ltd., Singapore, Singapore, [2]Department of Radiotherapy, the Affiliated Hospital of Xuzhou Medical University, Xuzhou, China, [3]Biostatistics Group, Helmholtz Centre for Infection Research, Braunschweig, Germany, [4]Institute for Information Engineering, Ostfalia University, Wolfenbuettel, Germany, [5]German Centre for Infection Research (DZIF), Partner Site Hannover-Braunschweig and Partner Site Cologne-Bonn, Cologne, Hannover, Germany, [6]Laboratory of Regenerative Immune Therapies Applied, Department of Hematology, Hemostasis, Oncology and Stem Cell Transplantation, Hannover Medical School, Hannover, Germany, [7]Clinic I for Internal Medicine, University Hospital Cologne, University of Cologne, Cologne, Germany, [8]Institute for Translational Immune-Oncology, Cancer Research Center Cologne-Essen (CCCE), University of Cologne, Cologne, Germany

Introduction: Epstein-Barr virus (EBV) is a widely spread pathogen associated with lymphoproliferative diseases, B/ T/ NK cell lymphomas, nasopharyngeal carcinoma (NPC) and gastric carcinoma (GC). EBV lytic reactivations contribute to the genomic instability, inflammation and tumorigenesis of NPC, promoting cancer progression. Patients with NPC refractory to standard therapies show dismal survival. EBV gp350 is an envelope protein detectable in NPC specimens intracellularly and on the cell membrane of malignant cells, and is a potential viral antigen for T cell-directed immunotherapies. The potency of T cells engineered with a chimeric antigen receptor (CAR) targeting gp350 against EBV$^+$ lymphoproliferative disease was previously shown.

Methods: Here, we advanced towards preclinical and non-clinical developments of this virus-specific CAR-T cell immunotherapy against NPC. Different gp350CAR designs were inserted into a lentiviral vector (LV) backbone.

Results: A construct expressing the scFv 7A1-anti–gp350 incorporating the CD8 transmembrane and CD28.CD3ζ signaling domain (ZT002) was selected. High titer ZT002 (~1x10^8 TU/ml) was manufactured in HEK 293T/17 suspension cells in serum free media as large-scale production under good manufacturing practices (GMP). A LV multiplicity of infection (MOI) of 1 resulted in high frequencies of functional gp350CAR$^+$ T cells (>70%) at a low (<2) vector copy numbers in the genome. ZT002 was therefore used to establish gp350CAR-T batch run production methods. GMP upscaling and validation of T cell transduction and expansion in several runs resulted in average 3x10^9 gp350CAR-T cells per batch. >80% CD3$^+$ gp350CAR-T cells bound to purified gp350 protein. *In vitro* cytotoxicity and cytokine secretion assays (IFN-γ and TNF-α) confirmed the

specificity of gp350CAR-T cells against gp350$^+$ NPC, GC and lymphoma cell targets. Immunocompromised B-NDG mice (NOD.CB17-*Prkdcscidll2rgtm1*/Bcgen) were challenged s.c. with a EBV$^+$ NPC C666.1 cell line expressing gp350 and then treated with escalating doses of gp350CAR-T cells or with non-transduced T cells. gp350CAR-T cells promoted antitumor responses, biodistributed in several tissues, infiltrated in tumors and rejected gp350$^+$ tumor cells.

Discussion: These results support the use of gp350CAR-T cells generated with ZT002 as an Innovative New Drug to treat patients with solid and liquid EBV-associated malignancies.

KEYWORDS

CAR-T cell, GMP, EBV, gp350, nasopharyngeal carcinoma, gastric carcinoma, lymphoma

Introduction

Epstein-Barr Virus (EBV) is an ubiquitous pathogen and infects more than 95% of healthy adults. Although EBV's primary infection is asymptomatic and mostly controlled by a potent CD8$^+$ T cellular response (1), this oncogenic virus is classified as a group 1 carcinogen by the World Health Organization and it is associated with 2% of the human cancers developing worldwide (2). The primary EBV lytic infection occurs in B cells and epithelial cells homing in the buccal cavity and EBV is an important etiological factor for development of epithelial cancers such as nasopharyngeal carcinoma (NPC) (3). The persistence of episomal EBV genome and expression of several latency-associated viral proteins (LMP-1, EBNA-1) have been linked with malignant transformation in NPC (4). Notwithstanding, the contribution of EBV lytic reactivation and expression of EBV lytic products showed significant carcinogenic effects by increasing the genomic instability and tumorigenesis of NPC cells (5). NPC patients with advanced and recurrent disease have high mortality rates, and therefore targeting the EBV lytic infection may be a novel effective strategy to develop new therapies (6).

Copies of the BLLF1 gene encoding the gp350 envelope protein is detected in 25% of NPC biopsies by real-time (RT)-PCR (7). In the viral envelope, gp350 is an entry protein which is abundantly expressed during lytic reactivations and is sporadically expressed on the surface of transformed cell lines (8) (9). We showed previously that T cells transduced with different retroviral vector designs and expressing chimeric antigen receptors (CARs) targeting gp350 detected and killed EBV$^+$gp350$^+$ lymphoblastoid cell lines (LCLs). The best *in vitro* performing CAR-T cells incorporated the 7A1-anti-gp350 scFv, an immunoglobulin (Ig) transmembrane domain and the CD28.CD3ζ signaling domain. Nod-Rag-gamma (NRG) mice fully humanized with human CD34$^+$ hematopoietic stem cells, infected with the lytic EBV-M81/fLuc strain and developing lymphoproliferative disease (LPD) demonstrated 75% therapeutic responses after CD8$^+$ 7A1-gp350CAR-T cell administration (9).

In this current work, we advance towards the clinical development of gp350CAR-T cells for future immunotherapy clinical trials against NPC. We generate gp350CAR-T cells using lentiviral vectors (LVs) produced under good-manufacturing practices (GMP). We show that gp350CAR-T cells manufacturing can be up-scaled to yield sufficient cell numbers and high purity for clinical use. We demonstrate *in vitro* potency of the preclinical gp350CAR-T cells using different types of gp350$^+$ tumor targets. We establish proof-of-concept of GMP-like gp350CAR-T cells used therapeutically in an EBV$^+$/gp350$^+$ NPC xenograft model to recognize and promote eradication of the NPC tumor *in vivo*. In sum, we confirm the applicability of gp350CAR-T cell immunotherapy against NPC.

Materials and methods

More information on materials and methods can be found in the supplemental information.

Ethics statements

Leukapheresis units or peripheral blood mononuclear cells were purchased from Allcells (Alameda, CA, US) or collected from donors from Shanghai Zhaxin Traditional Chinese and Western Medicine hospital (study protocol number: LP202006) with signed informed consent. All handling and care of animals were performed under the guidelines for the Care and Use of Animals for Scientific Purposes issued by the research ethics committee at Guangzhou Regenerative Medicine and Health, Guangdong Laboratory (GRMH-GDL) following the Guide for the Care and Use of Laboratory Mice (Institute of Laboratory Animal Resources, Commission on Life Sciences, National Research Council, China). Procedures used are designed to conform to accepted practices and to minimize or avoid causing pain, distress, or discomfort in the mice. In those circumstances in which the required study procedures could cause pain or distress, the mice received appropriate analgesics or anesthetics, as ascribed by the Study Director and/or the veterinary staff and approved by the Institutional Animal Care and Use Committee (IACUC) at GRMH-GDL (IACUC serial number:

2020125). When mice showed high levels or distress or reached the experimental endpoint, they were humanely euthanized with anesthesia overdose or CO_2 inhalation. NPC tissue sections were provided by Xuzhou Medical University upon ethic committee approval (XYFY2021-KL317-02).

Antibodies

The anti-gp350 monoclonal antibody clone 72A1 was obtained commercially (Merck Millipore, Kenilworth, NJ) and the clone 7A1 was kindly provided by Dr. Reinhard Zeidler and produced by the Core facility "Monoclonal Antibodies" at Helmholtz Zentrum Munich; Table S1). The mouse hybridoma cell line producing the OT6 anti-gp350 monoclonal antibody was kindly provided by Prof. Jaap Middeldorp, Amsterdam University Medical Center and the purified OT6 antibody was manufactured by Helmholtz Zentrum Munich, Germany.

Cell lines

The EBV^+ C666.1 human NPC cell line was purchased from Shunran Biology (Shanghai, China). Prof. Reinhard Zeidler (Ludwig-Maximilians-University Munich, Germany) kindly provided the PCI-1 human oropharyngeal cancer cell line. C666.1 and PCI-1 cells were cultured in Dulbecco's modified Eagle's medium (DMEM; Thermo Fisher Scientific, Waltham, MA, USA) supplemented with 10% fetal bovine serum (FBS; Nobimpex, Herbolzheim, Germany). The K562 human chronic myeloid leukemia cell line and the EBV^+ KATO-III human gastric cancer cell line were purchased from the American Type Culture Collection (ATCC, Manassas, VA) and cultured in Iscove's modified Dulbecco's medium (IMDM; Thermo Fisher Scientific, Waltham, MA, USA) supplemented with 10% FBS. Jurkat cells (Clone E6-1) were obtained from ATCC and cultured in Roswell Park Memorial Institute (RPMI, Thermo Fisher Scientific, Waltham, MA, USA) + 10% FBS. 293T cells were obtained from ATCC, and cultured in DMEM + 10% FBS. All cell lines were cultured at 37°C and 5% CO_2.

Cell lines expressing gp350

To generate cell lines stably overexpressing gp350, the parental cell lines were transduced with a gp350-expressing lentiviral vector (produced by the contract research organization TransferGene Co. Ltd, Dalian, China). After expansion, $gp350^+$ cells were selected after fluorescence activated cell sorting (FACS).

Generation of EBV^+ LCLs

The EBV^+ B95-8 Marmoset LCL was purchased from MITO Biological technology Co. Ltd (Shanghai, China). B95-8 cells were cultured in RPMI supplemented with 10% FBS. For lytic activation and release of EBV, B95-8 cells were treated with 20 ng/ml 12-O-tetradecanoylphorbol-13-acetate (TPA). Peripheral blood mononuclear cells (PBMCs) were obtained from AllCells (Alameda, CA, USA) after approval by the ethical committee of Shanghai Zhaxin Traditional Chinese and Western Medicine hospital. After TPA activation, B95-8 cell supernatants were 1:10 diluted in RPMI + 10% FBS culture medium and used to infect PBMCs in the presence of 20 nM Tacrolimus (FK506, Aladdin, Shanghai, China). Around 20 days after infection, outgrown LCLs were identified by flow cytometry as $CD23^{High}CD58^+$ cells.

Construction and production of lentiviral vectors expressing gp350CARs

The gp350CAR DNA sequences were synthesized and inserted between the BamHI and SalI sites of the pCDH-EF1-MCS-T2A-copGFP lentiviral vector (GENEWIZ, Suzhou, China). The T2A-copGFP sequences were deleted from the vector because GFP is known to be highly immunogenic (10). Batches of third generation lentiviral vectors were generated under GMP-compatible processes using proprietary methods from a contract research organization (CRO, TransferGene Co. Ltd, Dalian, China). Specifically, HEK 293T/17 cells (ATCC, Manassas, VA) first adapted to suspension cells in serum-free medium (Sino Biological, Beijing, China) by medium switching and continuous rocking at 37°C and cells were established and validated in Canvestbio (Wuhan, China). Transfergene (Dalian, China) manufactured and characterized high quality grade plasmids (vector backbone and three packaging plasmids) according to GMP requirements. All the plasmids were sequenced to confirm their structures. Third generation lentiviral vectors were produced after transient co-transfection of HEK 293T/17 suspension cells with four plasmids (the transfer plasmid pCDH-ZT002, the plasmid pMD2.G expressing the vesicular stomatitis virus G (VSV-G) envelope, and the packaging plasmids pMDLg/pRRE and pRSV-Rev) using a standard polyethyleneimine (PEI)-based method (PEIpro, polyplus-transfection, Illkirch, France). The cell supernatants were harvested 48 h after transfection. After pilot vector productions in flasks, the SOP for manufacturing of the LV was established and optimized (Table S1).

Concentration and purification of the lentiviral vector

After filtration with 0.5 µm filters (Cobetter, Hangzhou, China), cell supernatants were treated with 40 U/ml SuperNuclease (Sino Biological, Beijing, China) for 1 h at 37°C. LV batches were concentrated in a hollow-fiber system (Repligen, Waltham, MA, USA) and purified with Capto Core 700 chromatography resin (Cytiva, Marlborough, MA). After filtration with 0.22 µm filters (Merck Millipore, Kenilworth, NJ), the LV batches were aliquoted in 1.8 ml samples dispensed in cryopreservation tubes (Corning, NY, USA). The LV batches were stored at -80°C. Vector particle concentration was determined by p24 ELISA (Takara Bio, Japan). Infective lentivirus titer was determined by virus serial dilution, infection of Jurkat cells and the percentages of CAR^+ cells were determined by flow cytometry. Specifically, Jurkat cells were seeded in wells with $1x10^5$ cells each. Cells were transduced with 50, 10, 2, 0.4 or

0.08 µl of the LV sample. Controls were non-transduced mock cells. CAR expression was detected 72 hours post transduction by flow cytometry. gp350CAR expression was detected with APC-conjugated goat anti-human IgG-Fc directed against the IgG4 spacer (Jackson ImmunoResearch Laboratories, Philadelphia, PA, USA (Table S1). Activity titer was calculated using following formula: Activity titer (TU / ml) = P / V x 10^3 × 10^5 (P: Percentage of positive-stained cells; V: volume of cell supernatant with lentivirus used for infection).

Production of gp350CAR-T cells

PBMCs were isolated from leukapheresis units using Ficoll density gradient separation (GE Healthcare, Chicago, IL, USA) and cryopreserved. PBMCs were thawed and cultured in AIM-V (Thermo Fisher Scientific, Waltham, MA) supplemented with 5% CTS™ Immune Cell Serum Replacement (SR) (Thermo Fisher Scientific, Waltham, MA) and human IL-2 (300 IU/ml, Quangang, Shandong, China). PBMCs were activated and expanded with CTS™ Dynabeads™ CD3/CD28 (Thermo Fisher Scientific, Waltham, MA) for 24 h. T cells were transduced with LVs at multiplicity of infection (MOI) of 1. Three days after transduction, the cells were extensively washed to remove the LV particles. T cells were further expanded in AIM-V medium supplemented with 5% CTS™ Immune Cell SR (Thermo Fisher Scientific, Waltham, MA) for three to ten days in the presence of IL-2 (300 IU/ml, Quangang). The cell product was washed twice with normal saline (Qidu pharmaceuticals, Shandong, China) containing 2.5 % human serum albumin (CSL Behring, King of Prussia, PA, USA). Cells were resuspended in Cryostor® CS10 Cell Freezing Medium (STEMCELL Technologies, Vancouver, Canada) for cryopreservation and stored in liquid nitrogen.

Quality control of gp350CAR-T cells by flow cytometry analyses

Anti-human CD3, CD4 and CD8 monoclonal antibodies were obtained from Biolegend (San Diego, CA, USA (Table S1)). Staining of gp350CAR was performed with the APC-conjugated goat anti-human IgG-Fc or with gp350 recombinant protein labelled with Fluorescein-5-isothiocyanate (FITC, Sino Biological, Beijing, China). Flow cytometry data was acquired and analyzed with CytoFLEX (Beckman Coulter, Brea, CA, USA).

Analyses of secreted IFN-γ and TNF-α by ELISA

gp350CAR-T cells were co-cultured with gp350$^+$ or with wild-type (w.t.) control cells at various Effector : Target (E : T) ratios for 16 h. Cell supernatants were collected for measurement of IFN-γ (Biolegend, San Diego, CA, USA) or TNF-α (BD Biosciences, Franklin Lakes, NJ, USA) by ELISA according to the manufacturers' protocols. Samples were analyzed by microplate reader (TECAN, Männedorf, Switzerland).

Cytotoxicity assays

After co-culture with targets at different E:T ratios for 16 h, the cytotoxic activity of gp350CAR-T cells was measured using CytoTox 96® Non-Radioactive Cytotoxicity Assay (Promega, Madison, MI, USA) measuring release of lactate dehydrogenase (LDH). Alternatively, we used the DELFIA® EuTDA Cytotoxicity Reagents kit (Perkin Elmer, Waltham, MA, USA) based on loading cells with a fluorescence enhancing ligand that forms a fluorescent chelate once cells are lysed. Both assays were performed strictly following the manufacturer's instructions. Control groups were set up to measure: (i) the medium background (no cells added), (ii) the spontaneous release (target cells only), and (iii) the maximum release (target cells treated with 10 µl lysis buffer). Experiments were performed in triplicates. Data acquisition was performed using microplate reader (TECAN, Männedorf, Switzerland). For CytoTox 96® Non-radioactive cytotoxicity kit, killing efficacy was calculated by using the following formula: % Cytotoxicity= [Target plus Effector (OD 490nm) – Effector Spontaneous (OD 490nm)] / [(Target maximum (OD 490nm) – Target Spontaneous (OD 490nm)] x 100. For DELFIA® EuTDA Cytotoxicity kit, killing efficacy was calculated by using the following formula: % Specific release = [Target plus Effector (counts) - Spontaneous release (counts)] / [Maximum release (counts) - Spontaneous release (counts)] x 100.

NPC xenograft mouse model

Immunocompromised B-NDG mice (NOD.CB17-*Prkd*^{cscid}*Il2rgt*^{m1}/Bcgen) were purchased from Biocytogen (Beijing, China). A mouse xenograft model of human NPC was established by subcutaneous inoculating 5x10^6 C666.1/gp350 cells on day 0. Five days after tumor inoculation, tumor length (L) and width (W) were measured with a caliper and the tumor volume (V) was calculated with the formula V = (L x W x W) / 2 as baseline and treatments were administered. To test the potency of gp350CAR-T cells *in vivo*, mice were randomly distributed into treatment groups: (i) i.v. injected saline (control group), (ii) i.v. injected mock non-transduced T cells (at 5x10^5, 1x10^6, 5x10^6 cell doses), and (iii) i.v. injected gp350CAR-T cells (at 5x10^5, 1x10^6, 5x10^6 total cell doses). Blood was collected on days 8, 19 and 27 after treatment. Plasma IFN-γ was analyzed using cytometric bead assay (BD Biosciences, Franklin Lakes, NJ, USA) strictly according to manufacturer's protocol. Cross-sectional analyses to evaluate the bio-distribution of CAR-T cells in tissues were performed on days 6, 8, 12 and 19 and the numbers of CAR copies were measured by qPCR as described below. Tumor progression was monitored by tumor volume measurements. On day 27, mice were sacrificed and the weight of tumors was measured.

Tissue distribution analyses of gp350CAR-T cells by PCR

Various tissues were extracted and subjected to DNA extraction using QIAamp DNA Blood Mini Kit (Qiagen, Hilden, Germany). The primer set amplifying the DNA fragment by qPCR in the gp350CAR region of the vector (forward primer: 5'- AGTTCGCTTGCGACATCTAC; reverse

primer: 5'- GCCTAGACCTCTTGCTTCTATTT) was used. Gene-amplified products were detected with the probe: FAM TGCTGCTGCTGTCTCTGGTAGTC. Copies of CAR sequences were quantified in a QuantStudio 5 Real-Time PCR System (Thermo Fisher Scientific).

Immunohistochemistry analyses of gp350$^+$ and CD3$^+$ cells in mouse and human tissues

The NPC tissue sections obtained from patients and used as references for gp350 IHC analyses were provided by Xuzhou Medical University, China. Tumors obtained from mice were fixed and paraffin embedded using routine methods. The OT6 monoclonal antibody (hybridoma kindly provided by Prof. Jaap Middeldorp, Amsterdam University Medical Center and antibody manufactured by Helmholtz Zentrum Munich, Germany) was used for immunohistochemical staining to identify gp350-positive cells in the tissue. The anti-CD3D & CD3E heterodimer antibody was purchased from Sino Biological, Beijing, China. Paraformaldehyde-fixed, paraffin-embedded tissues are baked for 30 minutes at 60°C and cooled to room temperature. The sections were further deparaffinized in xylene for 3 times, and gradually rehydrated with 95%, 80%, 70%, and 60% alcohol, and finally washed with distilled water twice. Endogenous peroxidase activity was quenched with a 10-minute incubation of 3% hydrogen peroxide at room temperature. Sections were further incubated in sodium citrate antigen retrieval solution (Boster, Wuhan, China) at 100°C boiling water bath for 10 minutes. After antigen retrieval, sections were blocked with 5% BSA at 37°C for 30 minutes, and stained with mouse-derived OT6 antibody (1:200) or anti-CD3D & CD3E heterodimer antibody (1:200, Sino Biological, Beijing, China) at 4°C overnight. HRP polymer-labeled goat anti-mouse or rabbit IgG antibody (Boster, Wuhan, China) was used as secondary antibody. Sections were further stained with the ready-to-use SABC (Boster, Wuhan, China) and DAB (Boster, Wuhan, China). Slides were further counterstained with hematoxylin (Servicebio, Wuhan, China) for 10s, then use 60%, 70%, 80%, 95% alcohol to dehydrate, and finally transparent with xylene, and mount with neutral resin (Boster, Wuhan, China). Sections were further observed under microscope (Mshot, Guangzhou, China) and captured with Mshot camera (Mshot MD50, Guangzhou, China).

Statistical analyses

Statistical analyses were carried out with SPSS and R. Bar plots show mean ± s.d. Welch t-test with correction for Bonferroni-Holm multiple testing – if adequate – to evaluate differences in means.

Results

Pre-testing of LVs expressing different gp350CAR designs

We had previously produced gp350CAR-T cells using retroviral vectors (9) but since third generation self-inactivating (SIN) LVs remains currently as the leading the gene transfer tool for CAR-T cell manufacturing (11), we designed and tested four LVs containing the CD8 transmembrane domain (TM) and incorporating the 7A1 or 6G4 gp350-specific scFvs, the human IgG Fc or CD8 hinges, and the 4-1BB.CD3ζ or CD28.CD3ζ chimeric signaling domains (Figure 1A). One day after activation with cytokines, PBMCs were transduced with the LVs and further expanded *ex vivo*. Analyses of the cells seven days after transduction showed variable frequencies of CAR$^+$ T cells (Figure 1B). The cells transduced with LV-ZT002 (7A1-scFV/ Fc hinge/ CD28.CD3ζ) showed the highest frequency of gp350CAR$^+$ T cells (86%, representative results from triplicate experiments, Figure 1B). These results confirmed previous data comparing CARs generated with retroviral vectors, showing a higher expression for vectors containing the 7A1 scFv and CD28.CD3ζ (9). In order to compare them functionally, gp350CAR-T cell types produced with the four different LVs were co-cultured with human oropharyngeal cancer cell line PCI-1 engineered to express gp350 (PCI-1/gp350, results from triplicate experiments, Figure 1C). PCI w.t. cells were used as control targets and the release of IFN-γ and TNF-α were measured by ELISA. Secretion of cytokines was significantly higher for all types of gp350CAR-T cells co-cultured with gp350$^+$ cells than the control co-cultures (using Mock effectors or targeting PCI w.t.), confirming specific gp350 target recognition for all gp350CAR designs (Figure 1D). gp350CAR-T cells generated with the LV-ZT002 produced approximately tenfold higher cytokine levels than gp350CAR-T cells generated with the vector ZT001 incorporating the 4-1BB co-stimulatory domain (Figure 1D). gp350CAR-T cells generated with the vector ZT003 (6G4-gp350CAR-Fc-41BB.CD3ζ) or with the LV ZT004 (7A1-gp350CAR-CD8-41BB.CD3ζ) also showed much lower cytokine levels when stimulated with cells expressing gp350 than the CAR-T cells transduced with LV-ZT002. The *in vitro* killing activities of the different gp350CAR-T cells were analyzed by cytotoxicity assays performed as independent triplicates (Figure 1E). The CAR-T cells generated with the vector ZT002 showed the highest killing capacity of PCI/gp350$^+$ target cells, and up to approximately 70% cytotoxicity at E:T ratio of 10:1. The experiment was repeated using a range of E:T ratios 1:2, 1:1, 2:1, 4:1 and the superior cytotoxicity activity of CAR-T cells generated with the ZT002 vector was confirmed (Figure S1). These data showed that gp350CAR-T cells incorporating the 7A1-scFV and CD28.CD3ζ elements showed the highest expression and functionality, and the vector ZT002 was chosen for further clinical development.

LV design, GMP production, purification and testing

The ZT002 construct was used for LV scale-up production and purification (see main regulatory elements of the self-inactivating (SIN) vector in Figure 2A). GMP-compliant methods were established for upscaling, purification, filing and quality control (QC) of the vector product (Figure 2B). The validation of manufacturing of three independently produced consecutive batches LV-ZT002 by analyses of titers showed highly reproducible results (Table 1). All different production methods and scales, ranging from 50 ml flasks to the 5 l bioreactor system, resulted in satisfactory lentivirus yield (Table S2). Infection of Jurkat with the crude virus or with the purified/concentrated virus showed in average titers of 2.85 x 10^7 transduction units (TU) and 1.32 x 10^7 TU, respectively. The final volume of approximately 100 ml of virus product per batch showed

10.3389/fimmu.2023.1103695

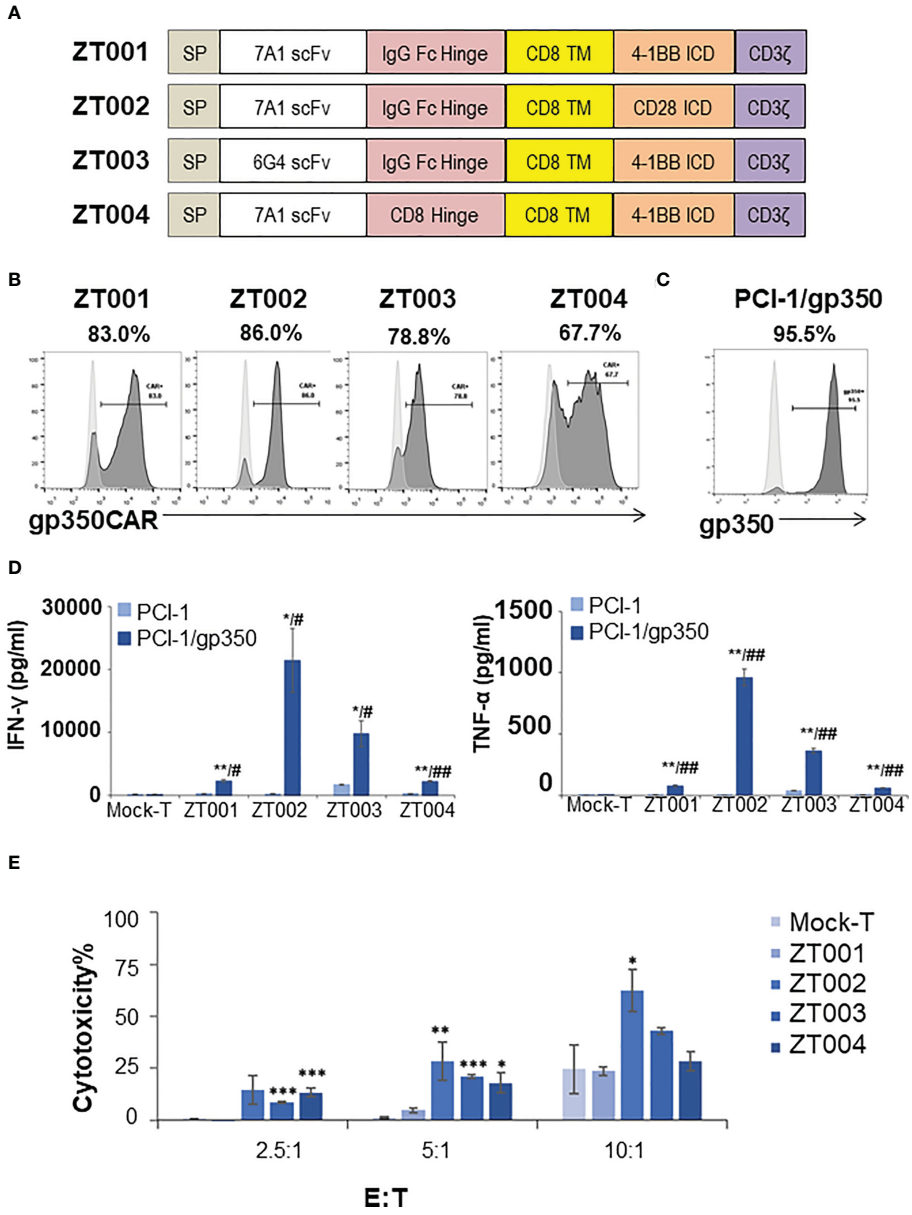

FIGURE 1
Testing of different lentiviral vectors incorporating different gp350CAR designs and selection of the best construct. **(A)** Schematic diagrams of LV constructs expressing gp350CAR. SP, signal peptide; scFv, single chain variable fragment (7A1 or 6G4); Hinge (IgG Fc or CD8); TM, transmembrane domain (all CD8); ICD, intracellular domain (CD28.CD3ζ or 4-1BB.CD3ζ). **(B)** Flow cytometry analyses showing surface expression of the CAR on T cells transduced with four lentiviral constructs (ZT001, ZT002, ZT003 or ZT004). Transduced T cells (dark grey) are compared with mock-T cells (light grey). Percentages of gp350CAR-expressing cells are shown; representative example from triplicate transduction experiments performed with T cells derived from one donor. **(C)** Flow cytometry analyses of PCI-1 cells transduced to express gp350 (dark grey) compared with un-transduced cells (light grey). **(D)** IFN-γ and TNF-α release. Mock-T and gp350 CAR-T cells were co-cultured with PCI-1 or PCI-1/gp350 cells for 16 hours at an E:T of 5:1 and the levels of IFN-γ and TNF-α released in the medium were measured by ELISA. Data are presented as means from triplicates ± SD. Welch t-test and p-values after correction for multiple comparisons, CAR-T versus Mock-T cells, *P ≤0.05, **P≤0.01, ***P ≤0.001. PCI-1/gp350 versus PCI-1, $^{\#}$P ≤0.05, $^{\#\#}$P≤0.01. **(E)** *In vitro* cytotoxicity comparison of four anti-gp350 CAR. Lactose dehydrogenase (LDH)-based cytotoxicity assay (16 hours culturing) was used to assess the cytotoxicity of four anti-gp350 CAR-T cells against gp350-positive human oropharyngeal cancer cell lines PCI-1 (PCI-1/gp350). Non-transduced T (Mock-T) cells were included as a control. These results are presented as means from triplicates ± s.d. Welch t-test and p-values after correction for multiple comparisons, compared to Mock-T, *, P < 0.05; **, P<0.01; ***, P < 0.001.

an average of 15% LV recovery after purification. The quality tests were performed according to the "International Council for Harmonization of Technical Requirements for Pharmaceuticals for Human Use" (ICH) (https://www.ich.org/) and the Chinese pharmacopeia (http://wp.chp.org.cn/front/chpint/en/). Detailed release criteria are listed in Table S3.

Up-scaled batch runs of gp350CAR-T cells

The GMP-grade clinical scale ZT002 vector was then used for upscaling production of CAR-T cells. Initially, we transduced T cells at different LV multiplicities of infection (MOIs; 0.25, 0.5, 1, 2). After transduction, T cells expanded approximately 100-fold for nine days.

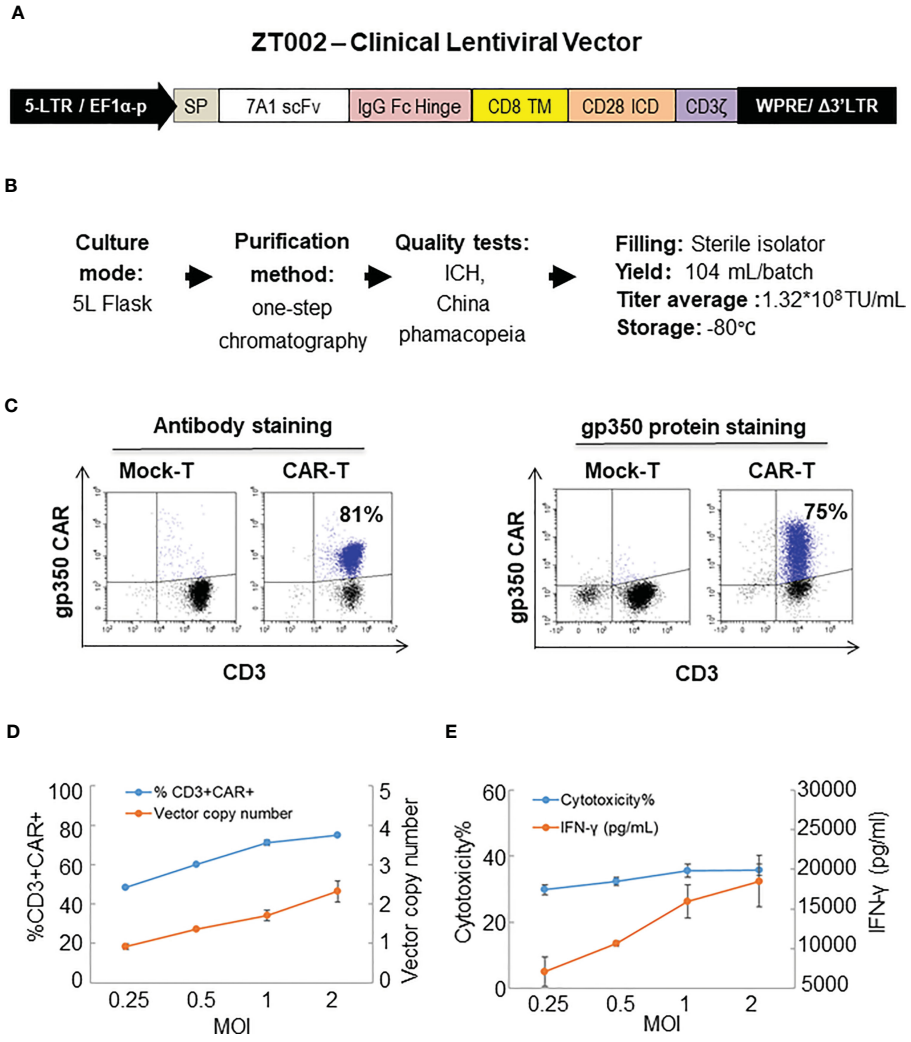

FIGURE 2
Production of ZT002 using GMP-compliant methods and generation of gp350CAR-T cells. **(A)** Detailed vector scheme of the self-inactivating third generation ZT002 vector selected for clinical use. The vector contains non-homologous 5′ and 3′ long-terminal repeats (LTRs). The 5′ LTR incorporates the EF1-α promoter and a WPRE element to improve the RNA stability upstream of the mutated (Δ) 3′ LTR. **(B)** Scheme of LV-ZT002 production, purification, testing and average results for three productions. **(C)** Flow cytometry detection of gp350CAR using an antibody for detection of the hinge (anti-IgG Fc, left) or labelled recombinant gp350 protein binding to the scFv (right). **(D)** Testing different transduction conditions with increasing multiplicity of infection (MOI) to correlate the efficiencies of gp350CAR$^+$ T cell generation with the integrated vector copy numbers. PBMCs were stimulated on day 0, transduced on the next day with ZT002 at increasing MOIs (0.25, 0.5, 1 and 2), and ten days later analyzed for the percentages of CD3$^+$CAR$^+$ cells (blue line) and number of CAR copies per cell genome (orange line). **(E)** Testing the functionality of gp350CAR-T cells generated with different ZT002 MOIs for target cytotoxicity and correlation with IFN-γ production. CAR-T cells were co-cultured with PCI-1/gp350 (E:T=2.5:1) and IFN- γ released in medium (orange line) and cytotoxicity activity (blue line) were analyzed. Results of independent triplicate experiments, performed with gp350CAR-T cells produced with one PBMC donor.

The identity analyses was performed by flow cytometry using a fluorochrome-labelled antibody recognizing the IgG Fc-Hinge region in the CAR or with a fluorochrome-labeled gp350 protein binding to the scFv (Figure 2C), confirming that the gp350CAR-T cells could bind the target protein. We observed a correlation between the transduction efficiency (measured by detection of CAR$^+$ CD3$^+$ T cells by flow cytometry) and the number of integrated vector copies in the genome (Figure 2D). We also observed that CAR-T cell produced with higher LV MOIs secreted higher levels of IFN-γ when incubated with PCI-1/gp350 target cells (Figure 2E). However, their cytotoxic activities reached the plateau at MOI = 1 (Figure 2E). According to "points to consider of quality control test and pre-clinical study for CAR-T cell therapy products" by the National Institutes for Food and Drug Control, a low vector copy number (VCN) (less than five copies per cell) is required to minimize the potential risks of insertional mutagenesis. Since the MOI of 1 resulted in high frequencies of functional gp350CAR$^+$ T cells (>70%) at a low (<2) CAR copy numbers, the MOI of 1 was chosen for gp350CAR-T batch run productions methods (Table 2). The recovery of T cells after expansion for ten days was in average 3.81 x 10^9 cells. >80% CD3$^+$ gp350CAR$^+$ T cells (at similar CD4$^+$CAR$^+$ and CD8$^+$CAR$^+$ ratios) were detected after staining with immunoconjugated gp350 protein and FACS analyses (Table 2). In average, 2.37 VCN per genome were detectable by real-time qPCR (Table 2). Based on the test-runs of gp350CAR-T cell productions, several relevant and required parameters for the batch release criteria were determined (Table S4). Therefore, the scale-up methods for generation of GMP-like gp350CAR-T cells were straightforward and resulted in CAR-T cells

10.3389/fimmu.2023.1103695

TABLE 1 Validation of LV-ZT002 GMP manufacturing after production and testing of three independent and consecutive viral lots.

Batch Number	Total volume before purification (ml)	Titer crude supernatant Jurkat cells (TU/ml x10^7)	Total volume after purification (ml)	Filling volume per vial (ml)	Activity titer Jurkat cells (TU/ml x10^8)	Recovery rate (%)
LV-ZT002-20210403	3,600	2.47	104	0.3	1.37	16.01
LV-ZT002-20210404	3,447	2.42	99	0.3	1.11	13.16
LV-ZT002-20210405	3,478	2.85	110	0.3	1.48	16.43
Average ± SD	3,508 ± 81	2.85 ± 0.24	104 ± 6	0.3	1.32 ± 0.19	15.20 ± 1.78

with the expected high expansion and viability, high purity, low vector copy numbers, and no detectable contaminations (bacteria and mycoplasma, Table S4).

In vitro potency testing of GMP-like gp350CAR-T cells

When NPC primary samples are immortalized to generate NPC lines, they commonly lose the expression of lytic antigens after extended culture. Therefore, we generated lentivirus-transduced gp350$^+$ cell lines: EBV$^-$ PCI-oropharyngeal carcinoma 1 (as shown in Figure 2), EBV$^-$ K562 myeloid leukemia, EBV$^-$ GC KATO-III, EBV$^+$ NPC C666.1. In addition, we obtained a LCL transformed and immortalized line expressing gp350 after *in vitro* infection of B cells with B95-8 EBV. The gp350-overexpressing cell lines showed >90% stable gp350 expression, and the EBV-transformed LCLs showed ~30% gp350 expression (Figure 3A). gp350CAR-T cells were co-cultured with those cell lines at variable E:T ratios for 16 h. Culture supernatants were harvested for IFN-γ ELISA measurements. For all co-cultures, gp350CAR-T cells showed significantly higher concentrations of secreted IFN-γ (100~3,000 fold) than control mock-T cells (Figure 3B). *In vitro* killing efficacy of gp350CAR-T cells was evaluated in triplicate experiments with various E:T ratios after 16 h of co-culture with the cell targets. For all E:T ratios used, gp350CAR-T cells showed significantly higher cytotoxicity against all cell targets than control mock-T cells (Figure 3C). Therefore, we confirmed the specificity, reactivity and cytotoxicity of gp350CAR-T cells produced after scale-up methods.

gp350CAR-T cells significantly reduce EBV$^+$ NPC C666.1/gp350 tumor burden *in vivo*

A batch of gp350CAR-T cells produced with the GMP-like methods and showing 86% CD8$^+$CAR$^+$ and 86% CD4$^+$CAR$^+$ cells (Figure 4A) was used for *in vivo* testing. Since subcutaneous (s.c.) implantation of the NPC cell line C666-1 cells into immune deficient mice consistently engraft and produce tumors (12), we used the C666-1/gp350 cells to establish a xenograft mouse model. C666.1/gp350 cells were injected s.c. on the flanks of B-NDG mice, and five days later we measured the baseline volume of the tumors (Figure 4B). On day five after challenge, the mice were then randomized into seven groups (n=6 mice per cohort) and injected with (i) Saline control, (ii) low dose (5x10^5/mouse) mock-T or (ii) gp350CAR-T cells, (iv) medium dose (1x10^6/mouse) mock-T or (v) gp350CAR-T cells, an (vi) high dose (5x10^6/mouse) mock-T or (vii) gp350CAR-T cells. The tumor volumes were measured longitudinally and mice were sacrificed at day 27 after tumor implantation for collection of biopsies and terminal analyses (Figure 4B). The tumor volumes were measured longitudinally (n=6) until day 26 after implantation. For all T cell doses tested, until day 26, gp350CAR-T cells promoted a dose-dependent and significant reduction of the tumor volumes compared with mock-T cells (Figure 4C). Accordingly, administration of gp350CAR-T cells at all different doses promoted a significant reduction of tumor weight measured at day 27 compared with mice injected with mock-T cells or saline (Figure 4D). gp350CAR-T cells were also injected at the highest 5x10^6 cell dose into B-NDG mice (n=2) five days after tumor implantation for a cross-sectional analyses of CAR-T cells bio-distribution. The mice were sacrificed at days 6, 8, 12 and 19 after

TABLE 2 Validation of gp350CAR-T cell manufacturing after production and testing of three independent and consecutive batch runs.

Batch Run	Expansion-fold day 10	Total cells (x10^9)	% CD3$^+$ CAR$^+$	% CD4$^+$	% CD8$^+$	LV copies/cell
1	205	2.77	83.4	51.3	45.4	2.10
2	334	5.01	86.5	38.9	55.2	1.91
3	405	3.65	82.1	44.6	52.8	3.10
Average ± SD	315 ±101	3.81 ±1.13	84.0 ±2.3	44.9 ±6.2	51.1 ±5.1	2.37 ±0.64

10.3389/fimmu.2023.1103695

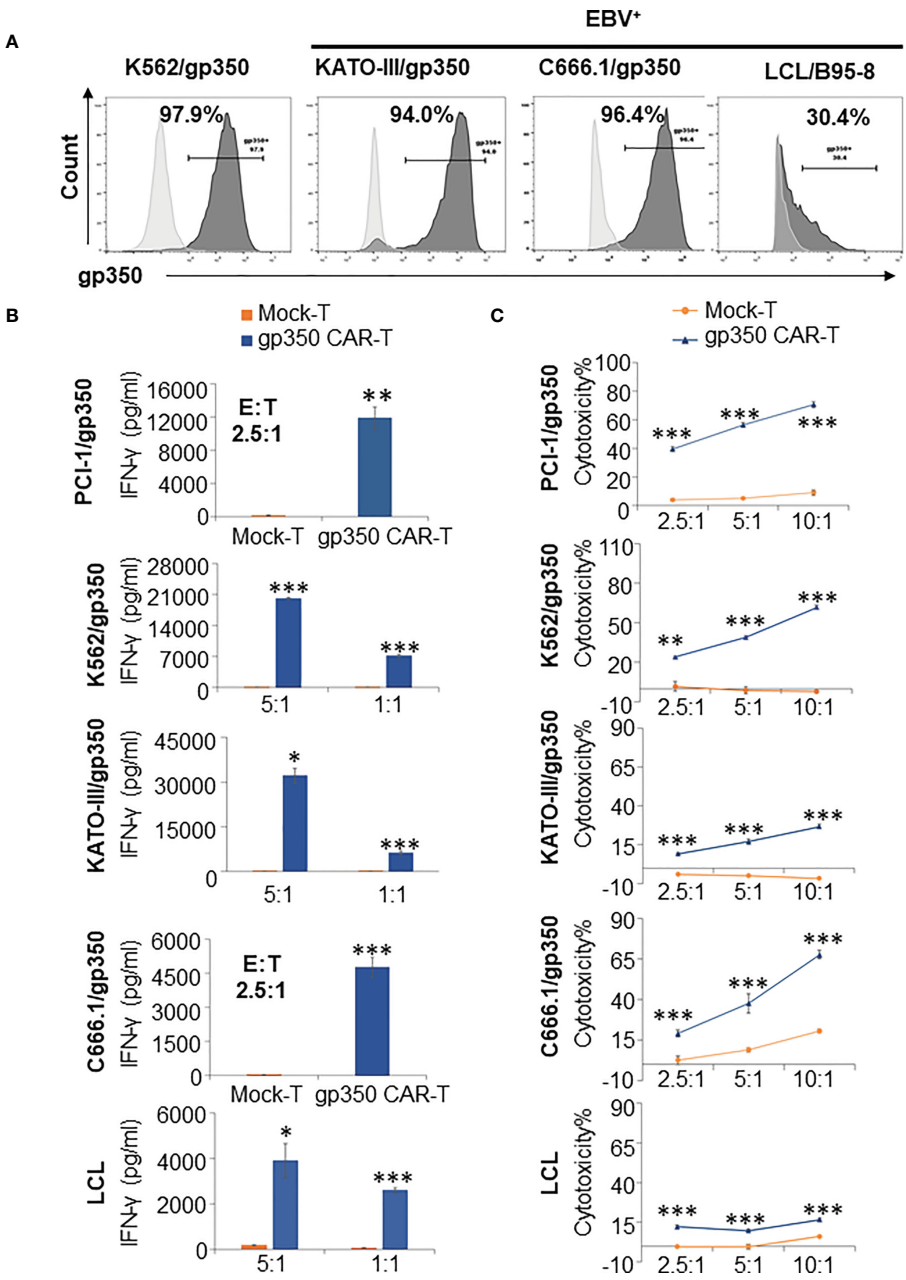

FIGURE 3
Potency testing of gp350CAR-T cells produced after scale-up against different cell targets expressing gp350. **(A)** Flow cytometry analyses of gp350 expression on various cancer cell lines: EBV$^-$ PCI-1 expressing gp350 (PCI-1/gp350), EBV$^-$ myeloid leukemia line K562 expressing gp350 (K562/gp350), EBV$^-$ gastric carcinoma KATO-III expressing gp350 (KATO-III/gp350), EBV$^+$ nasopharyngeal carcinoma C666.1 expressing gp350 (C666.1/gp350), and an EBV$^+$ B95-8-derived lymphoblastoid cell line (LCL). **(B)** Analyses of secreted IFN-γ. Gp350CAR-T cells were co cultured with above tumor cell lines for 16 h at indicated E:T ratios and IFN-γ release level was quantified by ELISA. t test, compared to mock-T, *P≤0.05, **P≤0.01, ***P≤0.001. **(C)** *In vitro* cytotoxicity assays. gp350CAR-T were co-cultured with PCI-1/gp350, KATO-III/gp350, C666.1/gp350 and LCLs and LDH-based cytotoxicity assay (performed after 16 h of co-culture) or Delfia EuTDA cytotoxicity assay (performed after 2 h of co-culture) were performed. Mock-T cells were included as controls. The results are presented as means ± s.d. t test, compared to mock-T, *P≤0.05, **P≤0.01, ***P≤0.001. Independent triplicate experiments were performed with gp350CAR-T cells produced with one PBMC donor.

tumor challenge for analyses. CAR copies were analysed by qPCR (CAR copies/ ng of tissue DNA) (Figure 4E). One day after gp350CAR-T cell infusion, CAR sequences were mostly detectable in spleen. From three to twelve days after CAR-T cell injections, CAR sequences were mostly noticeable in tumors. At day nineteen after CAR-T injections, the CAR PCR signal was widely distributed in tumors, spleen and lungs and in minor degrees in several other tissues. Hence, gp350CAR-T cells showed a dose-dependent therapeutic activity against gp350$^+$NPC tumor growth and CAR sequences were detectable in the tumor and afterwards redistributed systemically.

10.3389/fimmu.2023.1103695

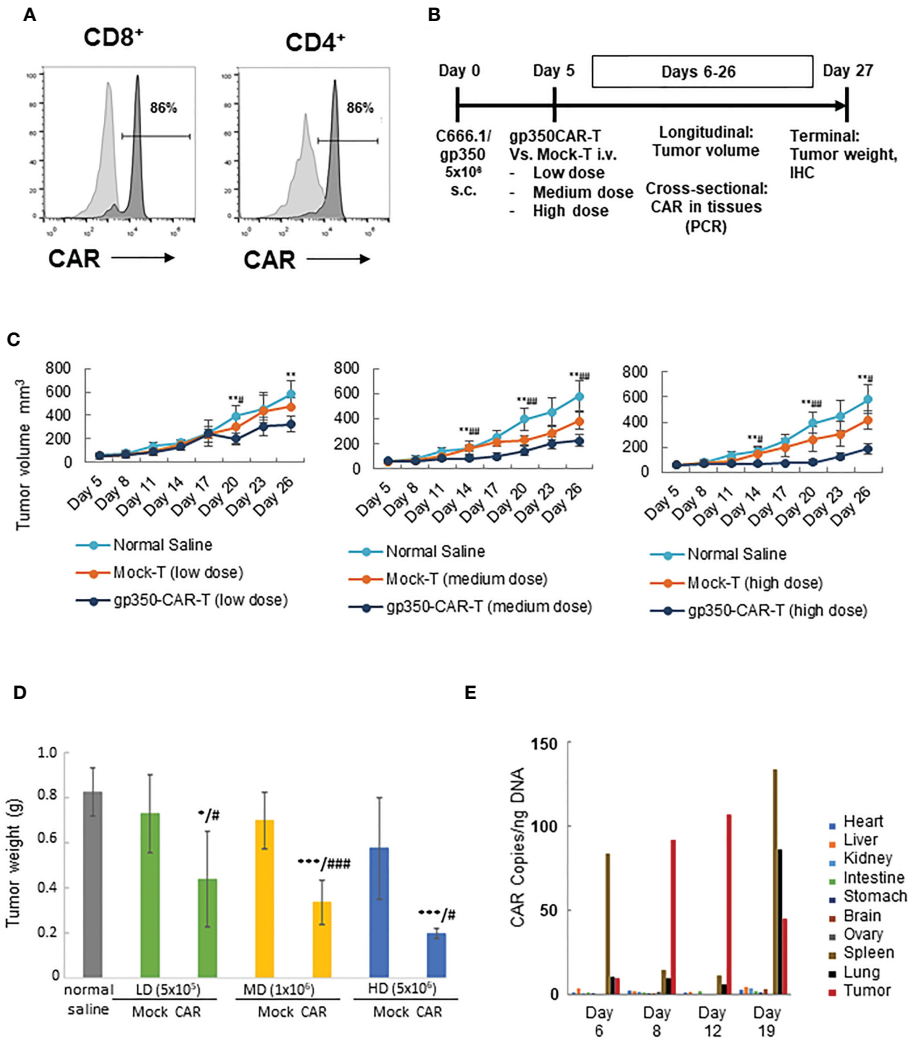

FIGURE 4
In vivo testing of gp350CAR-T cells in B-NDG mice challenged with NPC. **(A)** Flow cytometry analyses of GMP-like gp350CAR-T cells used for *in vivo* experiments showing high frequencies of gp350CAR$^+$ CD8$^+$ and CD4$^+$ T cells. **(B)** Schematic representation of *in vivo* experiment. Mice were injected with 5x10^6 NPC EBV$^+$C666.1/gp350 cells s.c. Five days later, mice were injected with saline, mock-T or CAR-T cells at escalating cell doses. Longitudinal, cross-sectional and terminal analyses were performed to follow tumor growth, CAR-T cell bio-distribution and therapeutic specificity. **(C)** Longitudinal analyses of tumor volume (mm^3). Left graph: low T cell dose (5x10^5); middle graph: medium T cell dose (1x10^6); right graph: high T cell dose (5x10^6). **(D)** Terminal analyses of tumor weight (g). Grey: saline control; green: low T cell dose; yellow: medium T cell dose; blue: high T cell dose. **(E)** Cross-sectional analyses for detection of CAR sequences in tissues (qPCR; copies/ng). Welch t-test and p-values after correction for multiple comparisons, compared to saline control group, *P<0.05; **P<0.01; ***P<0.001; compared to Mock-T, $^{\#}$P<0.05; $^{\#\#}$P<0.01; $^{\#\#\#}$P<0.001.

gp350 expression is decreased in C666.1/gp350 NPC tumors after therapy with gp350CAR-T cells

NPC biopsies obtained from patients occasionally express gp350 and we confirmed this using the OT6 mouse antibody for IHC analyses, showing strong gp350-positive staining in scattered cell populations (Figure 5A left panels, representative example). Applying the same staining methods, gp350 was detectable in the tumors of mice challenged with C666.1/gp350 tumors (Figure 5A right panels, representative example). This confirmed that our *in vivo* model reflected recent findings obtained with new tumor xenografts that could be established with EBV-positive NPC (13). We therefore evaluated if there was a correlation between gp350CAR-T cells homing the tumors and loss of gp350$^+$ cells (Figure 5B, Figure S2, Table S5). Whereas control mice treated with saline or with mock-T cells showed no or very little T cells homing in the tumor, mice treated with gp350CAR-T cells showed distinguishable single or clustered CD3$^+$ T cells infiltrating the tumor (Figure 5B left panels, representative example, Figure S2 with two additional cases, Table S5). IHC analyses for gp350 detection demonstrated that infiltration of gp350CAR-T cells in C666.1/gp350 tumors was inversely correlated with detection of gp350-positive cells (Figure 5B right panels, representative example, Figure S2 with two additional cases), indicating a causal effect for tumor eradication. An expert pathologist provided a semi-quantitative microscopic assessment of cell frequencies and expression levels of CD3 and gp350 in C666.1/gp350 tumor tissue sections obtained from mice treated with saline, Mock-T cells or gp350CAR-T cells. Cells with strong and moderate staining levels were quantified separately. Despite the limitations of

10.3389/fimmu.2023.1103695

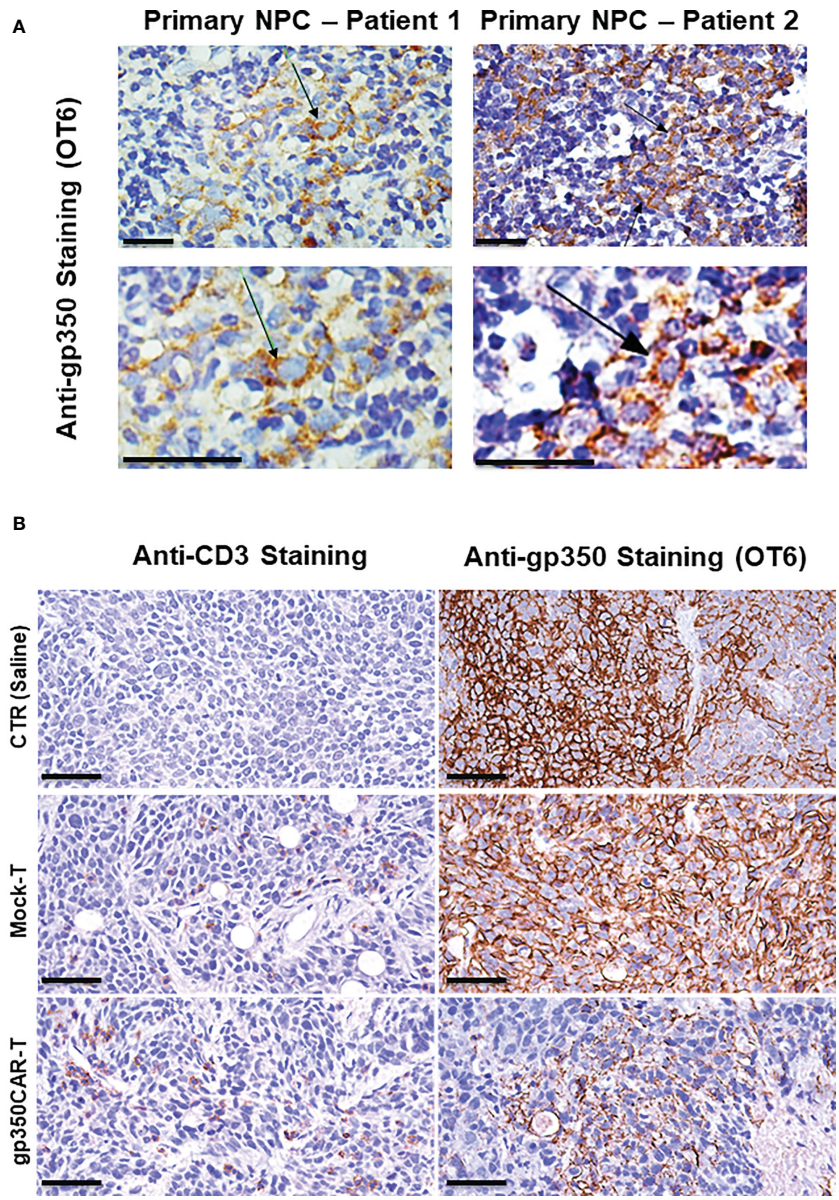

FIGURE 5
Immunohistochemistry staining of paraffin-embedded sections obtained from primary NPC patient tissues or obtained from a C666.1/gp350 tumor sample explanted from a mouse. **(A)** anti-gp350 OT6 staining on primary tumor biopsies from two NPC patients. Arrows, positive staining on tumor cell membrane. Scale bar, 50 µm. **(B)** Representative example of anti-human CD3 staining and anti-gp350 staining on C666.1/gp350 tumor samples. Additional two cases can be found in Figure S1. Scale bars represent 50 µm.

the semi-quantitative assessment, mice infused with gp350CAR-T cells showed in average lower gp350 expression in tumors and higher frequencies of $CD3^+$ cells than mock T cells (Table S5).

After completion of the preclinical experiments, we hired a contract research organization to conduct non-clinical experiments using good laboratory practices (GLP) and documentation for the submission of an Investigational New Drug (IND) for initialisation of clinical trials. Pharmacodynamics studies confirmed the immunotherapeutic activity of gp350CAR-T cells against C666.1/gp350 tumors at a dose dependent manner (Figure S3). The mice treated with gp350CAR-T cells in the non-clinical model did not show weight loss, signs of cytokine release syndrome or neurotoxicity. On the other hand, mice treated with mock-T cells showed pronounced weight loss, which was clinically defined by the CRO as Graft-versus-Host Disease (GvHD), which is a result of the xenograft reactivity of the human T cells against the mouse tissues. In addition, a pharmacokinetics study was performed under GLP to evaluate the bio-distribution of the test article in female and male mice (Figure S4). The biodistribution of the CAR-T cells was monitored by cross-sectional analyses by PCR analyses one day after administration and up to day 70 of the experiment. For both sexes, gp350CAR-T cell detection was initially mostly detected in tumors until day 21. From day 49 until 70, gp350CAR-T cells were also frankly detectable in blood, spleen and liver (Figure S4). Although gp350CAR-T cells were also detected in the spinal cord and several other tissues from day 49 onwards, mice did not show signs of cytokine release syndrome or neurotoxicity until the endpoint.

Discussion

After pioneering clinical trials by June et al showing impressive clinical responses, CAR-T cells have since then revolutionized the field of tumor immunotherapy, especially in the immunotherapy of refractory hematological tumors (14, 15). CAR-T cell therapies have produced sensational long-term remissions for approximately 40% of patients with multiply relapsed/refractory aggressive B-cell non-Hodgkin lymphomas, resulting in several approved advanced cell therapy products (14). However, most of the current CAR approaches have relied on the use of surface antigens expressed on normal cells and not cancer-specific. CD19 is the most explored antigen so far for targeting CAR-T cells against B cell hematologic malignancies, followed by CD20, B cell maturation antigen (BCMA) and others (14). The lack of specificity can lead to unwanted depletion of normal cell populations, which is a general concern in the field. In addition, overstimulation CAR-T cells *in vivo* due to abundant antigen existence can lead to severe immune-toxicities (15).

On the other hand, tumors associated with viral infections open the prospect of exploring viral antigens not expressed on the surface of normal cells for CAR-T cell engineering. The gp350 envelope protein is abundantly expressed on infected cells during EBV lytic reactivation and sporadically on the surface of latently infected cells, representing a potential virus-specific therapeutic target for CAR-T cells. Our current goal was to advance towards the clinical development of gp350CAR-T cells to treat patients with different types of EBV-associated malignancies.

Therefore, we tested several novel gp350CAR designs in LVs. SIN-LVs were used due to their ability and to efficiently transduce both dividing and non-dividing cells and to stably integrate in genomic locations not likely to be harmful for insertional mutagenesis. Further, GMP production of 3rd generation LVs (four plasmids transient transfection system) is well established in academic centers and companies. LV clinical utilization and boomed in recent years with several optimizations and tests confirming their consistent and broad usability in the immune and gene therapy fields leading to several approved cell therapies (16).

Among the four gp350CAR-T designs tested here, the LV 7A1-gp350CAR with the Fc Hinge and the CD28.CD3ζ signaling domain showed superior performance for reactivity and killing of gp350$^+$ targets. These results corroborate our previous studies showing higher performance of 7A1-gp350-CD28.CD3ζ-CAR T cells generated after retroviral vector transduction compared to other RV designs with the 6G4 scFv (9) or incorporating 4-1BB.CD3ζ (Stripecke et al, unpublished data). The Sadelain group extensively compared CD28.CD3ζ and 4-1BB.CD3ζ co-stimulation designs in stress tests using the CD19CAR-T cells in the Nalm-6 leukemia xenograft model (17). They showed that CAR-T cells incorporating CD28.CD3ζ and infused at low doses (1x10^5 - 2x10^5) produced significantly higher tumoricidal effects against leukemia development than CAR-T cells with 4-1BB.CD3ζ co-stimulation (17). Since EBV has evolved several mechanisms of immune evasion, we speculate that the CD28.CD3ζ signaling may provide superior potency for the T cells to subvert the EBV immune suppressive signals.

Using scale-up GMP methods, we therefore produced and purified the selected LV incorporating 7A1-gp350-CD28.CD3ζ-CAR and reached consistent high titers (range of 1x10^8 TU/ml) and purity characteristics. The GMP-grade purified and high-titer ZT002 vector enabled a straightforward upscaling of gp350CAR-T production, and the runs of the cell product showed high purity, viability and sterility. Our CAR-T cell manufacturing process was relatively simple, as the T cells were not enriched prior to transduction, the MOI was low (1), and after transduction the T cells could be cultivated for nine to ten days in the presence of generic clinical-grade IL-2. Three consecutive cell production batches resulted in >80% CAR$^+$, approximately 100-fold expansion, range of 4x10^9 total viable T cells, similar rations of CD8$^+$ and CD4$^+$ T cells and approximately two vector copies per genome. These results are comparable to CAR-T cells transduced with other lentiviral vectors (18, 19).

The GMP-like gp350CAR-T cells showed *in vitro* cytotoxic potency against five different types of gp350$^+$ cell lines as targets (lymphoma, NPC, GC). *In vivo*, gp350CAR-T cells showed a dose dependent incremental therapeutic effect against C6661-1/gp350 NPC growth, but all doses where therapeutic. The abrogation of NPC growth was associated with detectable CAR copies in several tissues and higher infiltration of T cells in tumors. The EBV$^+$ NPC model is highly relevant since it broadens the utility of gp350CAR-T cells against solid tumors.

These results underscore the forthcoming advance of gp350CAR-T cells for clinical studies for treatment of patients with EBV$^+$ gp350-positive NPCs associated with EBV lytic infections. Some specialized clinical centers are able to produce adoptive virus-specific T cells (VSTs) to treat EBV$^+$ LPD, lymphomas as well as nasopharyngeal cancers (20–22). Autologous or third party VSTs are stimulated *ex vivo* with viral latent antigens (such as EBNA1 and LMP2) and cell lots passing batch release are infused, resulting in overall beneficial clinical responses (23). However, for their generation, VSTs strongly rely on viral epitopes presented by the tumors *via* the human leukocyte antigen type I (HLA-I) for their recognition by cognate T cell receptors (TCRs) and their destruction. Nevertheless, EBV is known to down-regulate HLA-I, which may negative impact on the function of VSTs, whereas CAR-T cells are HLA-independent.

The uses of CAR-T cells are expanding beyond oncology and have already been validated against different infectious disease such as EBV (9, 24, 25), human cytomegalovirus (HCMV) (26), human immune deficiency (HIV) (27), and hepatitis C virus (HCV) (28). Therefore, an exciting and highly dynamic "synthetic biology" antiviral CAR-T field is evolving. Taken together, our data confirmed our initial proof-of-concept antitumor effects of gp350CAR-T cells, advanced the cell manufacturing to the GMP level, and the next goal is to evaluate their clinical potential against NPC.

Concluding remarks

- CAR-T cells targeting the EBV lytic antigen gp350 could be produced after lentiviral vector transduction using GMP-like methods and in sufficient numbers for clinical uses.
- gp350CAR-T cells recognized and killed several cell lines expressing gp350.
- A xenograft mouse model of NPC confirmed the *in vivo* potency of gp350CAR-T cells.

Data availability statement

The raw data supporting the conclusions of this article will be made available by the authors, without undue reservation.

Ethics statement

The studies involving human participants were reviewed and approved by Shanghai Zhaxin Traditional Chinese and Western Medicine hospital (study protocol number: LP202006). The patients/participants provided their written informed consent to participate in this study. The animal study was reviewed and approved by research ethics committee at Guangzhou Regenerative Medicine and Health, Guangdong Laboratory (GRMH-GDL) IACUC serial number: 2020125.

Author contributions

XZhang provided overall conceptualization and project leadership, wrote and the first draft of the manuscript and revised the final version. XZhang, TW, YL, ML, ZH developed technologies and assays, performed *in vitro* experiments and analyzed data. XZhu performed animal studies. DH provided funding, administered resources and provided project leadership. LZ, YW and LL provided NPC patient tissue samples. FK revised or conducted the statistical analyses. RS provided overall conceptualization supervised the data analyses and revised the final manuscript. All authors contributed to the article and approved the submitted version.

Funding

Upscaling and GMP adaptation for clinical development of gp350CAR-T cells and preclinical testing was financed by Biosyngen/ Zelltechs Pte. Ltd. Academic development and preclinical testing of additional CAR-T cells in mouse models in R.S.'s laboratories is ongoing and financed by grants of the German Center for Infections Research (DZIF-TTU07.912 to RS), by the German Cancer Aid (Deutsche Krebshilfe Nr. 70114234 to RS), by the Jackson Laboratory (JAX, USA, grant HLA-LV) and by the Cancer Research Center Cologne-Essen (CCCE), University of Cologne, Cologne, Germany.

Acknowledgments

We thank Prof. Reinhard Zeidler for providing the PCI-1 cell line and the 7A1 monoclonal antibody. We thank Prof. Jaap Middeldorp for kindly providing the OT-6 antibody. We thank TransferGene Co. Ltd. for providing details about the lentivirus production methods. We thank Dr. Baojian Pan for providing histology staining analyses. Upscaling and GMP adaptation for clinical development of gp350CAR-T cells was financed by Biosyngen/ Zelltechs Pte. Ltd.

Conflict of interest

Authors XZhang, TW, XZhu, YL, ML, ZH and DH are employees of Biosyngen/Zelltechs Pte. Ltd. developing and testing CAR-T cell products for clinical cancer immunotherapy. XZhang and DH are shareholders of Biosyngen Pte. Ltd., RS has filed a patent application for uses of gp350CAR-T cells and is a founding shareholder and scientific consultant of BioSyngen/Zelltechs Pte. Ltd.

The remaining authors declare that the research was conducted in the absence of any commercial or financial relationships that could be construed as a potential conflict of interest.

Publisher's note

All claims expressed in this article are solely those of the authors and do not necessarily represent those of their affiliated organizations, or those of the publisher, the editors and the reviewers. Any product that may be evaluated in this article, or claim that may be made by its manufacturer, is not guaranteed or endorsed by the publisher.

Supplementary material

The Supplementary Material for this article can be found online at: https://www.frontiersin.org/articles/10.3389/fimmu.2023.1103695/full#supplementary-material

References

1. Kanda T, Yajima M, Ikuta K. Epstein-Barr Virus strain variation and cancer. *Cancer Sci* (2019) 110(4):1132–9. doi: 10.1111/cas.13954

2. Munz C. Latency and lytic replication in Epstein-Barr virus-associated oncogenesis. *Nat Rev Microbiol* (2019) 17(11):691–700. doi: 10.1038/s41579-019-0249-7

3. Brennan B. Nasopharyngeal carcinoma. *Orphanet J Rare Dis* (2006) 1:23. doi: 10.1186/1750-1172-1-23

4. Hau PM, Lung HL, Wu M, Tsang CM, Wong KL, Mak NK, et al. Targeting Epstein-Barr virus in nasopharyngeal carcinoma. *Front Oncol* (2020) 10:600. doi: 10.3389/fonc.2020.00600

5. Wu CC, Fang CY, Huang SY, Chiu SH, Lee CH, Chen JY. Perspective: Contribution of Epstein-Barr virus (EBV) reactivation to the carcinogenicity of nasopharyngeal cancer cells. *Cancers (Basel)* (2018) 10(4), 120. doi: 10.3390/cancers10040120

6. Morales-Sanchez A, Fuentes-Panana EM. The immunomodulatory capacity of an Epstein-Barr virus abortive lytic cycle: Potential contribution to viral tumorigenesis. *Cancers (Basel)* (2018) 10(4):98. doi: 10.3390/cancers10040098

7. Martel-Renoir D, Grunewald V, Touitou R, Schwaab G, Joab I. Qualitative analysis of the expression of Epstein-Barr virus lytic genes in nasopharyngeal carcinoma biopsies. *J Gen Virol* (1995) 76(Pt 6):1401–8. doi: 10.1099/0022-1317-76-6-1401

8. Tsai MH, Lin X, Shumilov A, Bernhardt K, Feederle R, Poirey R, et al. The biological properties of different Epstein-Barr virus strains explain their association with various types of cancers. *Oncotarget* (2017) 8(6):10238–54. doi: 10.18632/oncotarget.14380

9. Slabik C, Kalbarczyk M, Danisch S, Zeidler R, Klawonn F, Volk V, et al. CAR-T cells targeting Epstein-Barr virus gp350 validated in a humanized mouse model of EBV infection and lymphoproliferative disease. *Mol Ther Oncol* (2020) 18:504–24. doi: 10.1016/j.omto.2020.08.005

10. Stripecke R, Carmen Villacres M, Skelton D, Satake N, Halene S, Kohn D. Immune response to green fluorescent protein: implications for gene therapy. *Gene Ther* (1999) 6 (7):1305–12. doi: 10.1038/sj.gt.3300951

11. Wagner DL, Koehl U, Chmielewski M, Scheid C, Stripecke R. Review: Sustainable clinical development of CAR-T cells - switching from viral transduction towards CRISPR-cas gene editing. *Front Immunol* (2022) 13:865424. doi: 10.3389/fimmu.2022.865424

12. Cheung ST, Huang DP, Hui AB, Lo KW, Ko CW, Tsang YS, et al. Nasopharyngeal carcinoma cell line (C666-1) consistently harbouring Epstein-Barr virus. *Int J Cancer* (1999) 83(1):121–6. doi: 10.1002/(sici)1097-0215(19990924)83:1<121::aid-ijc21>3.0.co;2-f

13. Lin W, Yip YL, Jia L, Deng W, Zheng H, Dai W, et al. Establishment and characterization of new tumor xenografts and cancer cell lines from EBV-positive nasopharyngeal carcinoma. *Nat Commun* (2018) 9(1):4663. doi: 10.1038/s41467-018-06889-5

14. June CH, O'Connor RS, Kawalekar OU, Ghassemi S, Milone MC. CAR T cell immunotherapy for human cancer. *Science* (2018) 359(6382):1361–5. doi: 10.1126/science.aar6711

15. Song EZ, Milone MC. Pharmacology of chimeric antigen receptor-modified T cells. *Annu Rev Pharmacol Toxicol* (2021) 61:805–29. doi: 10.1146/annurev-pharmtox-031720-102211

16. Olbrich H, Slabik C, Stripecke R. Reconstructing the immune system with lentiviral vectors. *Virus Genes* (2017) 53(5):723–32. doi: 10.1007/s11262-017-1495-2

17. Zhao Z, Condomines M, van der Stegen SJC, Perna F, Kloss CC, Gunset G, et al. Structural design of engineered costimulation determines tumor rejection kinetics and persistence of CAR T cells. *Cancer Cell* (2015) 28(4):415–28. doi: 10.1016/j.ccell.2015.09.004

18. Graham CE, Jozwik A, Quartey-Papafio R, Ioannou N, Metelo AM, Scala C, et al. Gene-edited healthy donor CAR T cells show superior anti-tumour activity compared to CAR T cells derived from patients with lymphoma in an *in vivo* model of high-grade lymphoma. *Leukemia* (2021) 35(12):3581–3584. doi: 10.1038/s41375-021-01324-z

19. Aleksandrova K, Leise J, Priesner C, Melk A, Kubaink F, Abken H, et al. Functionality and cell senescence of CD4/ CD8-selected CD20 CAR T cells manufactured using the automated CliniMACS Prodigy(R) platform. *Transfus Med Hemother* (2019) 46(1):47–54. doi: 10.1159/000495772

20. Heslop HE, Slobod KS, Pule MA, Hale GA, Rousseau A, Smith CA, et al. Long-term outcome of EBV-specific T-cell infusions to prevent or treat EBV-related lymphoproliferative disease in transplant recipients. *Blood* (2010) 115(5):925–35. doi: 10.1182/blood-2009-08-239186

21. Bollard CM, Heslop HE. T Cells for viral infections after allogeneic hematopoietic stem cell transplant. *Blood* (2016) 127(26):3331–40. doi: 10.1182/blood-2016-01-628982

22. Chia WK, Teo M, Wang WW, Lee B, Ang SF, Tai WM, et al. Adoptive T-cell transfer and chemotherapy in the first-line treatment of metastatic and/or locally recurrent nasopharyngeal carcinoma. *Mol Ther* (2014) 22(1):132–9. doi: 10.1038/mt.2013.242

23. Leen AM, Bollard CM, Mendizabal AM, Shpall EJ, Szabolcs P, Antin JH, et al. Multicenter study of banked third-party virus-specific T cells to treat severe viral infections after hematopoietic stem cell transplantation. *Blood* (2013) 121(26):5113–23. doi: 10.1182/blood-2013-02-486324

24. Tang X, Zhou Y, Li W, Tang Q, Chen R, Zhu J, et al. T Cells expressing a LMP1-specific chimeric antigen receptor mediate antitumor effects against LMP1-positive nasopharyngeal carcinoma cells *in vitro* and in vivo. *J BioMed Res* (2014) 28(6):468–75. doi: 10.7555/JBR.28.20140066

25. Dragon AC, Zimmermann K, Nerreter T, Sandfort D, Lahrberg J, Kloss S, et al. CAR-T cells and TRUCKs that recognize an EBNA-3C-derived epitope presented on HLA-B*35 control Epstein-Barr virus-associated lymphoproliferation. *J Immunother Cancer* (2020) 8(2). doi: 10.1136/jitc-2020-000736

26. Olbrich H, Theobald SJ, Slabik C, Gerasch L, Schneider A, Mach M, et al. Adult and cord blood-derived high affinity gB-CAR-T cells effectively react against human cytomegalovirus infections. *Hum Gene Ther* (2020) 31(7-8):423–439. doi: 10.1089/hum.2019.149

27. Carrillo MA, Zhen A, Zack JA, Kitchen SG. New approaches for the enhancement of chimeric antigen receptors for the treatment of HIV. *Transl Res* (2017) 187:83–92. doi: 10.1016/j.trsl.2017.07.002

28. Sautto GA, Wisskirchen K, Clementi N, Castelli M, Diotti RA, Graf J, et al. Chimeric antigen receptor (CAR)-engineered T cells redirected against hepatitis c virus (HCV) E2 glycoprotein. *Gut* (2016) 65(3):512–23. doi: 10.1136/gutjnl-2014-308316

frontiers | Frontiers in Immunology

TYPE Original Research
PUBLISHED 03 February 2023
DOI 10.3389/fimmu.2023.1085547

Check for updates

OPEN ACCESS

EDITED BY
Anand Rotte,
Arcellx Inc., United States

REVIEWED BY
Sadhak Sengupta,
Triumvira Immunologics, Inc., United States
Meenakshi Hegde,
Baylor College of Medicine, United States

*CORRESPONDENCE
Ravi V. Bellamkonda
ravi@emory.edu

SPECIALTY SECTION
This article was submitted to Cancer Immunity and Immunotherapy, a section of the journal Frontiers in Immunology

RECEIVED 31 October 2022
ACCEPTED 04 January 2023
PUBLISHED 03 February 2023

CITATION
Swan SL, Mehta N, Ilich E, Shen SH, Wilkinson DS, Anderson AR, Segura T, Sanchez-Perez L, Sampson JH and Bellamkonda RV (2023) IL7 and IL7 Flt3L co-expressing CAR T cells improve therapeutic efficacy in mouse EGFRvIII heterogeneous glioblastoma.
Front. Immunol. 14:1085547.
doi: 10.3389/fimmu.2023.1085547

COPYRIGHT
© 2023 Swan, Mehta, Ilich, Shen, Wilkinson, Anderson, Segura, Sanchez-Perez, Sampson and Bellamkonda. This is an open-access article distributed under the terms of the Creative Commons Attribution License (CC BY). The use, distribution or reproduction in other forums is permitted, provided the original author(s) and the copyright owner(s) are credited and that the original publication in this journal is cited, in accordance with accepted academic practice. No use, distribution or reproduction is permitted which does not comply with these terms.

IL7 and IL7 Flt3L co-expressing CAR T cells improve therapeutic efficacy in mouse EGFRvIII heterogeneous glioblastoma

Sheridan L. Swan[1], Nalini Mehta[1], Ekaterina Ilich[1], Steven H. Shen[2,3,4], Daniel S. Wilkinson[2], Alexa R. Anderson[1], Tatiana Segura[1,5], Luis Sanchez-Perez[2,3,6], John H. Sampson[2,3,4,6] and Ravi V. Bellamkonda[7,8]*

[1]Department of Biomedical Engineering, Pratt School of Engineering, Duke University, Durham, NC, United States, [2]Duke Brain Tumor Immunotherapy Program, Department of Neurosurgery, Duke University Medical Center, Durham, NC, United States, [3]The Preston Robert Tisch Brain Tumor Center, Duke University Medical Center, Durham, NC, United States, [4]Department of Pathology, Duke University Medical Center, Durham, NC, United States, [5]Clinical Science Departments of Neurology and Dermatology, Duke University, Durham, NC, United States, [6]Department of Neurosurgery, Duke University Medical Center, Durham, NC, United States, [7]Department of Biology, Emory University, Atlanta, GA, United States, [8]Wallace H. Coulter Department of Biomedical Engineering, Emory University, Atlanta, GA, United States

Chimeric antigen receptor (CAR) T cell therapy in glioblastoma faces many challenges including insufficient CAR T cell abundance and antigen-negative tumor cells evading targeting. Unfortunately, preclinical studies evaluating CAR T cells in glioblastoma focus on tumor models that express a single antigen, use immunocompromised animals, and/or pre-treat with lymphodepleting agents. While lymphodepletion enhances CAR T cell efficacy, it diminishes the endogenous immune system that has the potential for tumor eradication. Here, we engineered CAR T cells to express IL7 and/or Flt3L in 50% EGFRvIII-positive and -negative orthotopic tumors pre-conditioned with non-lymphodepleting irradiation. IL7 and IL7 Flt3L CAR T cells increased intratumoral CAR T cell abundance seven days after treatment. IL7 co-expression with Flt3L modestly increased conventional dendritic cells as well as the CD103+XCR1+ population known to have migratory and antigen cross-presenting capabilities. Treatment with IL7 or IL7 Flt3L CAR T cells improved overall survival to 67% and 50%, respectively, compared to 9% survival with conventional or Flt3L CAR T cells. We concluded that CAR T cells modified to express IL7 enhanced CAR T cell abundance and improved overall survival in EGFRvIII heterogeneous tumors pre-conditioned with non-lymphodepleting irradiation. Potentially IL7 or IL7 Flt3L CAR T cells can provide new opportunities to combine CAR T cells with other immunotherapies for the treatment of glioblastoma.

KEYWORDS

CAR T cells, glioblastoma, IL7, Flt3L, dendritic cells, T cell abundance

Introduction

Glioblastoma (GBM) is a highly aggressive cancer and the most common malignant brain tumor (1). While current treatments of resection, radiotherapy, and temozolomide (TMZ) have doubled two-year survival rates to 18%, median survival remains around 14 months (2, 3). Chimeric antigen receptor (CAR) T cell therapy has shown promise in B cell non-Hodgkin's lymphoma patients with 49% complete remission (4). Unfortunately, CAR T cell therapy is less successful in GBM with an overall median survival ranging from 7 to 24 months in various clinical trials (5–7). We sought out to enhance the efficacy of CAR T cell therapy in GBM by improving intratumoral CAR T cell abundance and modulating host immune cells in tumors pre-conditioned with non-lymphodepleting irradiation.

Lymphodepleting pre-conditioning using irradiation and/or chemotherapy can improve CAR T cell abundance by killing tumor cells, reducing competition for IL7 and IL15, and decreasing regulatory T cells (8–11). CAR T cell abundance in the peripheral blood was enhanced one week and four weeks post-infusion in neuroblastoma patients using lymphodepleting pre-conditioning (12). Despite these benefits, lymphodepletion severely reduces the host immune system. New strategies are needed to enhance CAR T cell abundance while preserving key immune cells like dendritic cells (DCs). DCs are antigen-presenting cells that generate specific T cell responses to combat disease. Exposure to 4 Gy irradiation depleted mouse splenic DCs whereas 0.5 Gy preserved around half of host DCs (13). In patients, tumor infiltrating lymphocytes can recognize and kill autologous tumor cells (14–16). Thus, there is a balancing act between the positive anti-tumor effects of lymphodepletion and the preservation of immune cells to maximize immunotherapeutic potential.

Significant efforts have been made to modify CAR T cells to improve intratumoral abundance. Modification of CAR T cells with a constituently active IL7 receptor enhanced CAR T cell expansion and survival in metastatic neuroblastoma and xenograft mouse models (17). However, this method was limited to intrinsically increasing the abundance of CAR T cells without targeting neighboring immune cells. IL7 is an attractive candidate to enhance the anti-tumor response of CAR T cells due to several key impacts on T cell biology. IL7 signaling in T cells promotes survival, proliferation, and, in certain circumstances, increases memory T cell formation and T cell receptor repertoire diversity (18–21). In comparison to IL2, IL12, and IL15, IL7 has shown low toxicity at a range of doses in clinical trials (22–26). However, IL7 has a limited half-life, around 9 hours in clinical studies, although some modifications have expanded this to 63 hours (26, 27). To circumvent poor half-life and localize IL7 delivery, CAR T cells can be engineered to secrete IL7. CAR T cells co-expressing IL7 and CCL19 or CCL21 improved overall survival and memory T cell formation in cyclophosphamide pretreated mastocytoma and pancreatic models (28, 29). These cells showed a complete response in 4 of 7 patients with refractory lymphoma when combined with anti-PD1 treatment (30). In a B cell lymphoma model, IL7 expressing CAR T cells have been shown to be in a less differentiated state with enhanced persistence (31). In glioma models, the use of IL7 is beginning to be explored. Subcutaneous delivery of modified IL7 increased systemic cytotoxicity of CD8 T cells and improved survival with co-administration of irradiation and temozolomide (TMZ) (32, 33). This therapy is in an ongoing clinical trial (NCT03687957) of intramuscular injections of modified IL7 in gliomas with irradiation/TMZ administration. While there is limited research on local IL7 delivery in brain tumors, one study demonstrated that co-delivery of intravenous CAR T cells with intratumoral IL7-loaded oncolytic adenovirus increased survival in GBM xenografts (34). These CAR T cells showed improved abundance but also increased exhaustion *in vivo*.

Another challenge of CAR T cell therapy is antigen heterogeneity resulting in the immunological escape of antigen-negative tumor cells. The epidermal growth factor receptor variant III (EGFRvIII) mutation can be found in approximately 30 – 40% of GBMs at varying levels and locations within a single tumor (35–38). Patients with recurrent GBM treated with a single dose of EGFRvIII CAR T cells experienced EGFRvIII antigen loss (39). Therefore, it is critical to utilize preclinical models that capture antigen heterogeneity to understand clinical translation. One approach utilized synNotch CAR T cells that have multi-antigen circuits for priming and killing in patient-derived xenografts (40). SynNotch CAR T cells significantly increased survival compared to conventional CAR T cells. While this animal model best represents patient heterogeneity, the use of immunocompromised mice eliminated the investigation of the endogenous immune response. Another approach delivered CAR T cells with oncolytic virus in a syngeneic GBM model with 100% or 10% EGFRvIII positive tumors (41). CAR T cells pre-loaded with virus in combination with oncolytic virus demostrated better therapeutic outcomes in 100% EGFRvIII positive tumors whereas 10% EGFRvIII positive tumors had limited efficacy. Similarly, in another study, CAR T cells in combination with a CAR T cell-boosting vaccine showed reduced efficacy with increasing ratios of antigen-negative tumors (42). Thus, it is critical to assess CAR T cell therapies in antigen heterogeneous tumors.

Maintaining the endogenous immune system is critical for mounting a T cell mediated response in antigen heterogeneous tumors. CAR T cell therapy has been shown to have enhanced efficacy in immunocompetent mice compared to immunodeficient mice (43). Endogenous T cells harvested from CAR T cell treated mice demonstrated significant anti-tumor activity *in vitro* and *in vivo* (43). Thus, enhancing the endogenous immune response could improve CAR T cell efficacy. Fms-like tyrosine kinase receptor 3 ligand (Flt3L) is a cytokine and growth factor essential for DC differentiation, expansion, and survival (44, 45). cDC1 is a key DC subset, known for surface expression XCR1, that can promote an anti-tumor CD8 T cell response (46). Therefore, increasing intratumoral cDC1 populations can potentially improve existing immunotherapies. Injections of Flt3L significantly increased CD103+ DCs (migratory DCs) in B16-OVA tumors (47). Another study, engineered CAR T cells to secrete Flt3L in Her2 tumors (13). These Flt3L CAR T cells increased conventional DCs and, in conjunction with polyinosinic-polycytidylic acid (poly(I:C)) and anti-41BB, enhanced T cell receptor diversity and epitope spreading. While promising, there are limited studies of Flt3L in the brain. Intratumoral injection of adenoviruses mediating tumor killing and delivering Flt3L in a rat GBM model resulted in increased plasmacytoid DCs (pDCs) and 70% long term survival (48, 49). A phase I dose escalation of this therapy in the glioma resection cavity demonstrated safety and promising preliminary survival outcomes (NCT01811992) (50). As far as we are aware, the exploration of Flt3L expression in the context of CAR T cell therapy in GBM has not been investigated.

In this study, we explored the effects of intratumoral delivery of CAR T cells expressing IL7 and/or Flt3L in a syngeneic EGFRvIII heterogeneous GBM model. We utilized non-lymphodepleting preconditioning to balance preserving the endogenous immune system while retaining the benefits of irradiation. IL7 and IL7 Flt3L CAR T cells enhanced intratumoral CAR T cell abundance and IL7 co-expression with Flt3L increased CD103+XCR1+ dendritic cells. IL7 and IL7 Flt3L CAR T cells enhanced overall survival in mouse EGFRvIII antigen heterogeneous tumors.

Materials and methods

Cell lines and media

CT2A, CT2A-EGFRvIII, and HEK293 cells were graciously donated by Dr. John Sampson's lab. CT2A and CT2A-EGFRvIII were modified to express GFP and/or luciferase by transducing lentivirus made by the Duke Viral Core Facility (Addgene #89608 and #105621). Tumor cell lines were referred to as CT2A-GFP-Luc or 2A and CT2A-EGFRvIII-Luc or vIII. The presence of human EGFRvIII on CT2A-EGFRvIII-Luc was confirmed by flow cytometry with anti-human EGFRvIII antibody [L8A4] (Kerafast) (data not shown). Tumor cell lines were cultured in complete DMEM (cDMEM): DMEM, 10% FBS, 1%: Pen/Strep, Non-Essential Amino Acids (NEAA), and L-Glutamine. HEK293 cells, unless otherwise noted, were cultured in D10 media: DMEM with 4.5 mg/ml glucose and 0.11 mg/ml pyruvate (Gibco) + 10% FBS. T cells were cultured in T cell media (TCM) with or without human IL2 (donated from Dr. Sampson's lab): RPMI 1640 (w/ L-glutamine and sodium pyruvate), 10% FBS, 1%: Pen/Strep, NEAA, sodium pyruvate, L-glutamine, and 0.1%: β2-mercaptoethanol (Thermo Fischer), and 50 mg/mL gentamycin (Sigma-Aldrich).

Retroviral CAR T cell production

CAR T cells were made using a previously established protocol (11). The pMSGV plasmid backbone with MSCV promoter was used to make third generation CAR T cells. Plasmids contained the human 139 single-chain antibody variable fragment (scFv) specific for EGFRvIII (19) along with transmembrane mouse CD8 and intracellular mouse CD3z, CD28, and 4-1BB signaling domains to enhance proliferation and function (51). When appropriate, plasmids were further modified to express mouse IL7 and/or Flt3L using an N-terminal secretion signal and P2A and/or T2A cleavage peptides. To make retrovirus, HEK293 cells were plated on a poly-l-lysine (Millipore Sigma) coated petri dish in D10 media. The following day, fresh D10 media was added to HEK293 cells and transfected using the previously described helper plasmid, pCL-Eco (Addgene), and lipofectamine 2000 (Invitrogen) in OptiMEM (Gibco). Spleens from 6- to 12-week-old female C57B6/J mice (Jackson Labs) were made into a single cell suspension using a 70 μm filter and washed with TCM without IL2. Cells were resuspended in RBC lysis buffer (BD) for 2 minutes and quenched with TCM. Cells were resuspended at 2x10^6 cells/mL in TCM with 2 μg/mL Concanavalin A (Sigma-Aldrich) and 50 IU/mL IL2 and plated in 24 well plates. The next day, fresh TCM without IL2 was added to HEK293 cells and, separately, a 24 well plate was coated with 25 μm/mL RetroNectin (Takara Bio) overnight at 4C. Concanavalin A activated splenocytes were transduced at 1x10^6 cells/mL with viral supernatant and spun for 1.5 hours at 2000 RPM at 32C. Fresh TCM with IL2 was added to each well. CAR expression on cells was assessed through flow cytometry on day 4 using a tetrameric peptide recognizing the CAR, CD3 Pe/Cy7 (17A2 BioLegend #100220), and CD8 PE (53-6.7 BioLegend #100708) on the NovoCyte 2060 or Cytek NL-3000. CAR T cells were used for *in vivo* experiments on day 5.

Tetrameric peptide construction

A fluorescently labeled peptide to identify CAR T cells specific to EGFRvIII was made similar to a previous study (11). A custom peptide conjugated with biotin (JPT Peptide Technologies) was added in a 10:1 molar ratio with streptavidin-Alexa 647 (Invitrogen) in PBS to make a 1 mg/mL peptide solution. After incubation for 1 hour at room temperature in the dark, the solution was diluted to 0.5 mg/mL in PBS and incubated for another 2 hours. The solution was further diluted to 0.1 mg/mL and passed through a 30 kDa MWCO polyethersulfone filter (Millipore Sigma) to remove the free conjugated peptide. The tetrameric peptide was aliquoted and stored in the dark at 4C until use.

In vitro enzyme-linked immunosorbent assay

ELISAs determined protein secretion of CAR T cells cultured alone or with tumor cells. 1x10^4 tumor cells in 200 μL of cDMEM were allowed to adhere for 5 hours in a 96-well plate. For the vIII + 2A condition, tumor cells were mixed in a 1:1 ratio with 0.5x10^4 EGFRvIII-positive and 0.5x10^4 EGFRvIII-negative cells before plating. cDMEM was removed from tumor cells and 1x10^5 CAR T cells were plated in 200 μL TCM without IL2. After 24 hours, the supernatant was harvested and frozen at -80C until assayed with IL7, Flt3L, IFNγ, or Granzyme B ELISA kits (R&D Systems) using the Spectramax i3x plate reader.

In vitro bioluminescence assay

We used the bioluminescent signal from tumor cells as a surrogate marker for the tumor killing ability of CAR T cells. 1x10^4 tumor cells in 200 μL cDMEM were plated for 5 hours in an opaque 96-well plate. cDMEM was removed and replaced with 1x10^5 CAR T cells in 200 μL TCM without IL2. After 24 or 72 hours, Xenolight-D-luciferin (Perkin Elmer) was added at 150 μg/mL and incubated for 5 min until acquiring the signal on a Spectramax i3x plate reader (24 hour data not shown).

Cell proliferation assay

We assessed CAR T cell proliferation by co-culturing CAR T cells with EGFRvIII-positive tumor cells. 1x10^6 CT2A-EGFRvIII-Luc cells were allowed to adhere to a 24-well plate for 5 hours.

Separately, CAR T cells were stained per the manufacturer's protocol with CellTrace Far Red (Thermo Fischer) for 20 minutes at 37C. Tumor media was removed from tumor cells and 1x10^6 CAR T cells were plated in TCM without IL2. Cells were incubated at 37C for three days and processed for flow cytometry. Samples were stained using Live/Dead Fixable Green reagent (Thermo Fischer) and anti-mouse CD8a PE antibody (53-6.7 BioLegend #100708).

Surgical procedure

6- to 12-week-old female C57B6/J mice (Jackson labs) were used in accordance with the approved Duke Institutional Animal Care and Use Committee (IACUC) protocol. Mice were given Buprenorphine SR at 1 mg/kg and anesthetized using 3 to 5% isoflurane or 90 mg/kg ketamine with 10 mg/kg xylazine. Mouse skin was shaved and cleaned thrice with chlorhexidine and 70% ethanol. A small incision exposed the cranium and 1 to 2 drops of 0.25% bupivacaine were placed on the skull. Using a stereotaxic microinjector, a Hamilton syringe with a 25-gauge needle injected either 55,000 CT-2A-EGFRvIII-Luc or 75,000 CT2A-GFP-Luc plus 75,000 CT2A-EGFRvIII-Luc cells 1.5 mm posterior and left of bregma and 4 mm deep in 5 µL of 4000 cP methylcellulose (Sigma-Aldrich) with DMEM/F-12 (Thermo Fischer), sodium bicarbonate (Sigma-Aldrich), and HEPES (Thermo Fischer). The injection site was sealed with bone wax and wound clips closed the incision. Animals were monitored every two days for signs of distress or illness. 5 days following tumor injection, animals were imaged with IVIS Kinetic (Caliper Life Sciences) using an injection of 0.2 µm filtered Xenolight D-luciferin (Perkin Elmer) at 150 mg/kg body weight. Animals were randomized into treatment groups based on tumor size to allow for an equal distribution in each group. Animals without tumors based on bioluminescent imaging were excluded. On the indicated day, animals were irradiated with 0.5 Gy or 5 Gy irradiation using a Cesium-irradiator. The following day, animals were injected with 2x10^6 CAR T cells in 24 µL PBS at 60 µL/min at the same injection location.

In vivo flow cytometry

Animals were euthanized 14 days following tumor inoculation. The brain was harvested and processed for flow cytometry based on previous protocols (52, 53). Briefly, animals were perfused with cold HBSS without Ca/Mg and the tumor-bearing hemisphere was placed in a digestion buffer (TCM without IL2, 50 mg/mL DNase I grade II from bovine pancreas (Roche), and 20,000 units/mL collagenase type IV (Gibco)). The digested tissue suspension was passed through a 100 µm filter and incubated on a tube rotator at 37C for 30 minutes. The suspension was filtered using a 70 µm filter, spun down at 500g, and resuspended in a 25% Percoll density gradient (GE Healthcare). After centrifuging at 521g at 18C for 20 minutes, the suspension went through multiple washes, red blood cell lysis buffer, and cell counting. The cells were blocked in mouse fc-block (BD biosciences), and stained with live/dead stain and antibodies. The following are the antibodies with clone noted and reagents from BioLegend unless otherwise noted: Zombie Aqua fixable viability kit (#423101), CD45 BV711 (30-F11 #103147), CD3 APC/Cy7 (17A2 #100222), CD8 BV650 (53-6.7 #100742), CD4 PE/Cy5 (GK1.5 #100410), CAR tetramer Alexa 647, PD-1 BV421 (29F.1A12 #135221), TIM3 BV605 (RMT3-23 #119721), LAG3 PE (C9B7W #125208), CD25 PE/Cy7 (3C7 #101916), CD69 BV785 (H1.2F3 #104543), CD11b APC/Cy7 (M1/70 #101226), F4/80 BV421 (BM8 #123137), CD11c BV605 (N418 #117334), MHCII PE (M5/114.15.2 #107607), CD103 PE-CF594 (M290 BD Biosciences #565849), CD45R PE/Cy7 (RA3-6B2 #103222), XCR1 APC (ZET #148206), CD86 BV785 (GL-1 #105043), and CD40 PE/Cy5 (3/23 #124618). The stained cells remained at 4C until read immediately on the BD LSRFortessa X-20. Animal studies were replicated twice. Data was analyzed using FlowJo v10.7.2.

Bulk RNA and TCR sequencing

RNA was isolated from the tumor-bearing hemisphere and extracted using the RNeasy Lipid Tissue Mini kit (Qiagen). RNA purity was determined using the NanodropOne (Invitrogen) along with integrity and concentration measured with a Fragment Analyzer. The bulk RNA sequencing library was prepared using polyA tail enrichment with the KAPA Stranded mRNA-Seq kit (Roche). Sequencing was performed on the NovaSeq (Illumina) with 151 paired-end reads. For TCR sequencing, RNA was further processed with the mouse T-cell Receptor Panel QIAseq Immune Repertoire RNA Library Kit (Qiagen) using unique molecular indices with gene specific primers. Samples were run on MiSeq Version 3 (Illumina) using 300 paired-end reads. TCRseq data was analyzed using the online Qiagen platform with the IMSEQ algorithm (54). RStudio (R 4.2.1) was utilized for data processing, visualization, and statistics. For bulk RNAseq data, quality control was performed using FastQC/MultiQC. Star Alignment was run using default parameters and soft clipping for the Illumina universal adapter sequence. FeatureCounts was used for expression quantification of alignment output. Downstream analysis of the FeatureCounts raw counts output matrix was performed using DESeq2 (version 1.36.0). For differential gene expression analysis, to find genetic differences from responders and non-responders determined by LUC counts, one sample from each group was excluded based on principal component analysis clustering. The alternative shrink estimator ashr with a benjamini-hochberg correction was used to control for false discovery rates (FDR) (55). Differential gene expression was determined using an FDR < 0.1. The CIBERSORTx tool was used to infer cell fractions based on RNA sequencing data using the wild type samples from Seurat objects created from GSE197879 with S-mode batch correction and 100 permutations (56-58). Kyoto Encyclopedia of Genes and Genomes (KEGG) pathway analysis was performed using fast gene set enrichment on genes with a non-adjusted p-value < 0.05 (59). Cytosig analysis was performed using mean-centered log transformed data (60).

Statistical analysis

When applicable, data has been presented using the mean + or - SEM. ELISA data was normalized using 10^x before statistical analysis. When applicable, a one-way analysis of variance

(ANOVA) with Tukey's posthoc test was used for analysis. When noted in the figure legend, groups were compared within tumor types (vIII, vIII + 2A, or 2A). The Kaplan-Meier plot was used for the survival curve and significant differences were assessed using the log-rank Mantel-Cox test. For TCR sequencing diversity metrics, a Kruskal-Wallis test with Dunn's multiple comparisons was used to determine significance. A p-value of < 0.05 was considered significant. * = denotes significance to all other groups in the comparison. ns = denotes not significant. Unless otherwise noted, all statistical analysis was conducted using Graphpad Prism version 9.0.2.

Results

Construction and validation of IL7 and IL7 Flt3L co-expressing CAR T cells

Our first goal was to determine the functionality of IL7 Flt3L CAR T cells *in vitro*. We modified third generation CAR T cells by cloning mouse IL7 and/or Flt3L with an N-terminal secretion signal along with self-cleaving P2A and/or T2A peptides (Figure 1A). We confirmed no significant differences in the amount of CAR T cells from transduced splenocytes between CAR (vCAR), Flt3L (vFL), IL7 (vIL7), or IL7 Flt3L (vIL7FL) CAR T cells (Figure 1B). Additionally, cells were mostly CD8 CAR T cells due to the culture conditions. We then quantified secreted Flt3L and IL7 when CAR T cells were cultured alone or co-cultured with either CT2A-EGFRvIII-Luc (vIII), CT2A-GFP-Luc (2A) or 50% vIII and 50% 2A (vIII+2A) tumor cells. After 24 hours, we observed secretion of Flt3L and IL7 from CAR T cells programed to express those respective cytokines (Figure 1C). Interestingly, the expression of Flt3L remained stable despite the introduction of antigen-negative tumor cells, while IL7 expression seemed to diminish as 2A cells were introduced, although not significant. We further investigated delivering 50% vIL7 and 50% vFL, referred to as 7&3. While not significant, we did find lower levels of Flt3L for 7&3 compared to vFL and vIL7FL. We confirmed that CAR T cells secreted effector proteins through the expression of pro-inflammatory cytokine interferon gamma (IFNγ) and cytotoxic protein granzyme B (Supplementary Figure 1). Next, we measured tumor killing through a surrogate marker of bioluminescence signal due to luciferase expression in tumor cells. When CAR T cells were co-cultured with vIII the signal diminished compared to non-transduced splenocytes demonstrating effective elimination of tumor cells (Figure 1D). CAR T cells in the presence of vIII + 2A failed to eliminate luminescence signal. Notably, vCAR and vIL7 both significantly reduced luminescence signal compared to the non-transduced control when cultured with 2A for 72 hours. Since we confirmed IL7 secretion for CAR T cells, we assessed the functional effect of IL7 on T cell proliferation. CAR T cells were co-cultured with vIII at a 1:1 ratio and cellular proliferation was quantified after three days. Low proliferation was defined as the peak with the highest amount of signal, medium proliferation represented the intermediate population, and high proliferation reflected the population with the lowest signal (Figure 1E). In comparison to vCAR, vIL7 and vIL7FL showed a significant increase in the percentage of medium and high proliferating CD8 T cells (Figure 1F). Thus, IL7 secreted from vIL7 and vIL7FL had the capacity to increase proliferation *in vitro*.

IL7 and IL7 Flt3L expressing CAR T cells increased CAR T cell abundance in 5 Gy TBI EGFRvIII positive tumors

Since we observed increased proliferation of CAR T cells secreting IL7 *in vitro*, we assessed the intratumoral presence of CAR T cells 7 days after *in vivo* delivery. Previous studies utilizing TMZ for lymphodepleting pre-conditioning demonstrated peak CAR T cell abundance in the blood one week post-treatment and showed significant increases in intratumoral CAR T cells 7 days after treatment (11). 100% EGFRvIII positive tumors were inoculated into mice that received 5 Gy total body irradiation (TBI) the day before intracranial injection of CAR T cells (Figure 2A). One week after CAR T cell delivery, tumor tissue was processed for flow cytometry. vIL7 and vIL7FL significantly increased the CD8+ CAR T cell percentage of CD45+ cells compared to vCAR and vFL (Figure 2B). There was no change in CAR-negative (CAR-) T cells between groups. This is most likely due to the lymphodepletion caused by 5 Gy irradiation (13).

IL7 Flt3L CAR T cells increased CAR T cell and dendritic cell populations in EGFRvIII heterogeneous tumors treated with non-lymphodepleting irradiation

Next, we examined the ability of vIL7FL to alter immune cell populations in a more rigorous animal model. Animals were inoculated with tumors containing 50% EGFRvIII positive and 50% EGFRvIII negative cells. Prior to CAR T cell injection, a non-lymphodepleting dose (0.5 Gy) of irradiation was administered (Figure 3A). Compared to 100% EGFRvIII syngeneic mouse tumors, this model better recapitulates antigen heterogeneity while preserving the endogenous immune system and the anti-tumor benefits of irradiation. Using a multi-color flow cytometry panel, the tumor-bearing hemisphere was analyzed one week after CAR T cell delivery for T cells and dendritic cells (DCs) (Supplementary Figure 2). vIL7 and vIL7FL significantly increased intratumoral CAR T cells compared to vCAR (Figure 3B and Supplementary Figure 3). Interestingly, vIL7FL had significantly higher CD8 CAR T cells compared to all groups, including vIL7. This could suggest a synergistic effect from IL7 and Flt3L. There was no significant difference in CAR- CD8 T cells. The introduction of any CAR T cell significantly reduced the proportion of PD1+TIM3+LAG3+ of CAR- CD8 T cells, referred to as phenotypically exhausted T cells, compared to PBS. Notably, vIL7 significantly decreased exhausted T cells compared to vFL. Additionally, we assessed activation of CAR- T cells through expression of CD25 or CD69. While the proportion of CD25+ or CD69+ T cells of CD8 CAR- T cells did not significantly differ, vIL7 significantly increased absolute counts of CD69+ CD8 CAR- T cells compared to PBS, vCAR, and vFL (Supplementary Figure 3 and Figure 3B). Next, we investigated intratumoral conventional DCs (cDCs) due to their importance in antigen presentation. cDCs were classified by surface expression of CD45+F480-CD11c+CD11b-CD45R-MHCII+. vIL7FL enhanced intratumoral cDCs as well as the CD103+XCR1+ subset known as migratory antigen-presenting DCs (Figure 3C). There was no significant difference in plasmacytoid DCs.

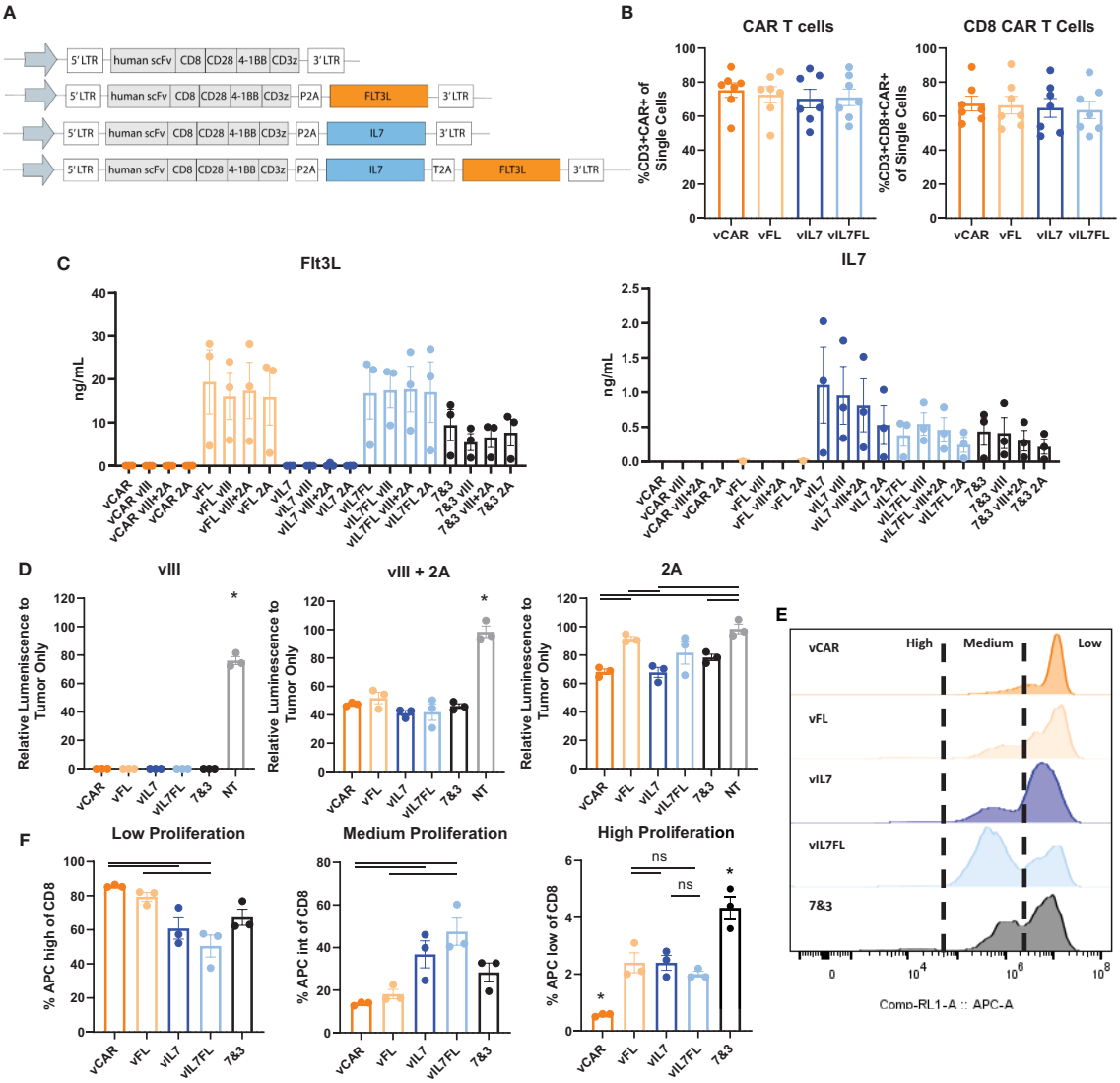

FIGURE 1
Construction and validation of IL7 and/or Flt3L CAR T cells. CAR T cells were made using activated mouse splenocytes and transduced on day 2. **(A)** Schematic of CAR T cell plasmids. **(B)** Flow cytometry of day 4 CAR T cells. Cells were stained with CD3, CD8, and a tetrameric peptide recognizing the CAR. **(C)** CAR T cells were cultured alone or co-cultured with tumor cells (vIII, vIII+2A, or 2A) with an effector:target (E:T) ratio of 10:1. 24 hours later the supernatant was collected for a Flt3L or IL7 ELISA. **(D)** CAR T cells were co-cultured with tumor cells with an E:T ratio of 10:1. 72 hours later bioluminescence signal was measured using a plate reader and normalized to tumor only signal. NT = non-transduced. **(E)** Cell proliferation of CAR T cells co-cultured with vIII tumor cells. CAR T cells were stained with CellTrace Far Red and plated at an E:T ratio of 1:1. After three days, cells were gated on live CD8 T cells and analyzed for APC expression indicating proliferation using a flow cytometer. Representative histograms of cell proliferation define low, medium, and high proliferation. **(F)** Quantification of cell proliferation from three replicates in one biological sample mean and SEM plotted. For all other experiments, each data point represents a biological replicate with mean and SEM plotted. Statistical analysis was conducted within each tumor group using a one-way ANOVA with a Tukey's multiple comparison test. * = denotes significance compared to all other groups. ns, not significant.

IL7 and IL7 Flt3L CAR T cells improved overall survival and altered gene expression in EGFRvIII heterogeneous tumors treated with non-lymphodepleting irradiation

We evaluated the therapeutic outcome of vIL7 and vIL7FL in EGFRvIII heterogeneous tumors treated with non-lymphodepleting irradiation. Animals were subjected to 0.5 Gy TBI 6 days after tumor inoculation with 50% EGFRvIII positive and 50% EGFRvIII negative tumor cells. On day 7, CAR T cells were delivered intracranially, and animals were monitored for survival. vIL7 and vIL7FL significantly enhanced survival compared to PBS, vCAR, and vFL (Figure 4A). Interestingly, vCAR and vFL had a survivor which could be due to the bystander effect from using irradiation (61). Bioluminescent imaging of tumors 5 days post-treatment indicated repression of tumor burden in vIL7 and vIL7FL (Supplementary Figure 4A). To understand the effect of vCAR, vIL7, or vIL7FL treatment on a transcriptional level, we evaluated tumor gene expression 7 days after CAR T cell delivery using bulk RNA sequencing. First, we assessed inferred cell fractions using CIBERSORTx. We utilized previously published single cell RNAseq data of mouse CD45 pre-sorted CT2A tumors to infer immune cell populations from bulk RNAseq data. The cDC1 population was significantly increased in vIL7FL compared to vIL7, which correlated with our flow cytometry

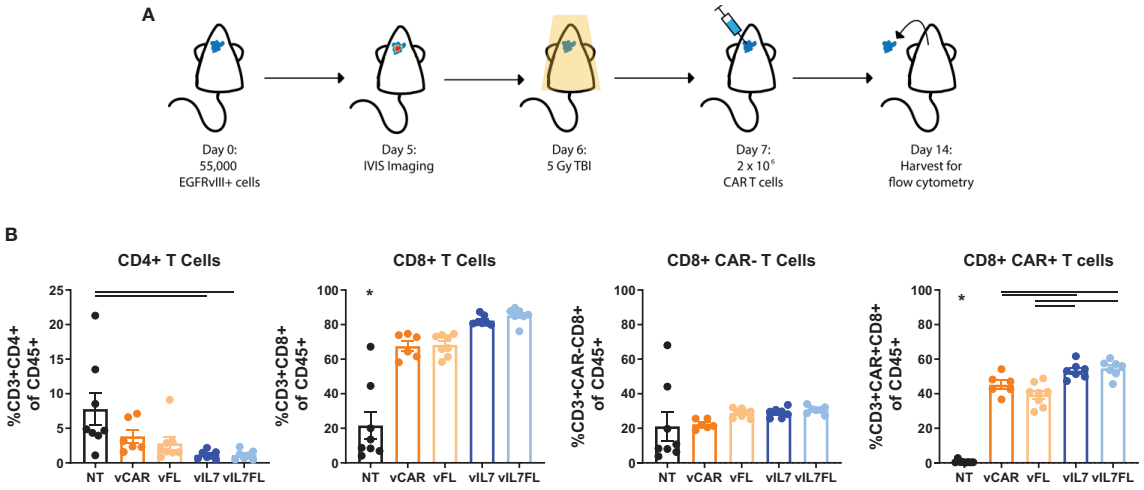

FIGURE 2
IL7 and IL7 Flt3L co-expressing CAR T cells increased the CD8 CAR T cell population in a 5 Gy TBI EGFRvIII homogenous model. **(A)** Experimental timeline. Animals were inoculated intracranially with 55,000 vIII tumor cells. Tumors were IVIS imaged five days later and subjected to 5 Gy irradiation on day 6. On day 7, 2x10^6 CAR T cells were injected intracranially. **(B)** The tumor was harvested for flow cytometry on day 14 and analyzed for T cell populations (n=6-8). A one-way ANOVA with a Tukey's multiple comparison test determined significance. Mean and SEM are plotted. * = denotes significance compared to all other groups.

data (Figure 4B). Since EGFRvIII positive tumor cells expressed EGFRvIII and luciferase (LUC) and EGFRvIII negative tumor cells expressed GFP and LUC, we used these transgenes as a surrogate markers for antigen-positive and negative tumor cells. GFP and LUC transgenes displayed a responder and non-responder effect (Figure 4C). The principal component analysis revealed that one sample from each group did not cluster with the other samples and samples were differentiated by LUC counts (Figure 4D). Additionally, the responder status did not necessarily indicate increased CAR reads (Figure 4D). Thus, to determine transcriptional differences between responders and non-responders to generate hypotheses for future studies we excluded the following samples that didn't cluster: vCAR 3, vIL7 2, and vIL7FL 3. LUC and GFP were differentially expressed between vIL7 vs. vCAR and vIL7FL vs vCAR (Figure 4E). This was to be expected based on our exclusion criteria. There were no differentially expressed genes between vIL7 vs vIL7FL. vCAR treatment upregulated various differentially expressed immunosuppressive and immunostimulatory cytokines, including IL7 (Figure 4F). KEGG pathway analysis found enrichment in the neuroactive ligand receptor interaction pathway (Figure 4G). Upregulation of this pathway has been associated with glioblastoma (62, 63). However, one study found GBM patients with deficiencies in the neuroligand receptor interaction pathway have a poor prognosis due to mutations or low expression of Calcr (64). vIL7 and vIL7FL increased differential gene expression of Calcr compared to vCAR. However, the role of Calcr in GBM remains ambiguous. One common adverse event in CAR T cell therapy is cytokine release syndrome (CRS). CRS can occur 1 to 14 days post-CAR T cell therapy resulting in elevated levels of cytokines, including IL2, IL6, IL10, and TNF (65, 66). We did not observe overt weight loss 14 or 15 days post CAR T cell delivery in either experimental cohort (Supplementary Figure 4B). Additionally, the Cytosig platform was used to predict cytokine signaling in tumors 7 days post CAR T cell injection using gene expression data from bulk RNA sequencing (60). While there was a slight upregulation of IL6 and CD40L, which is known to induce IL6, TNF and IL2 were down-regulated in the treatment responders (Supplementary Figure 4C) (67, 68).

IL7 and IL7 Flt3L CAR T cells effect on T cell receptor repertoire diversity

Finally, we investigated the impact of vIL7FL on T cell receptor beta chain (TRBC) diversity. We assessed the T cell receptor (TCR) alpha and beta chains due to their importance in immunotherapy (69). The alpha and beta protein chains are created through recombination of variable (V), joining (J) and, in certain cases, diversity (D) gene segments. The alpha chain utilizes V-J recombination, while the beta chain uses V-(D)J recombination. While both are required together for antigen recognition, the TRBC is recognized as more uniquely expressed in T cells than the alpha chain, due to the additional D recombination and allelic exclusion, and therefore is the focus of this study (70–72). First, we compared the observed number of clonotypes, and asymptotic diversity metrics found by extrapolating the unique molecular indices to infinity (Figure 5A). The asymptotic number of clonotypes was found using chao 1 statistics. While not significant, vIL7FL tended to have more clonotypes and higher indexes of diversity. We then visualized V-J gene segment pairings between groups. vIL7FL qualitatively showed more combinations of V-J pairings than vCAR or vIL7 (Figure 5B). Finally, we assessed T cell epitope spreading of the top 10 clones. While vIL7 groups showed the highest peak frequency, there was no consistency between groups (Figure 5C). When assessing the CD3 receptor nucleotide sequence between groups, qualitatively vIL7FL had a dense representation of sequences (Figure 5D). We observed similar trends for the TCR alpha chain (Supplementary Figure 5). While not significant, we did observe the potential for vIL7FL to alter T cell diversity.

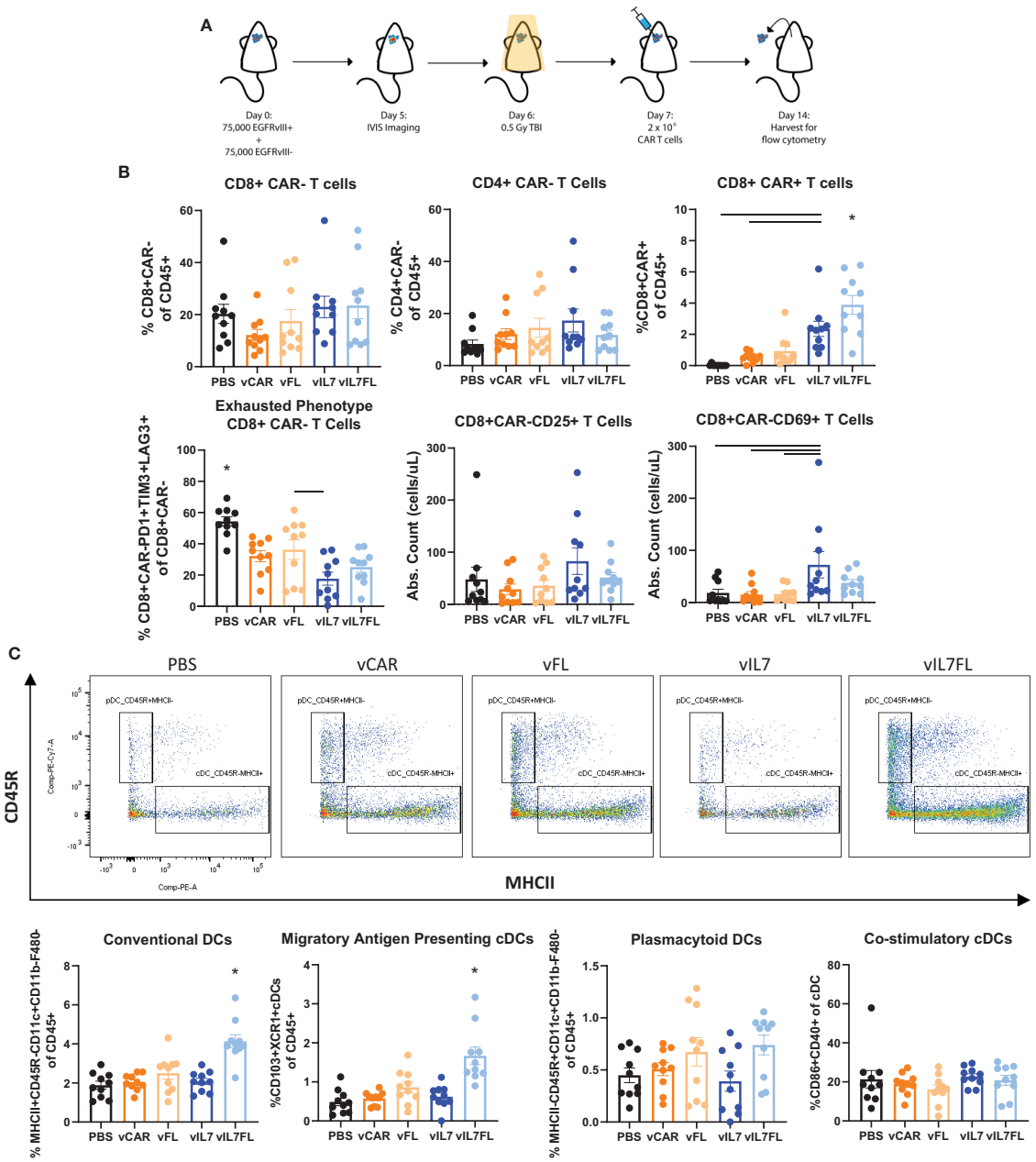

FIGURE 3
IL7 and IL7 Flt3L co-expressing CAR T cells increased CD8 CAR T cells and IL7 co-expression with Flt3L enhanced intratumoral DCs. **(A)** Schematic of experiment. Animals were inoculated with 50% vIII and 2A tumors and IVIS imaged 5 days later. On day 6, 0.5 Gy TBI was applied and 2x10^6 CAR T cells were injected intracranially the following day. **(B)** Flow cytometry was performed on the tumor-bearing hemisphere isolated on day 14 and split into two panels with the analysis of the T cell panel shown. **(C)** Analysis of DC populations using flow cytometry. Data represents a combination of two independent experiments (n=10). Statistical test was a one-way ANOVA with a Tukey's multiple comparison test with mean and SEM plotted. * = denotes significance compared to all other groups.

Discussion

CAR T cell therapy in GBM clinical trials has encountered significant challenges, including limited T cell trafficking to the tumor site, inadequate abundance, tumor antigen loss, tumor immunosuppression, and adverse effects (6, 73). While preclinical studies are making enormous strides in addressing these limitations, these models are mainly limited to immunocompromised/lymphodepleted mice and/or antigen homogenous glioma to achieve a therapeutic effect (40, 74–76). Here we utilized EGFRvIII heterogeneous glioma with non-lymphodepleting pre-conditioning to preserve the endogenous immune system and emulate antigen heterogeneity present in GBM. In our study, we demonstrated that IL7 expression in CAR T cells increased intratumoral CAR T cells, and co-expression with Flt3L enhanced cDC populations. IL7 and IL7 Flt3L CAR T cells, in combination with 0.5 Gy TBI, improved overall survival in EGFRvIII heterogeneous tumors.

We genetically modified third generation EGFRvIII CAR T cells to secrete mouse IL7 and/or Flt3L. Previous studies show the benefits of IL7 on T cell survival, proliferation, and memory T cell formation (18, 77, 78) and Flt3L on DC survival, differentiation, and expansion (44, 45). Similar

10.3389/fimmu.2023.1085547

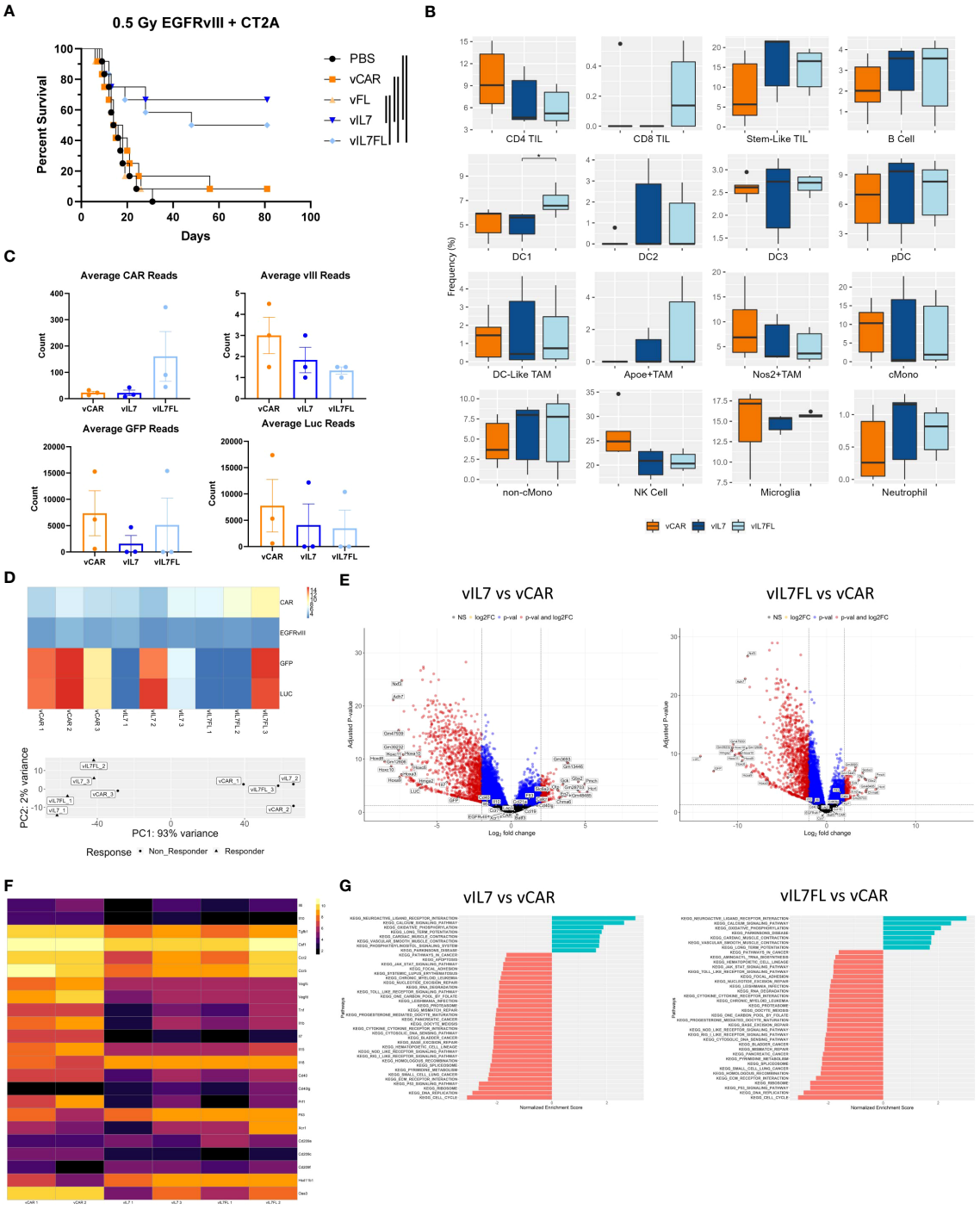

FIGURE 4
IL7 and IL7 Flt3L co-expressing CAR T cells increased survival in a 0.5 Gy TBI EGFRvIII heterogeneous model. Animals were inoculated with 50% vIII and 2A tumor cells and IVIS imaged 5 days later. **(A)** On day 6, 0.5 Gy TBI was applied and 2x10^6 CAR T cells were injected intracranially on day 7 and overall survival was assessed (n=12). Kaplan-Meier survival curves represent a combination of two independent experiments. Significance is noted with the log-rank Mantel-Cox test. **(B)** 7 days after tumor inoculation 0.5 Gy TBI was applied and 2x10^6 CAR T cells were injected intracranially on day 7. One week post CAR T cell injection, the tumor-bearing hemisphere was isolated for bulk RNA sequencing (n=3). **(C)** Transgene counts were found by averaging the lane reads in each sample. **(D)** Transgene heatmap using normalized data and principal component analysis. **(E)** Volcano plots with thresholds of log2 fold change = 2 and adjusted p-value = 0.05. **(F)** Normalized heatmap of selected differentially expressed genes. **(G)** KEGG analysis using non-adjusted p-value < 0.05 with an adjusted p-value of < 0.1 Differential expression between transgenes and all other genes was found using alternative shrink estimator ashr with a Benjamini-Hochberg correction with a FDR < 0.1.

to previous findings, IL7 signaling in CAR T cells enhanced cell proliferation *in vitro* (17, 28). When delivered in a 5 Gy TBI EGFRvIII homogenous tumor model, vIL7 and vIL7FL increased the proportion of intratumoral CD8 CAR T cells compared to conventional vCARs.

We assessed the efficacy of vIL7FL in a more rigorous model using 0.5 Gy TBI and 50% EGFRvIII positive and negative tumors. 0.5 Gy irradiation retains a proportion of leukocyte and splenic DC populations as opposed to 4 Gy irradiation, which severely depletes these cells (13).

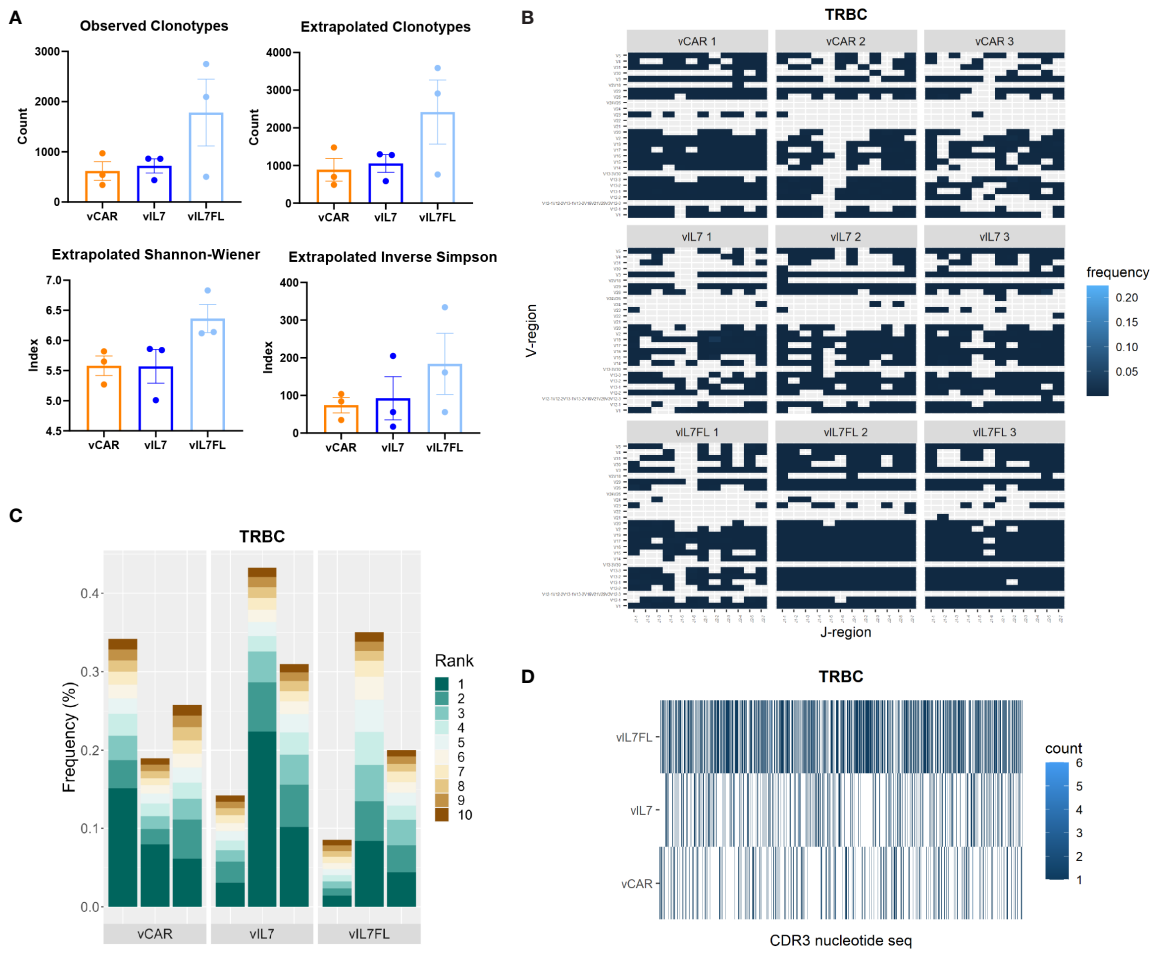

FIGURE 5
TRBC diversity of IL7 Flt3L co-expressing CAR T cells. Animals were inoculated with 50% vIII and 2A tumor cells and IVIS imaged 5 days later. On day 7, 0.5 Gy TBI was applied and 2x10^6 CAR T cells were injected intracranially the following day. RNA was extracted from the tumor-bearing hemisphere 7 days post CAR T cell injection and processed for immune repertoire sequencing (n = 3). **(A)** Diversity metrics of TRBC. Statistical analysis was a Kruskal-Wallis test with Dunn's multiple comparisons. **(B)** Heat map of V and J pairings of TRBC. **(C)** The frequency of the top 10 clonotypes of TRBC. **(D)** Visualization of TRBC clonotypes combing biological replicates.

Delivery of vIL7 and vIL7FL significantly increased intratumoral CD8 CAR T cells. Notably, vIL7FL increased CD8 CAR T cells compared to vIL7 CAR T cells *in vivo* despite tending to have lower mean secretion of IL7 (not significant) *in vitro*. This suggests the possibility of a synergistic effect of IL7 and Flt3L secretion on CAR T cell survival. Flt3L has been shown to prevent the decline of CD28 and IFNγ secretion in CD8 T cells as well as reduce PD-L1 expression on DCs and macrophages (79). However, we didn't observe significant differences in IFNγ secretion *in vitro*, PD1 expression on CAR T cells *in vivo*, or differential gene expression of PD-L1 (Supplementary Figures 1, 3). Interestingly, vIL7FL did not significantly enhance CD8 CAR T cells compared to vIL7 in the 5 Gy TBI model. Potentially, Flt3L is interacting with other immune cells in the 0.5 Gy model that were not present with 5 Gy TBI that promote CD8 CAR T cell survival. However, future studies of select populations would be necessary to determine this.

Additionally, we examined CAR- T cells because endogenous tumor infiltrating lymphocytes have the potential to recognize and kill autologous tumor cells (14–16). Delivering any CAR T cell significantly reduced the CAR- T cell exhaustion phenotype, furthermore vIL7 decreased exhaustion compared to vFL. While IL7 has been shown to reduce exhaustion and regulate metabolism in CAR T cells, we did not see any differences in the CAR+ T cell exhaustion phenotype, as exhaustion remained low in all T cell groups most likely due to the addition of the 4-1BB domain that has been shown to reduce exhaustion (Supplementary Figure 3) (31, 80). vIL7 enhanced absolute counts of CD8+CAR- CD69+ T cells compared to PBS, vCAR, and vFL. CD69 is surrogate marker of early T cell activation because it is rapidly produced after TCR engagement (81).

We evaluated the effect of vIL7FL on DC populations in the tumor-bearing hemisphere. In the steady-state mouse brain, subcutaneous Flt3L delivery has been shown to increase antigen-presenting cDC populations (82). Additionally, these cDCs arose from the differentiation of pre-DC progenitors that had migrated into the brain. Alternatively, Flt3L administration in rat brains has increased pDC populations (49). We elucidated that vIL7FL enhanced intratumoral cDCs including the migratory antigen-presenting population known as CD103+XCR1+ cDCs (83, 84).

Delivery of vIL7 or vIL7FL in an EGFRvIII heterogeneous 0.5 Gy model significantly enhanced overall survival. In our model, the effects of IL7 dominated despite DC infiltration from Flt3L co-expression.

Potentially, the lack of proper DC maturation affected T cell priming. Poly(I:C) is a toll-like receptor 3 (TLR3) agonist that can promote type I interferon (IFN) signaling in DCs as well as activate CD8 T cells (85, 86). Future investigations could adjuvant CAR T cells with poly(I:C) to potentially enhance anti-tumor T cell responses. While in our study one vCAR and vFL animal did survive, we speculate that this could be due to the bystander effect or immunogenicity. A previous study showed preconditioning mesothelin tumors with up to 25% antigen-negative cells with a non-lymphodepleting dose of cyclophosphamide resulted in CAR T cells having a curative effect (61).

A limitation of this study is the utilization of a syngeneic mouse model compared to spontaneously occurring tumors. Transplantable tumor cell lines tend to be more immunogenic and elicit non-naturally occurring immune responses compared to genetically induced mouse models. We chose the CT2A mouse model due to its low immunogenicity and immunosuppressive microenvironment compared to GL261 and SMA-560 models (87, 88). However, CT2A tumors can be less correlated to patient immune phenotypes than GL261 tumors and can become immunologically active after surgical resection (89). In addition, forced expression of luciferase in tumor cells was necessary to distribute animals based on bioluminescent tumor load, however, luciferase can increase tumor immunogenicity (90). Thus, the efficacy of vIL7FL should be tested in other models. Another limitation is tumor antigen expression. Patients with EGFRvIII positive tumors show varying levels of EGFRvIII expression at different locations within the tumor (35–37). In our study, treating mice with 50% EGFRvIII-positive and -negative tumors with vIL7 or vIL7FL increased survival compared to conventional CAR T cells. However, we can anticipate that decreasing the EGFRvIII positive tumor cell ratio could limit efficacy. Therefore, it remains to be seen whether vIL7FL will have the same efficacy in naturally occurring tumors with varying levels of heterogeneity.

Overall, this data emphasizes the ability of IL7 expression to improve CAR T cell abundance in GBM. While vIL7FL increased intratumoral dendritic cells, future studies are necessary to determine the therapeutic impact of intratumoral cDCs in brain tumors. IL7 expressing CAR T cells improved overall survival in mice pre-treated with a non-lymphodepleting dose of irradiation – allowing for retention of host immune cells – thus, the use of IL7 expressing CAR T cells can open opportunities for combinations of other immunotherapies in glioblastoma.

Data availability statement

The datasets presented in this study can be found in online repositories. The names of the repository/repositories and accession number(s) can be found below: GEO under accession ID: GSE215873.

Ethics statement

The animal study was reviewed and approved by Institutional Animal Care and Use Committee at Duke University.

Author contributions

SLS: conception, design, methodology, data acquisition, data analysis, writing original manuscript. NM: design, methodology, data acquisition, data analysis, manuscript review. EI: methodology, data acquisition, data analysis SHS: methodology and data acquisition DSW: data acquisition ARA: data acquisition TS: resources, supervision, manuscript review LS: conception, design, methodology, manuscript review JHS: methodology, resources, manuscript review RVB: methodology, resources, supervision, investigation, funding acquisition, manuscript review. All authors contributed to the article and approved the submitted version.

Funding

We are grateful to Ian's Friends Foundation and to the Center for Biomolecular and Tissue Engineering (CBTE) T32GM008555 grant by the National Institute of General Medical Sciences (NIGMS) NIH National Service Research Awards (NSRA) Program.

Acknowledgments

We thank the Duke University School of Medicine for the use of the Sequencing and Genomics Technology Shared Resource, which provided mRNA-sequencing service. Bulk RNA sequencing processing and analysis was provided by the Molecular Genomics Core at Duke University. We thank Martha Betancur for assistance monitoring animals and William Tomaszewski and Sarah Cook Quackenbush for their experimental guidance.

Conflict of interest

The authors declare that the research was conducted in the absence of any commercial or financial relationships that could be construed as a potential conflict of interest.

Publisher's note

All claims expressed in this article are solely those of the authors and do not necessarily represent those of their affiliated organizations, or those of the publisher, the editors and the reviewers. Any product that may be evaluated in this article, or claim that may be made by its manufacturer, is not guaranteed or endorsed by the publisher.

Supplementary material

The Supplementary Material for this article can be found online at: https://www.frontiersin.org/articles/10.3389/fimmu.2023.1085547/full#supplementary-material

References

1. Ostrom QT, Gittleman H, Farah P, Ondracek A, Chen Y, Wolinsky Y, et al. CBTRUS statistical report: Primary brain and central nervous system tumors diagnosed in the united states in 2006-2010. *Neuro Oncol* (2013) 15(SUPPL.2). doi: 10.1093/neuonc/not151

2. Delgado-Lopez PD, Corrales-Garcia EM. Survival in glioblastoma: A review on the impact of treatment modalities. *Clin Transl Oncol* (2016) 18(11):1062–71. doi: 10.1007/s12094-016-1497-x

3. Poon MTC, Sudlow CLM, Figueroa JD, Brennan PM. Longer-term (≥ 2 years) survival in patients with glioblastoma in population-based studies pre- and post-2005: A systematic review and meta-analysis. *Sci Rep* (2020) 10(1):1–10. doi: 10.1038/s41598-020-68011-4

4. Al-Mansour M, Al-Foheidi M, Ibrahim E. Efficacy and safety of second-generation CAR T-cell therapy in diffuse large b-cell lymphoma: A meta-analysis. *Mol Clin Oncol* (2020) 13(4):1–14. doi: 10.3892/mco.2020.2103

5. Brown CE, Badie B, Barish ME, Weng L, Ostberg JR, Chang WC, et al. Bioactivity and safety of il13rα2-redirected chimeric antigen receptor CD8+ t cells in patients with recurrent glioblastoma. *Clin Cancer Res* (2015) 21(18):4062–72. doi: 10.1158/1078-0432.CCR-15-0428

6. Maggs L, Cattaneo G, Dal AE, Moghaddam AS, Ferrone S. CAR T cell-based immunotherapy for the treatment of glioblastoma. *Front Neurosci* (2021) 15. doi: 10.3389/fnins.2021.662064

7. Goff SL, Morgan RA, Yang JC, Sherry RM, Robbins PF, Restifo NP, et al. Pilot trial of adoptive transfer of chimeric antigen receptor-transduced t cells targeting egfrviii in patients with glioblastoma. *J Immunother* (2019) 42(4):126–35. doi: 10.1097/CJI.0000000000000260

8. Karachi A, Dastmalchi F, Mitchell DA, Rahman M. Temozolomide for immunomodulation in the treatment of glioblastoma. *Neuro Oncol* (2018) 20(12):1566–72. doi: 10.1093/neuonc/noy072

9. Gattinoni L, Finkelstein SE, Klebanoff CA, Antony PA, Palmer DC, Spiess PJ, et al. Removal of homeostatic cytokine sinks by lymphodepletion enhances the efficacy of adoptively transferred tumor-specific CD8+ T cells. *J Exp Med* (2005) 202(7):907–12. doi: 10.1084/jem.20050732

10. Yeo AT, Rawal S, Delcuze B, Christofides A, Atayde A, Strauss L, et al. Single-cell RNA sequencing reveals evolution of immune landscape during glioblastoma progression. *Nat Immunol* (2022) 23:971–84. doi: 10.1038/s41590-022-01215-0

11. Suryadevara CM, Desai R, Abel ML, Riccione KA, Batich KA, Shen SH, et al. Temozolomide lymphodepletion enhances CAR abundance and correlates with antitumor efficacy against established glioblastoma. *Oncoimmunology* (2018) 7(6):1–10. doi: 10.1080/2162402X.2018.1434464

12. Heczey A, Louis CU, Savoldo B, Dakhova O, Durett A, Grilley B, et al. CAR T cells administered in combination with lymphodepletion and PD-1 inhibition to patients with neuroblastoma. *Mol Ther* (2017) 25(9):2214–24. doi: 10.1016/j.ymthe.2017.05.012

13. Lai J, Mardiana S, House IG, Sek K, Henderson MA, Giuffrida L, et al. Adoptive cellular therapy with T cells expressing the dendritic cell growth factor Flt3L drives epitope spreading and antitumor immunity. *Nat Immunol* (2020) 21(8):914–26. doi: 10.1038/s41590-020-0676-7

14. Liu Z, Meng Q, Bartek J, Poiret T, Persson O, Rane L, et al. Tumor-infiltrating lymphocytes (TILs) from patients with glioma. *Oncoimmunology* (2017) 6(2). doi: 10.1080/2162402X.2016.1252894

15. Dunn GP, Dunn IF, Curry WT. (2007). Focus on TILs: Prognostic significance of tumor infiltrating lymphocytes in human glioma. *Cancer Immun* 7:12.

16. Leko V, Cafri G, Yossef R, Paria B, Hill V, Gurusamy D, et al. Identification of neoantigen-reactive T lymphocytes in the peripheral blood of a patient with glioblastoma. *J Immunother Cancer* (2021) 9(7):1–7. doi: 10.1136/jitc-2021-002882

17. Shum T, Omer B, Tashiro H, Kruse RL, Wagner DL, Parikh K, et al. Constitutive signaling from an engineered IL7 receptor promotes durable tumor elimination by tumor-redirected T cells. *Cancer Discovery* (2017) 7(11):1238–47. doi: 10.1158/2159-8290.CD-17-0538

18. MacKall CL, Fry TJ, Gress RE. Harnessing the biology of IL-7 for therapeutic application. *Nat Rev Immunol* (2011) 11(5):330–42. doi: 10.1038/nri2970

19. Morgan RA, Johnson LA, Davis JL, Zheng Z, Woolard KD, Reap EA, et al. Recognition of glioma stem cells by genetically modified T cells targeting EGFRvIII and development of adoptive cell therapy for glioma. *Hum Gene Ther* (2012) 23(10):1043–53. doi: 10.1089/hum.2012.041

20. Schluns KS, Kieper WC, Jameson SC, Lefrançois L. Interleukin-7 mediates the homeostasis of naïve and memory CD8 T cells *in vivo*. *Nat Immunol* (2000) 1(5):426–32. doi: 10.1038/80868

21. Zhou J, Jin L, Wang F, Zhang Y, Liu B, Zhao T. Chimeric antigen receptor T (CAR-T) cells expanded with IL-7/IL-15 mediate superior antitumor effects. *Protein Cell* (2019) 10(10):764–9. doi: 10.1007/s13238-019-0643-y

22. Kim JH, Lee KJ, Lee SW. Cancer immunotherapy with T-cell targeting cytokines: IL-2 and IL-7. *BMB Rep* (2021) 54(1):21–30. doi: 10.5483/BMBRep.2021.54.1.257

23. Xue D, Hsu E, Fu YX, Peng H. Next-generation cytokines for cancer immunotherapy. *Antib Ther* (2021) 4(2):123–33. doi: 10.1093/abt/tbab014

24. Rosenberg SA, Sportès C, Ahmadzadeh M, Fry TJ, Ngo LT, Schwarz SL, et al. IL-7 administration to humans leads to expansion of CD8+ and CD4+ cells but a relative decrease of CD4+ T-regulatory cells. *J Immunother* (2006) 29(3):313–9. doi: 10.1097/01.cji.0000210386.55951.c2

25. Sportès C, Hakim FT, Memon SA, Zhang H, Chua KS, Brown MR, et al. Administration of rhIL-7 in humans increases *in vivo* TCR repertoire diversity by preferential expansion of naive T cell subsets. *J Exp Med* (2008) 205(7):1701–14. doi: 10.1084/jem.20071681

26. Sportès C, Babb RR, Krumlauf MC, Hakim FT, Steinberg SM, Chow CK, et al. Phase I study of recombinant human interleukin-7 administration in subjects with refractory malignancy. *Clin Cancer Res* (2010) 16(2):727–35. doi: 10.1158/1078-0432.CCR-09-1303

27. Lee SW, Choi D, Heo MK, Shin EC, Park SH, Kim SJ, et al. hIL-7-hyFc, a long-acting IL-7, increased absolute lymphocyte count in healthy subjects. *Clin Transl Sci* (2020) 13(6):1161–9. doi: 10.1111/cts.12800

28. Adachi K, Kano Y, Nagai T, Okuyama N, Sakoda Y, Tamada K. IL-7 and CCL19 expression in CAR-T cells improves immune cell infiltration and CAR-T cell survival in the tumor. *Nat Biotechnol* (2018) 36(4):346–51. doi: 10.1038/nbt.4086

29. Luo H, Su J, Sun R, Sun Y, Wang Y, Dong Y, et al. Coexpression of IL7 and CCL21 increases efficacy of CAR-T cells in solid tumors without requiring preconditioned lymphodepletion. *Clin Cancer Res* (2020) 26(20):5494–505. doi: 10.1158/1078-0432.CCR-20-0777

30. Qian W, Zhao A, Liu H, Lei W, Liang Y, Yuan X. Safety and efficacy of CD19 CAR-T cells Co-expressing IL-7 and CCL19 in combination with anti-PD-1 antibody for Refractory/Relapsed DLBCL: Preliminary data from the phase Ib trial (NCT04381741). *Blood* (2021) 138(Supplement 1):3843–3. doi: 10.1182/blood-2021-144523

31. Li L, Li Q, Yan ZX, Sheng LS, Fu D, Xu P, et al. Transgenic expression of IL – 7 regulates CAR – T cell metabolism and enhances *in vivo* persistence against tumor cells. (2022) 0123456789:1–14. doi: 10.1038/s41598-022-16616-2

32. Ghosh S, Yan R, Thotala S, Jash A, Mahadevan A, Hu T, et al. 565 a novel long-acting interleukin-7 agonist, NT-I7, increases cytotoxic CD8+ T cells and enhances survival in mouse glioma models. *J Immunother Cancer* (2020) 8(Suppl 3):A340 LP–A340. doi: 10.1136/jitc-2020-SITC2020.0565

33. Campian JL, Ghosh S, Kapoor V, Yan R, Thotala S, Jash A, et al. Long-acting recombinant human interleukin-7, NT-I7, increases cytotoxic CD8 T cells and enhances survival in mouse glioma models. *Clin Cancer Res* (2022) 28(6):1229–39. doi: 10.1158/1078-0432.CCR-21-0947

34. Huang J, Zheng M, Zhang Z, Tang X, Chen Y, Peng A, et al. Interleukin-7-loaded oncolytic adenovirus improves CAR-T cell therapy for glioblastoma. *Cancer Immunol Immunother* (2021) 70(9):2453–65. doi: 10.1007/s00262-021-02856-0

35. Montano N, Cenci T, Martini M, D'Alessandris QG, Pelacchi F, Ricci-Vitiani L, et al. Expression of EGFRvIII in glioblastoma: Prognostic significance revisited. *Neoplasia* (2011) 13(12):1113–21. doi: 10.1593/neo.111338

36. Doucette T, Rao G, Rao A, Shen L, Aldape K, Wei J, et al. Immune heterogeneity of glioblastoma subtypes: Extrapolation from the cancer genome atlas. *Cancer Immunol Res* (2013) 1(2):112–22. doi: 10.1158/2326-6066.CIR-13-0028

37. Brennan CW, Verhaak RGW, McKenna A, Campos B, Noushmehr H, Salama SR, et al. The somatic genomic landscape of glioblastoma. *Cell* (2013) 155(2):462. doi: 10.1016/j.cell.2013.09.034

38. Nishikawa R, Sugiyama T, Narita Y, Furnari F, Cavenee WK, Matsutani M. Immunohistochemical analysis of the mutant epidermal growth factor, ΔEGFR, in glioblastoma. *Brain Tumor Pathol* (2004) 21(2):53–6. doi: 10.1007/BF02484510

39. O'Rourke DM, Nasrallah MP, Desai A, Melenhorst JJ, Mansfield K, Morrisette JJD, et al. A single dose of peripherally infused EGFRvIII-directed CAR T cells mediates antigen loss and induces adaptive resistance in patients with recurrent glioblastoma. *Sci Transl Med* (2017) 9(399):eaaa0984. doi: 10.1126/scitranslmed.aaa0984

40. Choe JH, Watchmaker PB, Simic MS, Gilbert RD, Li AW, Krasnow NA, et al. SynNotch-CAR T cells overcome challenges of specificity, heterogeneity, and persistence in treating glioblastoma. *Sci Transl Med* (2021) 13(591):1–16. doi: 10.1126/scitranslmed.abe7378

41. Evgin L, Kottke T, Tonne J, Thompson J, Huff AL, van Vloten J, et al. Oncolytic virus–mediated expansion of dual-specific CAR T cells improves efficacy against solid tumors in mice. *Sci Transl Med* (2022) 14(640). doi: 10.1126/scitranslmed.abn2231

42. Ma L, Morgan DM, Sulkaj I, Yousefpour P, Whittaker CA, Abraham W, et al. Eradication of tumors with pre-existing antigenic heterogeneity by vaccine-mediated co-engagement of CAR T and endogenous T-cells. *bioRxiv* (2022) 10(5):511036. doi: 10.1101/2022.10.05.511036

43. Alizadeh D, Wong RA, Gholamin S, Maker M, Aftabizadeh M, Yang X, et al. IFNgis critical for CAR T cell–mediated myeloid activation and induction of endogenousimmunity. *Cancer Discovery* (2021) 11(9):2248–65. doi: 10.1158/2159-8290.CD-20-1661

44. Liu K, Nussenzweig MC. Origin and development of dendritic cells. *Immunological reviews* (2010) 234(1):45–54. doi: 10.1111/j.0105-2896.2009.00879.x

45. Cueto FJ, Sancho D. The flt3l/flt3 axis in dendritic cell biology and cancer immunotherapy. *Cancers (Basel)* (2021) 13(7):1525. doi: 10.3390/cancers13071525

46. Sichien D, Lambrecht BN, Guilliams M, Scott CL. Development of conventional dendritic cells: From common bone marrow progenitors to multiple subsets in peripheral tissues. *Mucosal Immunol* (2017) 10(4):831–44. doi: 10.1038/mi.2017.8

47. Salmon H, Idoyaga J, Rahman A, Leboeuf M, Remark R, Jordan S, et al. Expansion and activation of CD103+ dendritic cell progenitors at the tumor site enhances tumor

responses to therapeutic PD-L1 and BRAF inhibition. *Immunity* (2016) 44(4):924–38. doi: 10.1016/j.immuni.2016.03.012

48. King GD, Ghulam Muhammad AKM, Curtin JF, Barcia C, Puntel M, Liu C, et al. Flt3L and TK gene therapy eradicate multifocal glioma in a syngeneic glioblastoma model. *Neuro Oncol* (2008) 10(1):19–31. doi: 10.1215/15228517-2007-045

49. Curtin JF, King GD, Barcia C, Liu C, Hubert FX, Guillonneau C, et al. Fms-like tyrosine kinase 3 ligand recruits plasmacytoid dendritic cells to the brain. *J Immunol* (2006) 176(6):3566–77. doi: 10.4049/jimmunol.176.6.3566

50. Lowenstein P, Orringer D, Umemura Y, Sagher O, Heth J, Hervey-Jumper S, et al. Abstract CT105: First in human phase I trial of adenoviral vectors expressing Flt3L and HSV1-TK to treat newly diagnosed high-grade glioma by reprogramming the brain immune system. *Cancer Res* (2020) 80(16_Supplement):CT105–5. doi: 10.1158/1538-7445.AM2020-CT105

51. Land CA, Musich PR, Haydar D, Krenciute G, Xie Q. Chimeric antigen receptor T-cell therapy in glioblastoma: charging the T cells to fight. *J Transl Med* (2020) 18(1):1–13. doi: 10.1186/s12967-020-02598-0

52. Woroniecka KI, Rhodin KE, Chongsathidkiet P, Keith KA, Fecci PE. T-Cell dysfunction in glioblastoma: Applying a new framework. *Clin Cancer Res* (2018) 24 (16):3792–802. doi: 10.1158/1078-0432.CCR-18-0047

53. Pösel C, Möller K, Boltze J, Wagner DC, Weise G. Isolation and Flow Cytometric Analysis of Immune Cells from the Ischemic Mouse Brain. *JoVE* (2016) 108):e53658. doi: 10.3791/53658

54. Kuchenbecker L, Nienen M, Hecht J, Neumann AU, Babel N, Reinert K, et al. IMSEQ-a fast and error aware approach to immunogenetic sequence analysis. *Bioinformatics* (2015) 31(18):2963–71. doi: 10.1093/bioinformatics/btv309

55. Stephens M. False discovery rates: a new deal. (2017) 18(2):275–94. doi: 10.1093/biostatistics/kxw041

56. Tomaszewski W. *Processed seurat object of scRNAseq data from wildtype and CaMKK2 KO immune infiltrate of CT2a preclinical murine glioma* (2022). Available at: https://zenodo.org/record/6654420.

57. Varn FS, Johnson KC, Martinek J, Huse JT, Nasrallah MP, Wesseling P, et al. Glioma progression is shaped by genetic evolution and microenvironment interactions. *Cell* (2022) 185(12):2184–2199.e16. doi: 10.1016/j.cell.2022.04.038

58. Tomaszewski W, Waibl-Polania J, Racioppi L, Sanchez-Perez L, Michael G, Sampson J. immu-34. camkk2 promotes an immunosuppressive program and checkpoint blockade resistance in the glioblastoma tumor microenvironment. *Neuro Oncol* (2021) 23(Supplement_6):vi100–0. doi: 10.1093/neuonc/noab196.393

59. Korotkevich G, Sukhov V, Budin N, Shpak B, Artyomov MN, Sergushichev A. Fast gene set enrichment analysis. *bioRxiv* (2021). doi: 10.1101/060012

60. Jiang P, Zhang Y, Ru B, Yang Y, Vu T, Paul R, et al. Systematic investigation of cytokine signaling activity at the tissue and single-cell levels. *Nat Methods* (2021) 118:1181–91. doi: 10.1038/s41592-021-01274-5

61. Klampatsa A, Leibowitz MS, Sun J, Liousia M, Arguiri E, Albelda SM. Analysis and augmentation of the immunologic bystander effects of CAR T cell therapy in a syngeneic mouse cancer model. *Mol Ther - Oncolytics* (2020) 18:360–71. doi: 10.1016/j.omto.2020.07.005

62. Yang S, Gao K, Li W. Identification of hub genes and pathways in glioblastoma by bioinformatics analysis. *Oncol Lett* (2019) 17(1):1035–41. doi: 10.3892/ol.2018.9644

63. Wang JJ, Wang H, Zhu BL, Wang X, Qian YH, Xie L, et al. Development of a prognostic model of glioma based on immune-related genes. *Oncol Lett* (2021) 21(2):116. doi: 10.3892/ol.2020.12377

64. Pal J, Patil V, Kumar A, Kaur K, Sarkar C, Somasundaram K. Loss-of-function mutations in calcitonin receptor (CALCR) identify highly aggressive glioblastoma with poor outcome. *Clin Cancer Res* (2018) 24(6):1448–58. doi: 10.1158/1078-0432.CCR-17-1901

65. Frey N, Porter D. Cytokine release syndrome with chimeric antigen receptor T cell therapy. *Biol Blood Marrow Transplant* (2019) 25(4):e123–7. doi: 10.1016/j.bbmt.2018.12.756

66. Brudno JN, Kochenderfer JN. Toxicities of chimeric antigen receptor T cells: Recognition and management. *Blood* (2016) 127(26):3321–30. doi: 10.1182/blood-2016-04-703751

67. Giavridis T, van der Stegen SJC, Eyquem J, Hamieh M, Piersigilli A, Sadelain M. CAR T cell-induced cytokine release syndrome is mediated by macrophages and abated by IL-1 blockade letter. *Nat Med* (2018) 24(6):731–8. doi: 10.1038/s41591-018-0041-7

68. Elgueta R, Benson MJ, De Vries VC, Wasiuk A, Guo Y, Noelle RJ. Molecular mechanism and function of CD40/CD40L engagement in the immune system. *Immunol Rev* (2009) 229(1):152–72. doi: 10.1111/j.1600-065X.2009.00782.x

69. Keskin DB, Anandappa AJ, Sun J, Tirosh I, Mathewson ND, Li S, et al. Neoantigen vaccine generates intratumoral T cell responses in phase ib glioblastoma trial. *Nature* (2019) 565(7738):234–9. doi: 10.1038/s41586-018-0792-9

70. Khor B, Sleckman BP. Allelic exclusion at the TCRβ locus. *Curr Opin Immunol* (2002) 14(2):230–4. doi: 10.1016/S0952-7915(02)00326-6

71. Padovan E, Casorati G, Dellabona P, Meyer S, Brockhaus M, Lanzavecchia A. Expression of two T cell receptor α chains: Dual receptor T cells. *Sci (80-).* (1993) 262 (5132):422–4. doi: 10.1126/science.8211163

72. Woodsworth DJ, Castellarin M, Holt RA. Sequence analysis of T-cell repertoires in health and disease. *Genome Med* (2013) 5(10):98. doi: 10.1186/gm502

73. Li L, Zhu X, Qian Y, Yuan X, Ding Y, Hu D, et al. Chimeric antigen receptor T-cell therapy in glioblastoma: Current and future. *Front Immunol* (2020) 11:1–9. doi: 10.3389/fimmu.2020.594271

74. Krenciute G, Prinzing BL, Yi Z, Wu MF, Liu H, Dotti G, et al. Transgenic expression of IL15 improves antiglioma activity of IL13Rα2-CAR T cells but results in antigen loss variants. *Cancer Immunol Res* (2017) 5(7):571–81. doi: 10.1158/2326-6066.CIR-16-0376

75. Rousso-Noori L, Mastandrea I, Talmor S, Waks T, Globerson Levin A, Haugas M, et al. P32-specific CAR T cells with dual antitumor and antiangiogenic therapeutic potential in gliomas. *Nat Commun* (2021) 12(1):1–13. doi: 10.1038/s41467-021-23817-2

76. Sampson JH, Choi BD, Sanchez-Perez L, Suryadevara CM, Snyder DJ, Flores CT, et al. EGFRvIII mCAR-modified T-cell therapy cures mice with established intracerebral glioma and generates host immunity against tumor-antigen loss. *Clin Cancer Res* (2014) 20(4):972–84. doi: 10.1158/1078-0432.CCR-13-0709

77. Bradley LM, Haynes L, Swain SL. IL-7: Maintaining T-cell memory and achieving homeostasis. *Trends Immunol* (2005) 26(3):172–6. doi: 10.1016/j.it.2005.01.004

78. Rathmell JC, Farkash EA, Gao W, Thompson CB. IL-7 enhances the survival and maintains the size of naive T cells. *J Immunol* (2001) 167(12):6869–76. doi: 10.4049/jimmunol.167.12.6869

79. Patil NK, Bohannon JK, Luan L, Guo Y, Fensterheim B, Hernandez A, et al. FLT3 ligand treatment attenuates T cell dysfunction and improves survival in a murine model of burn wound sepsis. *Shock* (2017) 47(1):40–51. doi: 10.1097/SHK.0000000000000688

80. Long AH, Haso WM, Shern JF, Wanhainen KM, Murgai M, Ingaramo M, et al. 4-1BB costimulation ameliorates T cell exhaustion induced by tonic signaling of chimeric antigen receptors. *Nat Med* (2015) 21(6):581–90. doi: 10.1038/nm.3838

81. Cibrián D, Sánchez-Madrid F. CD69: from activation marker to metabolic gatekeeper. *Eur J Immunol* (2017) 47(6):946–53. doi: 10.1002/eji.201646837

82. Anandasabapathy N, Victora GD, Meredith M, Feder R, Dong B, Kluger C, et al. Flt3L controls the development of radiosensitive dendritic cells in the meninges and choroid plexus of the steady-state mouse brain. *J Exp Med* (2011) 208(18):1695–705. doi: 10.1084/jem.20102657

83. Audsley KM, McDonnell AM, Waithman J. Cross-presenting XCR1+ dendritic cells as targets for cancer immunotherapy. *Cells* (2020) 9(3):565. doi: 10.3390/cells9030565

84. Gutiérrez-Martínez E, Planès R, Anselmi G, Reynolds M, Menezes S, Adiko AC, et al. Cross-presentation of cell-associated antigens by MHC class I in dendritic cell subsets. *Front Immunol* (2015) 6. doi: 10.3389/fimmu.2015.00363

85. Matsumoto M, Takeda Y, Tatematsu M, Seya T. Toll-like receptor 3 signal in dendritic cells benefits cancer immunotherapy. *Front Immunol* (2017) 8:1–7. doi: 10.3389/fimmu.2017.01897

86. Salem ML, Diaz-Montero CM, EL-Naggar SA, Chen Y, Moussa O, Cole DJ. The TLR3 agonist poly(I:C) targets CD8+ T cells and augments their antigen-specific responses upon their adoptive transfer into naïve recipient mice. *Vaccine* (2009) 27 (4):549–57. doi: 10.1016/j.vaccine.2008.11.013

87. Letchuman V, Ampie L, Shah AH, Brown DA, Heiss JD, Chittiboina P. Syngeneic murine glioblastoma models: Reactionary immune changes and immunotherapy intervention outcomes. *Neurosurg Focus* (2022) 52:1–9. doi: 10.3171/2021.11.FOCUS21556

88. Sahu U, Barth RF, Otani Y, McCormack R, Kaur B. Rat and mouse brain tumor models for experimental neuro-oncology research. *J Neuropathol Exp Neurol* (2022) 81 (5):312–29. doi: 10.1093/jnen/nlac021

89. Khalsa JK, Cheng N, Keegan J, Chaudry A, Driver J, Bi WL, et al. Immune phenotyping of diverse syngeneic murine brain tumors identifies immunologically distinct types. *Nat Commun* (2020) 11(1):3912. doi: 10.1038/s41467-020-17704-5

90. Baklaushev VP, Kilpeläinen A, Petkov S, Abakumov MA, Grinenko NF, Yusubalieva GM, et al. Luciferase expression allows bioluminescence imaging but imposes limitations on the orthotopic mouse (4T1) model of breast cancer. *Sci Rep* (2017) 7(1):1–17. doi: 10.1038/s41598-017-07851-z

frontiers | Frontiers in Oncology

TYPE Original Research
PUBLISHED 17 March 2023
DOI 10.3389/fonc.2023.1122329

Check for updates

OPEN ACCESS

EDITED BY
Anand Rotte,
Arcellx Inc, United States

REVIEWED BY
Amandeep Godara,
The University of Utah, United States
Robert Weinkove,
Victoria University of Wellington, New Zealand

*CORRESPONDENCE
Sai-Ching J. Yeung
syeung@mdanderson.org

SPECIALTY SECTION
This article was submitted to Cancer Immunity and Immunotherapy, a section of the journal Frontiers in Oncology

RECEIVED 12 December 2022
ACCEPTED 08 March 2023
PUBLISHED 17 March 2023

CITATION
Lipe DN, Qdaisat A, Chaftari P, Wattana MK, Krishnamani PP, Reyes-Gibby C and Yeung S-CJ (2023) Emergency department use by patients who received chimeric antigen receptor T cell infusion therapy. *Front. Oncol.* 13:1122329. doi: 10.3389/fonc.2023.1122329

COPYRIGHT
© 2023 Lipe, Qdaisat, Chaftari, Wattana, Krishnamani, Reyes-Gibby and Yeung. This is an open-access article distributed under the terms of the Creative Commons Attribution License (CC BY). The use, distribution or reproduction in other forums is permitted, provided the original author(s) and the copyright owner(s) are credited and that the original publication in this journal is cited, in accordance with accepted academic practice. No use, distribution or reproduction is permitted which does not comply with these terms.

Emergency department use by patients who received chimeric antigen receptor T cell infusion therapy

Demis N. Lipe[1], Aiham Qdaisat[2], Patrick Chaftari[2], Monica K. Wattana[2], Pavitra P. Krishnamani[2], Cielito Reyes-Gibby[2] and Sai-Ching J. Yeung[2]*

[1]Department of Medical Services, IQVIA Biotech, Houston, TX, United States, [2]Department of Emergency Medicine, The University of Texas MD Anderson Cancer Center, Houston, TX, United States

Background: Chimeric antigen receptor T cell infusion (CAR T) therapy has revolutionized the treatment of hematologic malignancies, but treatment-related toxicities are of concern. Understanding the timing and reasons for which patients present to the emergency department (ED) after CAR T therapy can assist with the early recognition and management of toxicities.

Methods: A retrospective observational cohort study was conducted for patients who had undergone CAR T therapy in the past 6 months and visited the ED of The University of Texas MD Anderson Cancer Center between 04/01/2018 and 08/01/2022. The timing of presentation after CAR T product infusion, patient characteristics, and outcomes of the ED visit were examined. Survival analyses were conducted using Cox proportional hazards regression and Kaplan-Meier estimates.

Results: During the period studied, there were 276 ED visits by 168 unique patients. Most patients had diffuse large B-cell lymphoma (103/168; 61.3%), multiple myeloma (21/168; 12.5%), or mantle cell lymphoma (16/168; 9.5%). Almost all 276 visits required urgent (60.5%) or emergent (37.7%) care, and 73.5% of visits led to admission to the hospital or observation unit. Fever was the most frequent presenting complaint, reported in 19.6% of the visits. The 30-day and 90-day mortality rates after the index ED visits were 17.0% and 32.2%, respectively. Patients who had their first ED visit >14 days after CAR T product infusion had significantly worse overall survival (multivariable hazard ratio 3.27; 95% confidence interval 1.29–8.27; P=0.012) than patients who first visited the ED within 14 days of CAR T product infusion.

Conclusion: Cancer patients who receive CAR T therapy commonly visit the ED, and most are admitted and/or require urgent or emergent care. During early ED visits patients mainly present with constitutional symptoms such as fever and fatigue, and these early visits are associated with better overall survival.

KEYWORDS

chimeric antigen receptor T cells, emergency department, CAR T cells, utilization, Mortality, disposition, length of stay, oncologic emergency

Introduction

Since the advent of chimeric antigen receptor T cell infusion (CAR T) therapy for hematologic malignancies, much has been learned and recognized about the risks and complications associated with CAR T therapy. Toxicities such as cytokine release syndrome (CRS), immune effector cell-associated neurotoxicity syndrome (ICANS), and infections in the days to months following the infusion of CAR T products have been recognized. The incidence rates of CRS and ICANS have been reported in the literature to range from 57% to 93% and 20% to 70%, respectively (1–3). These toxicities vary greatly and are thought to be influenced by multiple factors, including patient characteristics, tumor burden, CAR T cell dose, and differences in manufacturing processes, among others (4). The current treatment strategy of associated toxicities is focused on reduction of the overall inflammation by use of corticosteroids or cytokine inhibition, which is based on the grading of the toxicity as defined by the American Society for Transplantation and Cellular Therapy (ASTCT) guidelines on the management of CAR T related toxicities (5).

Although much is known about how clinicians should recognize, work up, and manage these toxicities (1), there is insufficient published literature on the use of the emergency department (ED) by this cohort of patients. CAR T therapy recipients are generally believed to have a potential for increased health care use after CAR T therapy, with high rates of intensive care unit (ICU) admissions and prolonged lengths of stay in the hospital, although re-hospitalization patterns appear to vary based on whether the patient's CAR T therapy was an inpatient or outpatient event (6, 7). One study reported that hospital re-admission and ICU admission rates within the first 3 months after CAR T product infusion were 28.1% and 15.5%, respectively (7). Another study reported that nearly 40% were re-hospitalized and 21% visited the ED during the initial 12 months following CAR T product infusion (8). Reasons for re-hospitalizations or ED visits have been mostly related to the primary disease, pain, CAR T-related toxicities, and infection (6–8). However, despite these reports, much is still unknown, and more data is needed to better understand why patients who receive CAR T therapy visit the ED and what their outcomes are.

In the current study, we describe the reasons why patients at a single comprehensive cancer center visited the ED after CAR T product infusion, as well as their outcomes, including disposition (whether the patient was discharged, admitted, transferred, or other), hospitalization, and survival.

Methods

Population

A retrospective observational cohort study was conducted by identifying all cancer patients who visited the ED of The University of Texas MD Anderson Cancer Center (a comprehensive cancer center in Houston, Texas, USA) within 6 months after receiving any CAR T product infusion, using the institutional data warehouse. For each patient with multiple ED visits, the first ED visit after CAR T product infusion was identified as the index ED visit. The period studied was between 04/01/2018 and 08/31/2022 for the index ED visits. Patients who were less than 18 years of age at their index ED visit were excluded.

Study setting

Our institution is a comprehensive cancer center that established the first academic emergency medicine department in 2010. The ED is staffed by board certified emergency and internal medicine physicians and has 44 beds, serving approximately 26,000 patients annually. The patients that visit the ED are assessed and treated by the staff in the ED, in consultation with the patient's oncologist. There is also an ED-run observation unit in the hospital, which serves patients projected to need in-hospital care for less than 2 midnights. This unit is functional 24-hours a day and is staffed by an emergency or internal medicine physician along with advanced practice providers. Most patients who are placed in the observation unit originate from the ED; however, patients may also come directly from clinics or procedure areas (9). Additionally, patients may also be admitted directly to the hospital by their oncologists, while bypassing the ED.

Variables and data collection

Thirty-day and 90-day mortality rates for the ED visits were calculated from the time of the index ED presentation to the reported time of death. ICU admission was reported as any ICU admission during the patient's hospital stay associated with the index ED visit. In-hospital mortality was identified as a death during the ED visit or subsequently during the hospital admission associated with the index ED visit. The timing of the indexed ED visit was grouped based on the time from CAR T product infusion to the ED presentation, and was categorized as early (≤14 days after CAR T product infusion) or late (>14 days after CAR T infusion). CAR T product infusion was defined as the day the CAR T product was infused. Because the first 14 days after CAR T infusion are the most critical with regards to treatment-related toxicities (10, 11), we chose the time point of 14 days as the cut-off to define early versus late presentation. The acuity level assigned to the patient was based on the modified Emergency Severity Index (mESI) tool used to triage patients in our ED. Life-threatening is level 1, emergent level 2, urgent level 3, less urgent level 4, and non-urgent level 5. This five-level triage algorithm classifies patients based on disease severity at presentation and the expected resource utilization (12). The "presenting complaint" was defined as the patient's reported reason for visiting the ED at the time of the triage assessment.

Clinical and demographic information, ED visit-related data, and outcomes were collected from patients' electronic health records and the institution's data warehouse. Race and ethnicity groups were categorized according to the Office of Management and Budget standards for race and ethnicity (13). The diagnosis of CRS,

ICANS, or active infection(s) was collected by reviewing the physician(s) and ED visit notes, reporting the grade for the CRS and the ICANS at the time of the ED visit if present.

Statistical analysis

Patient-level and visit-level data were reported using descriptive statistics. Medians and interquartile ranges were reported for continuous variables. Numerical data were evaluated for normality using quantile-quantile plots, histogram plots, and the Shapiro-Wilk test. Categorical variables were reported as counts and percentages. Statistical significance was appraised for proportions of categorical variables using the chi-square test or the Fisher exact test, as indicated. The Wilcoxon-Mann-Whitney test was used to determine significant differences for continuous variables (all data were not normally distributed).

For the survival analysis, survival time was defined as the time interval from the date of CAR T product administration onto the date of death or the end of the observation period, censoring patients who were lost to follow-up on the dates of their last recorded clinic visit or communication (email, video conference or phone call). We used the Kaplan-Meier method followed by the log-rank test to assess differences in overall survival between patients with early and late ED presentations. Univariate and multivariable Cox proportional hazards regression models were used to assess the association between different clinical factors and overall survival, reporting the hazard ratio and its 95% confidence interval. For the final model, the proportional hazards, the non-linearity, and the influential observations assumptions were evaluated by examining the Schoenfeld residuals, the Martingale residuals, and the Deviance residuals.

All statistical analyses were performed using R software (version 4.0.3, The R Foundation, http://www.r-project.org). Two-sided P values less than 0.05 were considered statistically significant.

Ethics

The Institutional Review Board of The University of Texas MD Anderson Cancer Center approved the study and granted a waiver of informed consent.

Results

Patient characteristics

During the period studied, 409 patients received CAR T therapy, and 171 (41.8%) had at least one ED visit within 6 months of CAR T product infusion (Figure 1). The clinical and demographic characteristics of the patients included in the analysis (n=168) are summarized in Table 1. The median age for the patients in our cohort was 63 years (interquartile range: 54–69). Most were male (60.7%), white (70.8%), and not of Hispanic or Latino ethnicity (72.6%). The most common cancer types for which

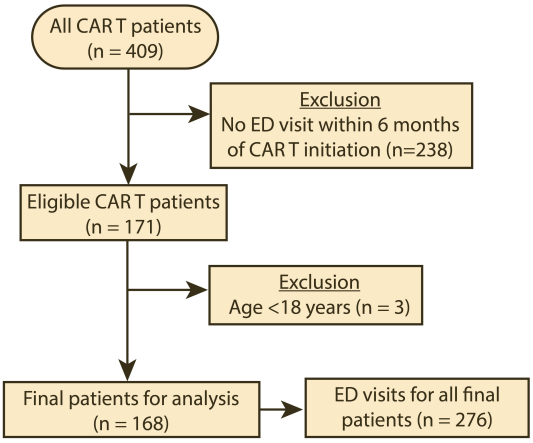

FIGURE 1
Flow diagram of the cohort selection for the period studied (04/01/2018–08/31/2022). CAR T, chimeric antigen receptor T-cell infusion therapy; ED, emergency department.

CAR T therapy was initiated were diffuse large B-cell lymphoma (61.3%), multiple myeloma (12.5%), mantle cell lymphoma (9.5%), and acute lymphoblastic leukemia (6.0%). Eighteen patients (10.7%) had other cancer types. During the period studied, the median number of ED visits was 1 (interquartile range 1–2). For the type of CAR T product, 108 patients (64.3%) were treated with axicabtagene ciloleucel within 6 months prior to their ED visit (Table S1). The remaining ED visits were by patients who were treated with idecabtagene vicleucel (12.5%), brexucabtagene autoleucel (11.3%), tisagenlecleucel (7.1%), and lisocabtagene maraleucel (4.8%). All the patients had their CAR T product infusion administered in an inpatient setting. Table S3 summarizes the presentation and characteristics of the ED visits stratified by CAR T product type, while Table S4 summarizes the presentation and characteristics of the ED visits stratified by the underlying cancer type.

ED visits and outcomes

During the period studied, patients included in our analysis made 276 unique visits to our ED. Most of the visits were of high acuity; 167 (60.5%) were urgent, and 104 (37.7%) were emergent or life-threatening. Only 5 visits (1.8%) had an acuity level of "less urgent" or "non-urgent". In terms of presenting complaints, around one-fifth of the visits (19.6%) were for a fever, and fatigue was reported in 9.1% of the visits. Altered mental status was reported in 5.1% of the visits, hypotension in 4.7%, and suspected sepsis in 4.3%. Abdominal pain (6.5%), shortness of breath (6.2%), cough (5.4%), nausea and/or vomiting (4.3%), and dizziness (1.8%) were also commonly reported as a presenting complaint. Other complaints are reported in Table 2. CRS was reported in 21 patients (7.6%) at the time of the ED visit, with the majority (19/21) being grade 1, while ICANS was reported in only 9 ED visits, 4 of which were higher than grade 1 (Table 2). Tocilizumab and corticosteroids were administered during the ED

TABLE 1 Clinical and demographic characteristics of patients presenting to the emergency department (ED) after chimeric antigen receptor T-cell infusion therapy (n = 168).

Characteristic	No. (%)
Age, median (IQR), years	63 (54–69)
Sex	
Female	66 (39.3)
Male	102 (60.7)
Race	
White	119 (70.8)
Black or African American	14 (8.3)
Asian	9 (5.4)
Others	23 (13.7)
Unknown or declined to answer	3 (1.8)
Ethnicity	
Not Hispanic or Latino	122 (72.6)
Hispanic or Latino	37 (22.0)
Unknown or declined to answer	9 (5.4)
Charlson comorbidity index, median (IQR)	4 (3–5)
Cancer type	
Diffuse large B-cell lymphoma	103 (61.3)
Multiple myeloma	21 (12.5)
Mantle cell lymphoma	16 (9.5)
Acute lymphoblastic leukemia	10 (6.0)
Others	18 (10.7)
Number of ED visits, median (IQR)	1 (1–2)

IQR, interquartile range.

stay in 1.1% and 5.8% of the visits, respectively (Table 3). In addition, infection was identified in 81 (29.3%) visits (Table 2), of which 18.5% (15/81) tested positive for COVID-19 at the ED visit. Within 14 days before the ED visit, COVID-19 was reported in 17 (6.2%) of the visits, including the aforementioned 15 (5.4%) active cases. Fever (≥38°C) was recorded in 9.8% of the ED visits. Antibiotics were administered in the ED in 50.7% of the visits (Table 3). Of significance, infections were higher in very late (>90 days after CAR T product infusion) visits compared to the early (≤14 days) visits (36.2% vs.13.8%, respectively; Table S2). Patients presented with severe neutropenia (<0.5 x 10^9/L) in 12.0% of the visits; while 48.6% of the ED visits were associated with severe thrombocytopenia (<50 x 10^9/L; Table 2).

As for the ED visit outcomes, 169 visits (61.2%) resulted in the patient being admitted to the hospital, and 68 (24.6%) resulted in discharge home (Table 3). Thirty-four visits resulted in the patient being placed in the observation unit. For patients who were admitted to the hospital, the median hospital length of stay was 6 days (interquartile range 4–9). When stratified by timing of the ED visit, visits that occurred within 14 days of CAR T product infusion had significantly higher rates of fever and fatigue as presenting complaints than those that occurred more than 90 days after CAR T product infusion (fever: 41.4% compared with 19.1%, P = 0.006; fatigue: 13.8% compared with 3.2%, P = 0.030; Table S2). For almost one-third of the visits (32.2%), the patient died within 90 days of the ED visit (Table 3). The thirty-day mortality rate for these ED visits was 17.0%.

Overall survival

The mortality rate during the study period was 37.5% (63/168). The cause and place of death are summarized in Table S5. Cancer progression (17.5%), infection/sepsis (14.3%), and organ failure (17.5%) were the most frequent causes of death in our cohort. Twenty-seven (42.9%) patients had their cause of death reported as unknown or not documented in the medical records. Only 42.9% deaths occurred in hospitals. For the subset of patients who died during the ED visit or subsequent hospital admission, infection was the most common cause of death (42.9%) for these patients (Table S6). Patients whose first ED visit occurred early (within 14 days of CAR T product infusion) had significantly (P=0.008) better overall survival than those whose first ED visit occurred late (more than 14 days after product infusion; Figure 2). Similar results were observed when a two-year survival was examined (Figure S1). As for the Cox regression analyses, non-linearity was detected for age and the Charlson comorbidity index, and we therefore categorized these variables into two groups. When compared with an early first ED visit (reference), patients whose first ED visit occurred >14 days after CAR T product infusion had significantly worse overall survival in both the univariate Cox regression analysis (hazard ratio 3.23, 95% confidence interval 1.29–8.10, P = 0.013) and the multivariable Cox regression analysis (hazard ratio 3.27, 95% confidence interval 1.29–8.27, P = 0.012; Table 4).

Discussion

Integrating CAR T therapy into the treatment of hematologic malignancies paved the way for better survival outcomes (14–16). However, as with every other cancer therapy, adverse events are a concern. In the current study, we examined the reasons for ED use by patients who received CAR T therapy and their outcomes. We found that when patients visited the ED after CAR T therapy, they mainly complained of constitutional symptoms, including fever and fatigue, and for most of these visits (73.5%), the patient was admitted to either the hospital or placed in the observation unit. It has been previously reported that the presence of fever does not seem to affect the safety and efficacy of CAR T therapy, however, the same study suggested that the absence of fever indicates a poor response to CAR T therapy (17). Although 19.6% of the presenting complaints included fever, an infectious etiology for the visit was found in over 29% of the cases. Of these cases, 5.4% were due to COVID-19; however, only two patients died as a direct cause of COVID-19, and 80.0% were admitted. While the outcomes of COVID-19 in patients treated with CAR T therapy remain

TABLE 2 Characteristics of emergency department visits by cancer patients in our analysis who had initiated chimeric antigen receptor T-cell infusion therapy within the past 6 months (total number of visits = 276).

Characteristic	No. (%)
Acuity	
Urgent	167 (60.5)
Emergent	104 (37.7)
Less urgent	4 (1.4)
Non-urgent	1 (0.4)
Top presenting complaints*	
Fever	54 (19.6)
Abnormal lab results	28 (10.1)
Fatigue	25 (9.1)
Abdominal pain	18 (6.5)
Shortness of breath	17 (6.2)
Cough	15 (5.4)
Altered mental status	14 (5.1)
Hypotension	13 (4.7)
Suspected sepsis	12 (4.3)
Fall	12 (4.3)
Nausea and/or vomiting	12 (4.3)
Diarrhea	7 (2.5)
Dizziness	5 (1.8)
Chest pain	4 (1.4)
Extremity weakness	3 (1.1)
Constipation	3 (1.1)
Leg swelling	3 (1.1)
Other pain	14 (5.1)
CRS	
No	255 (92.4)
Grade 1	19 (6.9)
Grade 2	2 (0.7)
ICANS	
No	267 (96.7)
Grade 1	5 (1.8)
Grade 2	2 (0.7)
Grade 3	2 (0.7)
Identified infection	
No	195 (70.7)
Yes	81 (29.3)
Temperature at presentation, median (IQR), °C	36.9 (36.6, 37.3)
Fever (≥38°C) recorderd in the ED	
No	249 (90.2)
Yes	27 (9.8)
WBC count, median (IQR) × 10^9/L	3.0 (1.7, 4.8)
Severe neutropenia (< 0.5 x10^9/L)	
No	243 (88.0)
Yes	33 (12.0)
Severe thrombocytopenia (<50 x 10^9/L)	
No	142 (51.4)
Yes	134 (48.6)
COVID-19 within 14 days of the ED visit	
No	259 (93.8)
Yes	17 (6.2)

CRS, cytokine release syndrome; ICANS, immune effector cell-associated neurotoxicity syndrome; °C, Celsius.
*Only complaints occurring in more than 1% of the visits were reported. In some visits, the patient presented with more than one complaint.

unclear, one study reported a prevalence of COVID-19 of 4.8% and a mortality rate of nearly 50% in patients who had received CAR T therapy (18). This is likely due to the immunocompromised state after CAR T product infusion but is also affected by other factors, such as malignant disease state and comorbidities. ED clinicians must recognize that these patients have a much higher rate of complications from COVID-19 and should have a lower threshold for admitting them.

Our study shows that of patients presenting to ED within 6 months of CAR T cell therapy, CRS and ICANS was present in 7.6% and 3.3%, respectively. This is likely because the CAR T product administration in all our patients was done in an inpatient setting, during which these toxicities were closely monitored and treated during their inpatient hospital stay. The CRS and ICANS diagnosed at their presentation to our ED were those cases with delayed or late occurrence. In our cohort, most of the CRS and the ICANS reported during the ED visit were of grades 1 or 2. Our institutional guidance recommends patients stay within 30 minutes of the hospital for 30 days after CAR T product infusion, therefore this might have prompted patients to present earlier in the course of their illness, however, as CAR T product administration is increasingly being done as an outpatient procedure, ED physicians need to be aware of these toxicities, including the optimal evaluation, grading, and management plans (1), as higher grades (grade 3 and grade 4) are to be expected with the shift to outpatient administration.

As for the timing of the ED visits, those that occurred within 14 days of CAR T product infusion had significantly higher rates of fever and/or fatigue as a presenting complaint, with CRS and ICANS reported in these visits. Patients who first visited the ED early after CAR T product infusion had better overall survival outcomes compared with those who initially visited the ED later.

TABLE 3 Outcomes of emergency department (ED) visits for cancer patients in our analysis who had received chimeric antigen receptor T-cell infusion therapy within the past 6 months (total number of visits = 276).

Characteristic	No. (%)
ED disposition	
Admit	169 (61.2)
Discharge	68 (24.6)
Observation	34 (12.3)
Others*	5 (1.8)
ED median length of stay (IQR), hours	7 (5–9)
ICU admission	
No	262 (94.9)
Yes	14 (5.1)
Administration of antibiotics during ED stay	
No	136 (49.3)
Yes	140 (50.7)
Administration of tocilizumab during ED stay	
No	273 (98.9)
Yes	3 (1.1)
Administration of corticosteroids during ED stay	
No	260 (94.2)
Yes	16 (5.8)
Hospital median length of stay† (IQR), days	6 (4–9)
Death during the ED visit or subsequent hospital admission	
No	262 (94.9)
Yes	14 (5.1)
Death within 30 days of ED visit	
No	229 (83.0)
Yes	47 (17.0)
Death within 90 days of ED visit	
No	187 (67.8)
Yes	89 (32.2)

IQR, interquartile range; ICU, intensive care unit.
*Includes visits in which the patient left without being seen (n = 2), was transferred (n = 2), or left against medical advice (n = 1).
†Includes only visits in which the patient was admitted (n = 169).

After CAR T therapy, some patients present to the ED for the management of inflammatory events associated with the CAR T product, with certain severe cases needing to be admitted to the ICU (8, 19, 20). Our study showed that only a minority of the ED visits (5.1%) resulted in an ICU admission. However, 26.2% of the patients that presented to the ED had an ICU admission at some point within three months after CAR T therapy, either through direct admission or transfer to the ICU from initial hospitalization for CAR T-cell infusion. While the ICU stays resulting from ED visits have not been explored before, the overall ICU admission rate is similar to a recent international multicenter report showing that up to 27% of patients required ICU admission after CAR T therapy. Other studies reported different ICU admission rates ranging from 10-47% (7, 19, 21). The overall differences in ICU admission rates may stem from differences in local practices, especially the use of in-hospital infusion versus outpatient infusion. In this study, all the patients had in-hospital CAR T therapy infusion; therefore, CAR T therapy toxicities were closely monitored during that patient's inpatient stay prior to their ED presentation and were admitted to the ICU during that stay if needed. Additionally, our institutional guidance recommends patients stay within 30 minutes of the hospital for 30 days after CAR T product infusion; therefore, this might have prompted patients to present early in the course of their illness. Only 1 (1.6%) patient had CAR T therapy toxicity as the main cause of death.

For patients who first visited the ED later (>14 days of CAR T product infusion), in whom we observed worse overall survival outcomes, it is known that cancer patients frequently visit the ED near the end of life, with reasons mainly related to cancer progression (22). Moreover, and as previously reported, post CAR T relapse can be observed early after infusion and is associated with poor overall survival, mainly due to the persistence or progression of the primary malignant disease (23, 24). In our study, cancer progression was a main cause of death especially for patients who died later after their ED visit and/or the subsequent hospital admission, suggesting the utilization of ED by these patients near the end of life and explaining the poor survival outcomes for these patients. However, the interpretation of these results should pay heed to the fact that all the patients in this study had at least one ED visit, and other patients who had CAR T infusions but never visited the ED after their treatment may have other characteristics and different survival outcomes.

Mortality rates after the ED visits in our study were high, with a 30-day mortality rate of 17.0% and a 90-day mortality rate of 32.2%. To the best of our knowledge, the current study is the first to evaluate mortality rates in patients who visited the ED after CAR T therapy. A systematic review reported that fatal toxic side effects may occur with up to a 5% mortality rate within the first 30 days of CAR T therapy, but the risk of death varied depending on the product administered and other disease-specific factors (25). Additionally, others have reported non-relapse mortality associated with CAR T therapy to be as high as 15% overall, with infections and neurologic toxicities being major contributors to mortality (26). For this reason, it is important that ED clinicians are able to recognize these toxicities quickly when patients present to the ED after CAR T therapy.

Certain limitations accompanied our study, mainly due to the retrospective nature of the study. First, our cohort consisted of only patients who presented to the ED within 6 months of initiating CAR T therapy. The characteristics of patients who did not come to the ED could be different and need to be further investigated. In this study, interpretation of the reported toxicities needs to take into consideration that the prevalence rates reported in our study are limited to those reported at the time of the ED visit, which happened after the patients were discharged from their inpatient stay for CAR T product infusion, where we anticipate most of the toxicities occurred. Second, in the

TABLE 4 Univariate and multivariable Cox proportional hazards analyses of overall survival in cancer patients who visited the emergency department within 6 months after CAR T product infusion (n = 168).

Variable	Univariate		Multivariable	
	HR (95% CI)	P	HR (95% CI)	P
Age				
<65 years	Reference			
≥65 years	1.18 (0.71–1.96)	0.516	1.17 (0.69–1.98)	0.571
Sex				
Female	Reference			
Male	1.33 (0.79–2.25)	0.283	–	–
Race				
Non-White	Reference			
White	1.16 (0.67–2.01)	0.594	–	–
Charlson comorbidity index				
≤2	Reference			
>2	1.00 (0.52–1.89)	0.990	0.90 (0.47–1.72)	0.742
Main cancer type				
Multiple myeloma	Reference			
Leukemia	1.33 (0.40–4.38)	0.641	1.38 (0.39–4.82)	0.617
Lymphoma	1.20 (0.47–3.02)	0.702	1.33 (0.52–3.42)	0.549
Time to first ED visit				
Early (≤14 days after product infusion)	Reference			
Late (>14 days after product infusion)	**3.23 (1.29–8.10)**	**0.013**	**3.27 (1.29–8.27)**	**0.012**

HR, hazard ratio; CI, confidence interval; ED, emergency department. Boldface indicates P < 0.05.

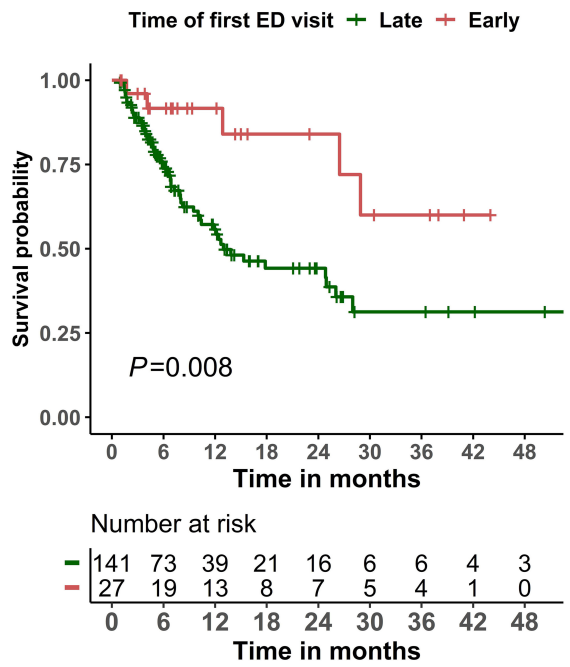

FIGURE 2
Kaplan-Meier overall survival curves among patients who visited the emergency department (ED) within 6 months of initiating chimeric antigen receptor T-cell infusion therapy, stratified by timing of the first ED visit (early: ≤14 days; late: >14 days).

current study, we reported specifically the reasons for presentation to the ED. Such an approach limited the integration of important clinical variables during pre- or post-ED visits, including adverse events that were presented elsewhere or events that occurred before or after the ED visit. Similarly, we could have possibly missed patients who presented to another ED or were admitted directly to the hospital. Finally, the cause of death was unknown or undocumented in 42.9% of the patients, for which a prospective study is needed to have a better and a complete understanding of the causes of death in these patients.

In conclusion, we found that cancer patients who receive CAR T therapy commonly visit the ED, and the timing of the visit is associated with different survival outcomes in these patients. Early ED visits appear to be related to the early systemic inflammatory response resulting from CAR T therapy and are associated with better overall survival. Most of the patients were admitted, and the 90-day mortality rate after these visits was high (32.2%). Additional future studies are needed to further investigate and identify characteristics of early presentation to the ED that can be used as a predictor of response to the treatment.

Data availability statement

The original contributions presented in the study are included in the article/Supplementary Material. Further inquiries can be directed to the corresponding author.

Ethics statement

The studies involving human participants were reviewed and approved by The University of Texas MD Anderson Cancer Center. Written informed consent for participation was not required for this study in accordance with the national legislation and the institutional requirements.

Author contributions

DL, AQ, and S-CY conceived and designed the study and developed the methods. AQ and PC collected the data. AQ was responsible for content analysis. S-CY supervised the statistical analysis. DL and AQ created the figures and tables. DL, AQ, PC, MW, PK, CR-G, and S-CY interpreted the results and drafted the first version of the manuscript. All authors contributed to the article and approved the submitted version.

Acknowledgments

The authors thank Erica Goodoff from the Research Medical Library at The University of Texas MD Anderson Cancer Center for editing this manuscript.

Conflict of interest

Author DL was employed by company IQVIA Biotech. S-CY was a member of an expert panel for Celgene, Inc. S-CYhad funding support from Bristol-Myer Squibb, Inc. and DepoMed, Inc.

The remaining authors declare that the research was conducted in the absence of any commercial or financial relationships that could be construed as a potential conflict of interest.

Publisher's note

All claims expressed in this article are solely those of the authors and do not necessarily represent those of their affiliated organizations, or those of the publisher, the editors and the reviewers. Any product that may be evaluated in this article, or claim that may be made by its manufacturer, is not guaranteed or endorsed by the publisher.

Supplementary material

The Supplementary Material for this article can be found online at: https://www.frontiersin.org/articles/10.3389/fonc.2023.1122329/full#supplementary-material

References

1. Santomasso BD, Nastoupil LJ, Adkins S, Lacchetti C, Schneider BJ, Anadkat M, et al. Management of immune-related adverse events in patients treated with chimeric antigen receptor T-cell therapy: Asco guideline. *J Clin Oncol* (2021) 39(35):3978–92. doi: 10.1200/JCO.21.01992

2. Sheth VS, Gauthier J. Taming the beast: Crs and icans after car T-cell therapy for all. *Bone Marrow Transplant* (2021) 56(3):552–66. doi: 10.1038/s41409-020-01134-4

3. Neelapu SS, Locke FL, Bartlett NL, Lekakis LJ, Miklos DB, Jacobson CA, et al. Axicabtagene ciloleucel car T-cell therapy in refractory Large b-cell lymphoma. *N Engl J Med* (2017) 377(26):2531–44. doi: 10.1056/NEJMoa1707447

4. Fischer JW, Bhattarai N. Car-T cell therapy: Mechanism, management, and mitigation of inflammatory toxicities. *Front Immunol* (2021) 12:693016. doi: 10.3389/fimmu.2021.693016

5. Lee DW, Santomasso BD, Locke FL, Ghobadi A, Turtle CJ, Brudno JN, et al. Astct consensus grading for cytokine release syndrome and neurologic toxicity associated with immune effector cells. *Biol Blood Marrow Transplant* (2019) 25(4):625–38. doi: 10.1016/j.bbmt.2018.12.758

6. Fowler NH, Dickinson M, Ghosh M, Chen AI, Andreadis C, Tiwari R, et al. Assessment of healthcare resource utilization and hospitalization costs in patients with relapsed or refractory follicular lymphoma undergoing car-T cell therapy with tisagenlecleucel: Results from the elara study. *Transplant Cell Ther* (2022) S2666-6367(22):01660–8. doi: 10.1016/j.jtct.2022.09.022

7. Johnson PC, Jacobson C, Yi A, Saucier A, Dhawale TM, Nelson A, et al. Healthcare utilization and end-of-Life outcomes in patients receiving car T-cell therapy. *J Natl Compr Canc Netw* (2021) 19(8):928–34. doi: 10.6004/jnccn.2020.7678

8. Kenzik KM, Johnson PC, Bhatia R, Bhatia S. Assessment of hospitalizations and emergency department visits after chimeric antigen receptor T-cell therapy among commercially insured patients. *JAMA Oncol* (2022) 8(7):1068–70. doi: 10.1001/jamaoncol.2022.1044

9. Chaftari P, Lipe DN, Wattana MK, Qdaisat A, Krishnamani PP, Thomas J, et al. Outcomes of patients placed in an emergency department observation unit of a comprehensive cancer center. *JCO Oncol Pract* (2022) 18(4):e574–e85. doi: 10.1200/OP.21.00478

10. Porter D, Frey N, Wood PA, Weng Y, Grupp SA. Grading of cytokine release syndrome associated with the car T cell therapy tisagenlecleucel. *J Hematol Oncol* (2018) 11(1):35. doi: 10.1186/s13045-018-0571-y

11. Porter DL, Levine BL, Kalos M, Bagg A, June CH. Chimeric antigen receptor-modified T cells in chronic lymphoid leukemia. *N Engl J Med* (2011) 365(8):725–33. doi: 10.1056/NEJMoa1103849

12. Lipe DN, Bourenane SS, Wattana MK, Gaeta S, Chaftari P, Cruz Carreras MT, et al. A modified emergency severity index level is associated with outcomes in cancer patients with covid-19. *Am J Emerg Med* (2022) 54:111–6. doi: 10.1016/j.ajem.2022.02.002

13. Revisions to the standards for the classification of federal data on race and ethnicity. (1997, October 30). Office of management and budget. Available at: https://obamawhitehouse.archives.gov/omb/fedreg_1997standards. Accessed on February 15, 2023.

14. Atrash S, Bano K, Harrison B, Abdallah AO. Car-T treatment for hematological malignancies. *J Investig Med* (2020) 68(5):956–64. doi: 10.1136/jim-2020-001290

15. Han D, Xu Z, Zhuang Y, Ye Z, Qian Q. Current progress in car-T cell therapy for hematological malignancies. *J Cancer* (2021) 12(2):326–34. doi: 10.7150/jca.48976

16. Zhao Z, Chen Y, Francisco NM, Zhang Y, Wu M. The application of car-T cell therapy in hematological malignancies: Advantages and challenges. *Acta Pharm Sin B* (2018) 8(4):539–51. doi: 10.1016/j.apsb.2018.03.001

17. Davis JA, Gaffney KJ, McGann M, Smith D, Edwards K, Baldino E, et al. Fever characteristics and impact on safety and efficacy of chimeric antigen receptor T-cell therapy. *Clin Lymphoma Myeloma Leuk* (2022) S2152-2650(22):01689–5. doi: 10.1016/j.clml.2022.09.005

18. Busca A, Salmanton-Garcia J, Corradini P, Marchesi F, Cabirta A, Di Blasi R, et al. Covid-19 and car T cells: A report on current challenges and future directions from the epicovideha survey by eha-idwp. *Blood Adv* (2022) 6(7):2427–33. doi: 10.1182/bloodadvances.2021005616

19. Azoulay E, Castro P, Maamar A, Metaxa V, de Moraes AG, Voigt L, et al. Outcomes in patients treated with chimeric antigen receptor T-cell therapy who were admitted to intensive care (Carttas): An international, multicentre, observational cohort study. *Lancet Haematol* (2021) 8(5):e355–e64. doi: 10.1016/S2352-3026(21)00060-0

20. Long B, Yoo MJ, Brady WJ, Holian A, Sudhir A, Gottlieb M. Chimeric antigen receptor T-cell therapy: An emergency medicine focused review. *Am J Emerg Med* (2021) 50:369–75. doi: 10.1016/j.ajem.2021.08.042

21. Li L, Liu J, Xu M, Yu H, Lv C, Cao F, et al. Treatment response, survival, safety, and predictive factors to chimeric antigen receptor T cell therapy in Chinese relapsed or refractory b cell acute lymphoblast leukemia patients. *Cell Death Dis* (2020) 11(3):207. doi: 10.1038/s41419-020-2388-1

22. Barbera L, Taylor C, Dudgeon D. Why do patients with cancer visit the emergency department near the end of life? *CMAJ* (2010) 182(6):563–8. doi: 10.1503/cmaj.091187

23. John S, Pulsipher MA, Moskop A, Hu Z-H, Phillips CL, Hall EM, et al. Real-world outcomes for pediatric and young adult patients with relapsed or refractory (R/R) b-cell acute lymphoblastic leukemia (All) treated with tisagenlecleucel: Update from the center for international blood and marrow transplant research (Cibmtr) registry. *Blood* (2021) 138(Supplement 1):428–. doi: 10.1182/blood-2021-146393

24. Vercellino L, Di Blasi R, Kanoun S, Tessoulin B, Rossi C, D'Aveni-Piney M, et al. Predictive factors of early progression after car T-cell therapy in Relapsed/Refractory diffuse Large b-cell lymphoma. *Blood Adv* (2020) 4(22):5607–15. doi: 10.1182/bloodadvances.2020003001

25. Cai C, Tang D, Han Y, Shen E, Abdihamid O, Guo C, et al. A comprehensive analysis of the fatal toxic effects associated with Cd19 car-T cell therapy. *Aging (Albany NY)* (2020) 12(18):18741–53. doi: 10.18632/aging.104058

26. Anand K, Burns E, Sano D, Pingali SR, Westin J, Nastoupil LJ, et al. Comprehensive report of anti-Cd19 chimeric antigen receptor T cells (Car-T) associated non-relapse mortality (Cart-nrm) from faers. *J Clin Oncol* (2019) 37 (15_suppl):2540–. doi: 10.1200/JCO.2019.37.15_suppl.2540

frontiers | Frontiers in Oncology

TYPE Original Research
PUBLISHED 24 March 2023
DOI 10.3389/fonc.2023.1124272

Check for updates

OPEN ACCESS

EDITED BY
Anand Rotte,
Arcellx Inc., United States

REVIEWED BY
Jakrawadee Julamanee,
Prince of Songkla University, Thailand
Paula Lam,
CellVec Pte Ltd., Singapore
Sarwish Rafiq,
School of Medicine, Emory University, United States

*CORRESPONDENCE
James K. C. Liu
james.liu@moffitt.org
Daniel Abate-Daga
daniel.abatedaga@moffitt.org

†These authors have contributed equally to this work and share first authorship

‡These authors have contributed equally to this work and share senior authorship

SPECIALTY SECTION
This article was submitted to Cancer Immunity and Immunotherapy, a section of the journal Frontiers in Oncology

RECEIVED 14 December 2022
ACCEPTED 21 February 2023
PUBLISHED 24 March 2023

CITATION
Potez M, Snedal S, She C, Kim J, Thorner K, Tran TH, Ramello MC, Abate-Daga D and Liu JKC (2023) Use of phage display biopanning as a tool to design CAR-T cells against glioma stem cells.
Front. Oncol. 13:1124272.
doi: 10.3389/fonc.2023.1124272

COPYRIGHT
© 2023 Potez, Snedal, She, Kim, Thorner, Tran, Ramello, Abate-Daga and Liu. This is an open-access article distributed under the terms of the Creative Commons Attribution License (CC BY). The use, distribution or reproduction in other forums is permitted, provided the original author(s) and the copyright owner(s) are credited and that the original publication in this journal is cited, in accordance with accepted academic practice. No use, distribution or reproduction is permitted which does not comply with these terms.

Use of phage display biopanning as a tool to design CAR-T cells against glioma stem cells

Marine Potez[1†], Sebastian Snedal[2†], Chunhua She[1], Jongmyung Kim[1], Konrad Thorner[2], Timothy H. Tran[3], Maria Cecilia Ramello[2], Daniel Abate-Daga[2,4*‡] and James K. C. Liu[1,4*‡]

[1]Neurosurgical Oncology, Department of Neuro-Oncology, H. Lee Moffitt Cancer Center and Research Institute, Tampa, FL, United States, [2]Department of Immunology, H. Lee Moffitt Cancer Center and Research Institute, Tampa, FL, United States, [3]Chemical Biology Core, H. Lee Moffitt Cancer Center and Research Institute, Tampa, FL, United States, [4]Department of Oncologic Sciences, Morsani College of Medicine, University of South Florida, Tampa, FL, United States

Background: Glioblastoma (GBM) is both the most common and aggressive type of primary brain tumor, associated with high mortality rates and resistance to conventional therapy. Despite recent advancements in knowledge and molecular profiling, recurrence of GBM is nearly inevitable. This recurrence has been attributed to the presence of glioma stem cells (GSCs), a small fraction of cells resistant to standard-of-care treatments and capable of self-renewal and tumor initiation. Therefore, targeting these cancer stem cells will allow for the development of more effective therapeutic strategies against GBM. We have previously identified several 7-amino acid length peptides which specifically target GSCs through *in vitro* and *in vivo* phage display biopanning.

Methods and results: We have combined two of these peptides to create a dual peptide construct (EV), and demonstrated its ability to bind GSCs *in vitro* and target intracranial GBM in mouse models. A peptide pull-down performed with peptide EV followed by mass spectrometry determined N-cadherin as the binding partner of the peptide, which was validated by enzyme-linked immunosorbent assay and surface plasmon resonance. To develop cytotoxic cellular products aimed at specifically targeting GSCs, chimeric antigen receptors (CARs) were engineered containing the peptide EV in place of the single-chain variable fragment (scFv) as the antigen-binding domain. EV CAR-transduced T cells demonstrated specific reactivity towards GSCs by production of interferon-gamma when exposed to GSCs, in addition to the induction of GSC-specific apoptosis as illustrated by Annexin-V staining.

Conclusion: These results exemplify the use of phage display biopanning for the isolation of GSC-targeting peptides, and their potential application in the development of novel cytotoxic therapies for GBM.

KEYWORDS

glioblastoma, glioma stem cells, novel binding domains, phage display biopanning, CAR-T, peptides, N-cadherin

Introduction

Glioblastoma (GBM) is the most common and malignant form of primary brain tumor and is associated with a poor prognosis with a median survival time of 16 months (1). The current standard-of-care treatment consists of maximal-safe surgical resection, followed by concurrent chemotherapy and radiotherapy, and maintenance chemotherapy (2). Recurrence is nearly inevitable, and less than 5% of patients survive 5 years after diagnosis (3). The resistance of GBM to conventional treatments remains an elusive challenge of this cancer, highlighting the need for novel therapeutic approaches.

Ex-vivo expansion of T cells followed by genetic modification with a chimeric antigen receptor (CAR) is used to redirect the immune cells to target various types of tumor cells. A CAR is a synthetic protein that typically consists of an extracellular antigen-recognition domain that contains the heavy and light chain variable fragments of a monoclonal antibody or B cell receptor, joined to a hinge and transmembrane domain, and an intracellular CD3ζ signaling domain from the T cell receptor, often in addition to a costimulatory domain such as CD28 (4). CAR-T cell activation and proliferation occur upon binding to their respective surface-exposed tumor antigen, thus leading to a cytotoxic attack on the antigen-bearing tumor cell (5). The clinical feasibility and safety of CAR-T cell therapy for patients with GBM has been demonstrated on three targets, interleukin-13 receptor alpha 2 (IL13-Rα2), human epidermal growth factor receptor 2 (HER2), and epidermal growth factor receptor variant III (EGFRvIII) (6–8). However, the clinical outcome remains unsatisfactory, with only partial responses being reported and a median survival time ranging between 8 and 11 months (9).

Tumor heterogeneity presently remains one of the main reasons for GBM resistance to treatment, largely due to the presence of cancer stem cells. Glioblastoma stem cells (GSCs) comprise a subpopulation of tumor cells that possess the unique abilities of self-renewal and tumor recapitulation, in addition to resistance to conventional radiotherapy and chemotherapy (10–12). Additional characteristics of these cells are the generation of differentiated progeny, invasive potential, and secretion of angiogenic factors (13–15). Several studies have identified and explored a variety of different markers of GSCs, such as CD133, CD15/SSEA, CD44, A2B5, SOX2, nestin, and OLIG2, however, none are able to universally define a GSC population (14, 16–20). Identification of a more ubiquitous GSC marker may allow for improved strategies to target and eliminate highly resistant tumors.

Phage display biopanning is a discovery tool that employs bacteriophages in which genes are inserted, and then displayed on their surface. Phage display allows for the isolation of peptides that can bind a specific cell type or protein through a series of positive and negative selection steps screening a library of random peptide sequences (21). The use of phage display biopanning to isolate peptides with specificity for GSCs has previously been employed (22, 23). Using a combination of 2 peptides previously isolated from phage display biopanning, we placed the dual peptide construct in the place of the scFv antigen-binding domain of a CAR, with the goal of designing a GSC-targeting cellular product. The peptide-based CAR-T cells were then evaluated for their reactivity and cytotoxicity.

Materials and methods

Approval and ethics statement

Experiments performed were approved by the Institutional Reviewed Board at the H. Lee Moffitt Cancer Center and Research Institute in accordance with the ethical guidelines set forth at each institution. GSCs, tumor tissue, and non-malignant normal brain were harvested from patient tumor samples or epileptic brain at Duke University Medical Center, Cleveland Clinic, and University Hospital Cleveland Medical Center in accordance with an approved protocol by the respective Institutional Review Boards. All animal studies were performed according to guidelines under Institutional Animal Care and Use Committee protocol approved at H. Lee Moffitt Cancer Center and Research Institute (IACUC# RIS00010727). Cg-Prkdcscid Il2rgtm1Wjl/SzJ (NSG) mice (male, 8 weeks old) were acquired from Jackson Laboratories (ME, USA), housed with ad libitum access to standard laboratory chow and water and with a 12-hour light/dark cycle.

Patient specimens and cell culture

T387 and T4121 glioblastoma stem cells were obtained from tissue dissociation of patient derived glioblastoma samples and maintained as previously described (13, 23). Both cell lines were pathologically described as glioblastoma at the time of resection from the patient. T4121 was a recurrent GBM. No additional molecular identifiers were available. To obtain differentiated glioma cells (DGCs), neurospheres were grown in DMEM containing 10% FBS and 1% Penicillin-Streptomycin. A172 glioblastoma cells (ATCC® CRL-1620™, Manassas, VA) and non-malignant brain cells (NM263) obtained from epileptic brain tissue were also maintained in DMEM supplemented by 10% FBS and 1% PS. Neural stem cells (NSCs) were obtained from EMD (Millipore, Temecula, CA) and cultured as described by the manufacturer. Human primary peripheral blood mononuclear cells (PBMCs) were obtained from de-identified buffy coats (OneBlood, Florida Blood Services, FL), cultured in X-VIVO medium (Lonza, Walkersville, MD) supplemented with 5% human serum (Access Biologicals, Vista, CA), 1% PS, 1% 200 mM L-glutamine, and 300 IU/mL of IL-2 (Clinigen, Yardley, PA), and activated with the anti-CD3ϵ monoclonal antibody OKT3 (Biolegend, San Diego, CA) for two days prior to transduction.

In vitro and *in vivo* phage display biopanning

In vitro and *in vivo* phage display biopanning was performed using a Ph.D.-7 Phage Display Peptide Library Kit (New England BioLabs, Ipswich, MA). The first step of the *in vitro* biopanning was a negative selection of the library against extracellular matrix and DGCs to remove non-GSC binding peptides. The peptide library was then screened against GSCs for four rounds of biopanning.

Phage clones were then isolated through bacterial infection and peptide sequences were isolated by sequencing. *In vivo* biopanning was performed by intravenously injecting the phage library in NSG mice bearing intracranial GBM. Following circulation of the peptide library for 24 hours, tumors were harvested, tumor cells were lysed, then bound phage peptides were isolated, purified, and transduced into E. coli for phage clone isolation and sequenced. The *in vivo* phage display performed against subcutaneous GBM was performed as previously described (22).

Peptides

The peptide AWEFYFPGGGGSGGGGSGGGGSSSQPFWS was conjugated with cyanine 3 (EV-Cy3) or with biotin (EV-b), and the scrambled non-targeting peptides FAYPEWFGGGGSGGG GSGGGGSPSWSFSQ (NT-Cy3 and NT-b) were synthesized by LifeTein, LCC (Hillsborough, NJ, USA). They were reconstituted in DMSO at a concentration of 10 mM and stored at -80°C.

Immunocytochemistry

After coating glass coverslips with Geltrex (1/100, Gibco, Waltham, MA) for 24 hours, cells were seeded and incubated overnight on the coated coverslips. The peptide cell staining was performed by removing the media and incubating the cells with PBS-1%-BSA for 15 minutes at 4°C. Biotinylated peptides (10 µM, EV-b or NT-b) were incubated for 20 minutes at 4°C, washed with PBS-1%-BSA for 5 minutes, and fluorescent-labeled streptavidin (1/100, AlexaFluor 647, Invitrogen, Waltham, MA) was added and incubated for 20 minutes at 4°C. The cells were then washed (PBS-1%-BSA, 5 minutes), fixed with 4% paraformaldehyde (20 minutes, RT), incubated with a 4',6-diamidino-2-phenylindole (DAPI) solution (PBS-1%-BSA + 100 ng/mL DAPI, 20 minutes, RT) and mounted with Anti-Fade Fluorescence Mounting Medium (Abcam, Cambridge, UK). Z-stack images were acquired with a Leica SP8 confocal microscope at 63 magnification 1X and 3X. All images were post-processed identically with Image J software (Bethesda, MD).

Flow cytometry

For the peptide-binding quantification and binding affinity assays, single cell suspensions of GSCs or DGCs (1×10^6 cells/mL) were saturated with PBS-1%-BSA for 15 minutes on ice, centrifuged at 150 x g for 3 minutes, then incubated at 4°C for 30 minutes with 10 µM or increased concentration of biotinylated peptide (EV-b or NT-b). Cells were washed two times and incubated with an AlexaFluor 647-streptavidin (1/100, Invitrogen, Waltham, MA) at 4°C for 30 minutes in the dark. Cells were washed two times with PBS-1%-BSA and resuspended in 50 µL of PBS-1%-BSA with DAPI (100 ng/mL, Invitrogen, Waltham, MA). An Amnis ImageStream flow cytometer (Luminex, Austin, TX) was used for recording and data was analyzed with Image Data Exploration and Analysis Software (IDEAS, EMD Millipore, Burlington, MA). Gating strategy shown in Supplemental Figure 1.

For the quantification of CAR transduction efficiency, T cells co-transduced with the EV CAR and truncated CD34, and untransduced (UT) T cells were washed, stained with CD34-PE (Invitrogen, MA5-16927), then incubated for 15 minutes at 4°C in the dark. Cells were then washed and resuspended in FACS buffer with DAPI and incubated for 15 minutes at 4°C in the dark. Data acquisition was performed with a BD FACSCanto II flow cytometer (Becton, Dickinson & Company, Franklin Lakes, NJ).

For apoptosis assay experiments, single cell suspensions of effector and target cells (4×10^5 and 8×10^5 cells, respectively) were surface-stained with CSPG4-APC (R&D Systems, FAB2585A), and CD3-BV711 (Biolegend, 317328), following a 4-6 hour co-culture, then incubated for 20 minutes at 4°C in the dark. Cells were then washed, secondarily stained with Annexin-V-FITC (Biolegend, 640906) and DAPI, incubated for 15 minutes at room temperature in the dark, and then analyzed. Data acquisition was performed with BD FACSCanto II or LSR II cytometers (Becton, Dickinson & Company, Franklin Lakes, NJ) and analyzed with FlowJo software (Becton, Dickinson & Company, Ashland, OR). Gating strategy shown in Supplemental Figure 6.

In vivo peptide injection

For *in vivo* imaging, a stereotaxic implantation was performed to inject 5 µL with 5×10^5 glioma stem cells transduced with luciferase, or 5 µL of PBS for the sham mice, in the right caudate nucleus with a Hamilton syringe. Two weeks after tumor implantation, 20 µM of EV-b stained by streptavidin-Alexa-Fluor 647 (1/100) was injected intravenously in the tail vein of the mice and intraperitoneal injection of 100 µL Luciferin (15 mg/mL, GoldBio, St Louis, MO) was performed to confirm the presence of GBM. Images were acquired on an IVIS Lumina (PerkinElmer, Waltham, MA) with excitation and emission filters of 660 and 710 nm, respectively, and a luminescence filter for luciferase cells. Measurements were performed by subtracting the fluorescence before injection from the fluorescence after injection on the lower back, and on the head.

Peptide pull-down assay

Cells were lysed using the IP Lysis Buffer Protocol (Pierce, Waltham, MA) as described by the manufacturer. Biotinylated peptides (EV-b and NT-b, 40 µg) were incubated with 100 µL of streptavidin agarose resin at 4°C for 1 hour on a rotator to generate the peptide-coupled streptavidin agarose resin. The protein samples were pre-cleared by incubation of 50 µL of NT-streptavidin agarose resins (4°C on rotator for 1 hour). After centrifugation, the pre-cleared samples were incubated with 150 µL of EV-coupled streptavidin agarose resin at 4°C overnight on rotator. After PBS wash, the resin was pelleted and sent for mass spectrometry analysis (see details in Supplementary Methods) or eluted with 4x Laemmli Sample Buffer (Bio-Rad, Hercules, CA) containing 1X DTT

reducing agent (dithiothreitol, Cell Signaling Technology, Danvers, MA) and boiled for SDS-PAGE. Pulled-down proteins were then separated with a Novex™ WedgeWell™ (ThermoFisher Scientific, Waltham, MA) and transferred to polyvinylidene fluoride (PVDF) membranes (Millipore, Burlington, MA). Membrane-transferred proteins were immunoblotted with an antibody recognizing N-cadherin (1/10000, NBP2-01498, Novus Biologicals, Littleton, CO) (Supplemental Figure 2).

Peptide-protein interaction profiling on HuProt™ arrays

The binding profile of EV-Cy3 peptide was evaluated on HuProt™ human proteome arrays, a human protein collection on a single array. The samples were sent to CDI Laboratories (Baltimore, MD) for the profiling assay of the samples. Candidates were identified using the following criteria: (1) The mean signal intensity of the sample group (EV-Cy3) is greater than 1.25-fold of the NT-Cy3 group; (2) p value < 0.05 (t-test); (3) the signal intensity of the candidates is at least three standard deviations above the mean signal intensity of the sample group (EV-Cy3).

Surface plasmon resonance

The direct binding measurements between N-cadherin and EV peptide by surface plasmon resonance was performed by immobilizing N-cadherin protein (Recombinant Human N-Cadherin extracellular domain, amino acids 160-724, 1388NC050, R&D Systems, Minneapolis, MN) to a CM5 sensor chip surface docked in Biacore T200 (Cytiva, Marlborough, MA) at 25°C using an amine-coupling method. Prior to immobilization, the chip was primed and equilibrated with a running buffer containing 20 mM HEPES, pH 7.4, 1 mM TCEP, 2 mM $CaCl_2$ and 150 mM NaCl at a flow rate of 10 µL/min. The carboxymethyl surface of the CM5 chip was manually activated for 7 minutes using a 1:1 ratio of 0.4 M 1-ethyl-3-(3-diaminopropyl) carbodiimide hydrochloride (EDC) and 0.1 M N-hydroxysuccinimide (NHS) to achieve a density of about 10,000 RU per flow cell. N-cadherin protein stock (1.12 µM) was diluted to 100 nM in 10 mM sodium acetate, pH 4.5, and manually injected over the surface at the same flow rate. Excess activated functional groups on the surface were blocked using a 7-minute injection of 1M ethanolamine, pH 8.5, at a flow rate of 10 µL/min. Using this manual injection protocol, approximately 3500 RU of N-cadherin was immobilized on the surface of the CM5 chip.

For kinetic titration experiments, the same running buffer was used except with the inclusion of 5% DMSO. SPR single cycle kinetic experiments with EV peptide were carried out in duplicate on two different sensor chips at 25°C. A threefold concentration series of EV peptide serially diluted in the running buffer ranging from 2 to 167 µM was injected over the sensor surface at 30 µL/min flow rate with 80-second contact time and 120-second dissociating time. For control experiments, a non-targeting (NT) peptide (GGGSGGG) was applied in place of EV peptide under identical condition. Sensorgrams were solvent corrected, buffer referenced, and the on-rate, off-rate, and equilibrium binding constants were calculated from the sensorgrams by global fitting of a 1:1 binding model, using analysis software (version 3.0) provided with Biacore T200 instrument (Cytiva).

Western blotting

T cells (5×10^6 per effector condition) were lysed with Laemmli buffer, and protein concentrations were quantified utilizing the Pierce BCA Protein Assay Kit (ThermoScientific, Waltham, MA). Membranes were incubated with 0.2 µg/mL mouse anti-human CD3ζ (Santa Cruz Biotechnology, SC-166275, Dallas, TX) and 0.04 µg/mL rabbit anti-human glyceraldehyde-3-phosphate dehydrogenase (Santa Cruz Biotechnology, SC-25778, Dallas, TX). Membranes were then washed and subsequently incubated with 0.05 µg/mL of corresponding secondary antibodies, goat anti-rabbit 680LT (LI-COR, 926-68021, Lincoln, NE), and goat anti-mouse 800CW (LI-COR, 32210, Lincoln, NE) in 5% blocking solution for 1 hour. After washing and drying, the membrane blots were developed utilizing the LI-COR Odyssey imaging system with both the 700 and 800 channels (Supplemental Figure 3).

Enzyme-linked immunosorbent assay

For evaluation of the peptide target, Nunc MaxiSorp, 96-well plates (ThermoFisher Scientific, Waltham, MA) were coated with 2.5 µg/mL of recombinant N-cadherin (Recombinant Human N-Cadherin extracellular domain, amino acids 160-724, 1388NC050, R&D Systems, Minneapolis, MN) diluted in 0.1 M $NaHCO_3$ overnight at 4°C. The wells were washed with PBS-0.025%-Tween 20 and blocked with PBS/BSA-3%-Milk at RT for 2 hours. Biotinylated peptides (EV-b or NT-b), diluted in PBS-2%-BSA at different concentrations, were incubated for 1 hour at RT and washed five times. The streptavidin-HRP (0.1 µg/mL) was incubated for 1 hour at RT followed by five washes and incubation with 3,3′,5,5′-tetramethylbenzidine substrate (TMB, 50 µL/well, ThermoFisher Scientific, Waltham, MA) for 10 minutes at RT. 50 µL of 2 M sulfuric acid (H_2SO_4) were added to each well to stop the coloration and the absorbance was immediately read at 450 nm. Five replicates were used for each concentration, and wells without N-cadherin coating served as control.

For evaluation of IFN-gamma secretion in co-culture experiments, Nunc MaxiSorp 96-well plates were coated at RT overnight with 0.63 µg/mL of recombinant human IFN-gamma M700A monoclonal antibody (ThermoFisher, Waltham, MA) diluted with 1X PBS. Wells were washed with PBS-0.2%-Tween 20 and blocked with PBS-4%-BSA at RT for 1 hour. IFN-gamma recombinant protein was prepared in a 1:1000 ratio with PBS-4%-BSA for use as a serially diluted standard for later interpolating concentrations of IFN-gamma in pg/mL. Co-culture supernatants were prepared with PBS-4%-BSA in a 1:10 ratio, then added to the ELISA plates and incubated at RT for 1 hour. 0.16 µg/mL

biotinylated recombinant IFN-gamma M701B monoclonal antibody (ThermoFisher, Waltham, MA) was prepared with PBS-4%-BSA, then added to the ELISA plates and incubated at RT for 1 hour. Precision Protein StrepTactin-HRP Conjugate (Bio-Rad, Hercules, CA) was prepared with PBS in a 1:5500 ratio, then added to the ELISA plates and incubated at RT for 30 minutes. 1-Step Ultra TMB Substrate (ThermoFisher, Waltham, MA) was added to the ELISA plates, then incubated for 10-15 minutes in the dark. Reactions were stopped by the addition of H_2SO_4, and the absorbance was immediately read at 450 nm and 550 nm. Experimental conditions were run in duplicate.

Retroviral vectors and cell transduction

For CAR cloning, gBlock gene fragments were designed to contain the codon-optimized coding sequence for the indicated target-binding domains, and synthesized by Integrated DNA Technologies. These were flanked by NcoI/NotI restriction sites, which were used for cloning by restriction enzyme digestion followed by ligation. Using this approach, we replaced the scFv-encoding sequence of PSCA-28t28z and PSCA8t28z plasmids, described previously (24). Chemically competent *E. coli* (Invitrogen, Waltham, MA) were transformed for amplification of the CAR plasmids. Retroviruses encoding for our CAR constructs were generated utilizing 293GP cells. These packaging cells were co-transfected for 7 hours on poly-D-lysine-coated plates with RD-114 envelope protein in addition to the CAR plasmid and lipofectamine 2000 (Invitrogen, Waltham, MA). For the T cell transductions, RetroNectin-coated plates (Takara, Kusatsu, Shiga, Japan) were coated with retrovirus and centrifuged for 2 hours at 4000 x g at 32°C, after which the virus was aspirated and 2×10^6 activated αβ T cells were seeded per well. The cells were centrifuged for 10 minutes at 1000 x g at 32°C, and then incubated for 24 hours before undergoing a second transduction.

Statistics

All statistics were performed with GraphPad Prism 8.2 (San Diego, CA). ImageStream flow cytometry data was analyzed with a one-way ANOVA and a Dunnett's multiple comparisons test. The binding affinities (Kd) were calculated with the One site-specific binding equation. A Kruskal-Wallis uncorrected test was used to compare the binding of EV and N-cadherin by ELISA. The difference between the *in vivo* fluorescence of the body and the head of the mice after EV injection was evaluated with a Wilcoxon paired test. IFN-gamma ELISA data was analyzed by two-way ANOVA and Tukey's multiple comparisons test to determine significance between CAR and GFP conditions within the same target cell group, and to compare CAR conditions across the different targets. The Annexin-V apoptosis data was analyzed by two-way ANOVA and Sidak's multiple comparisons test to determine significance between CAR and UT conditions against the target cell conditions. Proteome and mass spectrometry data was analyzed by T tests at Moffitt's core facilities.

Results

Tandem sequences combining two GSC-specific peptides target GSCs *in vitro* and *in vivo*

We have previously isolated glioblastoma stem cell targeting peptides through a combination of *in vitro* and *in vivo* biopanning strategies (22, 23). *In vitro* biopanning was performed by screening a random 7 amino acid phage peptide library against differentiated stem cells and glioblastoma stem cells grown in culture to isolate GSC-specific targeting peptides (Figure 1A). Two types of *in vivo* biopanning were performed, one against mice with intracranial GBM xenografts (Figure 1B) and one with subcutaneous flank xenografts (Figure 1C). Two peptides were selected for use in subsequent experiments. A single peptide sequence AWEFYFP (E) was isolated from both the *in vitro* and intracranial *in vivo* biopanning. Another peptide, SSQPFWS (V), was isolated from the subcutaneous flank biopanning. These two peptides were previously demonstrated to have specificity for targeting GSCs *in vitro* and therefore used to design new CAR constructs.

To combine the binding affinities, peptides AWEFYFP (E) and SSQPFWS (V) were joined by a flexible linker (GGGGSGG GGSGGGGS) resulting in a final length of 29 amino acids (EV). A scrambled sequence of both peptides joined by the same linker was used as a control peptide (NT) (Figure 2A). The EV peptide demonstrated specificity for binding GSCs compared to the NT peptide, and specificity over DGCs, GBM cell line, non-neoplastic brain cells (Figure 2B). Flow cytometry quantification of the EV staining on GSCs and DGCs showed significant differences between GSCs stained with EV compared to GSCs stained with NT ($p=0.0004$), DGCs stained with EV ($p=0.0028$), and DGCs stained with NT ($p=0.0011$) (Figure 2C). The evaluation of the peptide binding affinity by flow cytometry demonstrated a higher affinity of the peptide EV for GSCs compared to DGCs, with a KD of 32.3 μM for GSCs, and a higher KD of 220.7 μM for DGCs (Figure 2D). To determine the specificity of the EV peptide to target only glioblastoma, mice bearing intracranial T387 or T4121 xenograft GBM models, or mice that received a sham brain tumor implantation, were injected with 20 μM of EV. Fluorescence imaging demonstrated that only mice with intracranial xenografts had an increased fluorescence signal after peptide injection located only in the brain (Figure 2E). The mice with no brain tumors did not show any fluorescence localized in the brain after EV peptide injection.

EV peptide specifically binds to N-cadherin in GSCs

A peptide pull-down was performed with EV and NT peptides following incubation with GSC lysates to identify cellular binding partner(s) of EV (Figure 3A). Proteins that were collected through the pulldown were analyzed by mass spectrometry. Proteins isolated with EV were compared to proteins isolated with NT to determine the EV binding specificity. The mass spectrometry showed a 9.5-

10.3389/fonc.2023.1124272

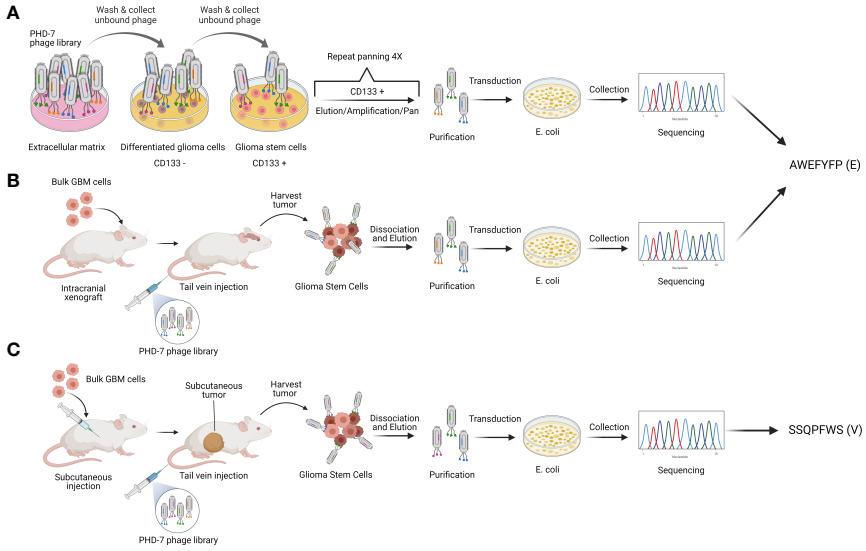

FIGURE 1
Peptide selection. Schematic representation of phage display strategies used to isolate the GSC-targeting peptides E (AWEFYFP) and V (SSQPFWS). **(A)** In vitro and **(B)** *in vivo* biopanning resulted in the identification of peptide E as one of the most enriched. **(C)** *In vivo* biopanning on subcutaneous tumors identified peptide V as one of the most enriched. Authors' elaboration based on prior data from (22, 23).

fold increase binding of EV to N-cadherin (CDH2) compared to NT on GSCs (Figure 3B). In parallel, binding of EV and NT to the HuProt Human Proteom Microarray (CDI Laboratories) was analyzed. In this analysis, N-cadherin showed a 4-fold increase binding of EV compared to NT peptide (Figure 3C).

Immunoblot performed with pulldown samples demonstrated positive signal with N-cadherin antibody in the EV peptide immunoprecipitates while absent in the NT peptide pulldown (Figure 3D). N-cadherin was also found to be present in a higher level in GSCs compared to DGCs. The binding affinity of EV to N-cadherin was confirmed by ELISA, which demonstrated dose-dependent binding with increasing concentration of EV to recombinant extracellular N-cadherin protein. All concentrations showed a strong affinity between EV and N-cadherin, compared to NT and N-cadherin ($p \leq 0.0348$, Figure 3E). Binding affinity evaluation was performed to rule out other binding partners isolated in the mass spectrometry and proteome array analysis to confirm binding to N-cadherin. Binding of EV and NT peptides to CTNNA1 or CTNNB1 in ELISA demonstrated no preference in binding of EV peptide over the NT peptide (Supplemental Figures 4A, B).

Surface plasmon resonance was also used to confirm the binding of EV peptide and N-cadherin *in vitro*. The single cycle kinetic results showed a very well fitted response curve by Biacore T200 Evaluation Software to derive an on-rate (k_a) of 2615 M-1 s-1 and an off-rate (k_d) of 0.01957 s-1, resulting in an equilibrium binding constant KD of 7.50 μM (Figure 3F). A repeated run under the same condition on another new CM5 sensor chip was fitted and resulted in a KD of 9.40 μM, giving an average KD of 8.45 μM. The NT peptide did not exhibit significant resonance units compared with those of the EV and could not be fitted for reliable extraction of the KD. The interaction of EV with N-cadherin was confirmed by flow cytometry after a knockdown of CDH2 in GSCs (Supplemental Figure 5).

CARs using tandem short peptides as the antigen-binding domain recognize GSCs

To determine the most efficacious design for our CAR-T cells, EV peptide was inserted in place of the scFv region for various CAR constructs (Figure 4A). The E-28t28z construct is comprised of a CD28 hinge/transmembrane domain, a CD28 co-stimulatory domain, and the intracellular signaling domain CD3ζ, while the E-8t28z construct instead contains a CD8 hinge/transmembrane domain. The E-28t28z-tCD34 and E-8t28z-tCD34 constructs are identical to the constructs described above but were co-expressed with a truncated CD34 (tCD34, used here as a cell-surface marker (25)), separated by a P2A cleavage site (Figures 4A, B). Staining of these CAR-T cells with anti-CD34-PE antibody allowed for the quantification of transduction efficiency by flow cytometry, showing robust cell transduction (75.4% and 63.1% for the E-28t28z and E-8t28z constructs, respectively, in the representative example shown, Figure 4C).

We next analyzed the ability of these CAR-T cells to recognize GSCs. To that end, we co-cultured (CAR-)T cells with GSCs or media alone overnight, and quantified the presence of IFN-gamma in the supernatants. All CAR-transduced T cells (except for E-8t28z-tCD34) showed a significant increase in IFN-gamma produced in response to co-culture with T387 GSCs when compared with mock-transduced (GFP) cells and with each respective CAR in presence of cell-free media ($p<0.0001$) (Figure 4D). To determine the cause of lack of reactivity by E-8t28z-tCD34, we analyzed the expression of the CAR molecules by

10.3389/fonc.2023.1124272

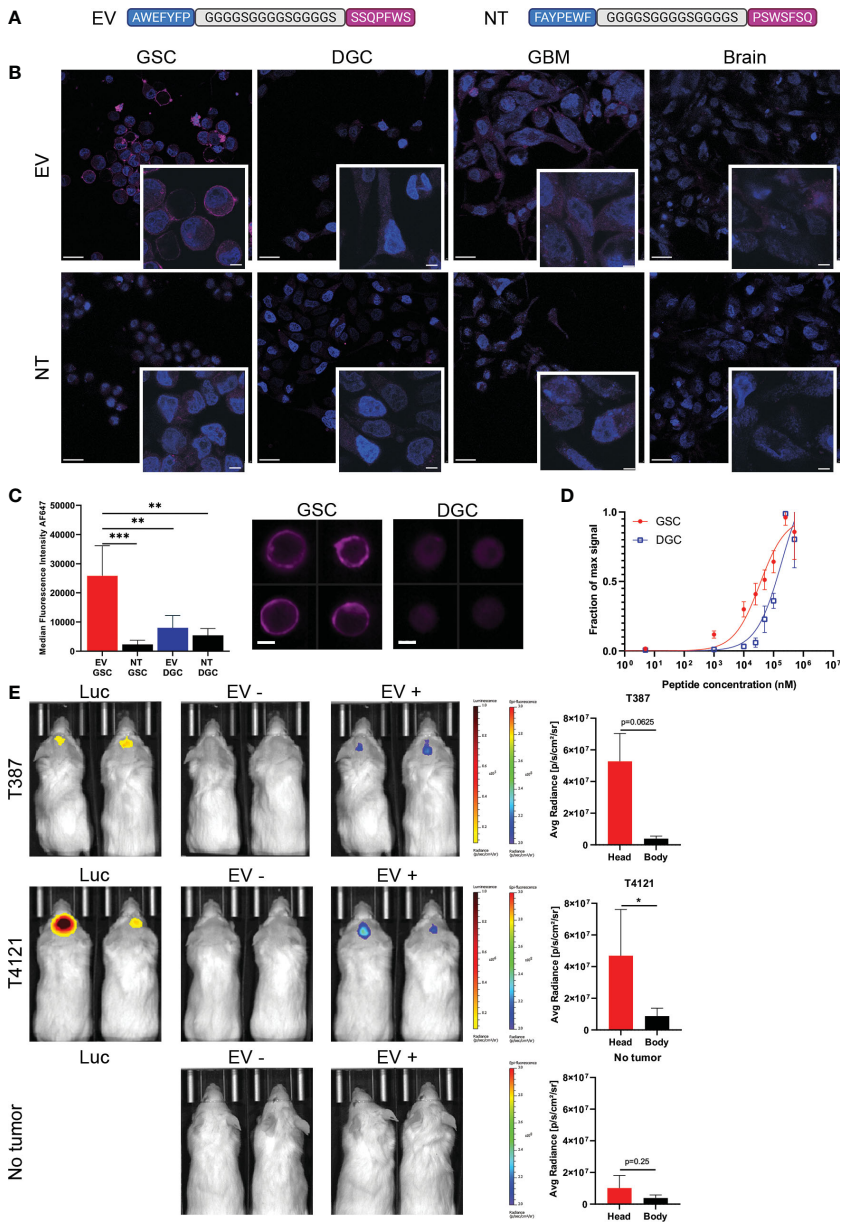

FIGURE 2
Specificity of the peptide for GSCs. **(A)** The two peptides recovered with phage display biopanning have been combined as a dual peptide (EV), linked by a sequence of glycine and serine. A non-targeting peptide (NT) employed the same amino acids in a scrambled sequence. **(B)** Immunocyto-fluorescent staining of different cells with EV or NT peptides (purple staining). Nuclei are stained with DAPI (blue staining). Scale bars: 20 µm, in zoomed images: 5 µm. **(C)** ImageStream quantification and representative images of EV staining on GSCs (red) and DGCs (blue), compared to NT (black bars), ** = $p < 0.01$, *** = $p < 0.001$. Signal intensity represented is actual measured median fluorescence intensity. Data in quadruplicate. Scale bars: 10µm. **(D)** Measure of the binding affinity of GSCs (red) or DGCs (blue) with increasing concentration of EV peptide by flow cytometry. Data in quadruplicate. **(E)** Representative images of mice and fluorescence measurements acquired with the IVIS Lumina. The presence of tumor was confirmed by luminescence after Luciferin injection. Images were acquired before (EV-) and after (EV+) EV injection for the T387 cells (top row), T4121 cells (middle row), and sham implanted (bottom row). The body measurements were taken at the lower back of the mice. The fluorescence scale remained the same for all the mice, and the luminescence scale was adapted between T387 and T4121 tumors, * = $p < 0.05$.

Western blot. An anti-CD3ζ antibody was used to identify the band corresponding to the CARs, which displayed a higher molecular weight than the endogenous CD3ζ. As shown in Figure 4E, the E-8t28z CAR was expressed when cloned in absence of tCD34, but its expression was impaired when co-expressed with the marker gene (full uncut membrane shown in Supplemental Figure 3). This finding indicates that the lack of GSC recognition by E-8t28z-tCD34 CAR-T cells observed in Figure 4D was due to abrogation of CAR expression. We therefore focused the rest of our experiments on the E-28t28z design.

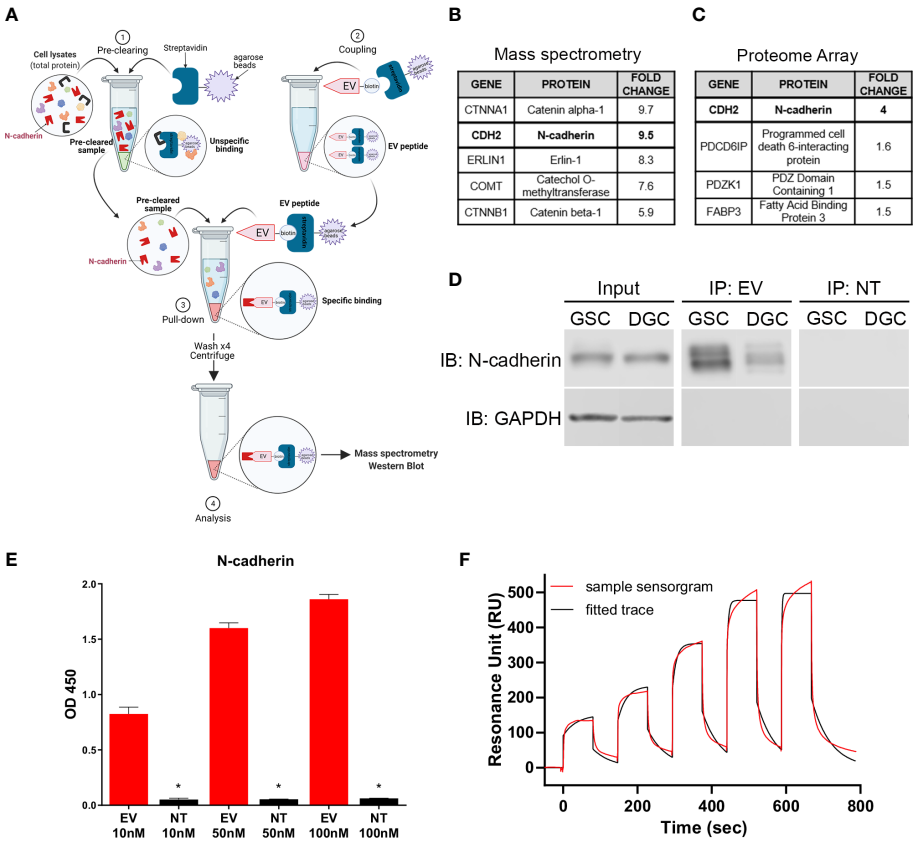

GENE	PROTEIN	FOLD CHANGE
CTNNA1	Catenin alpha-1	9.7
CDH2	**N-cadherin**	**9.5**
ERLIN1	Erlin-1	8.3
COMT	Catechol O-methyltransferase	7.6
CTNNB1	Catenin beta-1	5.9

GENE	PROTEIN	FOLD CHANGE
CDH2	**N-cadherin**	**4**
PDCD6IP	Programmed cell death 6-interacting protein	1.6
PDZK1	PDZ Domain Containing 1	1.5
FABP3	Fatty Acid Binding Protein 3	1.5

FIGURE 3
N-cadherin as the target of EV peptide. **(A)** Diagram of the peptide pull-down assay performed with EV-biotinylated peptide on GSCs and DGCs. **(B)** Highest scoring proteins from EV binding to GSC surface proteins identified by peptide pull-down followed by mass spectrometry analysis and **(C)** human proteome array. **(D)** Immunoblot results from the peptide pull-down, demonstrating a stronger binding to N-cadherin in GSCs compared to DGCs. **(E)** ELISA displaying the binding of different concentrations of EV or NT to N-cadherin. The stars show the significant differences between EV and NT for the same concentration, * = $p < 0.005$. Data in quadruplicate. **(F)** Surface plasmon resonance single cycle kinetic titration run showing the binding of EV peptide with N-cadherin using Biacore T200. Data were performed in duplicate.

Dual peptide CAR induces apoptosis of GSCs

We next evaluated if the selectivity of peptide binding to GSCs over DGCs was preserved in our CAR-T cells. In this experiment, we used two pairs of GSCs/DGCs, each pair derived from the same donor (T387 or T4121). In addition, due to the expression of CDH2 in healthy neural tissue, we tested if the E-28t28z selectively recognizes GSCs over non-malignant neural stem cells. To that end, E-28t28z-tCD34 engineered CAR-T cells were co-cultured with the abovementioned targets. Untransduced/mock-transduced T cells were used as negative controls, as well as CAR-T cells in media alone. CAR-transduced T cells secreted significantly more IFN-gamma in response to co-culture with either T387 and T4121 GSCs when compared with DGCs, NSCs, and cell-free media ($p<0.0001$). Additionally, CAR-transduced T cells demonstrated a significant increase in IFN-gamma produced in response to co-culture with either T387 and T4121 GSCs when compared with GFP-transduced T cells co-cultured with the same target cell type ($p<0.0001$) (Figure 5A). Although basal reactivity against DGCs was observed, our results confirm that the selectivity for GSCs is preserved. Most importantly, no recognition of NSCs was observed, suggesting that non-malignant stem cells would not be recognized by this CAR.

Finally, we tested the cytotoxic potential of E-28t28z-tCD34 CAR-T cells towards GSCs using Annexin-V staining (Figure 5B). Effector and target cells were cultured for 4-6 hours. We then quantified the percentage of Annexin-V-stained cells, in an attempt to capture both early (Annexin-V+/DAPI-) and late (Annexin-V+/DAPI+) apoptotic cells (gating strategy shown in Supplemental Figure 6). The assay demonstrated a significant increase of apoptosis induced to T387 ($p=0.0404$) and T4121 ($p=0.0223$) GSCs by E-28t28z-tCD34 CAR-T cells when compared to UT T cells, indicating that CAR-T cells can not only recognize but also eliminate GSCs. This difference was not observed in DGCs, reinforcing the notion of selectivity for cancer stem cells (Figure 5C).

Discussion

In this study, we employed peptides that were isolated from previous phage display biopanning (22, 23) with the aim of testing the hypothesis that these short synthetic peptides can be used as

10.3389/fonc.2023.1124272

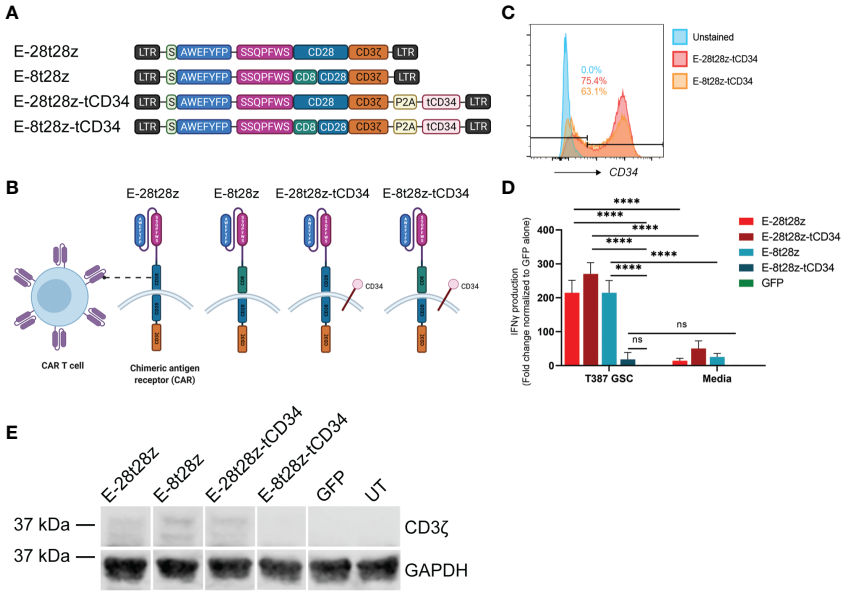

FIGURE 4
Dual peptide CAR-T cell design. **(A)** Diagram of the CAR construct designs. The E-28t28z and E-8t28z constructs use CD28 and CD8 as the hinge/transmembrane domains respectively, while both constructs employed CD28 for the co-stimulatory domain. The E-28t28z-tCD34 and E-8t28z-tCD34 constructs are identical to the E-28t28z and E-8t28z constructs but feature co-expression of truncated CD34 as an extracellular marker. **(B)** Diagram of a CAR-T cell with the different dual peptide-based constructs as the antigen-recognition domain. **(C)** CD34+ expression analysis by flow cytometry allows for a built-in quantification of transduction efficiency. **(D)** ELISA results displaying IFN-gamma secretion from CAR- or mock-transduced (GFP) T cells co-cultured overnight against T387 GSCs or cell-free media, **** = $p < 0.0001$. Values shown in the bar chart represent the average of two independent experiments. **(E)** CD3ζ western blotting with GAPDH as a housekeeping gene, used for additional support to confirm the presence or lack of the CAR following transduction. LTR, Long terminal repeat; S, signal peptide; P2A, Porcine teschovirus-1 2A self-cleaving peptide; tCD34, Truncated CD34.

antigen-binding domain to augment targeting of GSCs. Establishment of new therapies that will more effectively target and treat GBM must cross the BBB, target tumor cells without damaging the surrounding environment, and kill GSCs to prevent tumor relapse following standard of care treatment (13). These constraints have long served as obstacles against the development of effective interventions for primary malignant brain tumors.

Phage display biopanning has proven effective for the development of targeted therapeutics by isolating peptides that have preferential binding capacity for a given receptor or cell type (26). Extensive literature reports the application of peptides that specifically bind to different types of cells, such as tumor blood vessels, tumor lymphatic vessels, tumor cells, or to specific cell surface receptors, such as integrin and neuropilin, nestin, VPAC1 receptor, FGF9 in gastric and bladder cancer, or CD133 in glioblastoma (27–33). Based on the potential for using phage display biopanning to discover new therapeutic targets, multiple studies have conjugated their discovered peptides with nanoparticles, drugs or antisense oligonucleotides (34–38).

To focus on the targeting of GSCs, a subset of the tumor population which may be heavily involved in resistance to standard therapy, we have previously employed *in vitro* and *in vivo* phage display biopanning strategies to isolate peptides that specifically target and bind GSCs. Phage display biopanning can be used to isolate peptides that mimic a known ligand to replicate a specific ligand-receptor interaction. However, as definitive markers that specifically define GSCs remain elusive, we devised biopanning strategies to select for peptides that may target cellular receptors that are unique to the stem cell phenotype within GBMs. Our goal was then to leverage the specificity of these peptides to augment strategies for therapeutic delivery to GBM specifically by targeting GSCs.

We demonstrated that by combining two different peptides displaying GSC-targeting abilities, we maintained their specificity toward GSCs, and were also able to identify the targeted receptor, N-cadherin (CDH2). N-cadherin is an adhesion molecule with over 96% homology between human and mouse, which involved in the development of neural tissue and in various neurodegenerative processes (39). By using the dual peptide as the extracellular antigen-recognition domain of CAR constructs, we were able to create CAR-T cells that recognized GSCs *in vitro*. Extensive efforts to develop CAR-T cells targeting GBM have been made these past few years, and *in vitro* studies against GSCs with CAR-T cell therapies have demonstrated promising results (8, 40). The most studied tumor-associated antigen targets for CAR-T cells in GBM include interleukin-13 receptor alpha 2 (IL-13Rα2), EGFRvIII, and human epidermal growth factor receptor 2 (HER2) – molecules that can be expressed by GSCs (7, 8, 41). Therefore, CAR-T cell therapy represents an opportunity to eradicate this population of cells, largely implicated in treatment resistance and tumor relapse.

Our study has illustrated the utility and feasibility of designing novel antigen-binding domains for CAR-T cells by using two short peptides of just seven amino acids each to induce functional recognition of GSCs. We evaluated the expression and reactivity

10.3389/fonc.2023.1124272

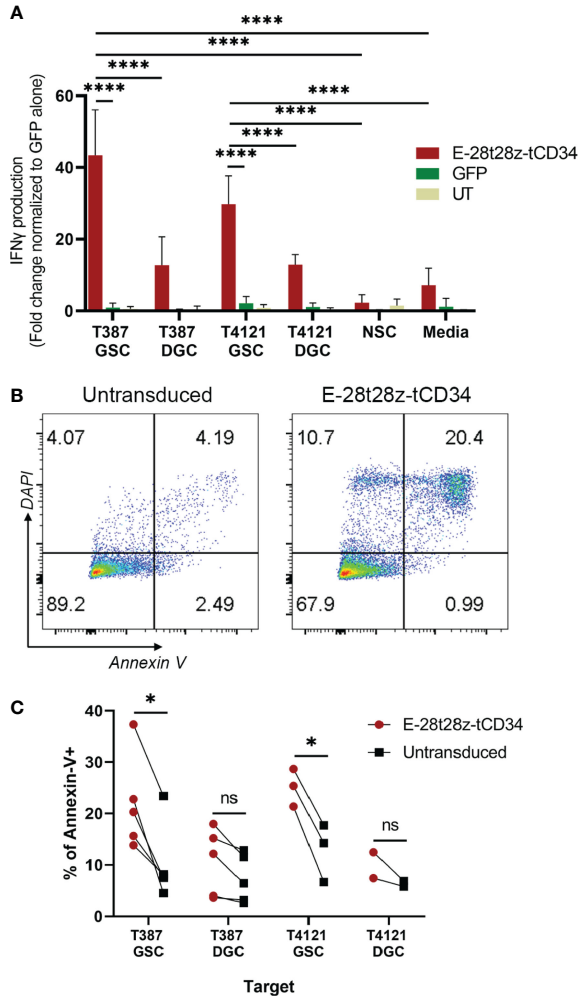

FIGURE 5
In vitro efficacy of the EV CAR-T cells. **(A)** IFN-gamma secretion results from the E-28t28z-tCD34 CAR-transduced, GFP-transduced and untransduced (UT) T cells after overnight co-culture with different cells, **** = $p < 0.0001$. **(B)** Representative dot plot of Annexin-V staining of GSCs after 4-6 hour co-culture with untransduced and E-28t28z-tCD34 cells. **(C)** Summary of percentage of Annexin-V+ cells following co-culture with the indicated effectors. Target cells include GSC and DGC from two independent donors: T387 and T4121. *$p < 0.05$ (T387 GSC, and T4121 GSC). n.s.= non statistically significant.

of several different EV-based CAR constructs in alpha-beta T cells, narrowing it down to use of CD28 or CD8 as the hinge/transmembrane domains and CD28 as the superior costimulatory domain, with our final CAR constructs exhibiting specific reactivity and cytotoxicity against GSCs with the dual peptide used in the place of the single-chain variable fragment (scFv) as the antigen-binding domain. By using mass spectrometry and human proteome analysis, we were able to isolate N-cadherin as the likely target of the peptide-based recognition of GSCs. N-cadherin is a transmembrane protein that plays a key role in cell-cell adhesion in the brain, and is involved in the epithelial-mesenchymal transition, with increase of its expression while E-cadherin expression is decreased (42–44). N-cadherin has a role in tumor invasion and is known to be expressed in GBM and GSCs (45–48). The expression of N-cadherin has also been associated with WHO glioma grading, correlating with a decreased patient survival when overexpressed (20). The study of Osuka et al. showed that a knockout of N-cadherin by CRISPR/Cas9 reduced the stemness and the resistance of GSCs to radiation therapy (49). Therefore, N-cadherin may be a viable target that allows specific targeting of GSCs. It is unclear at this time as to the exact region of N-cadherin that is targeted by the peptides. We do know that based on the recombinant N-cadherin (reference 1388NC050, R&D Systems Inc., Minneapolis, MN) used for the ELISA binding experiments (Figure 3E), that the EV peptide is binding to the extracellular domain between amino acids 160-724. We have previously tested the binding of peptide AWEFYFP (E) and found that by itself it demonstrated positive binding to N-cadherin (manuscript under review). Further studies will be needed to better understand how each peptide affects the binding of peptide EV to N-cadherin.

Despite the specificity of the dual peptide-based CAR-T cells for targeting GSCs over DGCs or NSCs, the targeting of N-cadherin can have some limitations. This protein is widely expressed in normal tissues, particularly in the brain, endocrine tissues, and muscle tissues (especially in the heart). Though we have demonstrated a lack of EV peptide targeting of non-neoplastic brain tissue, further studies are necessary to understand the role of N-cadherin in EV peptide specificity for the targeting of GSCs. However, the knowledge that we have advanced in producing a functional antigen-recognition domain with tandemly arranged short peptides derived from phage-display biopanning could prove useful for the generation of new tethering or costimulatory receptors. Such receptors can serve as a physical bridge linking tumor cell and T cell, increasing functional avidity, and stabilizing or enhancing the immunological synapse without resulting in an activation cascade on their own (50). On-target off-tumor toxicity remains a hurdle in CAR-T cell therapies, though the employment of a Boolean logic "AND" gate in T cell immunotherapy can circumvent this issue by requiring gene-edited T cells to recognize two or more antigens to result in effector function (51, 52). A potential dual-receptor strategy for GBM could involve an "AND" gate approach employing the GSC-targeting peptides in conjunction with other known GBM-targeting CARs.

Further studies utilizing GSC-targeting CAR-T cells will need to be tested to demonstrate the effectiveness of these cells in the *in vivo* setting. Given the potential ubiquity of N-cadherin receptors, different delivery methods may need to be tested, such as intrathecal or intratumoral delivery, to avoid non-specific binding outside of the central nervous system. As GSC-targeting CAR-T cells will be directed against a subset of the GBM tumor population, detailed studies will need to be constructed to safely and effectively deliver the CAR-T cells and to test their effectiveness on limiting on tumor recapitulation and invasion.

Conclusion

Our results exhibit the potential for utilizing *in vitro* and *in vivo* phage display biopanning approaches to obtain peptides that can serve as the antigen-binding domain of CAR constructs. Our CAR-T cells retained the same specificity toward GSCs as our initial peptides

and led to functional reactivity and cytotoxicity. This study demonstrates the potential of developing novel strategies for the treatment and diagnosis of different tumors currently incurable.

Data availability statement

The datasets presented in this article are not readily available because sharing of materials and data are subject to review and approval by Moffitt's Office of General Counsel and Office of Innovation. Some materials are bound to MTA. Requests to access the datasets should be directed to james.liu@moffitt.org.

Ethics statement

The animal study was reviewed and approved by USF IACUC (Protocol RIS00010727).

Author contributions

DA-D and JL jointly contributed to conception and design of the study. MP, SS, CS, JK, KT, TT, and MR contributed to experimental design and acquisition/analysis/interpretation of data. MP and SS wrote the first draft of the manuscript. All authors contributed to manuscript revision, read, and approved the submitted version.

Funding

This work has been partially funded by the Moffitt-Celgene Innovative Studies award, and supported by the Flow Cytometry and Proteomics Core Facilities at Moffitt Cancer Center, an NCI designated Comprehensive Cancer Center (P30-CA076292).

Acknowledgments

Figure images were generated with BioRender.

Conflict of interest

DA-D and JL are inventors or co-inventors in several patents and patent applications filed by the Moffitt Cancer Center, including one pertaining to this work US 11384118. DA-D also receives or has received funding from Intellia and bluebird bio/2-seventy bio, but neither of these relationships are associated with the subject matter of this manuscript.

The remaining authors declare that the research was conducted in the absence of any commercial or financial relationships that could be construed as a potential conflict of interest.

Publisher's note

All claims expressed in this article are solely those of the authors and do not necessarily represent those of their affiliated organizations, or those of the publisher, the editors and the reviewers. Any product that may be evaluated in this article, or claim that may be made by its manufacturer, is not guaranteed or endorsed by the publisher.

Supplementary material

The Supplementary Material for this article can be found online at: https://www.frontiersin.org/articles/10.3389/fonc.2023.1124272/full#supplementary-material

References

1. Omuro A, DeAngelis LM. Glioblastoma and other malignant gliomas: A clinical review. *JAMA* (2013) 310:1842–50. doi: 10.1001/jama.2013.280319

2. Stupp R, Hegi ME, Gilbert MR, Chakravarti A. Chemoradiotherapy in malignant glioma: Standard of care and future directions. *J Clin Oncol* (2007) 25:4127–36. doi: 10.1200/JCO.2007.11.8554

3. Thakkar JP, Dolecek TA, Horbinski C, Ostrom QT, Lightner DD, Barnholtz-Sloan JS, et al. Epidemiologic and molecular prognostic review of glioblastoma. *Cancer Epidemiol Biomarkers Prev* (2014) 23:1985–96. doi: 10.1158/1055-9965.EPI-14-0275

4. Stock S, Schmitt M, Sellner L. Optimizing manufacturing protocols of chimeric antigen receptor T cells for improved anticancer immunotherapy. *Int J Mol Sci* (2019) 20. doi: 10.3390/ijms20246223

5. Liu EK, Sulman EP, Wen PY, Kurz SC. Novel therapies for glioblastoma. *Curr Neurol Neurosci Rep* (2020) 20:19. doi: 10.1007/s11910-020-01042-6

6. Brown CE, Alizadeh D, Starr R, Weng L, Wagner JR, Naranjo A, et al. Regression of glioblastoma after chimeric antigen receptor T-cell therapy. *N. Engl J Med* (2016) 375:2561–9. doi: 10.1056/NEJMoa1610497

7. Ahmed N, Brawley V, Hegde M, Bielamowicz K, Kalra M, Landi D, et al. HER2-specific chimeric antigen receptor-modified virus-specific T cells for progressive glioblastoma: A phase 1 dose-escalation trial. *JAMA Oncol* (2017) 3:1094–101. doi: 10.1001/jamaoncol.2017.0184

8. O'Rourke DM, Nasrallah MP, Desai A, Melenhorst JJ, Mansfield K, Morrissette JJD, et al. A single dose of peripherally infused EGFRvIII-directed CAR T cells mediates antigen loss and induces adaptive resistance in patients with recurrent glioblastoma. *Sci Transl Med* (2017) 9. doi: 10.1126/scitranslmed.aaa0984

9. Bagley SJ, Desai AS, Linette GP, June CH, O'rourke DM. CAR T-cell therapy for glioblastoma: Recent clinical advances and future challenges. *Neuro Oncol* (2018) 20:1429–38. doi: 10.1093/neuonc/noy032

10. Eyler CE, Rich JN. Survival of the fittest: cancer stem cells in therapeutic resistance and angiogenesis. *J Clin Oncol* (2008) 26:2839–45. doi: 10.1200/JCO.2007.15.1829

11. Hadjipanayis CG, Van Meir EG. Tumor initiating cells in malignant gliomas: Biology and implications for therapy. *J Mol Med* (2009) 87:363–74. doi: 10.1007/s00109-009-0440-9

12. Zhou BB, Zhang H, Damelin M, Geles KG, Grindley JC, Dirks PB. Tumour-initiating cells: Challenges and opportunities for anticancer drug discovery. *Nat Rev Drug Discovery* (2009) 8:806–23. doi: 10.1038/nrd2137

13. Bao S, Wu Q, Mclendon RE, Hao Y, Shi Q, Hjelmeland AB, et al. Glioma stem cells promote radioresistance by preferential activation of the DNA damage response. *Nature* (2006) 444:756–60. doi: 10.1038/nature05236

14. Rich JN, Eyler CE. Cancer stem cells in brain tumor biology. *Cold Spring Harb Symp. Quant. Biol* (2008) 73:411–20. doi: 10.1101/sqb.2008.73.060

15. Mannino M, Chalmers AJ. Radioresistance of glioma stem cells: intrinsic characteristic or property of the 'microenvironment-stem cell unit'? *Mol Oncol* (2011) 5:374–86. doi: 10.1016/j.molonc.2011.05.001

16. Singh SK, Hawkins C, Clarke ID, Squire JA, Bayani J, Hide T, et al. Identification of human brain tumour initiating cells. *Nature* (2004) 432:396–401. doi: 10.1038/nature03128

17. Ogden AT, Waziri AE, Lochhead RA, Fusco D, Lopez K, Ellis JA, et al. Identification of A2B5+CD133- tumor-initiating cells in adult human gliomas. *Neurosurgery* (2008) 62:505–14. doi: 10.1227/01.neu.0000316019.28421.95

18. Son MJ, Woolard K, Nam DH, Lee J, Fine HA. SSEA-1 is an enrichment marker for tumor-initiating cells in human glioblastoma. *Cell Stem Cell* (2009) 4:440–52. doi: 10.1016/j.stem.2009.03.003

19. Anido J, Saez-Borderias A, Gonzalez-Junca A, Rodon L, Folch G, Carmona MA, et al. TGF-beta receptor inhibitors target the CD44(high)/Id1(high) glioma-initiating cell population in human glioblastoma. *Cancer Cell* (2010) 18:655–68. doi: 10.1016/j.ccr.2010.10.023

20. Chen Q, Cai J, Jiang C. CDH2 expression is of prognostic significance in glioma and predicts the efficacy of temozolomide therapy in patients with glioblastoma. *Oncol Lett* (2018) 15:7415–22. doi: 10.3892/ol.2018.8227

21. Smith GP. Filamentous fusion phage: Novel expression vectors that display cloned antigens on the virion surface. *Science* (1985) 228:1315–7. doi: 10.1126/science.4001944

22. Liu JK, Lubelski D, Schonberg DL, Wu Q, Hale JS, Flavahan WA, et al. Phage display discovery of novel molecular targets in glioblastoma-initiating cells. *Cell Death Differ*. (2014) 21:1325–39. doi: 10.1038/cdd.2014.65

23. Kim J, She C, Potez M, Huang P, Wu Q, Prager BC, et al. Phage display targeting identifies EYA1 as a regulator of glioblastoma stem cell maintenance and proliferation. *Stem Cells* (2021) 39:853–65. doi: 10.1002/stem.3355

24. Abate-Daga D, Lagisetty KH, Tran E, Zheng Z, Gattinoni L, Yu Z, et al. A novel chimeric antigen receptor against prostate stem cell antigen mediates tumor destruction in a humanized mouse model of pancreatic cancer. *Hum Gene Ther* (2014) 25(12):1003–12. doi: 10.1089/hum.2013.209

25. Park TS, Abate-Daga D, Zhang L, Zheng Z, Morgan RA. Gamma-retroviral vector design for the co-expression of artificial microRNAs and therapeutic proteins. *Nucleic Acid Ther* (2014) 24:356–63. doi: 10.1089/nat.2014.0486

26. Federici T, Liu JK, Teng Q, Yang J, Boulis NM. A means for targeting therapeutics to peripheral nervous system neurons with axonal damage. *Neurosurgery* (2007) 60:911–8. doi: 10.1227/01.NEU.0000255444.44365.B9

27. Laakkonen P, Porkka K, Hoffman JA, Ruoslahti E. A tumor-homing peptide with a targeting specificity related to lymphatic vessels. *Nat Med* (2002) 8:751–5. doi: 10.1038/nm720

28. Fogal V, Zhang L, Krajewski S, Ruoslahti E. Mitochondrial/cell-surface protein p32/gC1qR as a molecular target in tumor cells and tumor stroma. *Cancer Res* (2008) 68:7210–8. doi: 10.1158/0008-5472.CAN-07-6752

29. Sugahara KN, Teesalu T, Karmali PP, Kotamraju VR, Agemy L, Girard OM, et al. Tissue-penetrating delivery of compounds and nanoparticles into tumors. *Cancer Cell* (2009) 16:510–20. doi: 10.1016/j.ccr.2009.10.013

30. Beck S, Jin X, Yin J, Kim SH, Lee NK, Oh SY, et al. Identification of a peptide that interacts with nestin protein expressed in brain cancer stem cells. *Biomaterials* (2011) 32:8518–28. doi: 10.1016/j.biomaterials.2011.07.048

31. Tang B, Li Z, Huang D, Zheng L, Li Q. Screening of a specific peptide binding to VPAC1 receptor from a phage display peptide library. *PloS One* (2013) 8:e54264. doi: 10.1371/journal.pone.0054264

32. Vora P, Venugopal C, Salim SK, Tatari N, Bakhshinyan D, Singh M, et al. The rational development of CD133-targeting immunotherapies for glioblastoma. *Cell Stem Cell* (2020) 26:832–844.e836. doi: 10.1016/j.stem.2020.04.008

33. Wang J, Tan X, Guo Q, Lin X, Huang Y, Chen L, et al. FGF9 inhibition by a novel binding peptide has efficacy in gastric and bladder cancer per se and reverses resistance to cisplatin. *Pharmacol Res* (2020) 152:104575. doi: 10.1016/j.phrs.2019.104575

34. Henke E, Perk J, Vider J, De Candia P, Chin Y, Solit DB, et al. Peptide-conjugated antisense oligonucleotides for targeted inhibition of a transcriptional regulator *in vivo*. *Nat Biotechnol* (2008) 26:91–100. doi: 10.1038/nbt1366

35. Sugahara KN, Teesalu T, Karmali PP, Kotamraju VR, Agemy L, Greenwald DR, et al. Coadministration of a tumor-penetrating peptide enhances the efficacy of cancer drugs. *Science* (2010) 328:1031–5. doi: 10.1126/science.1183057

36. Pang HB, Braun GB, Friman T, Aza-Blanc P, Ruidiaz ME, Sugahara KN, et al. An endocytosis pathway initiated through neuropilin-1 and regulated by nutrient availability. *Nat Commun* (2014) 5:4904. doi: 10.1038/ncomms5904

37. Hamilton AM, Aidoudi-Ahmed S, Sharma S, Kotamraju VR, Foster PJ, Sugahara KN, et al. Nanoparticles coated with the tumor-penetrating peptide iRGD reduce experimental breast cancer metastasis in the brain. *J Mol Med* (2015) 93:991–1001. doi: 10.1007/s00109-015-1279-x

38. Paasonen L, Sharma S, Braun GB, Kotamraju VR, Chung TD, She ZG, et al. New p32/gC1qR ligands for targeted tumor drug delivery. *Chembiochem* (2016) 17:570–5. doi: 10.1002/cbic.201500564

39. Laszlo ZI, Lele Z. Flying under the radar: CDH2 (N-cadherin), an important hub molecule in neurodevelopmental and neurodegenerative diseases. *Front Neurosci* (2022) 16:972059. doi: 10.3389/fnins.2022.972059

40. Brown CE, Starr R, Aguilar B, Shami AF, Martinez C, D'apuzzo M, et al. Stem-like tumor-initiating cells isolated from IL13Ralpha2 expressing gliomas are targeted and killed by IL13-zetakine-redirected T cells. *Clin Cancer Res* (2012) 18:2199–209. doi: 10.1158/1078-0432.CCR-11-1669

41. Brown CE, Badie B, Barish ME, Weng L, Ostberg JR, Chang WC, et al. Bioactivity and safety of IL13Rα2-redirected chimeric antigen receptor CD8+ T cells in patients with recurrent glioblastoma. *Clin Cancer Res* (2015) 21:4062–72. doi: 10.1158/1078-0432.CCR-15-0428

42. Hatta K, Okada TS, Takeichi M. A monoclonal antibody disrupting calcium-dependent cell-cell adhesion of brain tissues: possible role of its target antigen in animal pattern formation. *Proc Natl Acad Sci U.S.A.* (1985) 82:2789–93. doi: 10.1073/pnas.82.9.2789

43. Inuzuka H, Redies C, Takeichi M. Differential expression of r- and n-cadherin in neural and mesodermal tissues during early chicken development. *Development* (1991) 113:959–67. doi: 10.1242/dev.113.3.959

44. Wheelock MJ, Shintani Y, Maeda M, Fukumoto Y, Johnson KR. Cadherin switching. *J Cell Sci* (2008) 121:727–35. doi: 10.1242/jcs.000455

45. Shinoura N, Paradies NE, Warnick RE, Chen H, Larson JJ, Tew JJ, et al. Expression of n-cadherin and alpha-catenin in astrocytomas and glioblastomas. *Br J Cancer* (1995) 72:627–33. doi: 10.1038/bjc.1995.384

46. Asano K, Duntsch CD, Zhou Q, Weimar JD, Bordelon D, Robertson JH, et al. Correlation of n-cadherin expression in high grade gliomas with tissue invasion. *J Neurooncol.* (2004) 70:3–15. doi: 10.1023/B:NEON.0000040811.14908.f2

47. Camand E, Peglion F, Osmani N, Sanson M, Etienne-Manneville S. N-cadherin expression level modulates integrin-mediated polarity and strongly impacts on the speed and directionality of glial cell migration. *J Cell Sci* (2012) 125:844–57. doi: 10.1242/jcs.087668

48. Velpula KK, Rehman AA, Chelluboina B, Dasari VR, Gondi CS, Rao JS, et al. Glioma stem cell invasion through regulation of the interconnected ERK, integrin alpha6 and n-cadherin signaling pathway. *Cell Signal* (2012) 24:2076–84. doi: 10.1016/j.cellsig.2012.07.002

49. Osuka S, Zhu D, Zhang Z, Li C, Stackhouse CT, Sampetrean O, et al. N-cadherin upregulation mediates adaptive radioresistance in glioblastoma. *J Clin Invest* (2021) 131. doi: 10.1172/JCI136098

50. Katsarou A, Sjostrand M, Naik J, Mansilla-Soto J, Kefala D, Kladis G, et al. Combining a CAR and a chimeric costimulatory receptor enhances T cell sensitivity to low antigen density and promotes persistence. *Sci Transl Med* (2021) 13:eabh1962. doi: 10.1126/scitranslmed.abh1962

51. Guedan S, Calderon H, Posey ADJr., Maus MV. Engineering and design of chimeric antigen receptors. *Mol Ther Methods Clin Dev* (2019) 12:145–56. doi: 10.1016/j.omtm.2018.12.009

52. Savanur MA, Weinstein-Marom H, Gross G. Implementing logic gates for safer immunotherapy of cancer. *Front Immunol* (2021) 12:780399. doi: 10.3389/fimmu.2021.780399

frontiers | Frontiers in Immunology

TYPE Review
PUBLISHED 05 May 2023
DOI 10.3389/fimmu.2023.1170968

Check for updates

OPEN ACCESS

EDITED BY
Anand Rotte,
Arcellx Inc, United States

REVIEWED BY
Jie Sun,
Zhejiang University, China
Pooria Safarzadeh Kozani,
Tarbiat Modares University, Iran

*CORRESPONDENCE
Mingfeng Zhao
mingfengzhao@sina.com

†These authors have contributed equally to this work and share first authorship

RECEIVED 22 February 2023
ACCEPTED 21 April 2023
PUBLISHED 05 May 2023

CITATION
Liu J, Zhang Y, Guo R, Zhao Y, Sun R, Guo S, Lu W and Zhao M (2023) Targeted CD7 CAR T-cells for treatment of T-Lymphocyte leukemia and lymphoma and acute myeloid leukemia: recent advances. *Front. Immunol.* 14:1170968. doi: 10.3389/fimmu.2023.1170968

COPYRIGHT
© 2023 Liu, Zhang, Guo, Zhao, Sun, Guo, Lu and Zhao. This is an open-access article distributed under the terms of the Creative Commons Attribution License (CC BY). The use, distribution or reproduction in other forums is permitted, provided the original author(s) and the copyright owner(s) are credited and that the original publication in this journal is cited, in accordance with accepted academic practice. No use, distribution or reproduction is permitted which does not comply with these terms.

Targeted CD7 CAR T-cells for treatment of T-Lymphocyte leukemia and lymphoma and acute myeloid leukemia: recent advances

Jile Liu[1†], Yi Zhang[1†], Ruiting Guo[1†], Yifan Zhao[1], Rui Sun[2], Shujing Guo[1], Wenyi Lu[3] and Mingfeng Zhao[3*]

[1]Department of Hematology, First Center Clinic College of Tianjin Medical University, Tianjin, China, [2]Department of Hematology, School of Medicine, Nankai University, Tianjin, China, [3]Department of Hematology, Tianjin First Central Hospital, Tianjin, China

The high expression of CD7 targets in T-cell acute lymphoblastic leukemia (T-ALL) and T-lymphoma has attracted considerable attention from researchers. However, because CD7 chimeric antigen receptor (CAR) T-cells undergo fratricide, CD7 CAR T-cells develop an exhaustion phenotype that impairs the effect of CAR T-cells. There have been significant breakthroughs in CD7-targeted CAR T-cell therapy in the past few years. The advent of gene editing, protein blockers, and other approaches has effectively overcome the adverse effects of conventional methods of CD7 CAR T-cells. This review, in conjunction with recent advances in the 64th annual meeting of the American Society of Hematology (ASH), provides a summary of the meaningful achievements in CD7 CAR T-cell generations and clinical trials over the last few years.

KEYWORDS

CD7 CAR T-cell therapy, base editing, protein blocker, American society of hematology, natural selection CD7 CAR T-cells

1 Introduction

Chimeric antigen receptor (CAR) T-cell therapy is a novel cell-based immunotherapy that has attracted considerable attention from researchers and healthcare professionals due to its outstanding therapeutic efficacy (1). Unlike major histocompatibility complex (MHC)-dependent T-cell receptors (TCRs), CAR can recognize antigens from any MHC background, allowing CAR T cells to target tumor cells that achieve immune evasion through down regulation of MHC expression or impaired proteasome antigen processing (2, 3). CAR T-cells are classified into five generations based on co-stimulatory structural domains, cytokine expression, and transcription factors (4–6). This therapy is typically completed in three steps: physicians first obtain sufficient healthy T cells from the patient or a donor;then, they engineer T-cells ex-vivo using techniques such as lentiviral or

electroporation to introduce CARs into the T cells; finally, these modified cells are infused into the patient's body, where they can efficiently and effectively kill tumor cells by targeting specific antigens (5, 7, 8). CAR T-cell therapy has revolutionized the treatment of hematologic malignancies, particularly in patients with CD19-positive B-cell malignancies, where CD19 CAR T-cell therapy has shown excellent efficacy (9–11). Based on this success, researchers are now seeking to identify suitable targets in other hematological malignancies, such as acute myeloid leukemia, multiple myeloma, and even solid tumor like lung cancer, in order to extend the success of the CD19 CAR T-cell therapy (4, 12–15).In this context, although with the success of anti-CD19 chimeric antigen receptor (CAR) T-cells have successfully treated patients with relapsed/refractory (R/R) B-cell leukemia/lymphoma (9–11). However, the use of CAR T-cells in the treatment of T-cell malignancies is challenging because many targets are co-expressed between normal and malignant cells (16).

The surface receptor CD7 is a cell membrane glycoprotein with a molecular weight of 40 kDa (17).As a member of the immunoglobulin supergene family, it is an important target for hematological immunotherapy (18, 19). CD7 is considered as a key factor in the treatment of T-cell acute lymphoblastic leukemia (T-ALL) and T-lymphoma due to its widespread distribution on tumors. Meanwhile, the expression of CD7 is also observed in 30% of acute myeloid leukemia (AML) (20, 21),and plays a critical role in the treatment. In fact, CD7 expression is associated with more progressive disease and worse prognosis in these 30% of AML cases. Increased drug resistance may result from positive CD7 expression (22–24). In view of the widespread expression of CD7 in these acute diseases, the importance of CD7 has been the focus of scientific attention from a very early stage. Frankel AE et al.(1997) prepared anti-CD7-dgA (consisting of a deglycosylated ricin A chain coupled with mouse monoclonal anti-human CD7 antibody) for treating of T-lymphocyte malignant hematologic tumors and evaluated its efficacy (25, 26). However, the anti-tumor activity of anti-CD7-dgA is limited. CD7-targeted drugs have not achieved significant results in the treatment of patients with T-cell lymphoma (26). CD7 surface antigens can also be detected on normal T lymphocytes and NK cells, as well as progenitors of thymocytes, lymphocytes, and myeloid cells (19, 27, 28). Therefore, the expression of uninhibited CD7 in CD7 CAR T-cells would trigger the above-mentioned fratricidal phenomenon. Meanwhile, infusion of CD7 CAR T-cells into patients could inadvertently deplete T and NK cells, reducing the patient's immune competence (16). Fratricide of CD7 CAR T-cells still affects their own proliferative function and cytotoxic effects *in vivo* in the context of traditional methods (16, 21). Therefore, it is the main direction for researchers to improve CD7 CAR-T by not expressing CD7 on the surface of CD7 CAR-T cells to avoid fratricide (Figure 1). Concerning this orientation, recent attempts have been made in the fields of gene editing, protein blockers, natural selection, and also some other aspects to improve the property of CD7 CAR-T in promoting the treatment of T-lymphocyte tumors. All these aspects will be critically analyzed from the viewpoints of preclinical experiment and clinical trial, followed by a comprehensive discussion.

2 Gene editing CD7 CAR T-cells

In order to remove the mechanism of fratricide (serving as a significant side effect), the gene editing methods mainly aim to carry out the knockout of the gene modulating CD7 expression, while preserving the normal development, proliferation, and the function of producing normal lymphoid organs and immune responses, which has been positively demonstrated by animal experiments (19, 29–31).

2.1 CRISPR/CAS9 gene-edited universal CD7 CAR T-cells

Clustered regularly interspaced short palindromic repeats/CRISPR associated nuclease 9(CRISPR/Cas9) system is a powerful genome editing tool originally adapted from the genetic defense

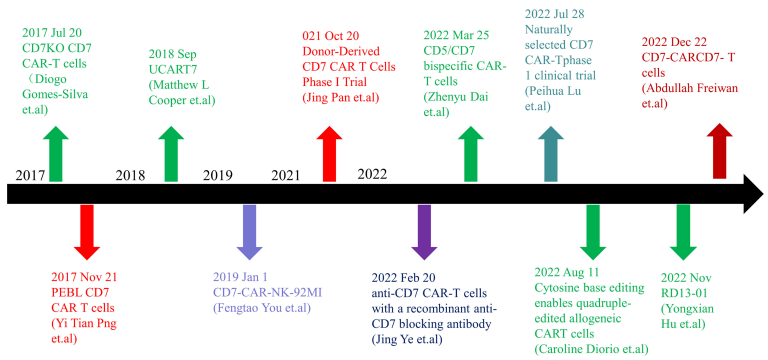

FIGURE 1
Timeline of CD7 target research. In 2017, anti-CD7 CAR-T cells that can get rid of fratricidal fate were successfully prepared by using gene editing technology and CD7 Protein blocker, which means that the application of CAR-T cells targeted at CD7 targets has become possible in clinical practice and has landmark significance in the research of CD7 targets. In the following five years, there were preparation methods such as allogenic anti-CD7 CAR-T cells, natural selection of anti-CD7 CAR-T cells, preparation of anti-CD7 CAR-T cells by recombinant antibody, and phase 1 and phase 2 clinical trials. With the extension of the time line, many breakthroughs have been made in CD7 target research. CD7 target research is still ongoing, and more successful patients will benefit in the future.

mechanism of info-prokaryotes to self-protect themselves from foreign genetic material (32). It consists of two components: the Cas9 endonuclease, which cleaves the DNA, and a guide RNA, which directs Cas9 to specific DNA sequences. By designing guide RNAs that target specific DNA sequences, researchers can use Cas9 to introduce double-strand breaks into DNA, resulting in gene knockouts or targeted modifications. As a prerequisite, the system requires the presence of a PAM adjacent to the target DNA sequence to function effectively (33).This system is classified into three types based on the presence of different effector complexes. The type II system, which uses a single Cas protein, is the most commonly used for genome editing due to its simplicity and precision (33, 34).

2.1.1 Preclinical experiments

In this method, CRISPR/CAS9 is used to remove the gene that modulates CD7 expression to prevent CD7 CAR T-cells from fratricide. [cell line: CCRF-CEM; animal model: male and female NGS mice] (16, 35). Since this knockout step is able to preserve the natural functions of CAR T-cells, previous studies have shown a significant viability of CD7 CAR T-cells in the relevant therapies. With this higher viability (compared with traditional methods), the engineered CD7 CAR ($CD7^{KO}$ CD7 CAR) T-cells are more capable of proliferating (16, 36). At the same time, it also performs well in a more potent and specific anti-tumor activity against malignant T cells. Consistent with the revealed mechanism, a protective effect has been observed in an *in vivo* experiment using T-ALL mice xenograft model (4). In this sense, CD7 CAR T-cells have generally shown promise in the treatment of malignant T lymphocytic cancers (Figure 2).

The first preclinical data on the effective treatment of T-cell malignancies with universal CAR-T therapy was reported by Matthew L. Cooper et al. (35) Universal CAR T-cells (UCAR-T cells) are typically made from T-cells donated by a healthy donor. The generation of UCAR T cells has the potential to overcome many of the disadvantages associated with the second-generation autologous CAR T cells currently in use: 1. The difficulty of obtaining sufficient healthy T cells from patients for the preparation of CAR T cells (37); Patients with malignancies often undergo multiple rounds of chemotherapy, radiation therapy, and immunotherapy, which can significantly reduce the viability and number of T cells compared to healthy individuals; 2. The lengthy process of CAR-T preparation. Extracting T-cells from the patient's body and reintroducing CAR-T cells into the body usually takes more than ten days. Due to disease progression, some patients may miss the optimal time for CAR T-cell therapy. Donor T cells can shorten the waiting time and are particularly beneficial for patients with rapidly progressing disease; 3. With autologous collection, there is a risk that T cells collected from patients with T-cell lymphoma may be contaminated with

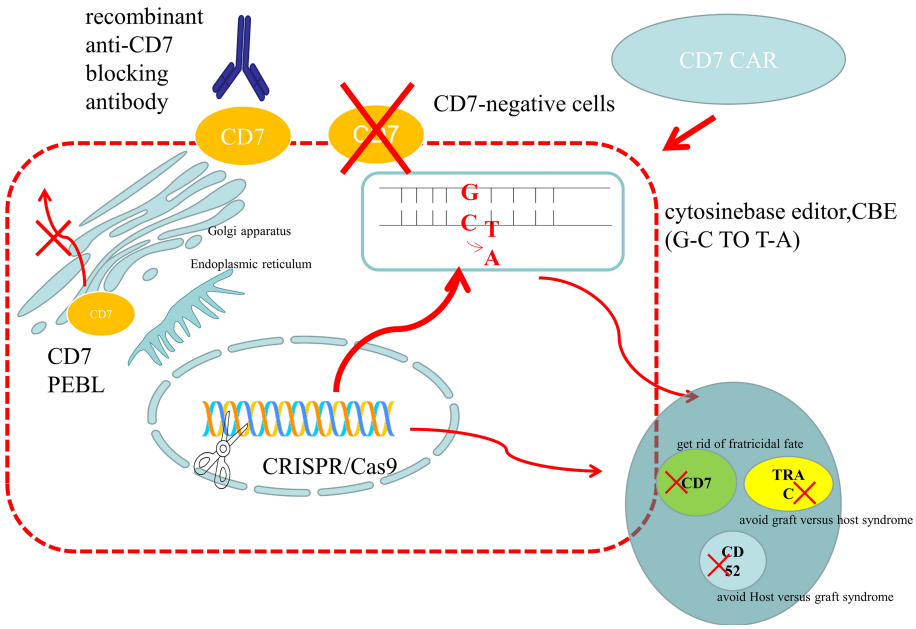

FIGURE 2
Preparation methods of anti-CD7 CAR-T cells. (1) Use gene editing technology to knock out the CD7 gene to avoid being killed because of the same expression of CD7 protein on the surface of CAR-T cells. For donor-derived T cells, it is also necessary to knock out the TRAC gene to avoid TCR on the surface of T cells and attack the recipient cells, leading to graft versus host syndrome. The purpose of CD52 gene knockout is to use CD52 monoclonal antibody to suppress the host immune system, while retaining the CAR-T cells that are CD52 negative, so that the CAR-T cells can be protected from the attack of host immune cells and ensure their proliferation. At present, the main gene editing used is CRISPR/CAS9, which cuts double-stranded DNA like scissors to achieve the goal of gene knockout. There is also a new gene editing technology – base editor, which improves the security by replacing bases without double strand breaks. At present, both gene editing techniques have been applied to the preparation of anti-CD7 CAR-T cells and have entered the clinical trial stage. (2) The CD7 protein is anchored on the endoplasmic reticulum and Golgi apparatus by CD7 protein inhibitor, which prevents it from being expressed on the cells surface and avoids the emergence of cannibalism. (3) Natural CD7 negative T cells were selected to prepare anti-CD7 CAR-T cells. And natural selection of viable anti-CD7 CAR-T cells through placement were selected. (4) The free anti-CD7 antibody containing the same binding domains as CAR was selected to block the CD7 antigen on the surface of T cells to avoid fratricidal in the preparation of anti-CD7 CAR-T cells.

cancer cells (37, 38); T cells collected from patients with malignant tumors in the lymphatic system may not be healthy T cells, but rather malignant tumor cells (39); 4. The cost of preparing autologous CAR-T cells is also unaffordable for patients to shoulder (40). UCAR-T cells has achieved the goal of mass production of CAR T-cells and reducing the difference of autologous preparation. However, there are some problems with the universal CAR T-cells: 1. The host immune system rejects allogeneic T cells; 2. Graft versus host disease (GvHD) of donor T cells against the host (40). To address these issues, researchers used gene editing to knock out the T cell receptor (TCR) gene, the human leukocyte antigen (HLA) class II gene, and CD52 (41). Using gene editing technology to knock out CD52, CAR T-cells can tolerate CD52 antibodies (42). Considering that CD52 is ubiquitously expressed on the surface of lymphocytes, monocytes, and various hematopoietic cells, the property created by the gene editing process could be exploited by clearing the host T-cells. Prior to the administration to allogeneic CAR T-cells, CD52-targeting agents such as alemtuzumab could be administered to aid to the clearance of host T-cells, thereby preventing host versus-graft reactions (HVGR) that may arise result from host T cell-mediated attack on the allogeneic CAR T-cells. Meanwhile, CAR T-cells could also maintain their viability in this environment with these targeting agents (43). 2022 American Society of Hematology Annual (ASH) meeting published that the universal CD7 CART edited by CRISPR/Cas9 could effectively proliferate and specifically kill T-ALL tumor cells *in vitro* (44). It can also significantly reduce the tumor burden and extend mice survival time (cell lines: Jurkat; animal model: NSG mice). Meanwhile, knocking out CD7 related genes also leads to an increase in the CD4 memory cell group without affecting the function of CAR T-cells. In Dai et al. (2022) (45), preclinical developmental data on dual target dual-targeted CAR T-cells were reported. They have combined the two antigens to achieve a higher treatment efficacy and to expand the applicability of this therapy to a broader patient population. After using CRISPR/Cas9 to knock out the genes that modulate CD5 and CD7 expression, the researchers compared the expression status and tumor-killing efficiency of tandem CARs and dual CARs (cell lines: Jurkat, CCRF-CEM, MOLT-4, SUP-T1, Raji; animal model: 6-week-old female NSG mice). Tandem CARs and Dual CARs are two different designs of construction that combine two targets. Each CAR of Dual CAR-T cells has a complete signaling domain that activates the anti-tumor effect in the presence of any homologous antigen. Tandem CAR is a form of CAR in which two distinct antigen-binding domains are co-expressed in one tandem (46). *In vitro* and *in vivo* experiments have been concluded that tandem CAR-T cells have higher transduction efficiencies and cytotoxic effects. Tandem CAR-T cells are even more advantageous than dual CAR T-cells in preventing relapse due to antigen escape (45). Dai et al. (2022) shed new lights on the application of CD7 CAR T-cells, and broaden the scope of the therapy by also targeting the malignant T-cells with CD5 expression, reducing the likelihood of CD7-negative relapse.

2.1.2 Clinical trials

The researchers used the CRISPR/Cas9 system to disrupt the genes that express CD7 and TCRα in T cells and named the edited anti-CD7 CAR T-cell product GC027, an "off-the-shelf" allogeneic CAR T-cells. Shiqi Li et al. (47) reported two cases of T-ALL patients treated with GC027 to evaluate the efficacy and safety of GC027 at *Clinical Cancer Research* in November 2020. This study found patients with both grade 3 cytokine release syndrome (CRS) (Table 1) and neurotoxicity, but without GvHD. As for CRS, they repeatedly applied Ruxolitinib, and found that the repeated use of Ruxolitinib did not affect the efficacy of CAR T-cells' in treatment and their proliferation. With this observation, it was concluded that Ruxolitinib could play a critical role in the prevention and treatment CRS following CAR T-cell therapy (47). However, this study is statistically underpowered (n=2). In this sense, further clinical trials are highly in need to verify their conclusion.

He Huang et al. eliminatedCD7/TRAC/RFX5-related genes using CRISPR/Cas9 technology (48). The researchers utilized a method to prevent host NK cells from attacking CAR T-cells by attaching NK cell inhibitory receptors to the intracellular domain of the T cell costimulatory protein CD28. To compensate for the lack of CD7, they used gene-editing technology to add CD132 to the CAR T-cells to increase the production of IL-2 (49), which enhanced the proliferation and anti-tumor efficacy of the CAR T-cells (cell line: Jurkat; animal model: NSG mice). The Phase I clinical trial used a single-arm, open-label, dose-escalation (Level 1: 1×10^7cells/kg; Level 2: 2×10^7cells/kg; Level 3: 3×10^7cells/kg) design to evaluate the safety and tolerability of CD7-targeting CAR-T cells (RD13-01), and to observe its anti-tumor activity and pharmacokinetic properties. The experimental results show that RD13-01 has high safety and anti-tumor activity with no dose-limiting toxicity (DLT), GvHD and ≥ 3 CRS events. The overall remission rate (ORR) was 82% and 6 leukemia patients achieved minimal residual disease (MRD) (-), with some patients achieving

TABLE 1 CRS grading scale.

Grade	Penn grading scale
Grade1 CRS	The patient has fever ≥ 38.0° C and some nonspecific signs, but no hypotension or hypoxia
Grade2 CRS	The patient has a fever ≥ 38.0° C and low blood pressure, but there is no need for vasopressor drugs. Patients with or without hypoxia only need low flow nasal catheters (≤ 6 L/min) for oxygen administration, or blow by oxygen administration.
Grade3 CRS	The patient has a fever ≥ 38.0° C with hypotension, and has no effect on fluid supplementation while requiring high flow oxygen administration (≥ 6 L/min).
Grade4 CRS	The patient has a fever ≥ 38.0° C with hypotension requiring multiple pressor medications and/or with no other causes of hypoxia requiring positive pressure ventilation disposal.

the level of complete response (CR)/complete response with incomplete hematologic recovery (CRi) (48). At this ASH meeting, the Phase I clinical trial of RD13-01 infusion in 10 enrolled patients was reported (NCT04620655) (50). On the 28th day of RD13-01 infusion (low does: 0.5-1×10^7cells/kg; medium does: 2×10^7cells/kg; high does:4×10^7cells/kg), 8 patients achieved complete bone marrow (BM)/peripheral blood (PB), 7 of whom were MRD negative. Only one patient experienced grade 3 CRS, and only one patient experienced grade 3 neurotoxicity. However, some patients died during follow-up (including from disease progression and bacterial infection). Based data from the Phase I trial, the investigators concluded that RD13-01 product is safe and has a dose-dependent effect in the treatment of patients with T-ALL/LBL following high-dose pretreatment. However, long-term follow-up is required and more patients are needed to further evaluate the safety and efficacy of CD7 UCAR-T cells.

2.2 Base editor

Although CRISPR/Cas9 is widely used, the mechanism of DNA double-strand breaks (DSBs) often leads to unpredictable adverse outcomes. For example, complex genome rearrangements and high-frequency translocations that are caused by the simultaneous induction of multiple DSBs (51–53). Considering that the preparation of UCAR-T requires several editions before the final application in clinical practice, DSB-based gene editing technology may have a negative impact on the efficacy and safety of universal CAR-T therapy (51–54). In recent years, the base editing technology has been gradually developed and matured. Compared with CRISPR/Cas9, the base editor does not need to break the double-stranded DNA, so it has higher safety and accuracy (55, 56). Cytosine base editors (CBEs) are made by fusing cytidine deaminase into Cas9 endonuclease (nicase) or TALEN sequence with uracil glycosylase inhibitory domain (UGI) to convert C • G base pairs to T • A base pairs at specific locations in the genome (57). Adenine base editors (ABEs) are another common type of base editor that facilitates the conversion of A•T base pairs into G•C base pairs (58). Another variant of base editors, the TadA-derived cytosine base editors (TadCBEs), have also been developed and shown to be effective for precise gene editing (59). To date, it has been demonstrated that TadCBEs can be used for efficient multi-site cytosine base editing of treatment-related targets in primary human T-cells, and cytosine base editing of treatment-related sites in primary hematopoietic blood stem cells and progenitor cells (HSPCs).

2.2.1 Preclinical experiments

Diori used CBE to develop a clinically acceptable quadruple-base-edited allogeneic CAR T-cell therapy targeting CD7 (7CAR8) for the treatment of T-ALL (60). 7CAR8 has blocked the expression of CD52, CD7, PD1 and TCRα protein. Their preclinical experimental results indicate that 7CAR8 avoids the challenge of collecting T cells from T-ALL patients because T cells are obtained from healthy donors. And it reduces the possibility of fratricide in CAR T-cells, GVHD, and receptor rejection of allogeneic CAR T-cells. Meanwhile, this study also proves that the CAR T-cells prepared in this way can effectively and safely eliminate tumor cells *in vitro* and *in vivo* (cell line: CCRF-CEM; animal model: NGS mice) (60).

In this ASH meeting, the excellent property of base editing has been demonstrated in the removal of TCR, CD52, the common AML/T lineage antigen CD7 (61). It produced the BE-CAR33 T-cells and BE-CAR7 T-cells originally obtained from donor sources, targeting the AML with CD7 and CD33 positive. *In vivo* experiments have shown that, in NGS mice, compared with the control group, which goes with the CAR T-cells targeting CD19 and CD7, AML cells (Molm14 and Kasumi) in the group with cells targeting only CD33 and the group with a combination of targeting CD33 and CD7 significantly decreased. The survival rates of mice treated with BE-CAR33 T-cells and BE-CAR33/BE-CAR7 T-cells were significantly prolonged. CAR T-cells showed strong persistence. This experiment demonstrated the reliability and efficacy of the combination of BE-CAR33 T-cells and BE-CAR7 T-cells for the treatment of AML.

2.2.2 Clinical trials

In 2022, the CD7 CAR-T basic editing clinical trial (ISRCTN15323014) was initiated (62). The CAR T-cells were administered prior to allogeneic stem cell transplantation. Eligible patients were pretreated with fludarabine, cyclophosphamide and alemtuzumab to promote lymphodepletion, and then infused with 0.2-2.0×10^6 BE-CAR7 T-cells. Patients in remission on day 28 underwent allogeneic stem cell transplantation to deplete BE-CAR7 T-cells and promote immune reconstitution. The Phase I study is designed to treat 10 children. One child has been enrolled currently. After receiving BE-CAR7 T cells, the patient observed grade 2 CRS and grade 1 ICANS without GvHD. After 28 days, the child showed morphologic remission without count recovery and received low-intensity allogeneic stem cell transplantation.

3 Protein blocker

Protein Blocker (PEBL) consists of a single chain variable fragment and an intracellular retention domain that anchors the cognate antigen in the endoplasmic reticulum and Golgi apparatus before degradation. CD7 PEBL is a technique that does not require the downregulation of endogenous CD7 by gene editing (63). This method anchors the CD7 protein in the endoplasmic reticulum and/or Golgi apparatus and prevents it from being expressed on the surface (63). Studies have shown that the retention of CD7 on T cells does not affect their function and proliferation. Therefore, PEBL is also an effective method to produce CAR T-cells without CD7 protein on the cell surface (21, 64).

3.1 Preclinical experiments

Since the preparation of autologous CAR T cells and the application of this therapy could depend on the amount of leukemia cells and/or the number of T cells (taking into account the potential contamination and the lower proportion of healthy

cells driven by the malignancy), two "universal" allogeneic CAR-T cells prepared by PEBL and lentivirus transduction technology were presented in this 2022ASH. The two teams both used PEBL technology, but to develop CD3 CAR-T and CD7 CAR-T, respectively.

Because peripheral T-cell lymphoma (PTCL) arises from mature T cells, both T lymphocytes and most tumor subtypes both maintain a high persistent CD3 expression. To overcome the drawbacks of this feature, Hongliang Qian's team used PEBL to downregulate surface CD3 to avoid the fratricide of CD3 CAR T-cells (65). They developed CD3 CAR T-cells for the treatment of PTCL, which showed excellent property in *in vitro* (CCRF-CEM T-ALL cell line) and *in vivo* experiments in mice.

In Xing Fah Alex Wong's team, the feasibility of the simultaneously using of two PEBLs for intracellular protein retention was well validated, indicating that the key functions of CAR T-cells were not affected. They developed the anti-CD7 CAR T-cells depleted of the CD7-CD3- (PCART7) expression for the treatment of R/R T-ALL or T-cell lymphoblastic lymphoma (66). To generate TCR/CD3-deficient PCART7 cells from healthy donor T-cells, a double transduction method is used. The method involves the use of two lentiviral vectors, the first vector being bicistronic and carrying CD7 PEBL and anti-CD7 CAR, while the second vector carries CD3 PEBL. In this study, more than 90% of the cells have displayed the phenotype of CAR+CD7$^-$CD3$^-$. After screening and purification, this number could be increased to 99%. This type of preparation for CAR T-cells shows the same effect as the genetically modified knockout of TRAC and CD7, while avoiding the risk of gene translocation and rearrangement. The potent cytotoxicity of CAR-T against CD7$^+$ leukemia cells was confirmed in both short-term and long-term *in vitro* assays. In the xenograft model using the CCRF-CEM T-ALL cell line, PCART7 effectively inhibited tumor growth and extended mice survival time.

3.2 Clinical trials

In one clinical trial, CD7 CAR T-cells derived from autologous nanoantibodies were used to treat R/R T-ALL/LBL (67). A CD7 blocking strategy was developed using a tandem CD7 nanoantibody VHH6 coupled to the endoplasmic reticulum/Golgi retention motif peptide to immobilize CD7 molecules in cells. Preclinical studies have shown that CAR T-cells are not fratricidal and exert potent cytolytic activity, significantly attenuating leukemia progression and extending the survival time of mice in NPG mice injected with Luc+ GFP+CCRF-CEM cells. Eight patients were subsequently enrolled in a clinical trial (NCT04004637). Clinical trial results showed that seven patients achieved CR after 3 months of CAR T-cell infusion, with most patients experiencing only grade 1 or 2 CRS and no T-cell aplasia or neurotoxicity (67). This CAR T-cell therapy merits further study in highly invasive CD7-positive malignancies.

In 2021, Pan Jing's team published the results of the Phase I clinical trial of CD7 CAR T-cells from PEBL-treated donors in the *Journal of Clinical Oncology* (21). 20 patients were enrolled in the Phase I clinical trial. Patients received high-dose pretreatment chemotherapy prior to the CAR T-cell infusion [5 × 105 or 1 × 106 (± 30%) cells/kg] with no subsequent DLTs. Grade 3 or higher CRS only occurred in only 10% of patients, and neurotoxicity is mild and self-limiting. Early GvHD occurred in 60% of the subjects, with a mild and controllable manifestation. The therapeutic effect in up to 90% of patients demonstrating CR is accounted for by CD7 CAR T-cells. Despite their allogeneic nature, CAR T-cells proliferate effectively in all patients and can be maintained in the absence of SCT, without evidence of rejection (21). The first phase of the trial was only conducted with only a single target dose of 1×10^6/kg proven to be safe and effective. However, the sample size of this study was not statistically powerful, and the participants were also followed for a relatively short period of time. Therefore, the long-term efficacy and toxicity of this therapy could not be determined in this study.

At the 2022 ASH, the PAN team presented an interim report from the Phase II clinical trial of donor-derived CD7 CAR T-cells for the treatment of R/R T-cell acute lymphoblastic leukemia/lymphoma (NCT04689659) (68). The interim analysis was performed when the first 20 patients who received CD7 CAR T-cells in the Phase I clinical trial completed or discontinued the infusion at the point of 3-month point after the start of the infusion. At the same time, additional patients with mediastinal malignancies were enrolled in the Phase II trial in addition to the original sample. The best overall response rate (BOR) at 3 months was 90%, with only two (10%) patients developing grade 3 or higher CRS, and eight (40%) patients developing grade 1-2 GvHD. However, it should be noted that these side effects were reversible, while the CD7 negative relapse was considered the most important issue affecting survival in this study.

In this sense, they also proposed an alternative in response to these adverse effects. Namely, the infusion of CD5 CAR T-cells, about which they also reported the Phase 1 clinical trial in treating five patients with negative recurrence after CD7 CAR T-cell therapy on the 2022 American Society of Clinical Oncology (ASCO), displaying satisfactory results (69). This trial demonstrated the potential of CD5 CAR T-cells as a subsequent therapy for CD7 negative relapse Jia Feng et al. (70) generated CD5 CAR T-cells that are specifically capable of secreting interleukin 15(IL-15). Meanwhile, this type of CD5-IL15/IL15 sushi CAR may have a beneficial influence on treating T-cell malignancies that have metastasized to the central nervous system (71).

4 CD7 CAR^{CD7-} T cells and natural selection CD7 CAR T-cells

The studies presented in the previous sessions mainly consider challenges for CD7-targeted immunotherapies posed by cell fratricide and eradication. However, whether using genome editing to modify the CAR T-cell gene or PEBL to restrict the expression of CD7 protein on the CAR T cell membrane, although all are reported to have avoided potential adverse effects, the possibility of compromising the normal physiological function of CAR T-cells being affected still exists as the "intact" declarations are all preliminary and based on statistically weak probabilistic evidence. Therefore, the present section will mainly focus on the

studies innovating in the preparation of CD7 CAR T cells in a more natural way to shed light on the absolute neutral effects on the cell itself, emphasizing on the mechanism of the resistance to the fratricide while limiting the use of cell modification, covering CD7 CAR^{CD7-} T cells and natural selection CD7 CAR T-cells.

4.1 Preclinical experiments

In response to the above-mentioned issues, natural or manually selected CD7$^-$ T-cells have come into the scientific focus as be a promising cell source for the production of CD7$^-$CAR T-cells (72). CD7 is involved in transcriptional regulation and the lack of CD7 messenger RNA results in a stable distribution of CD7$^-$T-cells. Naturally occurring CD7$^-$T-cells may be a promising cell source for the generation of CD7$^-$CAR T-cells. These CD7-T cells primarily have a CD4+ memory phenotype and typically display a Th0/Th2 phenotype after transplantation or in other immunodeficient environments. Researchers have found that CD7-negative T cells exist in the peripheral blood of healthy donors (0.72% to 19.5%) as well as patients with T-cell acute lymphoblastic leukemia (T-ALL) and B-cell acute lymphoblastic leukemia (B-ALL) (3% to 12.5%).

Some researchers screened out naturally occurring CD7$^-$ T-cells by 2-step magnetic bead separation to generate CD7 CAR^{CD7-} (72). Compared with the CD7 CAR T-cells that did not go through this process, no fratricide was reported in the production and proliferation process of the CD7 CAR^{CD7-} T-cells that went through the selection. At the same time, the studies found that CD7 CAR^{CD7-} T-cells have rich CD4$^+$effect memory phenotype, maintaining their ability in cytotoxic activity and cytokine secretion, and a stably lower expression of checkpoint inhibitory receptor. In addition, CD7 CAR^{CD7-}T-cells demonstrated *in vivo* persistence and protection of NGS mice receiving 1×10^4 CCRF (T-ALL) or 3×10^6 BV173 (B-ALL) cells from tumor relapse. The CD7 CAR^{CD7-} T-cells screened showed superior anti-tumor function and durability compared to conventional CAR T-cells, and a distinct transcriptional activation spectrum. However, access to sufficient healthy CD7-T cells in the peripheral blood is still a challenge, which also promotes difficulties in the subsequent selection, and overall proliferation and overall production of T-cells to meet the demands of this type of therapy (72). Therefore, the feasibility of studies in this pathway still remains to be tested.

Unlike the CD7 CAR^{CD7-} T-cells, Lu Peihua's team employed a natural screening method to prepare the CD7 CAR T-cells. No other operations were performed during the preparation of the CD7 CAR-T. The main move of this method is to place the generated CD7 CAR-T cells in a natural state without restricting fratricide to acquire the final surviving cells (48) Screened out by this targeted natural selection, these CD7 CAR T-cells demonstrated high therapeutic efficacy in both T-lymphocyte malignancies and AML, contributed by the high level of CAR and CD7 negative expression *in vitro*. This manifestation stands out as an excellent prominence in the context that normally 20-35% of AML patients have high CD7 expression, leading to a higher likelihood of poor prognosis (73–75). Although a proliferation fatigue and higher cell death have been reported after the fratricide screening, the amount of target cells is still sufficient for the dose required for transfusion back to patients to complete the therapy. Notably, although the CD7 receptor T-cell defect was caused, the CD7$^-$ T-cell subset simultaneously shouldered the main function of the first one, alleviating the treatment-related T-cell immune deficiency. After subsequent allotransplantation, the number of NK-cells and T lymphocytes can quickly return normal. Finally, the CD7 CAR T-cell depletion marker analysis of natural selection was performed, which showed that the expression of PD-1 and TIM-3 were reported with a statistically significant increase. This indicates that long-term placement may cause CAR-T cells to enter a depleted state, resulting in decreased anti-tumor activity and proliferation of CAR T cells after their re-export into the body. During the manufacturing process of NS7CAR-T cells, there is a risk that the final number of CAR T cells may not meet the standard for transfusion due to excessive self-killing of CAR T cells. These factors may limit the widespread use of NS7CAR-T cells.

4.2 Clinical trials

In 2022, Lu Peihua's team published the results of the clinical trial of the CD7 CART (NS7CAR) on the natural selection in *Blood (*38*)*. The results of the Phase I clinical trial are encouraging. Of the 20 patients selected in the Phase 1 trial (low dose: 0.5×10^6/kg; medium dose:1 to 1.5×10^6/kg; or high dose:2×10^6/kg), 19 patients achieved MRD-negative CR in BM at day 28 and only 1 patient had grade 3 CRS. At this ASH, Lu posted the long-term observation results of his Phase I/II clinical trial. Natural selection targeting CD7 CAR-T (NS7CAR-T) cells eliminates the need for gene editing, protein blockers and other technologies, and greatly reduces the cost of preparation. NS7CAR therapy includes 4-1BB and CD3ζ second-generation murine CAR-T with a costimulatory domain. A total of 53 patients were enrolled in the study. At day 28, 95.8% (46/48) of patients achieved MRD (-) CR) in BM/PB. In 53 patients, the 18-month overall survival (OS) and event-free survival (EFS) rates were 75.0% and 53.1%, respectively. 32 patients were bridged with allogeneic HSCT within 3 months, and OS and EFS at 18 months were 75.8% and 71.5%, respectively. Mild CRS occurred in 47/53 (88.7%) patients. Five patients developed Grade III CRS and one patient developed Grade IV CRS. Grade I neurotoxicity was observed in only 2 patients. Their Phase I/Phase II study showed that NS7CAR was safe and effective in R/R T-ALL/LBL patients receiving high-dose pretreatment, including those with extramedullary involvement and a history of allogeneic HSCT (Tables 2, 3).

5 Preparation of anti-CD7 CAR-T cells using recombinant anti CD7 blocking antibodies

In 2022, a research team proposed and demonstrated the feasibility of a new strategy to generate anti-CD7 CAR T cells using recombinant anti-CD7 blocking antibodies. To avoid the gene toxicity caused by genome editing and the unknown biological function caused by the lack of CD7 expression on the cell

TABLE 2 Safety and effectiveness of clinical trial of CD7 CAR T-cells.

	Clinical Trial [Reference]	Phase	Costimulatory Domain	Source of CAR T-cells	The Number of Patients	The Doses of Infusion	Response Status	CRS(≤ Grade2)	CRS (≥Grade3)	CRES/ ICANS	Other Adverse Effects
CRISPR/ CAS9	NCT04538599 [(48)]	I	Unknown	Healthy donors	12	1×10^7 cells/kg; 2×10^7 cells/kg;3×10^7 cells/kg	On the 28th day after the infusion, 7/11 patients had CR/CRi. (One patient died of septicemia.)	10	0	0	CMV/EBV reactivation; Neutropenia; Septicemia
CRISPR/ CAS9	NCT04620655 [(50)]	I	41BB	Healthy donors (Universal CAR T-cells)	10	0.5-1×10^7cells/kg; 2×10^7cells/kg;4×10^7cells/kg.	On the 28th day after the infusion, 8/10 (80%) patients' BM/PB achieved CR/CRi, two patients still NR in the low dose group.	9	1	1	None
Base-Editing	ISRCTN15323014 [(62)]	I	/	Healthy donors (Universal CAR T-cells)	1	0.2-2.0$\times10^6$ BE-CAR7 T-cells	Bone marrow evaluated at day 28 showed morphological response.	1	0	1	No GvHD
PEBL	NCT04004637 [(67)]	I	/	Patients themselves	8	One or two infusions, 0.5-5×10^6/kg	Three months after CAR T-cells infusion, the CR rate was 87.5% (7/8).	7/8	1/8	0	Abdominal infection; Thrombocytopenia; Moderate anemia
PEBL	ChiCTR2000034762 [(21)]	I	41BB	Healthy donors	20	1×10^6(± 30%) cells/kg. The patients allowed to receive low-dose infusion of 5 × 10 (± 30%)/kg if CAR T-cells did not reach the target dose.	Before receiving any other treatment, 19 patients were in response and 18/19 patients achieved CR.	18/20	2/20	3/15	GvHD; Anemia; Thrombocytopenia; Neutropenia; Lymphopenia; Viral-infection
PEBL	NCT04689659 [(68)]	I	41BB	Healthy donors	20	1×10^6(± 20%) cells/kg.	The BOR rate was 90% at 3 months.	/	2/20	3/20	GvHD; Fulminant hepatitis; Pneumonia; Severe infection
Natural selection	NCT04572308 [(38)]	I	CD28TM-41BB	Healthy donors or patients themselves	20	Low dose: 0.5$\times10^6$/kg;mid-dose:1~1.5$\times10^6$/kg; high-does: 2×10^6/kg.	19 patients obtained MRD (-) CR in BM on the 28th day.	18/20	1/20	2/20	Bacterial infection; CMV reactivation; Anemia; Neutropenia; Thrombocytopenia; Lymphopenia

(Continued)

10.3389/fimmu.2023.1170968

TABLE 2 Continued

	Clinical Trial [Reference]	Phase	Costimulatory Domain	Source of CAR T-cells	The Number of Patients	The Doses of Infusion	Response Status	CRS(≤ Grade2)	CRS (≥Grade3)	CRES/ ICANS	Other Adverse Effects
Natural selection	NCT04572308&NCT04916860 [(76)]	I/II	41BB	Healthy donors (2) or patients themselves (51)	53	Low dose: 0.5×10^6/kg;mid-dose:1~1.5×10^6/kg; high-does: 2×10^6/kg.	At day 28, 46/48 of the BM affected patients achieved MRD (-) CR in BM/PB.	47	5	2	None
The fourth generation CAR T-cells	NCT04033302 [(77)]	1	CD28-41BB-caspase 9 genetic-cassette	patients themselves	1	2×10^6 cells/kg.	At day 28, the patient achieved CR.	Grade 1 CRS	None	None	Neutropenia

CAR T-cells, chimeric antigen receptor T-cells; CRS, cytokine release syndrome; CRES, CAR-T Cell-related Encephalopathy Syndrome; ICANS, Immune Effector Cell-Associated Neurotoxicity Syndrome; CMV, Cytomegalovirus; EBV, Epstein-Barr virus; GvHD, Graft versus host disease; BM, bone marrow; PB, Peripheral blood; CR, complete response; CRi, complete response with incomplete hematological recovery; PEBL, Protein blockers; BE-CAR7 T-cells, base-editing CD7 CAR T-cells; BOR, Best overall rate; MRD, Minimal residual disease.

membrane, they selected free anti-CD7 antibodies containing the same binding domain as CAR to block the CD7 antigen on the surface of T cells, so as to avoid fratricidal killing during the preparation of anti-CD7 CAR-T cells. They demonstrated that anti CD7 CAR-T cells cultured with antibodies during the preparation phase had higher cell viability and proliferative capacity, and harvested sufficient numbers of expected anti CD7 CAR-T cells. This provides a rapid and safe method for the preparation anti-CD7 CAR T cells, which deserves in-depth research and attention for subsequent clinical trial results (78).

6 Comparison of the effects of auto- and allo-CAR T-cells

At the 2022 ASH meeting, the comparison of clinical efficacy, durability and safety of two types of autologous and donor CD7 CARTs was published (NCT04823091) (79). The costimulatory domain of the CAR-T is 4-1BB. The study has just enrolled 10 patients. Five patients were randomly assigned to receive autologous CAR T-cells and the other five to receive allogeneic CAR T-cells. Efficacy and safety comparisons from this clinical trial are shown in Table 3. During the follow-up period, 50% of the patients (4/8) showed a relatively high level of CAR-T by qPCR at month 2, of whom 3 received allogeneic CAR-T cells and 1 autologous CAR-T cells. They concluded that the selection of the source of CAR T-cells and the appropriate supportive care are key to efficacy. They concluded that the source of the CAR T-cells and the appropriate supportive care are the keys to good efficacy. The risk of relapse is higher after treatment with autologous CAR T-cells. Therefore, consolidation therapy is necessary. Because donor-derived CAR T cells may increase the likelihood of rejection, infection, it is necessary to maintain long-term detection to achieve better efficacy (Table 4). The sample size of this study is only 10 people, and it is still necessary to increase the sample size for further analysis and comparison to ensure the authenticity of the results.

7 CD7 CART cell therapy for MPAL

Mixed phenotype acute leukemia (MPAL), a rare malignancy among acute leukemias, can cause multiple organ failure in patients. MPAL is typically associated with a relatively poor prognosis (80). At the ASH meeting in 2021, the clinical trial of CD7 CAR-T therapy for R/R CD7-positive MPAL patients was published to verify the safety and efficacy of the treatment (80). The investigators selected the second-generation CD7 CAR T-cells with 4-1BB costimulatory domain to treat 4 patients with MPAL and 1 patient with FLT3 mutation. The patients were infused with different doses of CD7 CAR T-cells. Four weeks after infusion, four-fifths of these patients achieved either CR or CRi in the bone marrow, and all achieved MRD-negative CR. This study confirmed the efficacy of CD7 CAR T cell therapy for CD7-positive MPAL, expended the scope of CD7 CAR T-cell therapy and provided new ideas for the treatment of MPAL.

TABLE 3 Transplant status and various disease responses in clinical trials.

		T-ALL	T-LBL	AML	Number of bridge transplants	Post-transplant situation
(48)	**Number of people**	7	4	1	4	4CR
	Day28 evaluation	5CR	1CR,2PR	CR		
(21)	**Number of people**	20	0	0	7	6CR (One patient died 14 days after SCT from GvHD).
	Day28 evaluation	18CR 1PR				
(38)	**Number of people**	14	6	0	10	7CR
	Day28 evaluation	13CR/CRi	6CR/CRi			
(77)	**Number of people**	1	0	0	1	CR
	Day28 evaluation	CR				

T-ALL, T-cell acute lymphoblastic leukemia; T-LBL, T-cell lymphoblastic lymphoma; AML, Acute myeloid leukemia; CR, complete response; CRi, complete response with incomplete hematological recovery; PR, partial response.

TABLE 4 Comparison of the safety of autogenous and allogenic CAR T-cells in this clinical trial.

	Recurrence rate	Serve CRS	GvHD	Infection	Thrombocytopenia (median time)	Viral infection
autogenous	100%	0%	20%	60%	25days	40%
allogenic	25%	20%	20%	20%	28days	20%

CRS, cytokine release syndrome, Serve CRS≥Grade 3; GvHD, Graft versus host disease; BM, bone marrow.

8 CD7 CAR-NK

In addition to introducing of anti-CD7 CAR into T cells to generate CD7 CAR T cells, other investigators have also attempted to generate CD7 CAR NK-cells for the treatment of T-lymphocyte malignant blood tumors and have made progress (37). They constructed monovalent CD7-CAR-NK-92MI and bivalent dCD7-CAR-NK-92MI cells using the CD7 nanobody VHH6 sequence and found that they exhibited high efficiency and specific anti-tumor activity on T-cell leukemia cell lines and primary tumor cells. Bivalent dCD7-CAR-NK-92MI monoclonal cells promote granzyme B and interferon γ (IFN-γ) secretion. They demonstrated that CD7-CAR-NK-92MI cells can be used to treat T-ALL. At 2022ASH, researchers presented the experiment of using human invariant natural killer T (iNKT) to generate CD7-CAR iNKT-cells to treat all T-ALL subtypes and 30% of CD7+AML patients. They found earlier. There is a high proportion of CD7-negative cells in iNKT cells from healthy donors. CD7 CAR iNKT-cells prepared by researchers using donor-iNKT-cells are more effective in 70% of $CD7^{+}CD1d^{+}$T-ALL patients because they provide dual target specificity and reduce the possibility of relapse (81).

9 Discussion

In recent years, CD7 CAR T-cell therapy technology has made significant progress in avoiding or using CAR T-cell fratricide for therapeutic purposes. It has been demonstrated that CAR T-cells can maintain normal physiological functions even when the gene expressing CD7 is deleted, providing a solid basis for the application of genome editing in CD7 CAR T-cells. Using CRISPR/Cas9 genome editing to knock out the CD7 gene has been a feasible method in several preclinical and clinical trials to prepare CD7-targeted CAR T-cells that do not express CD7 on the cell surface. However, the editing of multiple gene loci, which requires different DNA double-strand breaks, may pose a risk of genotoxic side effects. Therefore, a critical evaluation of genotoxic side effects is essential for CD7 CAR-T cells generated by gene-editing techniques using DNA double-strand breaks (DSBs), such as the CRISPR/CAS9 system, to avoid potential risks in subsequent therapies and trials. The advent of base editors has ushered in a new wave of gene editing of CAR T-cells. Base Editors can precisely knock out CD7 and other target genes without fear of adverse effects from DNA double-strand breaks. Base editor-edited universal CD7 CAR T-cells can replace existing CD7 CAR T-cells and hold promise for patients with insufficient healthy T cells or rapid tumor progression. PBEL fixes the CD7 protein in the endoplasmic reticulum and Golgi apparatus from the organelle level, which is safer and more convenient without gene editing. Meanwhile, recent ASH studies have shown that a combination of CD3-PEBL may function similarly to TRAC knockout, making PBEL-generated universal CD7 CAR T-cells safer and reducing the risk of GvHD. New strategies to generate anti-CD7 CAR T-cells using CD7-negative cells, natural selection targeting CD7 CAR T-cells (NS7CAR-T) and recombinant anti-CD7 blocking antibodies have provided us with new ideas. These methods can achieve the desired results under CD7 expression on the surface of CAR T-cells, thus saving costs and avoiding the uncertainty caused by complex operations. Based on the studies reviewed in this article, we can expect more and better preparation methods in the future.

For the study of CD7 CAR T-cell therapy, further research is needed to prepare CAR T-cells from autologous or allogeneic T-

cells. The quality of T-cells from patients with malignant T lymphocyte hematologic tumors is poor and easily contaminated with malignant tumor cells. Therefore, the production of CD7 CAR T-cells from healthy donor T-cells may be a better choice. However, donor-derived CD7 CAR T-cells also have many problems, including graft-versus-host syndrome and the risk of genotoxicity caused by gene editing. Whether allogeneic CD7 CAR T-cells can achieve better curative effects remains to be determined. More clinical data are needed to explore the advantages and disadvantages of autologous and allogeneic CAR T-cells and to select the most appropriate source of CD7 CAR T-cells for different situations.

Cell therapy for the CD7 target is still in its infancy and many factors such as efficacy, side effects and relapse need to be evaluated. CD7-negative relapse and infection are currently prominent problems in clinical data. To cope with the negative recurrence of tumor patients after CD7 CAR-T treatment, it may be an excellent solution to find new targetsCD5 CAR T-cells may be a practical choice, and its efficacy in the treatment of T-cell malignant tumors has been verified in past experiments. We hope that CD5 CAR T-cells can become a follow-up treatment for CD7-negative relapse, just like the addition of CD20 CAR T-cells when CD19 CAR T-cells cannot work (82, 83). In addition, anti-CD4 CAR T-cells, anti-T cell receptor beta constant 1 (TRBC1) CAR T-cells and anti-chemokine receptor 9 (CCR9) CAR T-cells have also shown promising effects in preclinical research for the treatment of T-cell malignancies and may become new targets for the clinical treatment of T-cell malignancies in the future (84–86). Dual-targeted CAR T-cells are also a direction in which we can conduct in-depth research to reduce the possibility of tumor escape. A preclinical experimental study of CD5/CD7 CAR T-cells by Dai et al. has given us ideas for further clinical trials. At the same time, we hope to see more trials of double-targeted CAR T-cells in the treatment of T-lymphocyte malignancies. It is also worth exploring how to avoid and manage the risk of infection of CD7 CAR T-cells after treatment. The infusion dose of CD7 CAR T-cells and bridging transplantation, as well as the combination of CD7 CAR T-cells and drugs, may be the focus of future research. We need to continue to explore the process to find a more promising treatment. We have high hopes for CD7 CAR T-cells and hope that they can relieve pain for more patients.

Author contributions

JL and YZ are major contributors to writing the manuscript. RG has made substantial contributions to the conception. YZ and JL have drafted the work. RS, YFZ, WL, and SG have substantively revised it. MZ reviewed the draft. All authors contributed to the article and approved the submitted version.

Funding

This work was supported by grants from the General Project of the National Natural Science Foundation of China (81970180 to MZ), the Science and Technology Project of Tianjin Municipal Health Committee (TJWJ2022QN030 to MZ), the Key projects of Tianjin Applied Basic Research and Multi-Investment Fund (21JCZDJC01240), the Science and Technology Project of Tianjin Municipal Health Committee (TJWJ2022XK018 to MZ), and the Key Science and Technology Support Project of Tianjin Science and Technology Bureau (20YFZCSY00800 to MZ), as well as Tianjin Key Medical Discipline (Specialty) Construction Project (TJYXZDXK-056B) and Tianjin Municipal Natural Science Foundation (22JCQNJC00820 to WY).

Conflict of interest

The authors declare that the research was conducted in the absence of any commercial or financial relationships that could be construed as a potential conflict of interest.

Publisher's note

All claims expressed in this article are solely those of the authors and do not necessarily represent those of their affiliated organizations, or those of the publisher, the editors and the reviewers. Any product that may be evaluated in this article, or claim that may be made by its manufacturer, is not guaranteed or endorsed by the publisher.

References

1. Firor AE, Jares A, Ma Y. From humble beginnings to success in the clinic: chimeric antigen receptor-modified T-cells and implications for immunotherapy. *Exp Biol Med (Maywood NJ)* (2015) 240:1087–98. doi: 10.1177/1535370215584936

2. Sadelain M, Brentjens R, Rivière I. The basic principles of chimeric antigen receptor design. *Cancer Discov* (2013) 3:388–98. doi: 10.1158/2159-8290.CD-12-0548

3. Whilding LM, Maher J. CAR T-cell immunotherapy: the path from the by-road to the freeway? *Mol Oncol* (2015) 9:1994–2018. doi: 10.1016/j.molonc.2015.10.012

4. Wei W, Yang D, Chen X, Liang D, Zou L, Zhao X. Chimeric antigen receptor T-cell therapy for T-ALL and AML. *Front Oncol* (2022) 12:967754. doi: 10.3389/fonc.2022.967754

5. Cao X, Jin X, Zhang X, Utsav P, Zhang Y, Guo R, et al. Small-molecule compounds boost CAR-T cell therapy in hematological malignancies. *Curr Treat Options Oncol* (2023) 24:184–211. doi: 10.1007/s11864-023-01049-4

6. Kagoya Y, Tanaka S, Guo T, Anczurowski M, Wang CH, Saso K, et al. A novel chimeric antigen receptor containing a JAK-STAT signaling domain mediates superior antitumor effects. *Nat Med* (2018) 24:352–9. doi: 10.1038/nm.4478

7. Lana MG, Strauss BE. Production of lentivirus for the establishment of CAR-T cells. *Methods Mol Biol (Clifton NJ)* (2020) 2086:61–7. doi: 10.1007/978-1-0716-0146-4_4

8. Jayasooriya V, Ringwelski B, Dorsam G, Nawarathna D. mRNA-based CAR T-cells manufactured by miniaturized two-step electroporation produce selective cytotoxicity toward target cancer cells. *Lab Chip* (2021) 21:3748–61. doi: 10.1039/D1LC00219H

9. Lee DW, Kochenderfer JN, Stetler-Stevenson M, Cui YK, Delbrook C, Feldman SA , et al. T Cells expressing CD19 chimeric antigen receptors for acute lymphoblastic leukaemia in children and young adults: a phase 1 dose-escalation trial. *Lancet (London England)* (2015) 385:517–28. doi: 10.1016/S0140-6736(14)61403-3

10. Davila ML, Riviere I, Wang X, Bartido S, Park J, Curran K, et al. Efficacy and toxicity management of 19-28z CAR T cell therapy in b cell acute lymphoblastic leukemia. *Sci Trans Med* (2014) 6:224ra25. doi: 10.1126/scitranslmed.3008226

11. Zhang J, Hu Y, Yang J, Li W, Zhang M, Wang Q, et al. Non-viral, specifically targeted CAR-T cells achieve high safety and efficacy in b-NHL. *Nature* (2022) 609:369–74. doi: 10.1038/s41586-022-05140-y

12. Feng D, Sun J. Overview of anti-BCMA CAR-T immunotherapy for multiple myeloma and relapsed/refractory multiple myeloma. *Scandinavian J Immunol* (2020) 92:e12910. doi: 10.1111/sji.12910

13. Ma S, Li X, Wang X, Cheng L, Li Z, Zhang C, et al. Current progress in CAR-T cell therapy for solid tumors. *Int J Biol Sci* (2019) 15:2548–60. doi: 10.7150/ijbs.34213

14. Date V, Nair S. Emerging vistas in CAR T-cell therapy: challenges and opportunities in solid tumors. *Expert Opin Biol Ther* (2021) 21:145–60. doi: 10.1080/14712598.2020.1819978

15. Chen L, Chen F, Li J, Pu Y, Yang C, Wang Y, et al. CAR-T cell therapy for lung cancer: potential and perspective. *Thorac Cancer* (2022) 13:889–99. doi: 10.1111/1759-7714.14375

16. Gomes-Silva D, Srinivasan M, Sharma S, Lee CM, Wagner DL, Davis TH, et al. CD7-edited T cells expressing a CD7-specific CAR for the therapy of T-cell malignancies. *Blood* (2017) 130:285–96. doi: 10.1182/blood-2017-01-761320

17. Schanberg LE, Fleenor DE, Kurtzberg J, Haynes BF, Kaufman RE. Isolation and characterization of the genomic human CD7 gene: structural similarity with the murine thy-1 gene. *Proc Natl Acad Sci USA* (1991) 88:603–7. doi: 10.1073/pnas.88.2.603

18. Haynes BF, Eisenbarth GS, Fauci AS. Human lymphocyte antigens: production of a monoclonal antibody that defines functional thymus-derived lymphocyte subsets. *Proc Natl Acad Sci USA* (1979) 76:5829–33. doi: 10.1073/pnas.76.11.5829

19. Rabinowich H, Pricop L, Herberman RB, Whiteside TL. Expression and function of CD7 molecule on human natural killer cells. *J Immunol (Baltimore Md 1950)* (1994) 152:517–26. doi: 10.4049/jimmunol.152.2.517

20. AlDabbagh MA, Gitman MR, Kumar D, Humar A, Rotstein C, Husain S. The role of antiviral prophylaxis for the prevention of Epstein-Barr virus-associated posttransplant lymphoproliferative disease in solid organ transplant recipients: a systematic review. *Am J Transplant Off J Am Soc Transplant Am Soc Transplant Surgeons* (2017) 17:770–81. doi: 10.1111/ajt.14020

21. Pan J, Tan Y, Wang G, Deng B, Ling Z, Song W, et al. Donor-derived CD7 chimeric antigen receptor T cells for T-cell acute lymphoblastic leukemia: first-in-Human, phase I trial. *J Clin Oncol Off J Am Soc Clin Oncol* (2021) 39:3340–51. doi: 10.1200/JCO.21.00389

22. Chang H, Salma F, Yi QL, Patterson B, Brien B, Minden MD. Prognostic relevance of immunophenotyping in 379 patients with acute myeloid leukemia. *Leukemia Res* (2004) 28:43–8. doi: 10.1016/S0145-2126(03)00180-2

23. Ogata K, Yokose N, Shioi Y, Ishida Y, Tomiyama J, Hamaguchi H, et al. Reappraisal of the clinical significance of CD7 expression in association with cytogenetics in *de novo* acute myeloid leukaemia. *Br J Haematol* (2001) 115:612–5. doi: 10.1046/j.1365-2141.2001.03139.x

24. Chang H, Yeung J, Brandwein J, Yi QL. CD7 expression predicts poor disease free survival and post-remission survival in patients with acute myeloid leukemia and normal karyotype. *Leukemia Res* (2007) 31:157–62. doi: 10.1016/j.leukres.2006.06.001

25. Jansen B, Vallera DA, Jaszcz WB, Nguyen D, Kersey JH. Successful treatment of human acute T-cell leukemia in SCID mice using the anti-CD7-deglycosylated ricin a-chain immunotoxin DA7. *Cancer Res* (1992) 52:1314–21.

26. Frankel AE, Laver JH, Willingham MC, Burns LJ, Kersey JH, Vallera DA. Therapy of patients with T-cell lymphomas and leukemias using an anti-CD7 monoclonal antibody-ricin a chain immunotoxin. *Leukemia Lymphoma* (1997) 26:287–98. doi: 10.3109/10428199709051778

27. Reinhold U, Abken H, Kukel S, Moll M, Müller R, Oltermann I, et al. CD7- T cells represent a subset of normal human blood lymphocytes. *J Immunol (Baltimore Md 1950)* (1993) 150:2081–9. doi: 10.4049/jimmunol.150.5.2081

28. Satoh C, Tamura H, Yamashita T, Tsuji T, Dan K, Ogata K. Aggressive characteristics of myeloblasts expressing CD7 in myelodysplastic syndromes. *Leukemia Res* (2009) 33:326–31. doi: 10.1016/j.leukres.2008.07.006

29. Lee DM, Staats HF, Sundy JS, Patel DD, Sempowski GD, Scearce RM, et al. Immunologic characterization of CD7-deficient mice. *J Immunol (Baltimore Md 1950)* (1998) 160:5749–56. doi: 10.4049/jimmunol.160.12.5749

30. Bonilla FA, Kokron CM, Swinton P, Geha RS. Targeted gene disruption of murine CD7. *Int Immunol* (1997) 9:1875–83. doi: 10.1093/intimm/9.12.1875

31. Kim MY, Cooper ML, Jacobs MT, Ritchey JK, Hollaway J, Fehniger TA, et al. CD7-deleted hematopoietic stem cells can restore immunity after CAR T cell therapy. *JCI Insight* (2021) 6(16):e149819. doi: 10.1172/jci.insight.149819

32. Jinek M, Chylinski K, Fonfara I, Hauer M, Doudna JA, Charpentier E. A programmable dual-RNA-guided DNA endonuclease in adaptive bacterial immunity. *Sci (New York NY)* (2012) 337:816–21. doi: 10.1126/science.1225829

33. Wang SW, Gao C, Zheng YM, Yi L, Lu JC, Huang XY, et al. Current applications and future perspective of CRISPR/Cas9 gene editing in cancer. *Mol Cancer* (2022) 21:57. doi: 10.1186/s12943-022-01518-8

34. Makarova KS, Haft DH, Barrangou R, Brouns SJ, Charpentier E, Horvath P, et al. Evolution and classification of the CRISPR-cas systems. *Nat Rev Microbiol* (2011) 9:467–77. doi: 10.1038/nrmicro2577

35. Cooper ML, Choi J, Staser K, Ritchey JK, Devenport JM, Eckardt K, et al. An "off-the-shelf" fratricide-resistant CAR-T for the treatment of T cell hematologic malignancies. *Leukemia* (2018) 32:1970–83. doi: 10.1038/s41375-018-0065-5

36. Gomes-Silva D, Atilla E, Atilla PA, Mo F, Tashiro H, Srinivasan M, et al. CD7 CAR T cells for the therapy of acute myeloid leukemia. *Mol Ther J Am Soc Gene Ther* (2019) 27:272–80. doi: 10.1016/j.ymthe.2018.10.001

37. You F, Wang Y, Jiang L, Zhu X, Chen D, Yuan L, et al. A novel CD7 chimeric antigen receptor-modified NK-92MI cell line targeting T-cell acute lymphoblastic leukemia. *Am J Cancer Res* (2019) 9:64–78.

38. Lu P, Liu Y, Yang J, Zhang X, Yang X, Wang H, et al. Naturally selected CD7 CAR-T therapy without genetic manipulations for T-ALL/LBL: first-in-human phase 1 clinical trial. *Blood* (2022) 140:321–34. doi: 10.1182/blood.2021014498

39. Safarzadeh Kozani P, Safarzadeh Kozani P, Rahbarizadeh F. CAR-T cell therapy in T-cell malignancies: is success a low-hanging fruit? *Stem Cell Res Ther* (2021) 12:527. doi: 10.3389/fimmu.2021.765097

40. Depil S, Duchateau P, Grupp SA, Mufti G, Poirot L. 'Off-the-shelf' allogeneic CAR T cells: development and challenges. *Nat Rev Drug Discov* (2020) 19:185–99. doi: 10.1038/s41573-019-0051-2

41. Qasim W, Zhan H, Samarasinghe S, Adams S, Amrolia P, Stafford S, et al. Molecular remission of infant b-ALL after infusion of universal TALEN gene-edited CAR T cells. *Sci Trans Med* (2017) 9(374):eaaj2013. doi: 10.1126/scitranslmed.aaj2013

42. Al-Mansour Z, Nelson BP, Evens AM. Post-transplant lymphoproliferative disease (PTLD): risk factors, diagnosis, and current treatment strategies. *Curr Hematol Malig Rep* (2013) 8:173–83. doi: 10.1007/s11899-013-0162-5

43. Hu Y, Zhou Y, Zhang M, Ge W, Li Y, Yang L, et al. CRISPR/Cas9-engineered universal CD19/CD22 dual-targeted CAR-T cell therapy for Relapsed/Refractory b-cell acute lymphoblastic leukemia. *Clin Cancer Res an Off J Am Assoc Cancer Res* (2021) 27:2764–72. doi: 10.1158/1078-0432.CCR-20-3863

44. Xie L, Gu R, Yang X, Qiu S, Xu Y, Mou J, et al. Universal anti-CD7 CAR-T cells targeting T-ALL and functional analysis of CD7 antigen on T/CAR-T cells. *Blood* (2022) 140:4535–. doi: 10.1182/blood-2022-158682

45. Dai Z, Mu W, Zhao Y, Cheng J, Lin H, Ouyang K, et al. T Cells expressing CD5/CD7 bispecific chimeric antigen receptors with fully human heavy-chain-only domains mitigate tumor antigen escape. *Signal Transduct Target Ther* (2022) 7:85. doi: 10.1038/s41392-022-00898-z

46. Han X, Wang Y, Wei J, Han W. Multi-antigen-targeted chimeric antigen receptor T cells for cancer therapy. *J Hematol Oncol* (2019) 12:128. doi: 10.1186/s13045-019-0813-7

47. Li S, Wang X, Yuan Z, Liu L, Luo L, Li Y, et al. Eradication of T-ALL cells by CD7-targeted universal CAR-T cells and initial test of ruxolitinib-based CRS management. *Clin Cancer Res an Off J Am Assoc Cancer Res* (2021) 27:1242–6. doi: 10.1158/1078-0432.CCR-20-1271

48. Hu Y, Zhou Y, Zhang M, Zhao H, Wei G, Ge W, et al. Genetically modified CD7-targeting allogeneic CAR-T cell therapy with enhanced efficacy for relapsed/refractory CD7-positive hematological malignancies: a phase I clinical study. *Cell Res* (2022) 32:995–1007. doi: 10.1038/s41422-022-00721-y

49. Zhang Q, Hresko ME, Picton LK, Su L, Hollander MJ, Nunez-Cruz S, et al. A human orthogonal IL-2 and IL-2Rβ system enhances CAR T cell expansion and antitumor activity in a murine model of leukemia. *Sci Trans Med* (2021) 13:eabg6986. doi: 10.1126/scitranslmed.abg6986

50. Zhang X, Zhou Y, Yang J, Li J, Qiu L, Ge W, et al. A novel universal CD7-targeted CAR-T cell therapy for relapsed or refractory T-cell acute lymphoblastic leukemia and T-cell lymphoblastic lymphoma. *Blood* (2022) 140:4566–7. doi: 10.1182/blood-2022-165733

51. Leibowitz ML, Papathanasiou S, Doerfler PA, Blaine LJ, Sun L, Yao Y, et al. Chromothripsis as an on-target consequence of CRISPR-Cas9 genome editing. *Nat Genet* (2021) 53:895–905. doi: 10.1038/s41588-021-00838-7

52. Adikusuma F, Piltz S, Corbett MA, Turvey M, McColl SR, Helbig KJ, et al. Large Deletions induced by Cas9 cleavage. *Nature* (2018) 560:E8–e9. doi: 10.1038/s41586-018-0380-z

53. Kosicki M, Tomberg K, Bradley A. Repair of double-strand breaks induced by CRISPR-Cas9 leads to large deletions and complex rearrangements. *Nat Biotechnol* (2018) 36:765–71. doi: 10.1038/nbt.4192

54. Stadtmauer EA, Fraietta JA, Davis MM, Cohen AD, Weber KL, Lancaster E, et al. CRISPR-engineered T cells in patients with refractory cancer. *Sci (New York NY)* (2020) 367(6481):eaba7365. doi: 10.1126/science.aba7365

55. Komor AC, Kim YB, Packer MS, Zuris JA, Liu DR. Programmable editing of a target base in genomic DNA without double-stranded DNA cleavage. *Nature* (2016) 533:420–4. doi: 10.1038/nature17946

56. Gaudelli NM, Komor AC, Rees HA, Packer MS, Badran AH, Bryson DI, et al. Programmable base editing of A•T to G•C in genomic DNA without DNA cleavage. *Nature* (2017) 551:464–71. doi: 10.1038/nature24644

57. Yu Y, Leete TC, Born DA, Young L, Barrera LA, Lee SJ, et al. Cytosine base editors with minimized unguided DNA and RNA off-target events and high on-target activity. *Nat Commun* (2020) 11:2052. doi: 10.1038/s41467-020-15887-5

58. Jeong YK, Lee S, Hwang GH, Hong SA, Park SE, Kim JS, et al. Adenine base editor engineering reduces editing of bystander cytosines. *Nat Biotechnol* (2021) 39:1426–33. doi: 10.1038/s41587-021-00943-2

59. Neugebauer ME, Hsu A, Arbab M, Krasnow NA, McElroy AN, Pandey S, et al. Evolution of an adenine base editor into a small, efficient cytosine base editor with low off-target activity. *Nat Biotechnol* (2022). doi: 10.1038/s41587-022-01533-6

60. Diorio C, Murray R, Naniong M, Barrera L, Camblin A, Chukinas J, et al. Cytosine base editing enables quadruple-edited allogeneic CART cells for T-ALL. *Blood* (2022) 140:619–29. doi: 10.1182/blood.2022015825

61. Kloos A, Georgiadis C, Etuk A, Gkazi SA, Syed F, Braybrook T, et al. Single and combinational multiplex base-edited 'Universal' CAR T cells in a humanised model of primary CD7+CD33+ AML. *Blood* (2022) 140:7425–6. doi: 10.1182/blood-2022-168719

62. Chiesa R, Georgiadis C, Ottaviano G, Syed F, Braybrook T, Etuk A, et al. Tvt CAR7: phase 1 clinical trial of base-edited "Universal" CAR7 T cells for paediatric Relapsed/ Refractory T-ALL. *Blood* (2022) 140:4579–80. doi: 10.1182/blood-2022-169114

63. Png YT, Vinanica N, Kamiya T, Shimasaki N, Coustan-Smith E, Campana D. Blockade of CD7 expression in T cells for effective chimeric antigen receptor targeting of T-cell malignancies. *Blood Adv* (2017) 1:2348–60. doi: 10.1182/bloodadvances.2017009928

64. Kamiya T, Wong D, Png YT, Campana D. A novel method to generate T-cell receptor-deficient chimeric antigen receptor T cells. *Blood Adv* (2018) 2:517–28. doi: 10.1182/bloodadvances.2017012823

65. Qian H, Gay FPH, Pang JWL, Lee Y, Ang J, Tan HC, et al. Development of anti-CD3 chimeric antigen receptor (CAR)-T cells for allogeneic cell therapy of peripheral T-cell lymphoma (PTCL). *Blood* (2022) 140:4510–1. doi: 10.1182/blood-2022-162222

66. Wong XFA, Ng J, Zheng S, Ismail R, Qian H, Campana D, et al. Development of an off-the-Shelf chimeric antigen receptor (CAR)-T cell therapy for T-cell acute lymphoblastic leukemia (T-ALL) without gene editing. *Blood* (2022) 140:2358–9. doi: 10.1182/blood-2022-165822

67. Zhang M, Chen D, Fu X, Meng H, Nan F, Sun Z, et al. Autologous nanobody-derived fratricide-resistant CD7-CAR T-cell therapy for patients with relapsed and refractory T-cell acute lymphoblastic Leukemia/Lymphoma. *Clin Cancer Res an Off J Am Assoc Cancer Res* (2022) 28:2830–43. doi: 10.1158/1078-0432.CCR-21-4097

68. Tan Y, Pan J, Deng B, Ling Z, Weiliang S, Tian Z, et al. Efficacy and safety of donor-derived CD7 CAR T cells for r/r T-cell acute lymphoblastic Leukemia/ Lymphoma: interim analysis from a phase 2 trial. *Blood* (2022) 140:4602–3. doi: 10.1182/blood-2022-165819

69. Pan J, Yue T, Lingling S, Biping D, Zhuojun L, Weiliang S, et al. Phase I study of donor-derived CD5 CAR T cells in patients with relapsed or refractory T-cell acute lymphoblastic leukemia. *Am Soc Clin Oncol* (2022) suppl 16:abstr 7028. doi: 10.1200/JCO.2022.40.16_suppl.7028

70. Feng J, Xu H, Cinquina A, Wu Z, Chen Q, Zhang P, et al. Treatment of aggressive T cell lymphoblastic lymphoma/leukemia using anti-CD5 CAR T cells. *Stem Cell Rev Rep* (2021) 17:652–61. doi: 10.1007/s12015-020-10092-9

71. Waldmann TA. The shared and contrasting roles of IL2 and IL15 in the life and death of normal and neoplastic lymphocytes: implications for cancer therapy. *Cancer Immunol Res* (2015) 3:219–27. doi: 10.1158/2326-6066.CIR-15-0009

72. Freiwan A, Zoine JT, Crawford JC, Vaidya A, Schattgen SA, Myers JA, et al. Engineering naturally occurring CD7- T cells for the immunotherapy of hematological malignancies. *Blood* (2022) 140:2684–96. doi: 10.1182/blood.2021015020

73. Zheng J, Wang X, Hu Y, Yang J, Liu J, He Y, et al. A correlation study of immunophenotypic, cytogenetic, and clinical features of 180 AML patients in China. *Cytometry Part B Clin Cytometry* (2008) 74:25–9. doi: 10.1002/cyto.b.20368

74. Venditti A, Del Poeta G, Buccisano F, Tamburini A, Cox-Froncillo MC, Aronica G, et al. Prognostic relevance of the expression of tdt and CD7 in 335 cases of acute myeloid leukemia. *Leukemia* (1998) 12:1056–63. doi: 10.1038/sj.leu.2401067

75. Haubner S, Perna F, Köhnke T, Schmidt C, Berman S, Augsberger C, et al. Coexpression profile of leukemic stem cell markers for combinatorial targeted therapy in AML. *Leukemia* (2019) 33:64–74. doi: 10.1038/s41375-018-0180-3

76. Zhang X, Yang J, Li J, Qiu L, Li J, Lu P. Analysis of 53 patients with relapsed or refractory (R/R) T-cell acute lymphoblastic leukemia (T-ALL) and T-cell lymphoblastic lymphoma (T-LBL) treated with CD7-targeted CAR-T cell therapy. *Blood* (2022) 140:2369–70. doi: 10.1182/blood-2022-158878

77. Xie L, Ma L, Liu S, Chang L, Wen F. Chimeric antigen receptor T cells targeting CD7 in a child with high-risk T-cell acute lymphoblastic leukemia. *Int Immunopharmacol* (2021) 96:107731. doi: 10.1016/j.intimp.2021.107731

78. Ye J, Jia Y, Tuhin IJ, Tan J, Monty MA, Xu N, et al. Feasibility study of a novel preparation strategy for anti-CD7 CAR-T cells with a recombinant anti-CD7 blocking antibody. *Mol Ther Oncolytics* (2022) 24:719–28. doi: 10.1016/j.omto.2022.02.013

79. Zhang Y, Li C, Jiang H, Luo W, Du M, Zhou F, et al. Allogeneic and autologous anti-CD7 CAR-T cell therapies in relapsed or refractory T cell malignancies. *Blood* (2022) 140:4592–4. doi: 10.1182/blood-2022-170819

80. Zhang X, Yang J, Li J, Shi Y, Su Y, Liu Y, et al. First-in-Human clinical study of a novel CD7-targeted chimeric antigen receptor (CAR)-T cell therapy for Refractory/ Relapsed mixed phenotype acute leukemia (MPAL). *Blood* (2021) 138:1741. doi: 10.1182/blood-2021-146425

81. Zhou X. Preclinical development of non-edited CD7 CAR-modified invariant NKT cell therapy for T-cell malignancies and acute myeloid leukemia. *Blood* (2022) 140 (Suppl 1):7417–8. doi: 10.1182/blood-2022-166611

82. Chen Z, Liu Y, Chen N, Xing H, Tian Z, Tang K, et al. Loop CD20/CD19 CAR-T cells eradicate b-cell malignancies efficiently. *Sci China Life Sci* (2023) 66:754–70. doi: 10.1007/s11427-022-2173-9

83. Sang W, Shi M, Yang J, Cao J, Xu L, Yan D, et al. Phase II trial of co-administration of CD19- and CD20-targeted chimeric antigen receptor T cells for relapsed and refractory diffuse large b cell lymphoma. *Cancer Med* (2020) 9:5827–38. doi: 10.1002/cam4.3259

84. Pinz K, Liu H, Golightly M, Jares A, Lan F, Zieve GW, et al. Preclinical targeting of human T-cell malignancies using CD4-specific chimeric antigen receptor (CAR)-engineered T cells. *Leukemia* (2016) 30:701–7. doi: 10.1038/leu.2015.311

85. Maciocia PM, Wawrzyniecka PA, Philip B, Ricciardelli I, Akarca AU, Onuoha SC, et al. Targeting the T cell receptor β-chain constant region for immunotherapy of T cell malignancies. *Nat Med* (2017) 23:1416–23. doi: 10.1038/nm.4444

86. Maciocia PM, Wawrzyniecka PA, Maciocia NC, Burley A, Karpanasamy T, Devereaux S, et al. Anti-CCR9 chimeric antigen receptor T cells for T-cell acute lymphoblastic leukemia. *Blood* (2022) 140:25–37. doi: 10.1182/blood.2021013648

frontiers | Frontiers in Immunology

TYPE Original Research
PUBLISHED 09 June 2023
DOI 10.3389/fimmu.2023.1175920

Check for updates

OPEN ACCESS

EDITED BY
Anand Rotte,
Arcellx Inc., United States

REVIEWED BY
Maite Alvarez,
University of Navarra, Spain
Eliana Ruggiero,
Scientific Institute for Research, Hospitalization and Healthcare (IRCCS), Italy

*CORRESPONDENCE
Zhigang Hu
huzg_2000@126.com
Zhigang Guo
guo@njnu.edu.cn

†These authors have contributed equally to this work

RECEIVED 28 February 2023
ACCEPTED 01 June 2023
PUBLISHED 09 June 2023

CITATION
Yang F, Zhang F, Ji F, Chen J, Li J, Chen Z, Hu Z and Guo Z (2023) Self-delivery of TIGIT-blocking scFv enhances CAR-T immunotherapy in solid tumors. *Front. Immunol.* 14:1175920. doi: 10.3389/fimmu.2023.1175920

COPYRIGHT
© 2023 Yang, Zhang, Ji, Chen, Li, Chen, Hu and Guo. This is an open-access article distributed under the terms of the Creative Commons Attribution License (CC BY). The use, distribution or reproduction in other forums is permitted, provided the original author(s) and the copyright owner(s) are credited and that the original publication in this journal is cited, in accordance with accepted academic practice. No use, distribution or reproduction is permitted which does not comply with these terms.

Self-delivery of TIGIT-blocking scFv enhances CAR-T immunotherapy in solid tumors

Fan Yang[1†], Fan Zhang[1†], Feng Ji[1], Jiannan Chen[1], Jun Li[2], Zhengliang Chen[2], Zhigang Hu[1*] and Zhigang Guo[1*]

[1]Jiangsu Key Laboratory for Molecular and Medical Biotechnology, College of Life Sciences, Nanjing Normal University, Nanjing, China, [2]CAR-T R&D Department, Nanjing Blue Shield Biotechnology Co., Ltd., Nanjing, China

Chimeric antigen receptor T cell therapy has become an important immunotherapeutic tool for overcoming cancers. However, the efficacy of CAR-T cell therapy in solid tumors is relatively poor due to the complexity of the tumor microenvironment and inhibitory immune checkpoints. TIGIT on the surface of T cells acts as an immune checkpoint by binding to CD155 on the tumor cells' surface, thereby inhibiting tumor cell killing. Blocking TIGIT/CD155 interactions is a promising approach in cancer immunotherapy. In this study, we generated anti-MLSN CAR-T cells in combination with anti-α-TIGIT for solid tumors treatment. The anti-α-TIGIT effectively enhanced the efficacy of anti-MLSN CAR-T cells on the killing of target cells *in vitro*. In addition, we genetically engineered anti-MLSN CAR-T cells with the capacity to constitutively produce TIGIT-blocking single-chain variable fragments. Our study demonstrated that blocking TIGIT significantly promoted cytokine release to augment the tumor-killing effect of MT CAR-T cells. Moreover, the self-delivery of TIGIT-blocking scFvs enhanced the infiltration and activation of MT CAR-T cells in the tumor microenvironments to achieve better tumor regression *in vivo*. These results suggest that blocking TIGIT effectively enhances the anti-tumor effect of CAR-T cells and suggest a promising strategy of combining CAR-T with immune checkpoints blockade in the treatment of solid tumors.

KEYWORDS

MSLN, TIGIT, immunotherapy, CAR-T cell, solid tumors

Introduction

Chimeric antigen receptor (CARs) T cells therapy is emerging as a hot spot for cancer immunotherapy. CAR-T cells are genetically engineered to express antigen-specific T cells that recognize and eliminate specific cancer cells independent of major histocompatibility complex (MHC) molecules (1, 2). CAR consists of intracellular signaling and transmembrane (TM) structural domains and extracellular single-chain variable fragments (scFvs) (3). These scFvs are hinge-linked light chain (VL) and heavy chain (VH) variable regions that specifically recognize and bind tumor-associated antigens

(TAA) (4). As an emerging therapy after chemoradiotherapy, it has become an important treatment for attacking cancers due to its advantages such as MHC restriction and etc. CAR-T cell therapy has achieved remarkable therapeutic results on a variety of tumors, especially in hematologic tumors, but its therapeutic results in solid tumors are limited (5). The main limitations of CAR-T cells are the limited available target antigens, their vulnerability in the tumor microenvironment (TME), insufficient tumor killing capacity and low persistence (6). In the TME, tumors can evade immune-mediated recognition through multiple immune escape mechanisms thereby attenuating the killing ability of immune cells (7). Under chronic tumor antigen exposure, T cell dysfunction/dysregulation and upregulation of various checkpoint inhibitory receptors that limit T cell survival and function reduce tumor clearance (8–10). Interactions between immune cell types and non-tumor cells within the TME clearly affect tumor progression, invasion, and metastasis (11). Therefore, the question of how to attenuate the inhibitory effect of suppressive immune checkpoints in the TME has become a pressing need.

Mesothelin (MSLN) is normally expressed on the surface of mesothelial cells. It was found that MSLN is also overexpressed in a wide range of solid tumors (12). Due to its differential expression between cancer and normal tissues and its role in tumorigenesis, MSLN can be considered as a potential target for cancer immunotherapy (13–16). However, achieving a broader therapeutic application of CAR-T cells requires a multi-layered approach to improve efficacy and safety (6, 17). An increasing number of studies have shown that mesothelin plays an important role in the promotion of tumorigenesis and progression, although its function in physiological situations is not yet clear (18). Studies have shown that MSLN can promote tumor proliferation, metastasis, and resistance to chemotherapy. Since MSLN is a highly specific antigen in several cancers, CAR-T therapy has been considered to be a promising strategy for the treatment of these cancers.

T cell Ig and immune receptor tyrosine inhibitory motif (ITIM) structural domains (TIGIT) acts as an immune checkpoint that is highly expressed on the surface of natural killer cells (NK) and T cells, significantly limiting anti-tumor and other $CD8^+$ T cell-dependent chronic immune responses (19–21). TIGIT belongs to the immunoglobulin superfamily, which consists of an extracellular immunoglobulin variable region (IgV) structural domain, a type I transmembrane structural domain and an intracellular structural domain with a classical ITIM and an immunoglobulin tyrosine tail (ITT) motif (22). CD155 is a high-affinity ligand of TIGIT (23). Once CD155, which is highly expressed on tumor surface, binds to TIGIT on NK and T cells surface, its killing effect on tumor cells is inhibited (24). The blocking of TIGIT/CD155 interaction is a promising approach in cancer immunotherapy (25). Many literatures describing the inhibitory immune test site TIGIT have shown that TIGIT-blocking antibody can be used in a variety of tumor treatments and are associated with T cell infiltration (26–28). However, it is still unknown whether the combination of TIGIT-related antibodies and CAR-T can achieve good efficacy since no study has been established.

For this study, we designed anti-MSLN CAR-T cells in combination with α-TIGIT antibody (anti-α-TIGIT) to treat the target cells. We found that anti-α-TIGIT effectively blocked TIGIT on the surface of CAR-T cells to a certain extent and increased the release of cytokines in anti-MSLN CAR-T cells to enhance the killing of target cells *in vitro*. Additionally, we genetically modified anti-MSLN CAR-T cells to have the ability to secrete anti-α-TIGIT scFvs for the long term. We found that the anti-α-TIGIT scFvs expression and secretion could interrupt the interaction of TIGIT with its ligand CD155, therefore enhanced CAR T cells infiltration and activation to promote tumor regression *in vivo*. In summary, our study demonstrated that blocking TIGIT effectively enhances the anti-tumor effect of CAR-T cells, thereby suggesting a promising strategy for the treatment of solid tumors by combining CAR-T cells with immune checkpoint blockages.

Materials and methods

Cell culture

Peripheral blood mononuclear cells (PBMCs, TPCS#PB025C) were purchased from the miles-bio of Shanghai. Normal human embryonic kidney cell line HEK293, T cell leukemia cell line NFAT-Jurkat, human cervical cancer cell lines Hela, human ovarian cancer cell lines (Skov3) were purchased from the American Type Culture Collection. T lymphocytes were maintained in T cell growth medium (TCGM): X-VIVO 15% Serum-free Hematopoietic Cell Medium (Lonza, Switzerland) supplemented with 5% FBS 2 ng mL^{-1} human recombinant IL-2 (100U mL^{-1}, Sigma, Germany). HEK293 were maintained in Dulbecco's modified Eagle's medium (DMEM, Gibco, Grand Island, NY, USA). NFAT-Jurkat and Hela were maintained in RPMI 1640-media (Gibco, Grand Island, NY, USA). Skov3 were maintained in McCoy's 5A medium (Gibco, Grand Island, NY, USA). GFP- and luciferase-expressing Hela (Hela-GL) and Skov3 cells (Skov3-GL) were generated by transfection of Hela and Skov-3 cells with lentiviral supernatant containing luciferase-2A-GFP. All cells were cultured in recommended medium supplemented with 10% FBS (Gibco) in a 10% CO_2 incubator.

CARs design and lentivirus packaging

The amino acid sequence of the human MSLN antibody was screened previously in the laboratory. The anti-MSLN scFv used originated from P4-scFv.The TIGIT-blocking scFv was originated from patent (Patent No.US20160176963A1). CAR constructs were synthesized and cloned into the pCDH lentiviral plasmid backbone with a human CMV promoter. A lentiviral vector containing a CAR consisting of the anti-MSLN scFv, CD8 hinge region, CD8 transmembrane domain, CD28 and CD3 costimulatory signaling molecules, CD3ζ signaling endodomains. To generate CARs expressing anti-human TIGIT scFv, T2A peptide sequences were intercalated among the second-generation CAR genes. The pMDL-MSLN-CAR-based lentiviral plasmid and two packaging plasmids, pMD-gag-pol and pMD-VSVG, were co-transduced into HEK293 cells in 75 cm^2 flask at a ratio of 4:3:1, with a total amount of 24 μg.

Lentivirus-rich supernatants were collected 48 h, 72 h and filtered through a 0.22 μm filter. Lentiviral vectors supernatants concentrated by ultracentrifugation at 25,000 ×g, 4°C, for 2 h and preserved at −80°C.

T cell isolation and retroviral transfection

PBMCs from healthy donors and ovarian cancer patients were isolated by Lymphoprep (Stemcell, Canada), and then T cells were isolated from the cells by negative selection using EasySep™ Human T Cell Isolation Kit (Stemcell, Canada). Then activated using anti-human CD3 and CD28 microspheres (Miltenyi, Germany) at a 1:1 bead to cell ratio on day 0. Purified T cells were cultured in 5% FBS X-VIVO Serum-free Hematopoietic Cell Medium (Lonza, Switzerland) supplemented with recombinant human IL-2 (300 IU/mL). Detection of the CAR-T cell positive rate and detection of cell phenotype was performed following lentivirus infection and continuous culture for 48 h after T cell isolation. 1×10^6 T cells were inoculated into a 24-well plate and 100 μL of lentivirus concentrate were added. T cells were expanded for 2 weeks before downstream experiments. Using CAR-T cells, paired (from same donor) untransduced T cells, activated and cultured for equivalent time, served as control T cells.

Flow cytometry

All samples were acquired on a CytoFLEX S (Beckman Coulter, Indianapolis, IN), and data was analyzed using Kaluza 2.1 Flow Analysis. Software (Beckman Coulter Life Sciences). Staining for cell surface markers was carried out by incubating with antibodies for 30 min on ice. Antibodies involved in this study included Recombinant PE Anti-Mesothelin antibody(Abcam, Grand Island, NY), mouse IgG1 Isotype Control(R&D, Minneapolis, MN, USA), mouse F(ab)2 IgG (H+L) APC-conjugated Antibody (R&D, Minneapolis, MN, USA), human CD155/PVR PE-conjugated Antibody (R&D, Minneapolis, MN, USA), human TIGIT APC-conjugated Antibody (R&D, Minneapolis, MN, USA), CD226 (DNAM-1) Monoclonal Antibody, APC (eBioscience, San Diego, CA), mouse anti-human CD4-PE (BD, San Diego, CA), mouse anti-human CD8-APC (BD, San Diego, CA), mouse anti-human Foxp3-APC (BD, San Diego, CA). APC anti-mouse CD279 (PD-1) Antibody (biolegend, California, USA), PE anti-mouse CD197 (CCR7) Antibody (biolegend, California, USA), APC anti-human CD45RA Antibody (biolegend, California, USA).

Western blotting

The cells were lysed in SDS buffer (Invitrogen™, Waltham, MA, USA) containing a protease inhibitor cocktail (PMSF) in accordance with the manufacturer's protocol. Each sample was sonicated 4 times for 15 second intervals, with at least 15 seconds rest on ice in between successive sonication periods, before being boiled for 5 minutes at 95°C. Cell lysates were separated by SDS-PAGE, transferred to nitrocellulose membranes under the appropriate conditions, and blotted for the following antigens: total human CD155/PVR Antibody (R&D, Minneapolis, MN, USA), GAPDH (Upstate, 05-423) HRP-conjugated mouse-anti-myc tag antibody and HA-Tag (6E2) Mouse mAb (Cell Signaling Technology, Danvers, Massachusetts, USA). Each experiment was repeated at least 3 times. Blots were quantified using ImageJ image analysis software.

Immunofluorescence

Immunofluorescence was used to analysis the expression of CD155 in tumor cells (Hela and Skov3). The slides with cells were fixed with 4% paraformaldehyde (Boston Bioproducts) for 15 min. Normal goat serum was added to the slides were sealed at room temperature for 30 min. Each slide was dropped with enough Human CD155/PVR Antibody (R&D, Minneapolis, MN, USA) and placed in a wet box for incubation at 4°C overnight. After incubation, sample were washed and incubated with Goat Anti-Mouse IgG H&L (Alexa Fluor® 594) (Abcam, Grand Island, NY) for 60 min at room temperature. The samples were stained DAPI (R&D, Minneapolis, MN, USA) and incubated for 5 min. Then PBST was washed for 5 min, 4 times to remove the excess DAPI. Dry the liquid on the slipper with absorbent paper, seal the slipper with sealing liquid containing anti-fluorescence quench agent, and observe and collect the image under Laser scanning confocal microscope (LSCM).

Real Time Cytotoxicity Assay (RTCA)

Tumor cells (2×10^4) were plated in a 96-well. After 24 h, effector T cells were added into the unit at various effector (T cells, anti-MSLN CAR-T cells, anti-MSLN CAR-T cells +anti-α-TIGIT and MT CAR-T cells)/target cell (E/T) ratios (8:1, 4:1, 2:1, and 1:1). Using the impedance-based Real Time Cytotoxicity Assay, RTCA (ACEA, San Diego, CA), the kinetics of tumor cell lysis was evaluated over 80 h. Impedance was measured at 15-min intervals. The impedance-based cell index for each well and time point was normalized with the cell index before adding T or CAR-T cells. The kinetics of cell lysis was evaluated as the change in normalized cell index over time.

LDH release assay

Tumor cells (2×10^4) were plated in a 96-well, resistor-bottomed plate in triplicate. After 24 h, effector T cells were added into the unit at various effector (T cells, anti-MSLN CAR-T cells, anti-MSLN CAR-T cells +anti-α-TIGIT and MT CAR-T cells)/target cell (E/T) ratios (8:1, 4:1, 2:1, and 1:1) at 37°C for 4 h. LDH in the culture medium was measured by using commercial kits in 96-well enzyme immunoassay plates according to the manufacturer's instructions.

Luciferase report assay

Tumor cells (2×10^4) were plated in a 96-well. After 24 h, effector T cells were added into the unit at various effector (T cells, anti-MSLN CAR-T cells, anti-MSLN CAR-T cells +anti-α-TIGIT and MT CAR-T cells)/target cell (E/T) ratios (8:1, 4:1, 2:1, and 1:1) at 37°C for 6 h. The above 96-well plate was centrifuged at 1000 ×g for 5 min and some of the supernatant was removed. Then adding 100 μL of luciferase substrate to each well, mix by blowing, and leave for 3 min. The above mixture was transferred to a white 96-well plate and assayed on the machine. Tthe cytotoxicity is relatively to tumor cells grown without T cells (Control group). The relative cytotoxicity rate was calculated as follows: relative cytotoxicity (%) = [Control well OD- (experimental well OD - blank well OD)/(control well OD- blank well OD)]× 100%.

Enzyme-Linked Immunosorbent Assay (ELISA)

For *in vitro* trials, CAR-T cells (2×10^4) were co-cultured with tumor cells (2×10^4) in 96-well plates without the addition of exogenous cytokines. Following 24 h of coculture at 37°C, supernatant was collected and cytokines (IFN-γ, IL-2, TNF-α) were measured by ELISA in accordance with the manufacturer's instructions (R&D, Minneapolis, MN, USA). For *in vivo* trials, 100 μL of peripheral blood was collected from the treated mice at 4°C overnight and centrifuged for 10 min (1000 ×g) to collect the supernatant. Cytokines in blood serum (IFN-γ, IL-2, TNF-α) were analyzed by ELISA assay, according to the manufacturer's instruction (R&D, Minneapolis, MN, USA). The content of TIGIT scFvs tested by ELISA analysis. Human TIGIT Protein, His Tag (HPLC verified) (Acro, Delaware, US) were encapsulated in a 96-well enzyme-labeled plate and spent the night at 4°C. The TIGIT antigen was diluted to 100 μg by coating diluent, 100 μL was added into each pore at 4°C for 24 h. 5% calf serum was sealed at 37°C for 40 min. The diluted sample was added into the enzyme-labeled reaction hole at least two holes, 100μL per hole, at 37°C for 60 min. Anti-HA-Tag Mouse mAb was added to connect with HA-Tag in TIGIT scFv. 200 μL TMB color solution per hole was incubated at room temperature for 10 min and then read at 450 nm.

In vivo xenograft models

Female B-NDG mice (4 weeks) were purchased from Biocytogen (Beijing). All procedures were conducted in conformity with guidelines of the National Institutes of Health and Institutional Animal Care and Use Committee. And the animal experiments were approved by the Nanjing Normal University Animal Faculty. Mice were maintained under specific pathogen-free conditions for 3 days, then an equal number of $Hela^{CD155}$ cells (5×10^6/per mouse) were subcutaneously implanted on the right of the same B-NDG mice, respectively. The progression of xenograft tumors was monitored every three days through the measurement of the length (L) and width (W) of tumors using a digital Vernier caliper, and the tumor volume (V) was calculated as $V= (L\times W^2)/2$. The mice were randomly divided into 4 groups when the mean of tumor volumes reached 100 mm^3 mice and different groups were treated with intravenous infused of 5×10^6 cells (T cells, anti-MSLN CAR-T cells, anti-MSLN CAR-T cells +anti-α-TIGIT and MT CAR-T cells). Mice were given TIGIT antibody (100 μg/per mice) (Biointron, Taizhou, China) on days 0, 7 and 14 post effector cells inoculation, for a total of three doses. Collect blood from mice before execution for used to detect cytokine release levels *in vivo*.

Copy number of CAR gene in mice

100 μL mice blood were collected every 7 days and DNA was extracted from FastPure Blood DNA Isolation Mini Kit following manufacturer's instruction (Vazyme, Nanjing, China) CAR DNA was quantified by real-time PCR using primers WPRE-F 5' GGCACTGACAATTCCGTGGT 3', WPRE-R 5' AGGGACGTAGCAGAAGGACG 3'. ChamQ SYBR qPCR Master Mix (High ROX Premixed) (Vazyme, Nanjing, China). The samples were measured in a CFX384 Touch Real-Time PCR Detection System (Bio-Rad). All samples were tested at least in triplicates.

Immunohistochemistry (IHC)

Tissues were fixed with formalin and embedded in paraffin until further processing. Then 3-mm-thick sections were deparaffinized and treated with a heat-induced antigen IHC Tek epitope retrieval solution (IHC World) for 30 min. Slides were then blocked with tris-NaCl (TNB) blocking buffer (PerkinElmer) and stained with anti-human CD4/8 antibody (Abcam, Grand Island, NY) or anti-human TIGIT antibody (R&D, Minneapolis, MN, USA) in the blocking solution overnight at 4°C. Secondary antibodies were added after rinsing the section for 1 h at room temperature, and the results were visualized with a ChemMate Envision Detection Kit (DakoCytomation). Images were obtained using the 3DHISTECH Panoramic digital slide scanner and the associated CaseViewer software (3DHISTECH).

Statistical analysis

GraphPad Prism 8.0 software was used to construct all graphs and calculate statistical significance. Kaluza Analysis 2.1 software was used for FCM analysis and to generate plots. For two sets of fold-change measurements, a one sample t-test was used. For comparison of three or more sets of unpaired measurements, one-way ANOVA was performed with Tukey's *post-hoc* test if all sets were analyzed, or Sidak's *post-hoc* test if selected relevant pairs were analyzed. Significance from Kaplan-Meier survival curves were calculated with the Log-Rank test. Data is represented as mean ± SD of at least three independent experiments. In all plots, *, $P< 0.05$; **, $P < 0.01$; ***, $P < 0.001$.

Results

Construction of anti-MSLN CAR-T and its killing effect on tumor cells

To validate the tumor killing effect of CAR-T cells, we first designed and generated anti-MLSN CAR-T cells with a highly efficient second-generation human-derived scFv targeting MSLN, which was screened from a human-derived scFv phage display library (Figure 1A). The expression of anti-MSLN scFv in lentiviral vector-transfected T cells was detected using flow cytometry 4 days post-infection to verify the CAR transfection efficiency. The results showed that the proportion of stabilized CAR^+ cells were approximately 83% 4 days post-infection (Figure 1B). The proportion of $CD3^+CD8^+$ T cells and $CD3^+CD4^+$ T cells in anti-MSLN CAR-T and T cells were examined using flow cytometry. It was found that the proportion of $CD3^+CD8^+$T cells in both anti-MSLN CAR-T and T cells was around 32%. The proportion of $CD3^+CD4^+$ T cells was around 60%. No significant differences in the distribution of CD4 and CD8 expression were found between CAR-T or T cells (Figure 1C). We also examined the phenotypes of CD45RA and CCR7 cells in anti-MSLN CAR-T and T cells. There were no significant differences found in the distribution of CD45RA and CCR7 expression between CAR-T or T cells (Figure 1D). In addition, to detect the expression of MSLN in Hela and Skov3 cells, we collected the cells and incubated them with anti-MSLN antibodies by flow cytometry detection. The results demonstrated that MSLN was elevated and specifically expressed in Hela and Skov3 cells (Figure 1E). Then we quantified the anti-tumor activity of our anti-MSLN CAR-T cells *in vitro*. The results showed that anti-MSLN CAR-T cells had a significant killing effect on Hela-luciferase-GFP and Skov3-luciferase-GFP cells (Figures 1F-H). These results suggested that anti-MSLN CAR-T cells induced considerable cell lysis in target Hela and Skov3 cells.

TIGIT antibody enhances the anti-tumor effect of MSLN CAR-T cells

TIGIT interacts with CD155, resulting in a reduced anti-tumor effect. Correspondingly, targeting TIGIT can be an effective approach for treating cancers. Thus, we detected TIGIT expression in activated T lymphocytes from healthy subjects and ovarian cancer patients. Flow cytometry results showed that $TIGIT^+$ T lymphocytes was about 10% in healthy subjects and 20%-35% in ovarian cancer patients (Figures 2A, B). These results indicated that a higher proportion of activated T lymphocytes from ovarian cancer patients expressed TIGIT. Then we found that varying degrees of CD155 expression on the cell surface in Hela and Skov3 cells (Figure 2C, Figure S1A, B). To detect the influence of TIGIT/CD155 immune checkpoint on MSLN CAR-T cells, we constructed $Hela^{CD155}$, a Hela cell line overexpressing CD155 (Figure S1C). The effector cell-induced killing was quantified using a fluorescein reporter assay. The results showed that anti-MSLN CAR-T cells were more effective in killing wild-type Hela cells but less effective in killing $Hela^{CD155}$ cells (Figure 2D). Subsequently, we examined the influence of TIGIT on the long-time killing effect of MSLN CAR-T cells. The results showed that anti-α-TIGIT did not influence the killing effect of anti-MLSN CAR-T cells on Hela and $Hela^{CD155}$ cells on Day 1. On day 2, anti-α-TIGIT significantly increased the anti-MSLN CAR-T cell-induced killing on $Hela^{CD155}$ cells (Figures 2E, F). On day 4, anti-α-TIGIT enhanced anti-MSLN CAR-T cells continuous killing of both Hela and $Hela^{CD155}$ cells (Figure 2G). To further r show the importance of TIGIT on CAR-T cell efficacy, we constructed a Hela cell line knock down CD155, $Hela^{shCD155}$ (Figure S1D). Anti-MSLN CAR-T cells had more stronger killing effect on $Hela^{shCD155}$ cells (Figure S1E, F). However, the combination of anti-α-TIGIT treatment significantly enhanced the killing effect of CAR-T cells on Hela cells. These findings provide important insights into the role of anti-α-TIGIT in enhancing the sustained killing efficacy of anti-MSLN CAR-T cells against tumor cells over an extended period. Flow cytometry analysis revealed that approximately 18.31% of anti-MSLN CAR-T cells were $TIGIT^+$, while the percentage dropped to about 1.81% in the anti-α-TIGIT+anti-MSLN CAR-T cell population (Figure 2H). This indicates that anti-α-TIGIT can indirectly or directly block TIGIT on the surface of activated CAR-T cells. Furthermore, we examined the phenotype of anti-MSLN CAR-T cells after co-culture with tumor cells. The results indicated that the anti-MSLN CAR-T cells+anti-α-TIGIT group exhibited a downregulation of immunosuppressive receptors (LAG-3 and TIGIT) compared to the anti-MSLN CAR-T cells group. Conversely, the expressions of T cell activation markers (CD226 and CD25) were upregulated in the anti-MSLN CAR-T cells +anti-α-TIGIT group compared to the anti-MSLN CAR-T cells alone (Figure 2I, Figure S1G). In addition, we quantified the release of IFN-γ from CAR-T cells. The results showed that both anti-α-PD-1 and anti-α-TIGIT antibodies increased the release of IFN-γ from CAR-T cells. Importantly, when these two antibodies were used together, there was a significant increase in the level of IFN-γ released (Figure 2J). In summary, these results indicated that anti-α-TIGIT enhanced the sustained killing effect of anti-MSLN CAR-T cells on tumor cells.

TIGIT antibody promotes the activation of anti-MLSN CAR/TIGIT NFAT-Jurkat cells

We used Jurkat cells to mimic T cell responses *in vitro* to investigate the effect of TIGIT on T cell phenotypes. T cell activation bioassay is a bioluminescent cell-based assay that overcomes the limitations of existing assays for the discovery and development of cellular therapies designed to induce, enhance, or mimic T cell responses. The assay consists of a genetically engineered Jurkat cell line that expresses a luciferase reporter gene driven by the nuclear factor of activated T cells response element (NFAT-RE) (Figure 3A). NFAT-Jurkat cells were transfected with anti-TIGIT, anti-MSLN CAR lentivirus for 24 h and cultured continuously. The results showed that there was 94.93% $TIGIT^+$ cells and 92.37% anti-$MLSN\ CAR^+$ cells, which were both high levels (Figure 3B). Next, we analyzed the binding of anti-α-TIGIT to NFAT-Jurkat cells. We used a mouse Fc IgG(H+L) APC-conjugated antibody bound to the FC fragment of the anti-TIGIT antibody, thereby indirectly detecting the binding efficiency of the anti-TIGIT antibody to

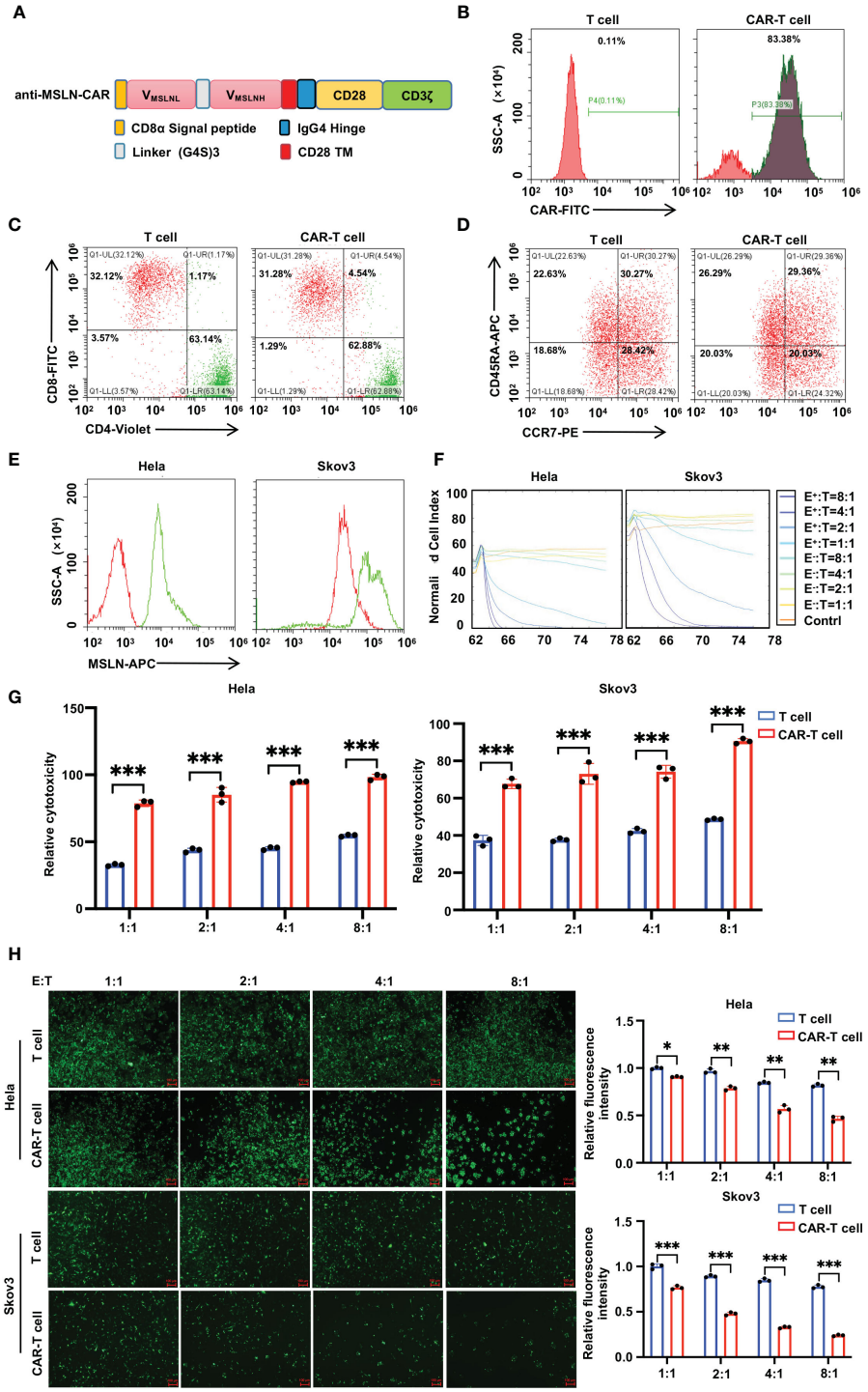

FIGURE 1
Construction anti-MSLN-CAR-T cells and its killing effect on tumor cells. **(A)** Schemas of MSLN-CARs incorporating different spacers [CD8α Signal peptide, IgG4 Hinge, (G4S)3 Linker, and CD8α^{TM}] and costimulatory domains (CD28). **(B)** The transfection efficiency was measured by GFP positive cells using flow cytometric analysis. **(C, D)** Efficient lentiviral transfection of primary human T cells encoding anti-MSLN, with similar CD4/CD8 ratios **(C)**, CD45RA and CCR7 **(D)** in control and CAR transduced T cells. (4 days after lentivirus CAR transfection, the subsets and phenotype of T cells, anti-MSLN CAR-T cells were analyzed by FACS, including the expression of CD4 and CD8.) **(E)** Expression of MSLN in human cell lines were evaluated by FACS. Cells were incubated with anti-MSLN antibody (green) or its corresponding isotype control (red). **(F)** RTCA was used to evaluate the lysis of the indicated tumor cells when treated with T (E^-) cells or CAR-T (E^+) cells at a 1:1, 2:1, 4:1, 8:1 effector/target (E/T) ratios over a 78-h period. **(G)** Luciferase report assay results showed lysis of spheres of target cell cultures in the presence of anti-MSLN CAR-T cells or control T cells at the indicated E/T ratios. **(H)** Lysis of spheres of Hela and Skov3 target cell cultures in the presence of T cells (control), or anti-MSLN CAR-T cells at a 1:1, 2:1, 4:1, 8:1 E/T ratios, subjected to immunofluorescence (IF) analysis. Scale bar: 100 μm. Data is represented as mean ± SD of at least three independent experiments. In all plots, *, $P< 0.05$; **, $P < 0.01$; ***, $P < 0.001$.

10.3389/fimmu.2023.1175920

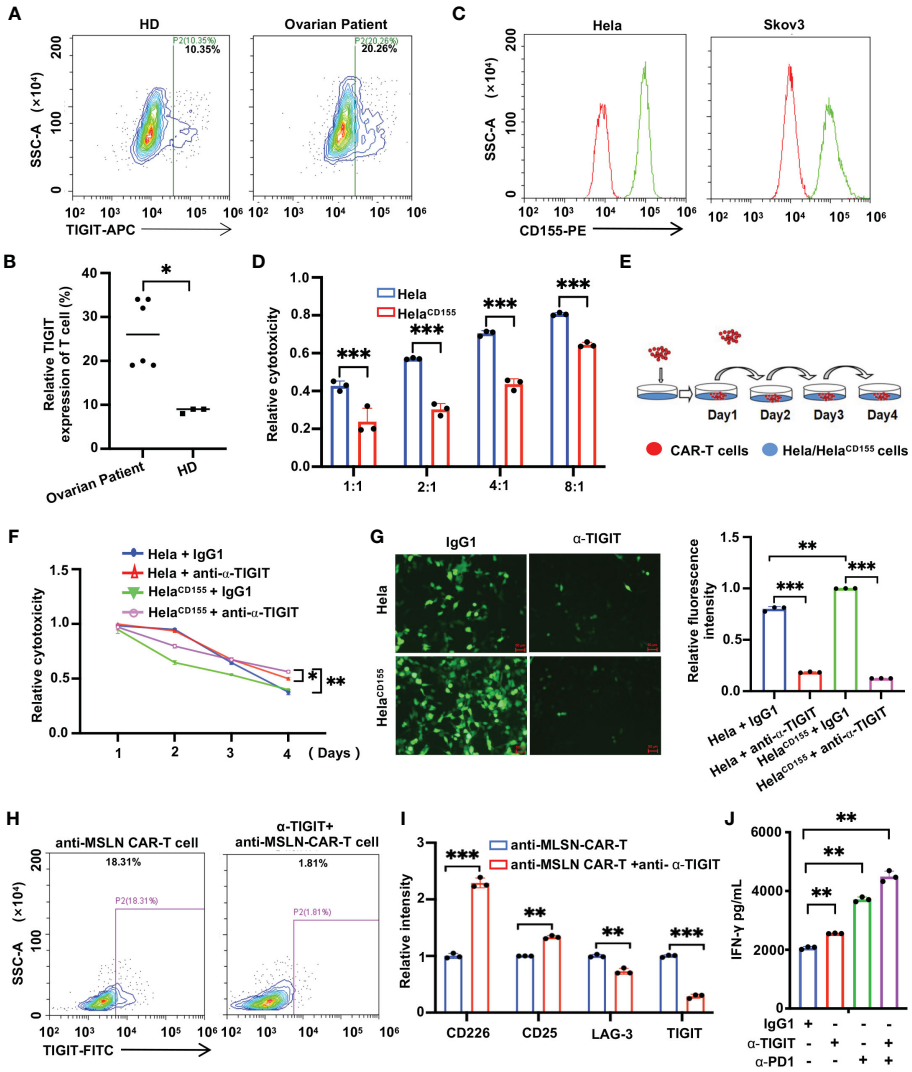

FIGURE 2
TIGIT antibody enhances the killing effect of anti-MSLN CAR-T cells on tumor cells. **(A)** Flow cytometry determines the expression of TIGIT in activated T lymphocytes from healthy donors or ovarian cancer patients. **(B)** Statistical graph of TIGIT expression in activated T lymphocytes of healthy subjects and ovarian cancer patients. **(C)** Flow cytometry for total CD155 protein levels in human cell lines. **(D)** Luciferase report assay results showed lysis of spheres of Hela/Hela^{CD155} cultures treated anti-MSLN CAR-T cells at the indicated E/T ratios for 6 (h) **(E)** The Schematic diagram of CAR-T continuous killing for 4 consecutive days. **(F, G)** Lysis of spheres of Hela/Hela^{CD155} target cell cultures in the presence of anti-MSLN CAR-T cells, at a 1:1 E/T ratio with or without anti-TIGIT (10^4 ng/mL) on 4 days, subjected to fluorescein reporting assay **(F)** and IF analysis **(G)**. Scale bar: 50 μm. **(H)** The TIGIT expression was measured in CAR-T cells cocultured with tumor cells in the case of with or without anti-α-TIGIT by GFP positive cells using flow cytometric analysis. **(I)** Anti-MSLN CAR-T cells-treated tumors were harvested 4 h post-treatment at a 1:1 E/T ratio, detecting the phenotype of CAR-T cell activation (CD226 and CD25) and depletion (LAG-3 and TIGIT) by flow cytometry. **(J)** ELISA results showed the IFN-γ secretion levels by anti-MSLN CAR-T combined with IgG1, anti-α-TIGIT, anti-α-PD1, anti-α-TIGIT+anti-α-PD1 for 24 (h) Data is represented as mean ± SD of at least three independent experiments. In all plots, *, $P < 0.05$; **, $P < 0.01$; ***, $P < 0.001$.

TIGIT on the surface of Jurkat cells by flow cytometry. The results showed that anti-α-TIGIT bound to Jurkat^{TIGIT} at a rate of 60.86% and Jurkat $^{CAR+TIGIT}$ cells at a rate of 67.6% (Figure 3C). In addition, we suggest that Jurkat cell activation status is positively correlated with TIGIT concentration in a certain range (Figure 3D). These results showed that the overexpression of CD155 suppressed Jurkat activation level, while anti-α-TIGIT increased Jurkat activation level and reverted the immunosuppression caused by CD155 (Figure 3E). In conclusion, anti-α-TIGIT can promote anti-MLSN CAR/TIGIT NFAT-Jurkat cell activation.

Self-delivery TIGIT-blocking scFv enhances the anti-tumor effects of CAR-T cells *in vitro*

Although CAR-T cells have made important advances in the treatment of multiple tumors, there are multiple adverse effects on clinical treatment. Improving the efficacy and safety of CAR-T cell therapy by modifying the structure of CARs is a promising strategy. Thus we introduced the MT CAR gene into T cells by gene transfection to make T cells express secretory TIGIT scFvs,

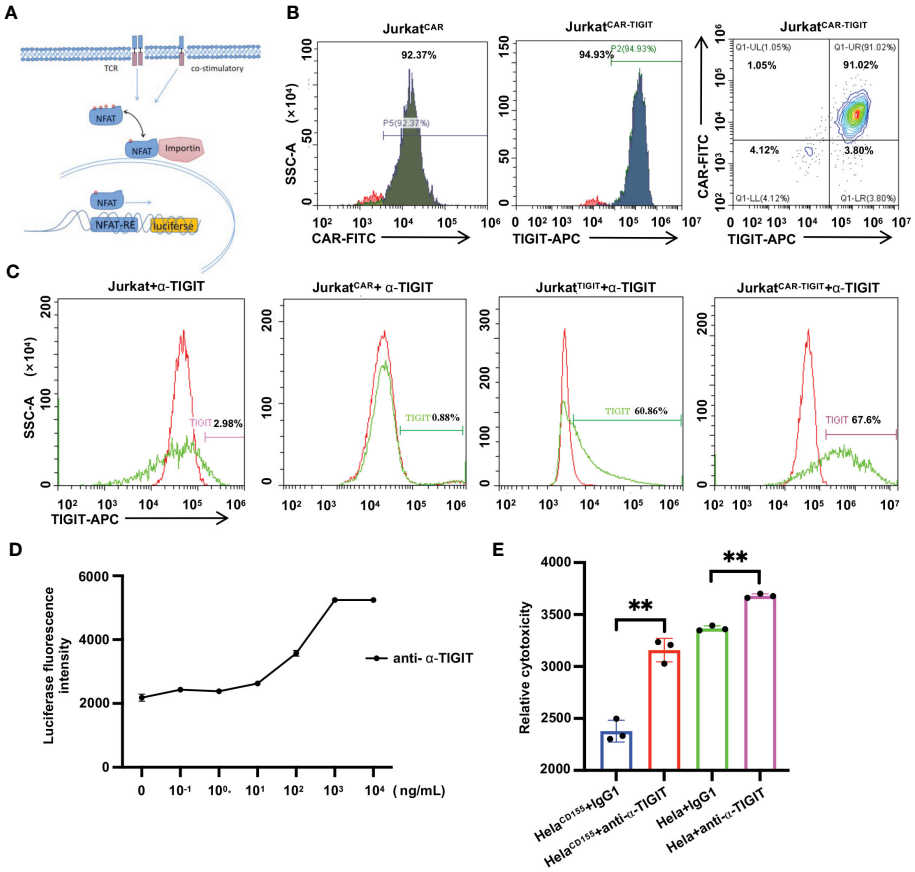

FIGURE 3
TIGIT antibody promotes T cell activation in NFAT-Jurkat cells report system. **(A)** Schematic diagram of NFAT-luciferin gene structure. **(B)** The transfection efficiency was measured by GFP positive cells using flow cytometric analysis on the 7th day after transfection. **(C)** The binding efficiency of anti-α-TIGIT in NFAT-Jurkat cells was measured by flow cytometry. Cells were incubated with anti-α-TIGIT (green) or its corresponding isotype control (red). **(D)** The degree of activation of anti-MLSN CAR/TIGIT NFAT-Jurkat cells cocultured with Hela^{CD155} for 24 h was shown after treatment with indicated concentrations of anti-α-TIGIT for 24 h **(E)** Luciferase report assay results showed lysis of spheres of target cell cultures treated by anti-MSLN CAR-T cells with or without anti-α-TIGIT (10^4 ng/mL) at a 1:1 E/T ratio for 24 **(h)** Data is represented as mean ± SD of at least three independent experiments. In all plots, **, $P < 0.01$.

which might block TIGIT on the surface of T cells. Then we designed and generated anti-MLSN CAR-T cells with self-delivery of TIGIT-neutralizing scFv, as shown in Figure 4A. The anti-α-TIGIT scFv expression of T cells after lentiviral vector transfection was detected by flow cytometry 4 days after transfection to verify the CARs transfection efficiency. The results showed that there was 48.93% CAR$^+$ in MT CAR-T cells after lentiviral transfection (Figure 4B). Western blot analysis showed that there was almost no expression of TIGIT scFvs in anti-MSLN CAR-T cells but significant in MT CAR-T cells (Figure 4C). In addition, ELISA analysis also indicated that anti-MSLN CAR-T cells had almost no expression of anti-α-TIGIT scFv, while MT CAR-T cells had a high expression of scFvs (Figure 4D). We performed a flow cytometry assay to validate TIGIT on the surface of T cells (Figure 4E). These results revealed that the expressed anti-α-TIGIT scFv blocked TIIGIT on MT CAR-T cells relative to anti-MSLN CAR-T cells. We quantified the anti-tumor activity of MT CAR-T cells *in vitro*. The results showed that MT CAR-T cells had a great killing effect on Hela, Hela ^{CD155} and Skov3 cells (Figures 4F, G). Then, we examined the tumor-killing effect of anti-MSLN CAR-T and MT CAR-T cells by LDH release level. The results showed that the anti-α-TIGIT scFv-expressing group had a better tumor-killing effect compared to the antibody and IgG groups in Hela, Hela^{CD155} and Skov3 cells (Figure 4H). Furthermore, the release of IFN-γ, IL-2 and TNF-α was detected using ELISA Kit. Consistently, an increase in cytokine production was observed in the supernatant of MT CAR-T cells and MSLN$^+$ tumor cells (Figures 5A–C). In addition, we examined the anti-MSLN CAR-T and MT CAR-T cell phenotype after co-culture with tumor cells (Figures 5D, E). MT CAR-T cells showed a downregulation of the immunosuppressive receptors (TIGIT, PD-1, and LAG-3) compared to those in the normal anti-MSLN CAR-T cells. In contrast, the expressions of T cell activation markers (CD226, CD25 and CD69) were upregulated in MT CAR-T cells compared with those in anti-MSLN CAR-T cells. These results indicated that self-delivery TIGIT-blockading scFv enhanced the efficacy of anti-tumor function of CAR-T cells on solid tumor cells *in vitro*.

10.3389/fimmu.2023.1175920

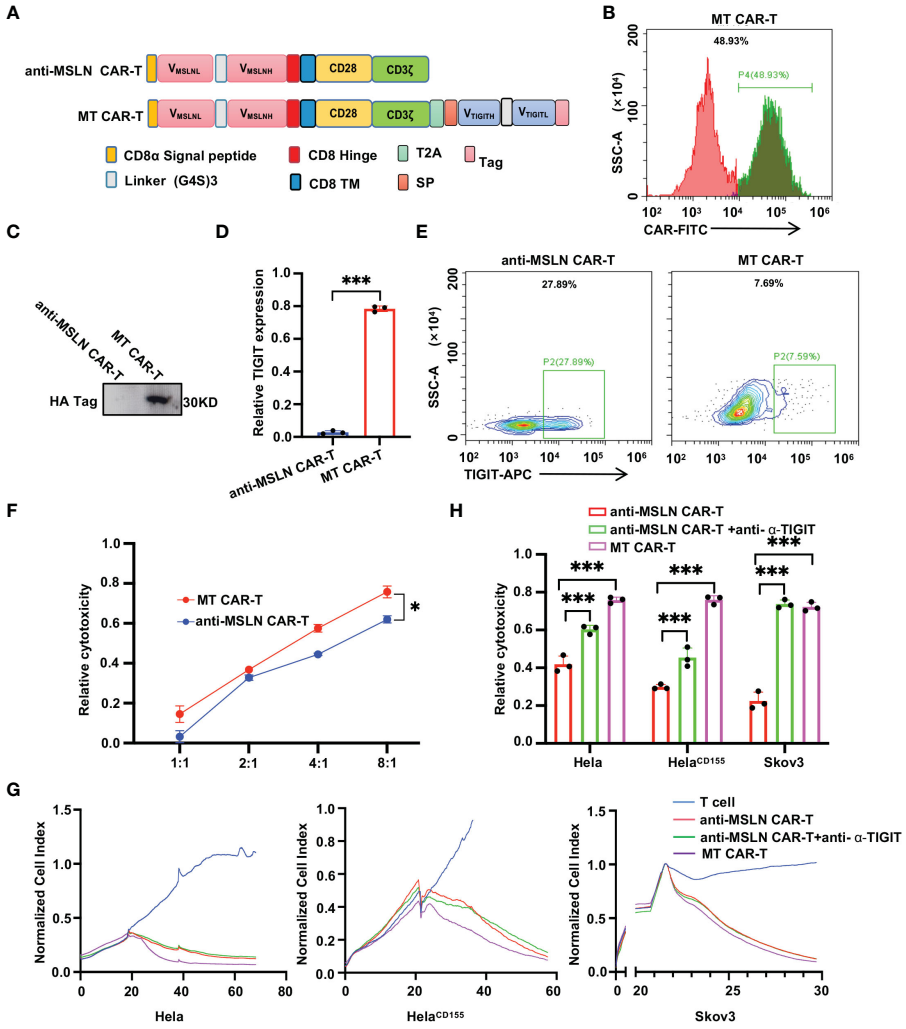

FIGURE 4
Self-delivery TIGIT-blocking scFv enhances CAR-T cells cytotoxicity to tumor cells. **(A)** Schemas of anti-MSLN-CARs and MT CARs incorporating different spacers [CD8α Signal peptide, IgG4 Hinge, (G4S)3 Linker, CD8α^{TM}, T2A peptide sequence, Tag protein and Signal peptide] and costimulatory domains (CD28). **(B)** The transfection efficiency was measured by GFP positive cells using flow cytometric analysis. **(C, D)** Western blot **(C)** and relative quantification **(D)** for TIGIT levels in MT or anti-MSLN CAR-T cells, with three independent assays. **(E)** Detecting TIGIT on the surface of CAR-T cells by flow cytometric analysis. **(F)** Luciferase report assay results showed lysis of spheres of Hela^{CD155} cultures treated by MT cells or anti-MSLN CAR-T cells at a 1:1, 2:1, 4:1, 8:1 E/T ratios for 4 h **(G)** RTCA was used to evaluate the lysis of the indicated tumor cells when treated with control T cells, anti-MSLN CAR-T cells, anti-MSLN CAR-T cells+anti-α-TIGIT and MT CAR-T cells, at a 1:1 E/T ratio over a 60-h period. **(H)** Lysis of spheres of target cell cultures in treated by control T cells, anti-MSLN CAR-T cells, anti-MSLN CAR-T cells+anti-α-TIGIT and MT CAR-T cells, at a 1:1 E/T ratio for 4 **(h)** MT CAR-T cells are more effective against multiple cell lines. Data is represented as mean ± SD of at least three independent experiments. In all plots, *, $P < 0.05$; ***, $P < 0.001$.

Blocking TIGIT enhances CAR-T therapy *in vivo*

Lastly, to determine whether blocking TIGIT could enhance the anti-tumor effect of anti-MASL CAR-T cells *in vivo*, six-week-old B-NDG mice were reared for subcutaneous infused of Hela^{CD155} cells for tumorigenesis *in vivo*. The protocol of specific treatment is shown in Figure 6A. The body weight and tumor size of mice were constantly monitored during the treatment (Figures 6B, C). There was no significant difference in tumor size between mice in the MT CAR-T cells treatment, anti-MSLN CAR-T cells ± anti-α-TIGIT, and T cells. The tumor growth rate of mice with the CAR-T cells treatment slowed down compared to the one with T cells treatment. The anti-MSLN CAR-T cells showed signs of tumor recurrence in the late stage of the experiment, while the MT CAR-T cells and anti-MSLN CAR-T ± anti-α-TIGIT mice showed no tumor recurrence. MT CAR-T cells treated mice exhibited longer survival times (Figure 6D). Peripheral blood samples from mice 3 days after treatment were collected for ELISA to detect serum levels of cytokines (IFN-γ, IL-2 and TNF-α) (Figure 6E). The result showed that the mice treated with the CAR-T cells group had higher cytokine level than the T cell treatment group. Meanwhile, higher cytokine levels were detected in the peripheral blood of mice treated with MT CAR-T cells than those treated with anti-MSLN CAR-T ± anti-α-TIGIT. These results indicated that MT CAR-T cells were beneficial to tumor regression. In addition, it was found that there was higher MT CAR expression in the peripheral blood of mice (Figure 6F). The results then

10.3389/fimmu.2023.1175920

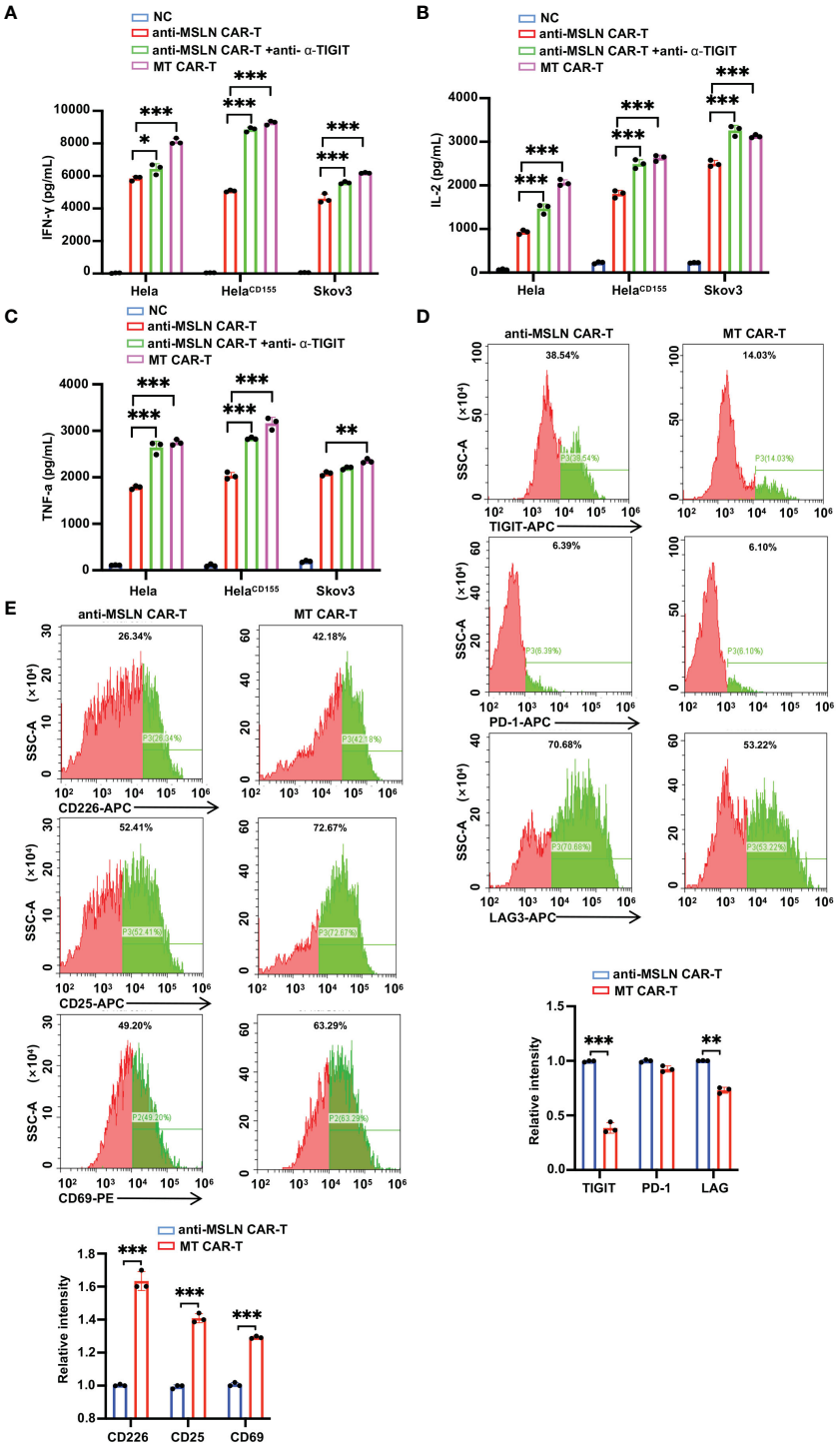

FIGURE 5
Self-delivery TIGIT-blocking scFv promotes cytokine secretion and modifies the characterization of CAR-T cells. **(A-C)** ELISA results showed the IFN-γ **(A)**, IL-2 **(B)**, and TNF-α **(C)** secretion levels treated by control T cells, anti-MSLN CAR-T cells, anti-MSLN CAR-T cells+anti-α-TIGIT and MT CAR-T cells. **(D)** MT cells or anti-MSLN CAR-T cells-treated tumors were harvested 4 h post-treatment at a 1:1 E/T ratio for 4 h, detecting the phenotype of CAR-T cell depletion (TIGIT, PD-1, and LAG-3) by flow cytometry. **(E)** MT cells or anti-MSLN CAR-T cells-treated tumors were harvested 4 h post-treatment at a 1:1 E/T ratio, detecting the phenotype of CAR-T cell activation (CD226, CD25 and CD69) by flow cytometry. Data is represented as mean ± SD of at least three independent experiments. In all plots, *, $P< 0.05$; **, $P < 0.01$; ***, $P < 0.001$.

showed that in the tumor tissues, the group of MT CAR-T cells treatment showed higher CD4 and CD8 infiltration compared to the group of anti-MSLN CAR-T cells (Figure 6G). Furthermore, TIGIT expression was lower in tumor tissues with the treatment of MT CAR-T cells (Figure 6H). No non-target organ tissue damage was detected in the heart, liver, spleen, and kidney (Figure 6I). In summary, these results indicated that self-delivery TIGIT-blocking scFv could enhance the anti-tumor function of CAR-T cells on solid tumors *in vivo*.

10.3389/fimmu.2023.1175920

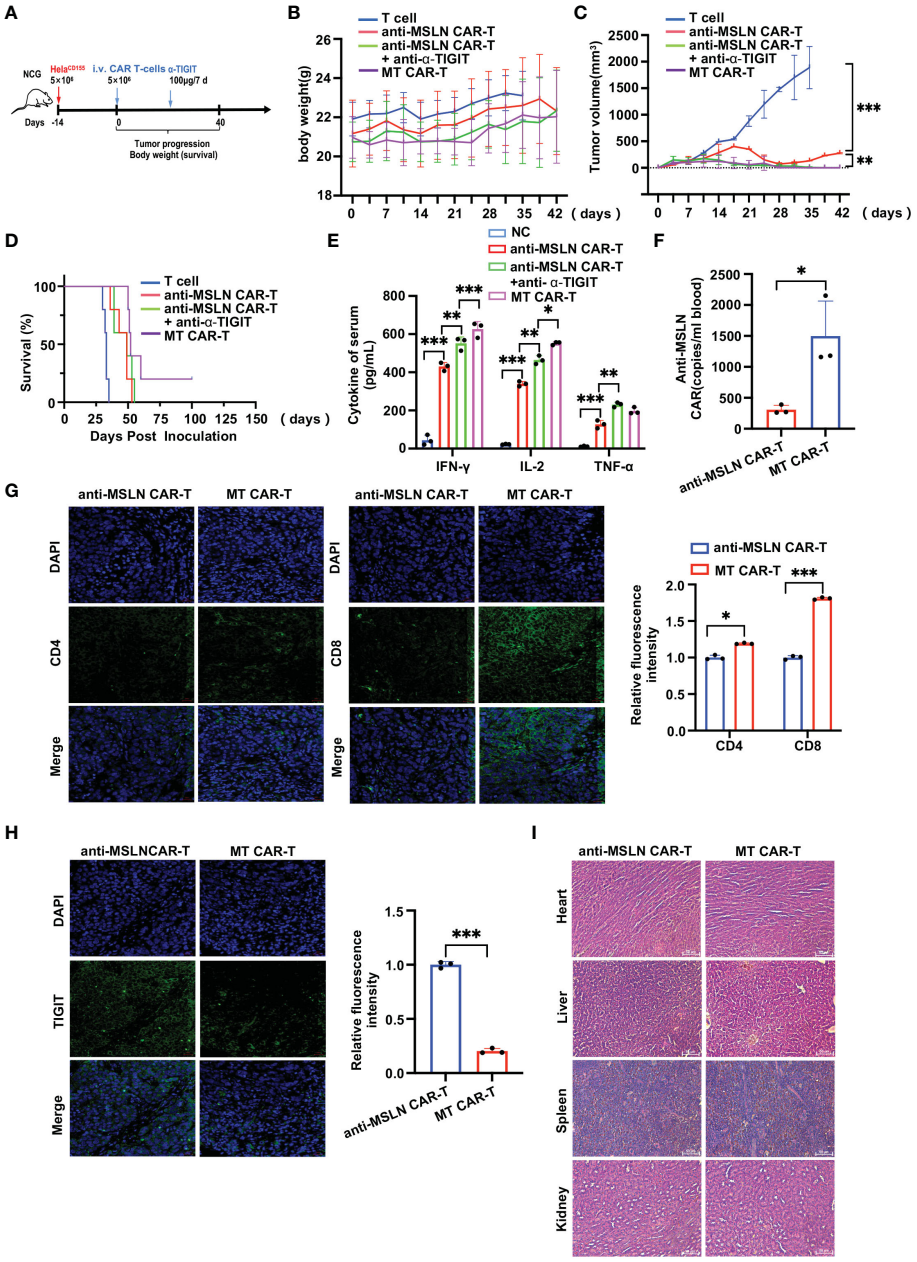

FIGURE 6
Self-delivery TIGIT-blocking scFv enhances anti-tumor effects of CAR-T cells *in vivo*. **(A)** Treatment scheme used in the Hela^{CD155} xenograft model treated with CAR-T cells and anti-α-TIGIT. B-NDG mice were treated with 5x10^6 CAR-T cells/mice and anti-α-TIGIT 100 μg/7d. **(B)** Mice body weights monitored during treatment. **(C)** Data showing the tumor volume (mm3) change trend of B-NDG mice in 4 different treat groups. **(D)** Kaplan-Meier survival curve was performed 100 days after Hela^{CD155} cells infused. Mice treated with MT CAR-T cells had a significantly longer survival probability in comparison with mice treated with control T cells, anti-MSLN CAR-T cells, anti-MSLN CAR-T cells+anti-α-TIGIT and MT CAR-T cells. **(E)** ELISA results showed the IFN-γ, IL-2, TNF-α secretion levels in mice blood treated by control T cells, anti-MSLN CAR-T cells, anti-MSLN CAR-T cells+anti-α-TIGIT and MT CAR-T cells. **(F)** Detection of anti-MSLN CAR expression in peripheral blood of mice. **(G)** MT and anti-MSLN CAR-T treated tumors were harvested 3 days post-treatment, subjected to IF analysis for CD4/CD8. Scale bar: 50 μm. **(H)** The TIGIT IF staining were performed in tumors from the resected Hela^{CD155} tumors after MT or anti-MSLN CAR-T cells treated. Representative images of staining intensity are shown. Scale bar, 50 μm. **(I)** MT cells or anti-MSLN CAR-T cells treatment without significant non-target organ damage. Scale: 50 μm. Data is represented as mean ± SD of at least three independent experiments. In all plots, *, $P < 0.05$; **, $P < 0.01$; ***, $P < 0.001$.

Discussion

CAR-T cell therapy is in full swing due to their rapid onset of action, high remission rates and long duration of remission compared to traditional biological drugs (29). In contrast, one of the main reasons for non-response or weak response to CAR-T cell therapy is poor T cell expansion and reduced sustained T cell killing capacity (30). Ineffective CAR-T treatment is due to immunosuppression of TME (31). The numerous immune inhibitory sites in the TME pose difficulties for tumor killing, making the combined use of immune checkpoint inhibitors of great interest. TIGIT, as an immune checkpoint, interacts with

CD155 expressed on the surface of tumor cells thereby inhibiting the $CD8^+$ T cells cytotoxicity in the TME (32). In this study, we demonstrated that blocking TIGIT significantly enhanced CAR-T therapy on solid tumor cells (Figure 7).

MSLN is highly expressed in mesothelioma, lung cancer, pancreatic cancer, breast cancer, ovarian cancer, and other cancers (12, 33, 34). Due to its differential expression between cancer and normal tissues and its role in tumorigenesis, MSLN can be considered a potential target. An increasing number of studies have shown that MSLN plays an important role in the promotion of tumorigenesis and progression, although its function in physiological situations is not yet clear (35). MSLN can promote tumor proliferation, metastasis, and resistance to chemotherapy (36). Since MSLN is a highly specific antigen in several cancers, CAR-T therapy has been shown to be a promising strategy for the treatment of these cancers. Here, we constructed anti-MSLN CAR-T cells that significantly induced target cell lysis of Hela and Skov3 cells. However, traditional CAR-T therapy is ineffective in treating solid tumors due to antigen escape, poor tumor infiltration, and immunosuppressive microenvironment (37). Therefore, achieving a broader therapeutic application of CAR-T cells requires a multi-level approach to improve efficacy and safety.

TIGIT acts as an immune checkpoint inhibitory protein that effectively suppresses both innate and adaptive immunity through a variety of mechanisms. It was shown that TIGIT is highly expressed in NK and T cells and associated with $CD8^+$ T cell infiltration (20). TIGIT can directly inhibit the functions of $CD8^+$ T cell and prevent the clearance of cancer cells (21). CD155 is barely expressed in various normal human tissues but is frequently overexpressed in human malignancies (38). When CD155 on the tumor surface binds to TIGIT on the surface of NK and T cells, it leads to immune escape of tumor cells and the anti-tumor effect is inhibited (39). In addition, TIGIT can further indirectly inhibit anti-tumor immunity by promoting T regulatory cell function of tumor-infiltrating lymphocytes and transmitting inhibitory signals through interaction with CD155 (24). In this study, based on previous studies, we confirmed that blocking TIGIT on the surface of CAR-T cells effectively increased cytokine release in CAR-T cells and enhanced the killing of target tumor cells. Moreover, we have modified the structure of the CAR-T cells to be able to produce TIGIT scFvs (MT CAR-T cells) to achieve the same effect of blocking TIGIT. It was found that MT CAR-T cells could exhibit significant toxicity against solid tumor cells and achieved tumor regression *in vivo*. The modification of CAR-T cells structure reduces the expenditure of treatment and enhances safety of treatment. However, there is a pressing need to continue to evaluate its safety and effectiveness in practical applications in the future.

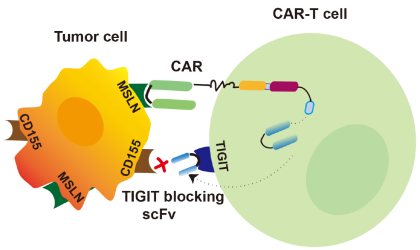

FIGURE 7
Diagram illustrating the augment of CAR-T cell therapy on tumors by blocking TIGIT. In the proposed model, secreted TIGIT-blocking scFv prevents the interaction of TIGIT on CAR-T cells with CD155 on tumor cells. CAR-T cells specifically recognize the tumor cell surface antigen MLSN to kill tumor cells. Blocking TIGIT enhances anti-tumor immunity of CAR-T cells.

In summary, this study focuses on the bottleneck of CAR-T cells in immunotherapy of solid tumors. Our study demonstrated that the TIGIT antibody effectively promoted cytokines release and enhanced the killing effects of anti-MSLN CAR-T cells on tumor cells. Moreover, self-delivery TIGIT-blocking scFvs augmented the infiltration and activation of CAR-T cells to enhance tumor regression *in vivo*. CAR-T cells armored for the expression of immunosuppressive protein scFvs may provide a promising strategy for advancing the application of CAR-T and checkpoint blockage therapies in solid tumors.

Data availability statement

The original contributions presented in the study are included in the article/Supplementary material. Further inquiries can be directed to the corresponding authors.

Ethics statement

The animal study was reviewed and approved by Animal Experiential Ethical Inspection form of Nanjing Normal University.

Author contributions

ZH, JL, and ZG designed the study. FY, FZ, FJ, and JC contributed to the analysis and interpretation of data. JL, ZC, and ZG contributed to the administrative, technical, or material support. FY, FZ, ZH, and ZG drafted the article. ZH and ZG were responsible for the critical revision. All authors contributed to the article and approved the submitted version.

Funding

This study was supported by the National Natural Science Foundation of China (81872284) and the Priority Academic Program Development of Jiangsu Higher Education Institutions.

Conflict of interest

Authors JL and ZC were employed by the company Nanjing Blue Shield Biotechnology Co., Ltd.

The remaining authors declare that the research was conducted in the absence of any commercial or financial relationships that could be construed as a potential conflict of interest.

Publisher's note

All claims expressed in this article are solely those of the authors and do not necessarily represent those of their affiliated organizations, or those of the publisher, the editors and the reviewers. Any product that may be evaluated in this article, or claim that may be made by its manufacturer, is not guaranteed or endorsed by the publisher.

Supplementary material

The Supplementary Material for this article can be found online at: https://www.frontiersin.org/articles/10.3389/fimmu.2023.1175920/full#supplementary-material

References

1. Maalej KM, Merhi M, Inchakalody VP, Mestiri S, Alam M, Maccalli C, et al. CAR-cell therapy in the era of solid tumor treatment: current challenges and emerging therapeutic advances. *Mol Cancer* (2023) 22(1):20. doi: 10.1186/s12943-023-01723-z

2. Zhao Z, Chen Y, Francisco NM, Zhang Y, Wu M. The application of CAR-T cell therapy in hematological malignancies: advantages and challenges. *Acta Pharm Sin B* (2018) 8(4):539–51. doi: 10.1016/j.apsb.2018.03.001

3. Abreu TR, Fonseca NA, Goncalves N, Moreira JN. Current challenges and emerging opportunities of CAR-T cell therapies. *J Control Release* (2020) 319:246–61. doi: 10.1016/j.jconrel.2019.12.047

4. Lesch S, Benmebarek MR, Cadilha BL, Stoiber S, Subklewe M, Endres S, et al. Determinants of response and resistance to CAR T cell therapy. *Semin Cancer Biol* (2020) 65:80–90. doi: 10.1016/j.semcancer.2019.11.004

5. Van de Donk N, Themeli M, Usmani SZ. Determinants of response and mechanisms of resistance of CAR T-cell therapy in multiple myeloma. *Blood Cancer Discovery* (2021) 2(4):302–18. doi: 10.1158/2643-3230.BCD-20-0227

6. Bagley SJ, O'Rourke DM. Clinical investigation of CAR T cells for solid tumors: lessons learned and future directions. *Pharmacol Ther* (2020) 205:107419. doi: 10.1016/j.pharmthera.2019.107419

7. Hong M, Clubb JD, Chen YY. Engineering CAR-T cells for next-generation cancer therapy. *Cancer Cell* (2020) 38(4):473–88. doi: 10.1016/j.ccell.2020.07.005

8. Martinez M, Moon EK. Car T cells for solid tumors: new strategies for finding, infiltrating, and surviving in the tumor microenvironment. *Front Immunol* (2019) 10:128. doi: 10.3389/fimmu.2019.00128

9. Marin-Acevedo JA, Kimbrough EO, Lou Y. Next generation of immune checkpoint inhibitors and beyond. *J Hematol Oncol* (2021) 14(1):45. doi: 10.1186/s13045-021-01056-8

10. Ji F, Zhang F, Zhang M, Long K, Xia M, Lu F, et al. Targeting the DNA damage response enhances CD70 CAR-T cell therapy for renal carcinoma by activating the CGAS-STING pathway. *J Hematol Oncol* (2021) 14(1):152. doi: 10.1186/s13045-021-01168-1

11. Carlino MS, Larkin J, Long GV. Immune checkpoint inhibitors in melanoma. *Lancet* (2021) 398(10304):1002–14. doi: 10.1016/S0140-6736(21)01206-X

12. Chen J, Hu J, Gu L, Ji F, Zhang F, Zhang M, et al. Anti-mesothelin CAR-T immunotherapy in patients with ovarian cancer. *Cancer Immunol Immunother* (2023) 72(2):409–25. doi: 10.1007/s00262-022-03238-w

13. Morello A, Sadelain M, Adusumilli PS. Mesothelin-targeted cars: driving T cells to solid tumors. *Cancer Discovery* (2016) 6(2):133–46. doi: 10.1158/2159-8290.CD-15-0583

14. Beatty GL, O'Hara MH, Lacey SF, Torigian DA, Nazimuddin F, Chen F, et al. Activity of mesothelin-specific chimeric antigen receptor T cells against pancreatic carcinoma metastases in a phase 1 trial. *Gastroenterology* (2018) 155(1):29–32. doi: 10.1053/j.gastro.2018.03.029

15. Schoutrop E, El-Serafi I, Poiret T, Zhao Y, Gultekin O, He R, et al. Mesothelin-specific CAR T cells target ovarian cancer. *Cancer Res* (2021) 81(11):3022–35. doi: 10.1158/0008-5472.CAN-20-2701

16. Tchou J, Wang LC, Selven B, Zhang H, Conejo-Garcia J, Borghaei H, et al. Mesothelin, a novel immunotherapy target for triple negative breast cancer. *Breast Cancer Res Treat* (2012) 133(2):799–804. doi: 10.1007/s10549-012-2018-4

17. Luo L, Zhou X, Zhou L, Liang Z, Yang J, Tu S, et al. Current state of CAR-T therapy for T-cell malignancies. *Ther Adv Hematol* (2022) 13:20406207221143025. doi: 10.1177/20406207221143025

18. Vivekanandhan S, Bahr D, Kothari A, Ashary MA, Baksh M, Gabriel E. Immunotherapies in rare cancers. *Mol Cancer* (2023) 22(1):23. doi: 10.1186/s12943-023-01720-2

19. Stanietsky N, Simic H, Arapovic J, Toporik A, Levy O, Novik A, et al. The interaction of TIGIT with PVR and PVR2 inhibits human NK cell cytotoxicity. *Proc Natl Acad Sci U.S.A.* (2009) 106(42):17858–63. doi: 10.1073/pnas.0903474106

20. Johnston RJ, Comps-Agrar L, Hackney J, Yu X, Huseni M, Yang Y, et al. The immunoreceptor tigit regulates anti-tumor and antiviral CD8(+) T cell effector function. *Cancer Cell* (2014) 26(6):923–37. doi: 10.1016/j.ccell.2014.10.018

21. Zhang Q, Bi J, Zheng X, Chen Y, Wang H, Wu W, et al. Blockade of the checkpoint receptor TIGIT prevents NK cell exhaustion and elicits potent anti-tumor immunity. *Nat Immunol* (2018) 19(7):723–32. doi: 10.1038/s41590-018-0132-0

22. Chiang EY, Mellman I. TIGIT-CD226-PVR axis: advancing immune checkpoint blockade for cancer immunotherapy. *J For Immunother Cancer* (2022) 10(4):e004711. doi: 10.1136/jitc-2022-004711

23. Freed-Pastor WA, Lambert LJ, Ely ZA, Pattada NB, Bhutkar A, Eng G, et al. The CD155/TIGIT axis promotes and maintains immune evasion in neoantigen-expressing pancreatic cancer. *Cancer Cell* (2021) 39(10):1342–60 e14. doi: 10.1016/j.ccell.2021.07.007

24. Liu L, Wang Y, Geng C, Wang A, Han S, You X, et al. CD155 promotes the progression of cervical cancer cells through Akt/MTOR and nf-Kb pathways. *Front In Oncol* (2021) 11:655302. doi: 10.3389/fonc.2021.655302

25. He W, Zhang H, Han F, Chen X, Lin R, Wang W, et al. CD155/TIGIT signaling regulates CD8(+) T-cell metabolism and promotes tumor progression in human gastric cancer. *Cancer Res* (2017) 77(22):6375–88. doi: 10.1158/0008-5472.CAN-17-0381

26. Hansen K, Kumar S, Logronio K, Whelan S, Qurashi S, Cheng H-Y, et al. Com902, a novel therapeutic antibody targeting tigit augments anti-tumor T cell function in combination with pvrig or PD-1 pathway blockade. *Cancer Immunol Immunother* (2021) 70(12):3525–40. doi: 10.1007/s00262-021-02921-8

27. Niu J, Maurice-Dror C, Lee DH, Kim DW, Nagrial A, Voskoboynik M, et al. First-in-Human phase 1 study of the anti-TIGIT antibody vibostolimab as monotherapy or with pembrolizumab for advanced solid tumors, including non-Small-Cell lung cancer☆. *Ann Oncol* (2022) 33(2):169–80. doi: 10.1016/j.annonc.2021.11.002

28. An anti-TIGIT antibody with a PD-1 inhibitor shows promise in solid tumors. *Cancer Discovery* (2022) 12(1):14. doi: 10.1158/2159-8290.CD-RW2021-170

29. Brog RA, Ferry SL, Schiebout CT, Messier CM, Cook WJ, Abdullah L, et al. Superkine IL-2 and IL-33 armored CAR T cells reshape the tumor microenvironment and reduce growth of multiple solid tumors. *Cancer Immunol Res* (2022) 10(8):962–77. doi: 10.1158/2326-6066.CIR-21-0536

30. Yang P, Meng M, Zhou Q. Oncogenic Cancer/Testis antigens are a hallmarker of cancer and a sensible target for cancer immunotherapy. *Biochim Biophys Acta Rev Cancer* (2021) 1876(1):188558. doi: 10.1016/j.bbcan.2021.188558

31. Tiwari A, Trivedi R, Lin S-Y. Tumor microenvironment: barrier or opportunity towards effective cancer therapy. *J BioMed Sci* (2022) 29(1):83. doi: 10.1186/s12929-022-00866-3

32. Chauvin J-M, Pagliano O, Fourcade J, Sun Z, Wang H, Sander C, et al. TIGIT and PD-1 impair tumor antigen-specific $CD8^+$ T cells in melanoma patients. *J Clin Invest* (2015) 125(5):2046–58. doi: 10.1172/JCI80445

33. Zeng W, Pan J, Fang Z, Jia J, Zhang R, He M, et al. A novel PD-L1-Containing MSLN targeting vaccine for lung cancer immunotherapy. *Front Immunol* (2022) 13:925217. doi: 10.3389/fimmu.2022.925217

34. Stromnes IM, Hulbert A, Rollins MR, Basom RS, Delrow J, Bonson P, et al. Insufficiency of compound immune checkpoint blockade to overcome engineered T cell exhaustion in pancreatic cancer. *J Immunother Cancer* (2022) 10(2):e003525. doi: 10.1136/jitc-2021-003525

35. Schoutrop E, Poiret T, El-Serafi I, Zhao Y, He R, Moter A, et al. Tuned activation of MSLN-CAR T cells induces superior anti-tumor responses in ovarian cancer models. *J Immunother Cancer* (2023) 11(2):e005691. doi: 10.1136/jitc-2022-005691

36. Li Y, Tian W, Zhang H, Zhang Z, Zhao Q, Chang L, et al. MSLN correlates with immune infiltration and chemoresistance as a prognostic biomarker in ovarian cancer. *Front Oncol* (2022) 12:830570. doi: 10.3389/fonc.2022.830570

37. Zhang C, Wang Y, Xun X, Wang S, Xiang X, Hu S, et al. TIGIT can exert immunosuppressive effects on $CD8^+$ T cells by the CD155/TIGIT signaling pathway for hepatocellular carcinoma in vitro. *J Immunother (Hagerstown Md: 1997)* (2020) 43 (8):236–43. doi: 10.1097/CJI.0000000000000330

38. Li X-Y, Das I, Lepletier A, Addala V, Bald T, Stannard K, et al. CD155 loss enhances tumor suppression *Via* combined host and tumor-intrinsic mechanisms. *J Clin Invest* (2022) 132(6):e159825. doi: 10.1172/JCI159825

39. Ozmadenci D, Shankara Narayanan JS, Andrew J, Ojalill M, Barrie AM, Jiang S, et al. Tumor fak orchestrates immunosuppression in ovarian cancer *Via* the CD155/TIGIT axis. *Proc Natl Acad Sci U.S.A.* (2022) 119(17):e2117065119. doi: 10.1073/pnas.2117065119

frontiers | Frontiers in Oncology

TYPE Case Report
PUBLISHED 10 August 2023
DOI 10.3389/fonc.2023.1217714

Check for updates

OPEN ACCESS

EDITED BY
Binod Dhakal,
Medical College of Wisconsin,
United States

REVIEWED BY
Frits Van Rhee,
University of Arkansas for Medical Sciences,
United States
Joselle Cook,
Mayo Clinic, United States

*CORRESPONDENCE
Javier Nogués-Castell
nogues@clinic.cat

RECEIVED 05 May 2023
ACCEPTED 14 July 2023
PUBLISHED 10 August 2023

CITATION
Nogués-Castell J, Feu-Basilio S, Felguera García Ó, Fernández de Larrea C, Oliver-Caldés A, Balagué Ponz O and Fassi JM (2023) Bilateral orbital plasmacytomas as first sign of extramedullary progression post CAR-T therapy: case report and literature review. *Front. Oncol.* 13:1217714. doi: 10.3389/fonc.2023.1217714

COPYRIGHT
© 2023 Nogués-Castell, Feu-Basilio, Felguera García, Fernández de Larrea, Oliver-Caldés, Balagué Ponz and Fassi. This is an open-access article distributed under the terms of the Creative Commons Attribution License (CC BY). The use, distribution or reproduction in other forums is permitted, provided the original author(s) and the copyright owner(s) are credited and that the original publication in this journal is cited, in accordance with accepted academic practice. No use, distribution or reproduction is permitted which does not comply with these terms.

Bilateral orbital plasmacytomas as first sign of extramedullary progression post CAR-T therapy: case report and literature review

Javier Nogués-Castell[1,2*], Silvia Feu-Basilio[1,2], Óscar Felguera García[1,2], Carlos Fernández de Larrea[2,3], Aina Oliver-Caldés[2,3], Olga Balagué Ponz[2,4] and Jessica Matas Fassi[1,2]

[1]Institut Clínic d'Oftalmologia, Hospital Clínic de Barcelona, Universitat de Barcelona, Barcelona, Spain, [2]Institut D' Investigacions Biomèdiques August Pi i Sunyer (IDIBAPS), Fundació Clínic per a la Recerca Biomèdica (FCRB), Universitat de Barcelona, Barcelona, Spain, [3]Amyloidosis and Myeloma Unit, Department of Hematology, Hospital Clínic de Barcelona, Universitat de Barcelona, Barcelona, Spain, [4]Centre de Diagnòstic Biomèdic, Hospital Clínic de Barcelona, Universitat de Barcelona, Barcelona, Spain

Background: Plasma cell leukemia (PCL) is an aggressive and rare form of plasma cell dyscrasia characterized by peripheral blood expression, poor prognosis, and high relapse rates. Extramedullary plasmacytomas are common in this entity and can affect various organs and soft tissues. Chimeric antigen receptor–T-cell (CAR-T) therapy is a novel immunotherapy for hematological malignancies with promising results. However, it is not indicated for PCL, and experience in this condition is limited. This case is a rare presentation of bilateral orbital plasmacytomas after CAR-T therapy in a patient with PCL history.

Case presentation: We present the case of a 51-year-old female patient with a history of previous primary PCL treated with CAR-T therapy achieving complete response and without evidence of systemic progression. Six months after the treatment, she developed subacute proptosis and ptosis on the left eye. An orbital CT scan was performed and showed an orbital tumor in both eyes. A surgical biopsy with histological examination revealed plasma cells, consistent with a plasmacytoma. PET-CT and MRI confirmed the presence of tumors in both orbits. The patient was treated with dexamethasone and chemotherapy along with palliative radiation therapy to the left orbit which had a good response.

Conclusion: Orbital involvement in multiple myeloma and PCL is rare, with plasmacytomas being more common in other parts of the body. In this report, we present a case of a patient with PCL history, treated with multiple therapeutic lines including CAR-T therapy, who presented bilateral orbital plasmacytomas as the first sign of extramedullary progression after the treatment. This case should be considered by specialist to be aware that the orbits are a possible location of extramedullary progression.

KEYWORDS

plasma cells leukemia, chimeric antigen receptor therapy, CAR-T, orbital plasmacytoma, orbital multiple myeloma

1 Introduction

Plasma cell leukemia (PCL) is a rare form of plasma cell dyscrasia and the most aggressive form of the human monoclonal gammopathies. Previous studies have reported an incidence rate of PCL between 2% and 4% of patients with multiple myeloma (MM) (1–4). Recent European studies from the HAEMCARE project found a crude incidence of PCL in the European population of 0.4 per million, accounting for approximately 0.5% of MM cases (5).

PCL diagnosis criteria have been recently redefined from 20% plasma cells in peripheral blood leukocytes or an absolute plasma cell count of $\geq 2 \times 10^9$/L to the presence of more than 5% plasma cells in peripheral blood leukocytes or an absolute plasma cell count of $\geq 0.5 \times 10^9$/L (6). Studies from the International Myeloma Working Group (IMWG) have shown that the presence of peripheral blood cells leads to more aggressive MM, and the presence of ≥5% circulating plasma cells in patients with MM has an adverse prognostic value similar to the patients with higher percentage rates (7, 8). Thus, the incidence of PCL has shown an increase between 0.7% and 2.5%, being the latter from a multicenter Catalan series (7, 8).

The clinical presentation of PCL is usually aggressive and develops from a fast and furious tumor burden, with deep cytopenia and a high rate of extramedullary involvement. The most common locations of extramedullary involvement in PCL are the liver, spleen, lymph nodes, lungs, central nervous system (CNS) or soft tissue plasmacytomas (3). Unlike MM, PCL rarely presents with osteolysis (3). Given the very high rate of extramedullary disease, the IMWG has suggested that fluorodeoxyglucose (FDG)–PET/CT should be considered in the diagnosis, evaluation, and monitoring of PCL (9). Survival of patients with PCL is short due to resistance to therapy, despite receiving multiple lines (6). Treatment of PCL typically includes induction combination regimens with immunomodulatory drugs and proteasome inhibitors followed by autologous hematopoietic stem cell transplantation (ASCT) and post-ASCT multidrug maintenance therapy with novel agents. Allogeneic stem cell transplantation (alloSCT) has also been also performed in these patients to improve survival rates (10).

Plasmacytomas are soft tissue neoplasms formed by a monoclonal plasma cell and may be associated with MM or PCL (11). Orbital plasmacytomas are extremely rare, accounting for only 1% of orbital tumors (12, 13). They may occur in association with plasma cell dyscrasias or isolated, although 50% of isolated plasmacytomas progress to MM within a year. Orbital Plasmacytomas may be the first manifestation of a systemic disease and the first sign of relapse (12–15).

The most common presenting sign of orbital plasmacytomas is proptosis. Reduced visual acuity, oedema, and diplopia are also commonly reported. In MM, they tend to be unilateral and have a slow progression. The most commonly affected quadrant is the superior-temporal (14). Plasmacytomas in MM have usually good response to radiotherapy (4, 14).

2 Case presentation

We present a 51-year-old woman who consulted the ophthalmology emergency department with proptosis on the left eye, oedema, and superior palpebral induration of one week duration (Figure 1A). Medical relevant history included a breast cancer in 2012 treated surgically and with tamoxifen until 2015, and she had a prothrombin 20210A mutation and was diagnosed in 2015 of PCL for which she received multiple therapy lines, as detailed in Table 1. Ophthalmologically, she had a history of dry eye due to graft-versus-host disease (GVHD).

The patient was diagnosed of primary PCL in a different center in August 2015. The initial presentation was of a severe pneumonia with bad evolution due to cytopenia. The laboratory test made at the moment of presentation manifested leucocytosis with a high number of circulating atypic plasma cells (49%). The patient also showed proteinuria, high blood levels of B2-microglobulins, and presence of light chains in serum. Examination of the marrow bone showed more than 69% plasma cell invasion. A PET-CT scan was run without signs of extramedullary disease. The plasma cells karyotype showed structural and numeric alterations including 1q trisomy and chromosome 13 monosomy, conclusive of a bad prognosis. The patient was diagnosed of IgG-lambda isotype primary PCL with no signs of extramedullary involvement. She received several lines of treatment, including alloSCT, as described in Table 1. Thus, 6 months prior to the ophthalmology emergency room consultation, she was treated with ARI0002h, an academic chimeric antigen receptor (CAR)–T-cell (CAR-T) therapy against BCMA (TNFRSF17) as a compassionate use.

Before CAR-T administration, patient had extramedullary affection in the form the hepatic hilum plasmacytomas with severe hepatic compromise, proteinuria, and high IgG levels in serum. However, marrow bone examination before treatment only showed 1% of plasma cells. After CAR-T administration, complete remission was achieved, with good clinical response and no evidence of disease in peripheral blood, as well as bone marrow examination and radiological stability in PET-CT imaging.

Ophthalmic examination revealed a visual acuity of 80/80 in both eyes. Extraocular and intraocular movements were intact, and she denied diplopia or pain. Orbital palpation revealed a mass in the temporal superior quadrant. Intraocular pressure was within normal limits in both eyes. Orbital CT scan revealed an orbital mass in the superior-temporal quadrant. Because of the presentation and history of breast cancer and PCL, the first suspected diagnosis was of a malignant tumor. A surgical biopsy

Abbreviations: PCL, plasma cell leukemia; CAR-T therapy chimeric antigen receptor–T-cell therapy; CAR, chimeric antigen receptor; RT, radiotherapy; MM, multiple myeloma; IMWG, international Myeloma Working Group; CNS, central nervous system; FDG, fluorodeoxyglucose; ASCT, autologous stem cell transplant; AlloSCT, allogeneic stem cell transplant; VTD-PACE, bortezomib, thalidomide, and dexamethasone–cisplatin, doxorubicin, cyclophosphamide, and etoposide; GVHD, chronic graft-versus-host disease; KRD, carfilzomib, lenalidomide, and dexamethasone; VCD, bortezomib, cyclophosphamide, and dexamethasone; PoCyDex, pomalidomide, cyclophosphamide, and dexamethasone; IOP, intraocular pression; GVL, graft versus leukemia.

10.3389/fonc.2023.1217714

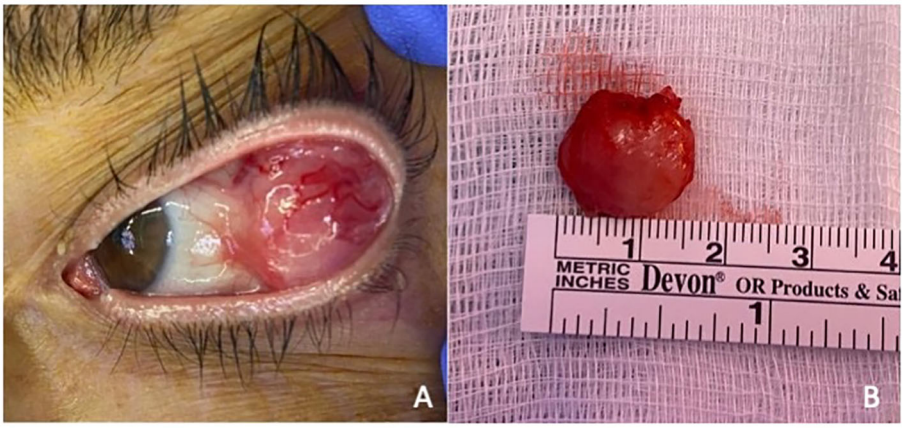

FIGURE 1
(A) Orbital tumor presentation. Orbital mass in the left eye presenting subconjunctival extension and no evidence of adherence to the globe or eyelids. **(B)** Surgical biopsy of the left orbital mass. Macroscopic view of the excised red colored mass measuring 16 mm × 14 mm × 12 mm with an elastic consistency.

of the lesion was performed through superior-temporal conjunctival incision (Figure 1B). The pathology analysis revealed a plasma cell dyscrasia with light-chain lambda restriction and a high proliferative index. All findings were consistent with a diagnosis of plasmacytoma, suggestive of extramedullary progression (Figure 2).

Body PET-CT scan and orbital MRI were performed after the pathology results to exclude other tumor lesions, evidencing an orbital mass in the right orbit without any other signs of activity in other organs (Figure 3). Blood and urine analysis revealed the presence of monoclonal lambda chains (65.00 U/mg/L) and an elevated b2 microglobuline level. Plasma cell count in peripheral blood samples showed no evidence of plasma cells in the smear. Marrow bone analysis performed after the biopsy results showed 1% plasma cells. Hematologists initiated a palliative treatment due to plasmacytoma rapid progression with steroids and chemotherapy. Radiation therapy of 20 Gy in 10 fractions was administered to the right orbit with a good radiological and clinical response.

Two weeks after the surgery on the left eye, the orbital and ocular examinations revealed residual hyperemia and fibrosis at the surgical site. Four months later, there was a clinical plasmacytoma recurrence of the left orbit with proptosis and a palpable extraocular mass in the superior- temporal quadrant. A local radiotherapy at 16 Gy in 4 fractions was performed with both clinical and radiological resolution. Blood tests were repeated periodically showing a progressive increase in lambda chain count of more than a hundred times in the following 3 months (1,590.00 U/mg/L). CT scans were run periodically after the relapse, showing signs of extramedullary progression in the mesenterial affecting the intrahepatic biliary duct and the right cardiophrenic fat with pleural involvement. Six months after the orbital plasmacytoma biopsy, the patient suffered from ascites. The ascitic cytology analysis showed plasma cell infiltration. Because of extramedullary progression and sepsis, palliative measures were provided.

3 Treatment timeline

TABLE 1 Lines of treatment in the patient.

Line	Treatment	Date	Treatment-related complications
First line	VTD-PACE × 4 (bortezomib, thalidomide, and dexamethasone–cisplatin, doxorubicin, cyclophosphamide, and etoposide) with a very good partial response (VGPR); allogeneic stem cell transplantation	2016	Chronic graft-versus-host disease (GVHD)
Second line	KRD (carfilzomib, lenalidomide, and dexamethasone) and local radiotherapy to extramedullary plasmacytomas in liver and bones	2017	GVHD reactivation
Third line	Daratumumab monotherapy	2017	-
Fourth line	VCD (bortezomib, cyclophosphamide, and dexamethasone)	2017	Peripheral neuropathy
Fifth line	PoCyDex (pomalidomide, cyclophosphamide, and dexamethasone) × 25 cycles every 28 days: complete remission	2018	-
Sixth line	CAR-T against BCMA (ARI0002h) with compassionate use; previous lymphodepletion regimen with cyclophosphamide and fludarabine	2021	–
Eighth line	Local radiotherapy + cyclophosphamide, C carfilzomib, and prednisone	February 2022	–
Ninth line	Cyclophosphamide + local radiotherapy	May 2022	–

10.3389/fonc.2023.1217714

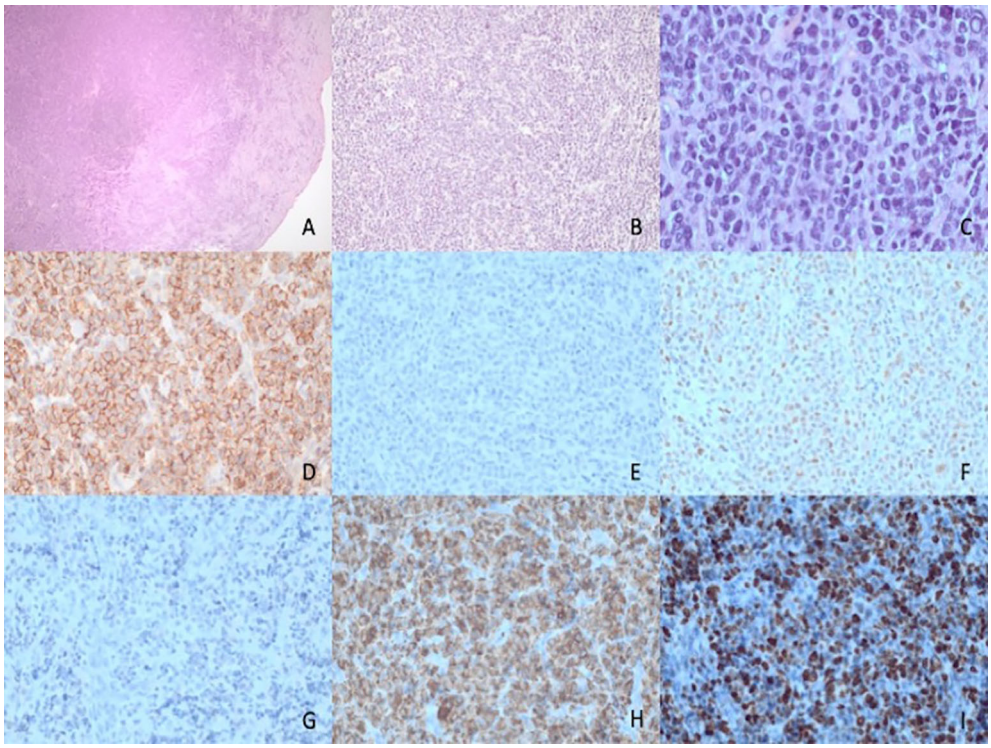

FIGURE 2
Histopathological features of plasma cell neoplasm with pleomorphic features. **(A–C)** Histopathological features showing a dense subepithelial infiltrate **(A)** of a medium-sized cells with diffuse distribution. **(B)** At higher magnification, **(C)** the tumor cells show plasma cell differentiation with Dutcher bodies but a higher level of pleomorphism than expected for a mature plasma cell proliferation. **(D)** Positive staining for CD138 and negative staining for CD20 **(E)** with partial positivity for cyclin D1 **(F)**. Staining for kappa **(G)** and lambda **(H)** shows lambda light-chain restriction. In addition, staining for KI67 **(I)** shows a proliferation index of around 70%, higher than expected for a mature plasma cell proliferation.

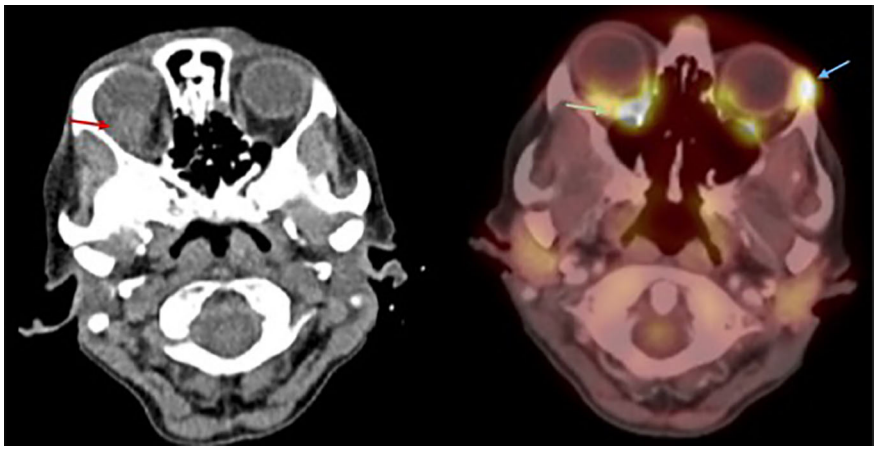

FIGURE 3
Axial MRI and PET-CT. Red arrow: Right orbital mass in the superior-temporal quadrant. Green arrow: Right orbital mass with increased FDG uptake. Blue arrow: Surgical bed after left orbital biopsy with high FDG uptake, possibly related to postsurgical inflammation.

4 Discussion and conclusions

Plasmacytomas can be classified as medullary, occurring only within the bone, or extramedullary, occurring in soft tissues. The latter may be paraskeletal (in contact with a bone) or due to hematogenous dissemination.

In 2009, Burkat et al. reviewed the existent literature and found that half of all documented cases of orbital plasmacytomas occurred

in patients who had already been diagnosed with MM (14). However, orbital involvement in PCL, as in the reported case, has been described in very few cases (16).

Our patient presented with proptosis and oedema on the left eye, with a mass in the superior-temporal quadrant. According to the literature, this is the most common form of presentation of orbital plasmacytoma, with proptosis being a common finding and the superior-temporal quadrant being the most common location, due to a rich blood supply that may favor metastasis. Reduced vision, swelling, and ptosis have also been frequently reported. Rarely, ecchymosis, cellulitis, and necrobiotic xanthogranuloma may be seen (14).

Orbital symptoms in orbital MM are typically insidious, with an average of 5 months from symptom onset to presentation (14). Bone involvement is also characteristic of MM. In contrast, our case presented with rapid growth and no bone involvement. Such a different clinical presentation could be due to the aggressive presentation of PCL compared with the insidious presentation of MM. Previous immunotherapies, including alloSCT and CAR-T cells, may have also affected the type of presentation.

Although orbital plasmacytomas are usually unilateral, bilateral manifestations, as in our case, have been reported (16–18). Orbital plasmacytomas have been described as the first manifestation of systemic disease and also as the first sign of relapse, like in our case (12–15). Some organs may act as sanctuaries, where graft-versus-leukemia (GVL) effect and chemotherapy cannot penetrate sufficiently (17). The eyes, testes, and CNS may act as such, with a lack of GVL effect. The orbit, with its direct relationship to CNS, is thought to have the same effect. Reports of isolated orbital relapse after alloSCT suggest a similar shielding effect in other diseases such as non-Hodgkin lymphoma (19, 20). Bilateral involvement as a form of relapse in our patient and the previously described cases may be explained by this theory.

In addition, orbital imaging is not easy to assess. In our case, CT and body PET-CT scans were performed after CAR-T therapy periodically to exclude any type of early systemic relapse, and no signs of orbital affection were detected by imaging before orbital presentation, with the latest PET-CT scan being performed only 20 days before. PET-CT can be misinterpreted in this area, as normal PET uptake can be seen at the apex and along the length of the extraocular muscles, masking tumors (21). Furthermore, body CT and PET-CT scans usually do not include orbital and CNS cuts if not asked specifically. Thus, orbital presentation can become a delayed diagnosis, so it is important for the radiologist to be highly trained in orbital imaging.

New treatments such as CAR-T therapy are being tested for plasma cells discrasias. CAR-T therapy consists in using genetically engineered autologous T cells that are programmed to bind specific antigens on target cells. Promising results have been reported in the treatment of some lymphomas, leukemia, and MM, but there are still few data on the response on PCL as is not indicated (4, 9, 22, 23).

Allogeneic transplantation is now rarely used in MM, especially in the first-line setting (24). However, because of the lack of long-term disease control with the therapeutic strategies used in recent years for primary PCL, the use of this immunotherapy in the first line has been proposed as a potential option in the last decade (9). More recently, several publications have shown that allogeneic transplantation may not be very useful compared with autologous transplantation, even in such aggressive disease. A tandem approach may still be useful in this setting. The early incorporation of advanced targeted immunotherapies, such as CAR-T cells and bispecific antibodies, should be explored in early lines for this disease.

Between 2020 and 2022, several new CAR-T therapies have emerged for both newly diagnosed MM and relapsed or refractive MM, and two have been approved in European Union although without reimbursement in Spain (25). ARI2000H is a second-generation lentiviral autologous CAR-T targeting BCMA with a 4-1BB and signal transduction CD3 co-stimulatory domain and a humanized single-chain variable fragment. ARI2000H has shown potency *in vitro* and *in vivo* activity in preclinical studies and has demonstrated an excellent feasibility in a clinical trial with deep and durable responses and a promising safety profile (26). Compassionate use of ARI2000H is ongoing (26).

The efficacy of CAR-T therapy in extramedullary MM is still in under debate. Previous reports have shown that plasmacytomas may not respond to this therapies in patients with extramedullary disease (27).

This case is the first reported case of bilateral orbital plasmacytoma presentation in a patient with history of PCL after the use of any CAR-T. In the future, it would be of clinical interest to be aware of this orbital condition in patients treated with these novel therapies.

In conclusion, we present a case of bilateral orbital plasmacytoma as the first sign of myeloma relapse after CAR-T therapy. To our knowledge, it is the first case of PCL orbital involvement after this therapy described in the literature and one of the few described cases of bilateral orbital plasmacytomas in PCL; its rapid growth and lack of bone involvement differ from the orbital plasmacytomas seen in MM.

Bilateral orbital involvement of this unusual entity seems extremely rare, which might indicate an orbital predisposition. Therefore, the possibility of orbital affection should be known by specialist to detect it promptly. If, in the future, more cases of orbital affection are reported, then a comprehensive orbital examination in patients with this disease who have been treated with CAR-T therapy might have to be contemplated. This also highlights the importance of interdisciplinary collaboration in this setting.

Patient perspective

Unfortunately, due to the PCL progression the patient was deceased before publishing this article.

Ethics approval and consent to participate

Not applicable.

Ethics Statement

Written informed consent was obtained from the patients/participants for the publication of any potentially identifiable images or data included in this case study.

Author contributions

JNC participated in the case description, background research, and discussion. SFB, OFG and JMF reviewed the ophthalmological data and ensured the accuracy of the bibliography used. AOC and CFL reviewed the haematology data of the case and the final discussion. OBP provided the histopathological description. All authors read and approved the final version of the manuscript.

Funding

This work has been supported, in part, by grants from the Instituto de Salud Carlos III (ISCIII) and co-founded by the European Union (FIS PI22/00647 and ICI19/00025) and 2021SGR01292 (AGAUR; Generalitat de Catalunya).

Acknowledgments

We would like to thank the patient and her family for their cooperation.

Conflict of interest

The authors declare that the research was conducted in the absence of any commercial or financial relationships that could be construed as a potential conflict of interest.

Publisher's note

All claims expressed in this article are solely those of the authors and do not necessarily represent those of their affiliated organizations, or those of the publisher, the editors and the reviewers. Any product that may be evaluated in this article, or claim that may be made by its manufacturer, is not guaranteed or endorsed by the publisher.

References

1. Dimopoulos MA, Palumbo A, Delasalle KB, Alexanian R. Primary plasma cell leukaemia. *Br J Haematol* (1994) 88(4):754–9. doi: 10.1111/j.1365-2141.1994.tb05114.x

2. Tiedemann RE, Gonzalez-Paz N, Kyle R Santana-Davila RA, Price-Troska T, Van S, Wier, et al. Genetic aberrations and survival in plasma cell leukemia. *Mol Cell Biochem* (2012) 23(1):1–7. doi: 10.1038/leu.2008.4

3. Rojas EA, Gutiérrez NC. Genomics of plasma cell leukemia. *Cancers (Basel)* (2022) 14(6):1–13. doi: 10.3390/cancers14061594

4. Gundesen MT, Lund T, Moeller HEH, Abildgaard N. Plasma cell leukemia: definition, presentation, and treatment. *Curr Oncol Rep* (2019) 21(1):8. doi: 10.1007/s11912-019-0754-x

5. Sant M, Allemani C, Tereanu C, De Angelis R, Capocaccia R, Visser O, et al. Incidence of hematologic malignancies in Europe by morphologic subtype: Results of the HAEMACARE project. *Blood* (2010) 116(19):3724–34. doi: 10.1182/blood-2010-05-282632

6. Jung SH, Lee JJ. Update on primary plasma cell leukemia. *Blood Res* (2022) 57 (S1):62–6. doi: 10.5045/br.2022.2022033

7. Fernández de Larrea C, Kyle R, Rosiñol L, Paiva B, Engelhardt M, Usmani S, et al. Primary plasma cell leukemia: consensus definition by the International Myeloma Working Group according to peripheral blood plasma cell percentage. *Blood Cancer J* (2021) 11(12):1–5. doi: 10.1038/s41408-021-00587-0

8. Granell M, Calvo X, Garcia-Guiñón A, Escoda L, Abella E, Martínez CM, et al. Prognostic impact of circulating plasma cells in patients with multiple myeloma: Implications for plasma cell leukemia definition. *Haematologica* (2017) 102(6):1099–104. doi: 10.3324/haematol.2016.158303

9. Fernández de Larrea C, Kyle R, Durie BG, Ludwig H, Usmani S, Vesole D, et al. Plasma cell leukemia: consensus statement on diagnostic requirements, response criteria and treatment recommendations by the International Myeloma Working Group. *Leukemia* (2013) 16(1):2658–63. doi: 10.1038/leu.2012.336

10. Drake MB, Iacobelli S, van Biezen A, Morris C, Apperley JF, Niederwieser D, et al. Primary plasma cell leukemia and autologous stem cell transplantation. *Haematologica* (2010) 95(5):804–9. doi: 10.3324/haematol.2009.013334

11. Jiménez-Segura R, Rosiñol L, Cibeira MT, Fernández de Larrea C, Tovar N, Rodríguez-Lobato LG, et al. Paraskeletal and extramedullary plasmacytomas in multiple myeloma at diagnosis and at first relapse: 50-years of experience from an academic institution. *Blood Cancer J* (2022) 12(9):1–8. doi: 10.1148/rg.336135502

12. Adkins JW, Shields JA, Shields CL, Eagle RC, Flanagan JC, Campanella PC. Plasmacytoma of the eye and orbit. *Int Ophthalmol* (1997) 20(6):339–43. doi: 10.1007/BF00176888

13. Tailor TD, Gupta D, Dalley RW, Dirk Keene C, Anza Y. Orbital neoplasms in adults: Clinical, radiologic, and pathologic review. *Radiographics* (2013) 33(6):1739–58. doi: 10.1148/rg.336135502

14. Burkat CN, Van Buren JJ, Lucarelli MJ. Characteristics of orbital multiple myeloma: A case report and literature review. *Surv Ophthalmol* (2009) 54(6):697–704. doi: 10.1016/j.survophthal.2009.04.012

15. Eckardt AM, Lemound J, Rana M, Gellrich NC. Orbital lymphoma: Diagnostic approach and treatment outcome. *World J Surg Oncol* (2013) 11:73. doi: 10.1186/1477-7819-11-73

16. Rodriguez T, Bon V. Secondary extramedullary bilateral orbital plasmacytoma in a 65-year-old man. *J Fr Ophtalmol* (2019) 42(6):e267–9. doi: 10.1016/j.jfo.2018.11.016

17. Barmas-Alamdari D, Sodhi GS, Shenouda TA. Bilateral proptosis in a case of recurring multiple myeloma: Uncommon orbital presentation of plasmacytoma. *Int Med Case Rep J* (2020) 13:297–301. doi: 10.2147/IMCRJ.S260472

18. Pyon RE, Wang GC, Chu Y, Tulpule S. Bilateral orbital plasmacytomas with orbital compartment syndrome. *Cureus* (2022) 14(6):10–3. doi: 10.7759/cureus.26269

19. Kottler UB, Cursiefen C, Holbach LM. Orbital involvement in multiple myeloma: First sign of insufficient chemotherapy. *Ophthalmologica* (2003) 217 (1):76–8. doi: 10.1159/000068251

20. Lekos A, Glantz MJ. Diagnosis in oncology. *J Clin Oncol* (1997) 15(8):3019–20. doi: 10.1200/JCO.1997.15.8.3019

21. Zincirkeser S, Şahin E, Halac M, Sager S. Standardized uptake values of normal organs on 18F-fluorodeoxyglucose positron emission tomography and computed tomography imaging. *J Int Med Res* (2007) 35(2):231–6. doi: 10.1177/147323000703500207

22. Mikkilineni L, Kochenderfer JN. Chimeric antigen receptor T-cell therapies for multiple myeloma. *Blood* (2017) 130(24):2594–602. doi: 10.1182/blood-2017-06-793869

23. Li C, Cao W, Que Y, Wang Q, Xiao Y, Gu C, et al. A phase I study of anti-BCMA CAR T cell therapy in relapsed/refractory multiple myeloma and plasma cell leukemia. *Clin Transl Med* (2021) 11(3):e346. doi: 10.1002/ctm2.346

24. Passweg JR, Baldomero H, Ciceri F, Corbacioglu S, de la Cámara R, Dolstra H, et al. Hematopoietic cell transplantation and cellular therapies in Europe 2021. The second year of the SARS-CoV-2 pandemic. A Report from the EBMT Activity Survey. *Bone Marrow Transplant* (2023) 7:660. doi: 10.1038/s41409-023-01943-3

25. Wang Z, Chen C, Wang L, Jia Y, Qin Y. Chimeric antigen receptor T-cell therapy for multiple myeloma. *Front Immunol* (2022) 13(December):1–20. doi: 10.3389/fimmu.2022.1050522

26. Fernandez de Larrea C, Gonzalez-Calle V, Cabañas V, Oliver-Caldes A, Español-Rego M, Rodriguez-Otero P, et al. Results from a pilot study of ARI0002h, an academic BCMA-directed CAR-T cell therapy with fractionated initial infusion and booster dose in patients with relapsed and/or refractory multiple myeloma. *Blood* (2021) 138(Supplement 1):2837–7. doi: 10.1182/blood-2021-147188

27. Deng H, Liu M, Yuan T, Zhang H, Cui R, Li J, et al. Efficacy of humanized anti-BCMA CAR T cell therapy in relapsed/refractory multiple myeloma patients with and without extramedullary disease. *Front Immunol* (2021) 12(August):1–13. doi: 10.3389/fimmu.2021.720571

frontiers | Frontiers in Immunology

TYPE Original Research
PUBLISHED 13 March 2024
DOI 10.3389/fimmu.2024.1202017

Check for updates

OPEN ACCESS

EDITED BY
Sébastien Wälchli,
Oslo University Hospital, Norway

REVIEWED BY
Anand Rotte,
Arcellx Inc, United States
Britta Eiz-Vesper,
Hannover Medical School, Germany

*CORRESPONDENCE
Patricia Mercier-Letondal
patricia.letondal@efs.sante.fr

†These authors have contributed equally to this work and share last authorship

RECEIVED 07 April 2023
ACCEPTED 27 February 2024
PUBLISHED 13 March 2024

CITATION
Mercier-Letondal P, Kumar A, Marton C, Bonnefoy F, Fredon M, Boullerot L, Dehecq B, Adotévi O, Godet Y and Galaine J (2024) Characterization of atypical T cells generated during *ex vivo* expansion process for T cell-based adoptive immunotherapy. *Front. Immunol.* 15:1202017. doi: 10.3389/fimmu.2024.1202017

COPYRIGHT
© 2024 Mercier-Letondal, Kumar, Marton, Bonnefoy, Fredon, Boullerot, Dehecq, Adotévi, Godet and Galaine. This is an open-access article distributed under the terms of the Creative Commons Attribution License (CC BY). The use, distribution or reproduction in other forums is permitted, provided the original author(s) and the copyright owner(s) are credited and that the original publication in this journal is cited, in accordance with accepted academic practice. No use, distribution or reproduction is permitted which does not comply with these terms.

Characterization of atypical T cells generated during *ex vivo* expansion process for T cell-based adoptive immunotherapy

Patricia Mercier-Letondal[1]*, Abhishek Kumar[1], Chrystel Marton[2], Francis Bonnefoy[1], Maxime Fredon[1], Laura Boullerot[1], Barbara Dehecq[1], Olivier Adotévi[1,3], Yann Godet[1†] and Jeanne Galaine[1†]

[1]UMR 1098 RIGHT INSERM, Etablissement Français du Sang Bourgogne Franche-Comté, Université de Franche-Comté, Besançon, France, [2]Centre Hospitalier Universitaire de Lille, Service des Maladies du Sang, Lille, France, [3]Centre Hospitalier Universitaire de Besançon, Service D'oncologie Médicale, Besançon, France

Engineered T cell-based adoptive immunotherapies met promising success for the treatment of hematological malignancies. Nevertheless, major hurdles remain to be overcome regarding the management of relapses and the translation to solid tumor settings. Properties of T cell-based final product should be appropriately controlled to fine-tune the analysis of clinical trial results, to draw relevant conclusions, and finally to improve the efficacy of these immunotherapies. For this purpose, we addressed the existence of atypical T cell subsets and deciphered their phenotypic and functional features in an HPV16-E7 specific and MHC II-restricted transgenic-TCR-engineered T cell setting. To note, atypical T cell subsets include mismatched MHC/co-receptor CD8 or CD4 and miscommitted CD8+ or CD4+ T cells. We generated both mismatched and appropriately matched MHC II-restricted transgenic TCR on CD8 and CD4-expressing T cells, respectively. We established that CD4+ cultured T cells exhibited miscommitted phenotypic cytotoxic pattern and that both interleukin (IL)-2 or IL-7/IL-15 supplementation allowed for the development of this cytotoxic phenotype. Both CD4+ and CD8+ T cell subsets, transduced with HPV16-E7 specific transgenic TCR, demonstrated cytotoxic features after exposure to HPV-16 E7-derived antigen. Ultimately, the presence of such atypical T cells, either mismatched MHC II-restricted TCR/CD8+ T cells or cytotoxic CD4+ T cells, is likely to influence the fate of patient-infused T cell product and would need further investigation.

KEYWORDS

T cell-based adoptive cell immunotherapy, transgenic TCR T cells, CD8 and CD4 expression, MHC restriction, *ex vivo* T cell culture process, T cell function

Introduction

For the past decade, numerous breakthroughs in cancer therapy have occurred. Among them, the area of T cell-based Adoptive Cell Therapy (ACT) has particularly met promising success. Tumor-associated antigen (TAA) specific ACT includes *ex vivo* expanded Tumor Infiltrating Lymphocytes (TIL), or engineered-T cells such as Chimeric Antibody Receptor (CAR-T) and transgenic T Cell Receptor expressing T cells (TCR-T), both reprogrammed to target TAA (1).

TCR-T cells are engineered to express a TCR derived from a TAA-specific T cell clone (2) to target extra or intracellular antigens, in an MHC-dependent manner. The first encouraging clinical trial of TCR-T infusion was performed in 2008 in metastatic melanoma (3). To date, many clinical trials are ongoing in the field of TCR-T-based ACT (2, 4, 5) and some of them have already displayed promising clinical results in the case of, for instance, MAGE-A3 or NY-ESO-1 expressing cancers (6, 7) or high-risk Human Papillomavirus (HPV) related malignancies (8).

TCR-T are usually isolated from a T cell clone, either MHC I-restricted (TCR I) CD8+ T cells or MHC II-restricted (TCR II) CD4+ T cells, depending on whether a cytotoxic or a helper function is initially expected. The canonical role of CD8+ and CD4+ T cells is to eliminate pathogenic cells *via* cytotoxic mechanisms and to coordinate a specific immune global response, respectively. However, these roles can be blurred for non-conventional reprogrammed T cells. On the one hand, the TCR-T vector can integrate the CD8+ or CD4+ T cell genome, regardless of its MHC class I or II restrictions. Consequently, mismatched TCR-T I/CD4+ and TCR-T II/CD8+ engineered T cells can be generated at an expected similar level to matched TCR-T I/CD8+ or TCR-T II/CD4+ T cells. This MHC/co-receptor mismatch is likely to impact the functions of engineered TCR-T cells. On the other hand, standard IL-2 supplementation of culture medium during the stage of *ex vivo* expansion of engineered T cells is prone to induce cytotoxic (CTX) CD4+ T cells (9, 10).

Previously, atypical T cells, namely T cells that do not behave as usually expected according to matching and commitment-associated rules, have already been described in several physiological and pathological settings. Thus, regarding CD4+ and CD8+ T cells, it has been documented that naturally mismatched TCR-T I/CD4+ and TCR-T II/CD8+ can occur and both of them behave mainly like classical CTX CD8+ T cells (11–15). This mismatched T cell generation has also previously been reported in transgenic contexts, along with CD8+ T cell-associated characteristics (16–24). Moreover, irrespective of defined canonical functions, miscommitted T cells (*i.e.* T cells exhibiting a different role than the canonical one) have already been described. Indeed, natural CD8+ T cells displaying helper features have been identified (25). Similarly, it has been reported more than 30 years ago that CD4+ T cells are able to mount an antigen-specific cytotoxic response in diverse infectious settings, as reviewed by Juno and colleagues (26). This characterization has been recently confirmed in the context of cancer antigen recognition (27). Oh & Fong (10) reviewed current knowledge on the topic and described a cytotoxic-associated CD4+ T cell phenotypic pattern.

Our team previously developed (17) an MHC II-restricted HPV-16 E7 TCR-T and demonstrated both CD8+ and CD4+ engineered-T cell specificity and functionality in terms of cytokine secretion after co-culture with relevant antigen-bearing target cells. Here, we aim to unravel cytotoxic features of mismatched TCR II/CD8+ along with matched TCR II/CD4+ transduced T cells, and thereafter focus on CD4 T cells to assess the role of *ex vivo* production process on CD4+ T cell cytotoxic polarization.

Materials and methods

Biological material

Peripheral blood mononuclear cells (PBMC) were collected from healthy donors at the Etablissement Français du Sang (EFS) as apheresis kit preparations after informed consent and according to the collection agreement AC-2020-4129. EBV-transformed B lymphoblastoid cell line (BLCL) was generated from an HLA-DRB1*04 healthy donor PBMC as previously described (28). The SKMEL-28 cell line, known to express HLA-DRB1*04 at its surface, was obtained from ATCC (HTB-72) and cultured according to manufacturer's instructions. Both cell lines were periodically checked for mycoplasma contamination. NOD/SCID IL-2R$\gamma^{-/-}$ (NSG) mice were bred in the animal facility of the University of Franche-Comté, according to the approved experimental project 2021-004-OA12PR.

Peptides

HPV16-E7$_{70\text{-}89}$ peptide (QSTHVDIRTLEDLLMGTLGI) was selected as previously described (17) and purchased from Proteogenix. Peptide purity is superior to 90%.

Retroviral vector

TCR α and β chains obtained from HPV16-E7-specific and HLA-DRB1*04-restricted CD4 T cell clones were introduced into a pSFG retroviral vector backbone, along with ΔCD19 selection and tracking marker, as previously described (17).

HPV-16 E7 encoding pLXSN plasmid was kindly supplied by Dr. A. Baguet (UMR RIGHT). The Neomycin resistance (NeoR) gene is included in the vector, as a selection gene.

T cell activation, retroviral transduction, selection, and expansion

Healthy donor T cells were magnetically isolated and activated by using CD3/CD28 microbeads (Fisher Scientific, 111.31D) according to manufacturer's instructions. Beads-attached T cells were cultured in RPMI-1640 medium (Fisher Scientific, 11544526) with 10% human serum (local production) in presence of 500 IU/

mL Interleukin (IL)-2 (Clinigen Healthcare BV, Proleukin®) or 350 IU/mL IL-7 (Miltenyi Biotec, 130-095-362) + 60 IU/mL IL-15 (Miltenyi Biotec, 130-095-762), according to specific experiment. The complete medium was renewed every 2-3 days until day 10 of culture. At day 2, activated and IL-2-cultured cells were transduced (GMTC) using HPV16-E7/HLA-DRB1*04-specific TCR retroviral supernatant, whose retroviral particles were trapped on RetroNectin® (Takara, T100B). At day 6, transduction efficiency was assessed through membrane staining with CD3 BV421 (BD Biosciences, 562426), and CD19 APC (Miltenyi Biotec, 130-113-165) antibodies, and analyzed by flow cytometry (FCM). Transduced T cells were then magnetically sorted using CD19 microbeads (Miltenyi Biotec, 130-050-301) following manufacturer's instructions. Sorting efficiency was performed through the same FCM analysis as transduction efficiency. At day 10, T cell bulk composition was evaluated *via* membrane staining with CD3 BV421, CD4 FITC (Diaclone, 954.031.010) and CD8 PE (Diaclone, 854.962.010) antibodies. An activated and untransduced cellular counterpart (UTC) from the same donor was also cultured for all experiments as a negative control of the anti-tumoral effect.

CD4+ and CD8+ T cells sorting

T cells were stained with CD4 FITC and CD8 PE antibodies according to manufacturer's instructions and resuspended in PBS 1X (Fisher Scientific, 11530546) 2mM EDTA. CD8+/CD4- and CD8-/CD4+ cells were further sorted using an FCM-based cell sorter (Sony, SH800) and cultured for four additional days in complete medium with 500 IU/mL IL-2. A sorted cell sample was set aside to assess enrichment efficacy through FCM analysis.

Phenotypic and functional assessment of cultured and engineered- T cells

Regarding IL-2 cultured TCR-T or UTC, the exhaustion-associated phenotype was evaluated through a staining with Fixable viability Dye (FvD) eFluor780 (Life Technologies, 65-0865-14), and CD3 FITC (BD Biosciences, 555332), CD8 BV510 (BD Biosciences, 563919), CD19 APC, anti-PD-1 PE-Cy7 (BD Biosciences, 561272), anti-TIM-3 PerCP-Cy5.5 (Sony, RT2325080), anti-TIGIT BV421 (BD Biosciences, 747844) antibodies and analyzed by FCM. CD8+ and CD4+ TCR-T cell exhaustion score was calculated as described by Chen et al. (29). Briefly, the formula is (where MFI is the mean fluorescence intensity):

$$\text{Exhaustion score} = (\text{MFI}^{\text{PD}-1}/\text{MFI}^{\text{CD19}} + \text{MFI}^{\text{TIM}-3}/\text{MFI}^{\text{CD19}} + \text{MFI}^{\text{TIGIT}}/\text{MFI}^{\text{CD19}})/3$$

The activation-related phenotype was assessed through a staining with FvD eFluor780, CD19 APC, CD3 BV421, CD8 BV510, CD25 FITC (Sony, RT2113020), CD69 APC-R700 (BD Biosciences, 565154) and anti-HLA-DR PE (BD Biosciences, 555561) antibodies before FCM analysis. CD4+ and CD8+ TCR-T cell activation score was obtained through the formula given by Chen et al. (29). Briefly, the formula is:

$$\text{Activation score} = (\text{MFI}^{\text{CD25}}/\text{MFI}^{\text{CD19}} + \text{MFI}^{\text{CD69}}/\text{MFI}^{\text{CD19}} + \text{MFI}^{\text{HLA DR}}/\text{MFI}^{\text{CD19}})/3$$

Transgenic TCR functionality was evaluated by co-culturing IL-2-exposed sorted CD4+ and CD8+ T cells, both transduced and untransduced, with HPV16-E7$_{70\text{-}89}$ peptide-pulsed (2µM) or unpulsed allogeneic HLA-DRB1*04 BLCL, at the effector:target (E:T) ratio of 1:1, as previously described (17). CD107a expression was assessed by adding Golgi Stop (BD Biosciences, 554724) and CD107a PE antibody (BD biosciences, 555801) simultaneously to cell culture during a 5-hour co-culture before staining with FvD eFluor780, CD3 BV421 and CD19 APC antibodies prior to FCM analysis. Cytotoxicity assay was performed after an overnight co-culture through CD3 BV421 and CD19 APC antibodies, Annexin-V FITC, and 7-AAD (Beckman Coulter, IM3614) cell staining. Additionally, peptide-pulsed or not and CFSE-stained target cell lysis was evaluated by a Trucount™ device (BD Bioscience, 340334) after an overnight co-culture with TCR-T cells or UTC (E:T ratio from 1:1 to 1:5).

The phenotype and functionality of resting PBMC-derived T cells and IL-2 or IL-7+IL-15 cultured UTC cells were assessed after a 5-hour stimulation with 25ng/mL PMA (Sigma-Aldrich, P8139) and 1.25µg/mL ionomycin (Sigma Aldrich, I0634) and treatment with Golgi Stop. CD107a expression was assessed after 5 hours through staining with CD107a PE-CF594 antibody (BD Biosciences, 562628) according to manufacturer instructions, before staining with FvD eFluor780, CD3 BV421, and CD4 FITC antibodies. Cytotoxicity-associated CD4+ T cell phenotype was evaluated after staining with FvD, CD3, CD4, CD8, CD137, CD134, anti-TRAIL, anti-FasL, anti-SLAMF7 antibodies, followed by intracellular staining with anti-Granzyme B and anti-Perforin, using a fixation and permeabilization kit (BD Biosciences, 550028); panel 1 and panel 2 are further described in Table 1.

Target cell line generation and mouse model design for *in vivo* CD4+ and CD8+ TCR-T cells functionality evaluation

SKMEL-28 cell line was checked for HLA-DR expression (HLA-DR PE). Its capacity to present HPV-16 E7$_{70\text{-}89}$ to TCR-T cells was assessed after pulsing SKMEL-28 cells with 2µM peptide and a co-culture with Golgi Plug-treated TCR-T cells, as well as UTC (18h, 37° C). IFN-γ secretion was assessed after membrane staining with FvD eFluor780, CD3 BV421, CD4 FITC, and CD8 PE antibodies followed by intracellular staining (BD Biosciences, 550028) with anti-IFN-γ APC antibody (BD Biosciences, 554702), and FCM analysis.

SKMEL-28 cells were transfected with HPV-16 E7 pLXSN encoding DNA plasmid vector using Lipofectamine™ LTX reagent (Thermo Fisher, A12621), selected during 3 weeks with 1mg/mL Geneticin (Thermo Fisher, 10092772) and evaluated for HPV-16 E7 expression through western blotting, as previously described (17).

Two million HPV-16 E7-expressing SKMEL-28 cells were subcutaneously injected into 8-week-old female NSG mice (Charles River, 614NSG) in the presence of Matrigel™ (Thermo Fisher, 11593620). Three to five mice per group were analyzed. After tumors developed in mice flank, $5*10^6$ sorted CD4+ and CD8+, or total unsorted TCR-T or UTC cells were intravenously injected. Ten µg HPV-16 $E7_{70-89}$ were injected at the tumor site 2 hours before T cell infusion to potentiate TCR-T cells-mediated immune response against HPV-16 E7-expressing tumor. A second TCR-T injection was performed 7 days after the first one, regarding all GMTC (*i.e.* IL-2-cultured and transduced cells) fractions and the total UTC control group. Tumor volume was monitored for 17 days according to the following formula before mice sacrifice and TCR-T cell tumor-infiltration evaluation (L and l mean tumor length and width, respectively):

$$\text{Tumor volume} = L \times l^2 \times \pi/6$$

Upon subsequent mice sacrifice, tumors were harvested and thereby disrupted using a Tumor Dissociation Kit (Miltenyi Biotec, 130-096-730), according to manufacturer instructions. FvD eFluor780, anti-human CD45 BV510 (Sony, RT2120180), anti-mouse CD45 PE-Cy7 (Sony, RT1115570), CD3 BV421, CD4 FITC, CD8 PE and anti-murine constant TCR β chain APC (BD Biosciences, 553174 – transgenic TCR construct contains a murine constant β chain to avoid TCR mispairing between the endogenous and the transgenic TCRs) antibodies were used along with Trucount™ tubes to stain tumor cell extract before FCM analysis.

Flow cytometry analysis

Appropriate isotypic controls were included in all staining designs.

Staining implying CD107a PE-CF594 antibody, as well as exhaustion, activation panels, and mice-injected TCR-T follow-up, were acquired on a BD FACS LSR Fortessa flow cytometer and analyzed through BD FACS Diva software (version 8.0).

Cytotoxic-associated CD4+T cells phenotypic evaluation panel 1 was assessed through a Beckman Coulter CytoFLEX LX flow Cytometer and analyzed through Kaluza software (version 2.1).

All additional stainings were acquired using a BD FACS CANTO II flow cytometer and analyzed with BD FACS Diva software (version 8.0).

Statistical analysis

Statistical analysis were performed through Graphpad Prism v9 software and consisted, as specifically mentioned in figure captions, of a one or two-tailed and paired or unpaired t-test. An Aspin Welch correction was applied in case of heterogeneous standard deviation between the compared groups. P-values< 0.05 were considered to be statistically significant. P-values between 0.05 and 0.1 were considered to be testifying to a trend towards statistical significance. P-values > 1 were considered to be statistically non-significant and are not mentioned.

Results

Post-*ex vivo* expansion and transduction T cell bulk composition

Gene-modified TCR-T along with untransduced control T cells exposed to IL-2 (Figure 1A) were evaluated for CD8+ and CD4+ T cell composition. The retroviral vector is likely to transduce both

TABLE 1 Antibody panels used for cytotoxic-associated CD4+ T cell phenotypic evaluation.

	Panel 1			Panel 2		
	Fluorochrome	Supplier	Reference	Fluorochrome	Supplier	Reference
FvD	Alexa Fluor 700	BD Biosciences	564997	eFluor780	Life Technologies	65-0865-14
CD3	APC-Cy7	Biolegend	300470	BV421	BD Biosciences	562426
CD4	BV510	BD Biosciences	562970	FITC	Diaclone	954.031.010
CD8	BV786	Biolegend	344740	ND	ND	ND
anti-SLAMF7	PE	Biolegend	331806	PE	Sony	RT2259030
anti-Granzyme B	PE-CF594	BD Biosciences	562462	BV510	BD Biosciences	563388
anti-perforin	Alexa Fluor 488	BD Biosciences	563764	ND	ND	ND
CD134 (OX40)	BV605	Biolegend	350028	ND	ND	ND
CD137 (4-1BB)	PE-Cy7	Biolegend	309818	ND	ND	ND
anti-TRAIL	BV650	BD Biosciences	743721	ND	ND	ND
anti-FasL	BV421	Biolegend	306411	ND	ND	ND

CD4+ and CD8+ T cells in a similar fashion (Figure 1B). Subsequent ΔCD19-based GMTC sorting allows for a high purity percentage of GMTC, with a mean of 97.88%+/-0.48 (SD) (Figure 1C). The final TCR-T cell product is thus constituted of both CD4+ and CD8+ T cells (Figure 1D).

Phenotypic characterization of CD4+ and CD8+ TCR-T cells

First, GMTC expansion capacities are lower than those of UTC ($p = 0.011$) (Figure 2A). GMTC and UTC CD4/CD8 ratios are 2.84 [0.96-4.85] and 2.20 [0.31-6.24], respectively (Figure 2B); this difference is not statistically significant. The phenotypic profile of activation evaluation does not show any differences between CD4+ and CD8+ T cells, either transduced or not, regarding CD25, CD69, and HLA-DR expression patterns (Figure 2C). Moreover, CD4+ and CD8+ GMTC activation scores are not statistically different (Figure 2D). CD8+ GMTC and UTC exhaustion phenotypes are similar in terms of PD-1+ TIM-3+ cell population (exhausted T cells, T_{EX}) or PD1+ TIM-3- TIGIT+ cell population (progenitor exhausted T cells, T_{PEX}). A trend to increase is revealed regarding CD4+ TCR-T_{PEX} compared to CD4+ UTC-T_{PEX} ($p=0.06$), but not CD4+ TCR-T_{EX} (Figure 2E). Exhaustion scores are similar for CD4+ and CD8+ TCR-T cells (Figure 2F).

In vitro cytotoxic capacity characterization of both CD8+ and CD4+ TCR-T II transduced T cells

CD4+ and CD8+ were sorted from TCR-T and untransduced T cells after expansion in the presence of IL-2. Sorting efficiency is high enough [97.95% (mean)+/-1.14 (SD) and 98%+/-1.93 for CD4+ and CD8+ GMTC, respectively] to ensure that further observed results are attributed to sorted T cell subsets (Figure 3A). CD107a degranulation marker expression on sorted gene-modified CD8+ T cells (Figure 3B) is significantly increased after HPV16-$E7_{70-89}$-pulsed BLCL co-culture when compared with either sorted unmodified CD8+ T cells or unpulsed BLCL co-culture experimental conditions ($p< 0.05$ and 0.01, respectively). A comparable upward trend is observed regarding CD107a expression by CD4+ T cells (Figure 3B), even if statistical significance at a 5% α risk is not fully achieved ($p = 0.059$ and 0.056 by comparing HPV16-$E7_{70-89}$-pulsed BLCL co-cultured gene-modified CD4+ T cells with unpulsed BLCL and untransduced CD4 + T cells experimental conditions, respectively).

Cytotoxicity-related data perfectly mirror CD107a expression (Figure 3C). Indeed, HPV16-$E7_{70-89}$ peptide-pulsed BLCL-specific target lysis is significantly higher after co-culture with transduced CD8+ T cells compared with unpulsed BLCL experimental conditions ($p< 0.05$). A similar strong trend is observed between

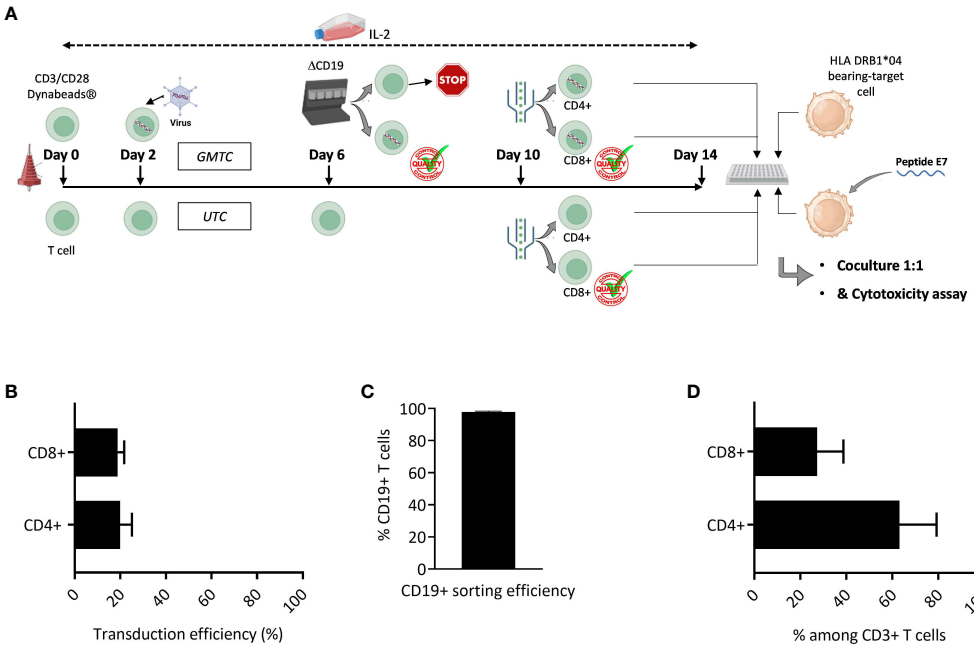

FIGURE 1
Final T cell bulk characterization. T cells are activated, cultured in the presence of IL-2, transduced with HPV16-E7/HLA-DRB1*04-specific TCR-T and selected on the basis of ΔCD19 expression. **(A)** Graphic representation of experiment design. Figure adapted from images created with BioRender.com. **(B)** CD4+ and CD8+ T cell transduction efficiency is evaluated through the expression of ΔCD19 selection gene among CD3+ CD4+ or CD3+ CD8+ T cells by flow cytometry; data represent mean+/-SD from 3 independent experiments; two-tailed paired t-test. **(C)** ΔCD19-based sorting efficiency; data represent mean+/-SD from 4 independent experiments. **(D)** CD4+ & CD8+ T cell percentage among T cell bulk is evaluated by the expression of CD4 and CD8 co-receptors among CD3+ T cells by flow cytometry; data represent mean+/-SD from 7 independent experiments.

10.3389/fimmu.2024.1202017

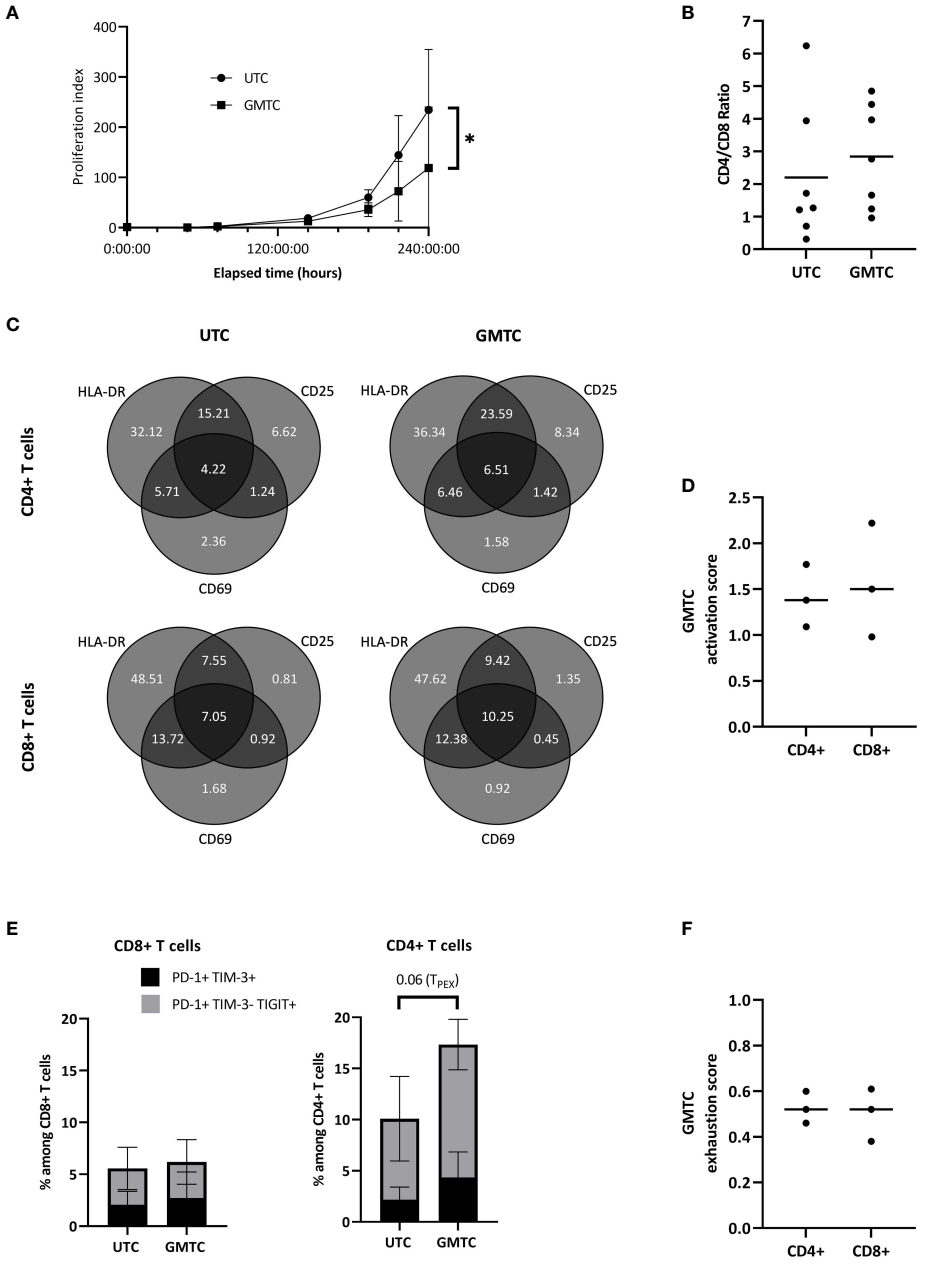

FIGURE 2
Phenotypic characterization of transduced CD8+ and CD4+ T cells. T cells are activated, cultured in the presence of IL-2, and transduced with HPV16-E7/HLA-DRB1*04-specific TCR-T. **(A)** Selected transduced (GMTC) and untransduced (UTC) T cells culture-related fold expansion; data represent mean+/-SD from 3 independent experiments; two-tailed paired t-test, *: p< 0.05. **(B)** Selected transduced and untransduced T cell CD4/CD8 ratio. Data represent individual values and mean from 7 independent experiments; two-tailed paired t-test. **(C)** Transduced and untransduced, CD4+ and CD8+, T cell activation pattern expression; data represent mean from 3 independent experiments; two-tailed paired t-tests for each subset. **(D)** Activation score of CD4+ and CD8+ TCR-T cells; data represents individual values and median from 3 independent experiments; two-tailed paired t-test. **(E)** Transduced and untransduced, CD4+ and CD8+, T cell exhaustion pattern expression; data represent mean+/-SD from 3 independent experiments; two-tailed paired t-test. **(F)** Exhaustion score of CD4+ and CD8+ TCR-T cells; data represents individual values and median from 3 independent experiments; two-tailed paired t-test.

transduced and untransduced CD8+ T cells (p= 0.06). Regarding CD4+ T cells, the differences observed after co-culture of either transduced T cells with peptide-pulsed or unpulsed target cells and transduced or untransduced T cells with peptide-pulsed target cells, are not statistically significant at a 5% α risk (p = 0.085 and 0.088, respectively). Nevertheless, the risk that these differences are only due to a random event is less than 9%. CD4+ TCR-T cells seem to exhibit less cytotoxic capacities than their CD8+ TCR-T counterparts, even if statistical significance is not fully achieved (p= 0.085).

Taken together, these results demonstrate that TCR-T II CD8+, and to a lesser extent CD4+, transduced T cells exhibit *in vitro* cytotoxic features toward cognate antigen-bearing target cells.

10.3389/fimmu.2024.1202017

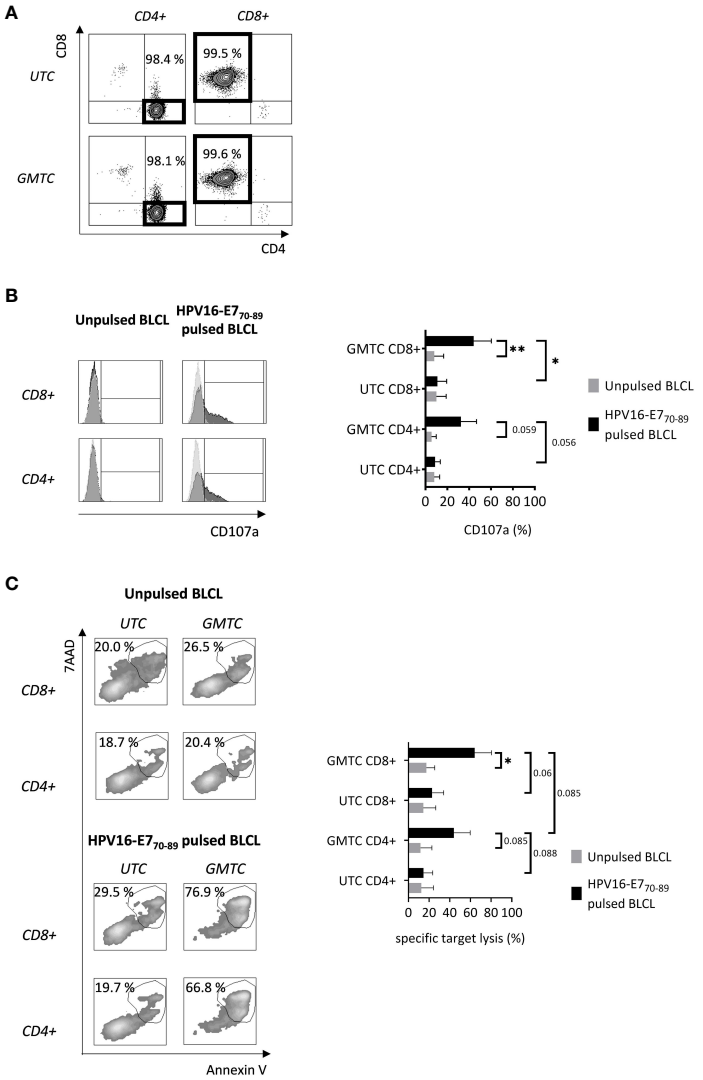

FIGURE 3
In vitro cytotoxic features of transduced CD8+ & CD4+ T cells. T cells are activated, cultured in the presence of IL-2, transduced (and selected) or not with HPV16-E7/HLA-DRB1*04-specific TCR-T, and sorted on the CD4 or CD8 co-receptors expression before being restimulated with HPV16-$E7_{70-89}$-pulsed or not HLA-DRB1*04 BLCL. **(A)** CD4+ and CD8+ T cell sorting efficiency is evaluated through flow cytometry. Data are representative of 4 independent experiments. **(B)** Antigen-activated CD4+ and CD8+ T cell CD107a expression is evaluated through flow cytometry. Left: flow cytometry histograms representing CD107a expression of CD8+ or CD4+ T cells after restimulation; light and dark grey histograms corresponding to UTC and GMTC respectively; values obtained from one experiment, representative of 3. Right: bar graph representing CD107a expression of transduced or not CD8+ or CD4+ T cells after restimulation; mean+/-SD from 3 independent experiments; one-tailed paired t-test, *: p< 0.05 and **: p< 0.01. **(C)** CD4+ and CD8+ T cell-mediated target cell cytolysis is assessed through Annexin V/7AAD co-staining of target cells by flow cytometry. Left: flow cytometry plots representing Annexin V/7AAD expression of peptide-pulsed or not BLCL after co-culture with UTC or GMTC CD4+ or CD8+ T cells; values obtained from one experiment, representative of 3. Right: bar graph representing specific target lysis of transduced or not CD8+ or CD4+ T cells after restimulation; specific target lysis = [(% Annexin V+/7AAD+ $_{\text{cocultured target}}$ - % Annexin V+/7AAD+ $_{\text{alone target}}$)/(100 - % Annexin V+/7AAD+ $_{\text{alone target}}$)] x 100; mean+/-SD from 3 independent experiments; one-tailed paired t-test, *: p< 0.05.

Cytotoxic-associated CD4+ T cells phenotype evaluation of *ex vivo* activated and expanded T cells

Ex vivo culture conditions are likely to be involved in the development of CTX CD4+ T cells. We first hypothesized that IL-2 supplementation could be related to this phenomenon (Figure 4A). CD4+ T cell CD107a expression and cytotoxic profile were assessed after initial activation through CD3/CD28, *ex vivo* culture with 500 IU/mL IL-2 supplementation, and antigenic rechallenge mimicking PMA/ionomycin stimulation (Figures 4B, C). Stimulated CD4+ T cells express a high amount of CD107a, Granzyme B, and Perforin, and a significant amount of SLAMF7, OX40, and 4-1BB. A very low level of death receptors TRAIL and FasL co-expression is detected. This phenotype is consistent with a cytotoxic-associated CD4+ T cell phenotype.

We then evaluated the cytokine environment impact on CD4+ T cell cytotoxic features during *ex vivo* culture. CD107a, Granzyme B, and SLAMF7 expression were assessed for resting *versus* cultured T cells after initial activation through CD3/CD28 magnetic beads,

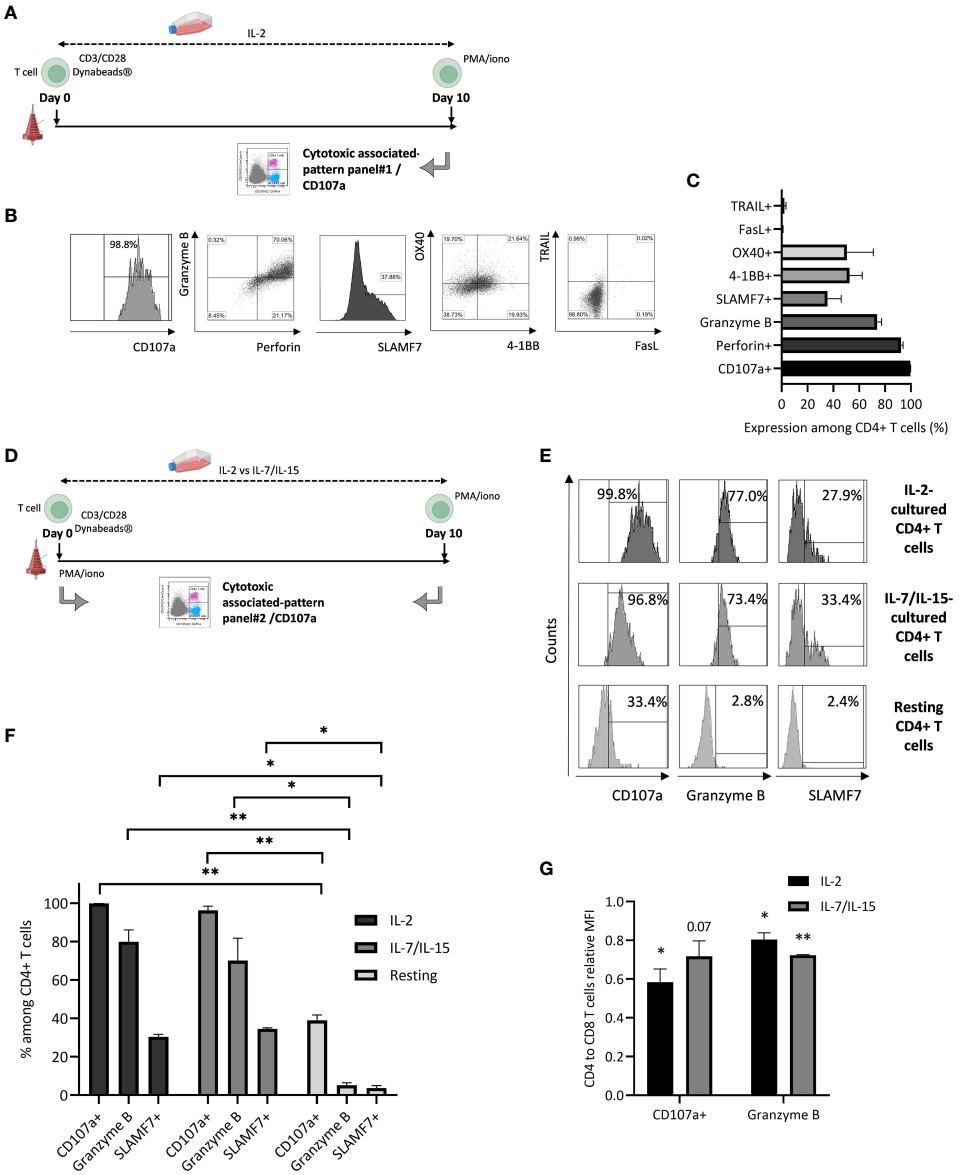

FIGURE 4
Cytotoxic phenotypic features of ex vivo cultured CD4+ T cells. **(A)** T cells are activated and cultured in the presence of IL-2 before PMA/iono restimulation and cytotoxicity-associated expression pattern evaluation (panel 1). Figure adapted from images created with BioRender.com. **(B)** Flow cytometry plots representing CD4+ T cell expression of CD107a, Granzyme B, Perforin, SLAMF7, OX40, 4-1BB, FasL, and TRAIL; data from one experiment, representative of 3. **(C)** Bar graph representing mean+/-SD from 3 independent experiments for all cytotoxicity-associated CD4+ T cell evaluated markers. **(D)** T cells are resting or activated and cultured in the presence of IL-2 or IL-7 and IL-15 before PMA/iono restimulation and cytotoxicity-associated expression pattern evaluation (panel 2). Figure adapted from images created with BioRender.com. **(E)** CD4+ T cell cytotoxicity-associated expression pattern: flow cytometry plots representing CD4+ T cell expression of CD107a, Granzyme B, SLAMF7 after restimulation or not; data from one experiment, representative of 3. **(F)** Bar graph representing mean+/-SD from 3 independent experiments for all cytotoxicity-associated CD4+ T cell evaluated markers, after restimulation; two-tailed paired t-test, *: $p< 0.05$ and **: $p< 0.01$. **(G)** CD4+ T cells degranulation marker expression intensity, relative to what is observed for their cytotoxic CD8+ T cell counterparts: T cells are either activated and cultured in the presence of IL-2 or IL-7/IL-15 before PMA/iono restimulation and degranulation marker expression intensity (Mean of Fluorescence Intensity or MFI) evaluation, through flow cytometry (panel 2). Bar graph represents mean+/-SD from 3 independent experiments. Pictured statistical analysis are made by comparing the mean of MFI observed for CD4+ and CD8+ T cells, for each culture condition; two-tailed paired t-test, *: $p< 0.05$ and **: $p< 0.01$.

ex vivo culture with either 500 IU/mL IL-2 or IL-7 350 IU/mL and IL-15 60 IU/mL supplementation and antigenic rechallenge mimicking PMA/ionomycin stimulation (Figure 4D). A similar expression pattern is observed regarding CD107a, Granzyme B and SLAMF7 expression after exposure to IL-2 compared to IL-7 and IL-15. Resting CD4+ T cell cytotoxic expression pattern is significantly different compared to the one of IL-2 or IL-7 and IL-15 exposed T cells (Figures 4E, F). CD107a and Granzyme B mean fluorescence intensities are lower for CTX CD4+ T cells compared to their classical cytotoxic CD8+ T cell counterparts. Similar results are obtained after both IL-2 ($p< 0.05$ regarding CD107a and Granzyme B) and IL-7/IL-15 ($p= 0.07$ and $p< 0.01$ regarding

CD107a and Granzyme B, respectively) exposure (Figure 4G). This observation is consistent with previously observed data regarding cytotoxicity assessment (Figure 3C).

Altogether, these results demonstrate that our *ex vivo* T cell culture conditions are likely to induce CTX CD4+ T cells and that IL-2 is not the only responsible parameter for this phenomenon.

In vivo cytotoxicity, infiltration and persistence capacity characterization of both CD8+ and CD4+ TCR-T II transduced T cells

We first validated the suitability of the SKMEL-28 cell line as an appropriate TCR-T target tumor cell for *in vivo* preclinical functionality studies. Indeed, membrane HLA-DR expression on SKMEL-28 cells was assessed (Supplementary Figure S1A). HPV-16 $E7_{70-89}$-pulsed SKMEL-28 cells specifically induce TCR-T IFN-γ secretion, either from CD4+ (14.3%) or CD8+ (9.2%) cells, after an overnight co-culture (Supplementary Figure S1B). Both results suggest the ability of SKMEL-28 cells to present HPV-16 E7-derived peptide to TCR-T, in an MHC II restriction fashion. HPV16-E7 plasmid transfection efficiency and subsequent NeoR selection of SKMEL-28 cells were confirmed by Western blotting (Supplementary Figure S1C).

We then produced, as described above, a TCR-T batch including CD4+, CD8+, total GMTC as well as UTC from one healthy donor-derived T cells. This GMTC-specific lysis capacity was validated with CFSE-stained HPV16-$E7_{70-89}$-pulsed HLA-DRB1*04 target cell line, either BLCL or SKMEL-28 cell line. Indeed, all GMTC subsets demonstrate a detectable cytotoxic capacity at an E:T ratio of 1:1. First, it is interesting to note that CD4+ GMTC are not as efficient in eliminating peptide-pulsed BLCL as their CD8+ counterparts or total GMTC. This result is consistent with Annexin V/7AAD staining results (Figure 3C). Second, all GMTC subsets demonstrate lower cytotoxic potential against peptide-pulsed SKMEL-28 cell line compared to BLCL. Moreover, CD8+ GMTC are less efficient to lyse peptide-pulsed SKMEL-28 cell line than their CD4+ counterpart and total GMTC population, in contrast to what occurs regarding BLCL (Supplementary Figure S1D). Overall, except for CD8+ GMTC which demonstrate the same low level of peptide-pulsed SKMEL-28 cell line-specific lysis at an E:T ratio of 1:1 and 1:5, all GMTC subsets show a decreased cytotoxicity against peptide-pulsed targets when diminishing the E:T ratio (Supplementary Figure S1E).

When SKMEL-28/E7-derived tumor volume reached a mean of around 100 mm^3 in NSG mice, all fractions of TCR-T and UTC cells were injected (Figure 5A). Tumor volume was calculated 3 times a week until sacrifice (Figure 5B) and tumor fold expansion ratio was calculated at Day (D)7, D10, D12, D14 and D17 post-treatment (Figure 5C). At D7, no effect on tumor growth control is observed regardless of the UTC subset. At D7 and D10, we demonstrate a tumor growth control mediated by CD4+ ($p< 0.01$ and $p= 0.055$, respectively for D7 and D10) and total GMTC ($p< 0.01$ and $p< 0.05$, respectively for D7 and D10), but not by CD8+ GMTC group, compared to total UTC control group. These data are consistent with the *in vitro* counterpart experiment shown in Supplementary Figure S1B. Tumor growth control mediated by CD4+ GMTC has the same amplitude but is less durable than the one mediated by the total GMTC. The second T-cell injection has no additional impact on tumor growth. From D14, GMTC-induced tumor growth control declines and is ultimately abolished at D17. Tumor infiltration by xenogeneic persistent T cells was assessed at D17, after sacrificing the mice. Few but detectable TIL are present in the tumor TCR-T-treated mice only (untreated vs total GMTC: $p= 0.081$; untreated vs CD8+ GMTC: $p= 0.078$; untreated vs CD4+ GMTC: $p< 0.05$; total UTC vs total GMTC: $p= 0.079$ and total UTC vs CD4+ GMTC: $p= 0.09$) (Figure 5D). Total GMTC and UTC TIL are composed of both CD4+ and CD8+ T cells. CD8+ and CD4+ GMTC TIL are only composed of CD8+ and CD4+ T cells, respectively. These data are consistent with what is expected according to effector subset quality controls shown in Figure 3A. Regarding the total UTC-injected mice group, we observe a trend to a fewer TIL infiltration and/or persistence in the tumor, when compared to the GMTC-injected mice. GMTC-derived TIL partially express TCR-T, with a trend to higher residual expression in CD8+ cells compared to CD4+ T cells (Figure 5E).

Taken together, these results emphasize the capacity of total GMTC and, to a lesser extent, of CD4+ GMTC, to delay the SKMEL-28/E7 growth in mice. Persistent infiltrating TCR-T, either CD8+ or CD4+, are detected in mice tumors and partially express the transgenic TCR.

Discussion

Ex vivo retroviral transduction and TCR-T cell expansion allow for a cellular product constituted of both CD4+ and CD8+ T cells, transduced to a similar extent, consistent with previously published data by Schmueck et al. (30) and Dillard et al. (19). Consequently, these observations emphasized the systematic generation of a mismatch between T cell co-receptor and MHC transgenic TCR restriction. Regarding phenotypic characterization, we show here a lower GMTC expansion capacity during culture with IL-2, confirming data from Marton et al. (31). CD4/CD8 ratio is similar between GMTC and UTC, and is comparable to the one described for PBMC from healthy adults (32). Both subsets are present at levels considered as physiological in TCR-T and are prone to play a significant role in clinical settings. We do not demonstrate any differences between CD4+ and CD8+ T cells in terms of activation and low exhaustion profiles. Nevertheless, we observe a weak trend to higher T_{PEX} rate in CD4+ GMTC compared to UTC, which could be further investigated. In contrast to a CAR-T strategy where tonic signaling induced by antigen-independent triggering is prone to lead to T cell exhaustion, we did not expect an increase in either exhaustion or activation status of TCR-T (33).

In the present study on HPV16-E7 TCR-T, we confirm Dillard and colleagues' *in vitro* data regarding cytotoxic CD8+ cell existence in a setting of MHC II-restricted TCR-T transduction, directed against the hTERT-derived peptide (19). We also demonstrate a strong trend of transgenic CD4+ T cells to exhibit similar cytotoxic capacities as CD8+ T cells. It has been previously demonstrated that

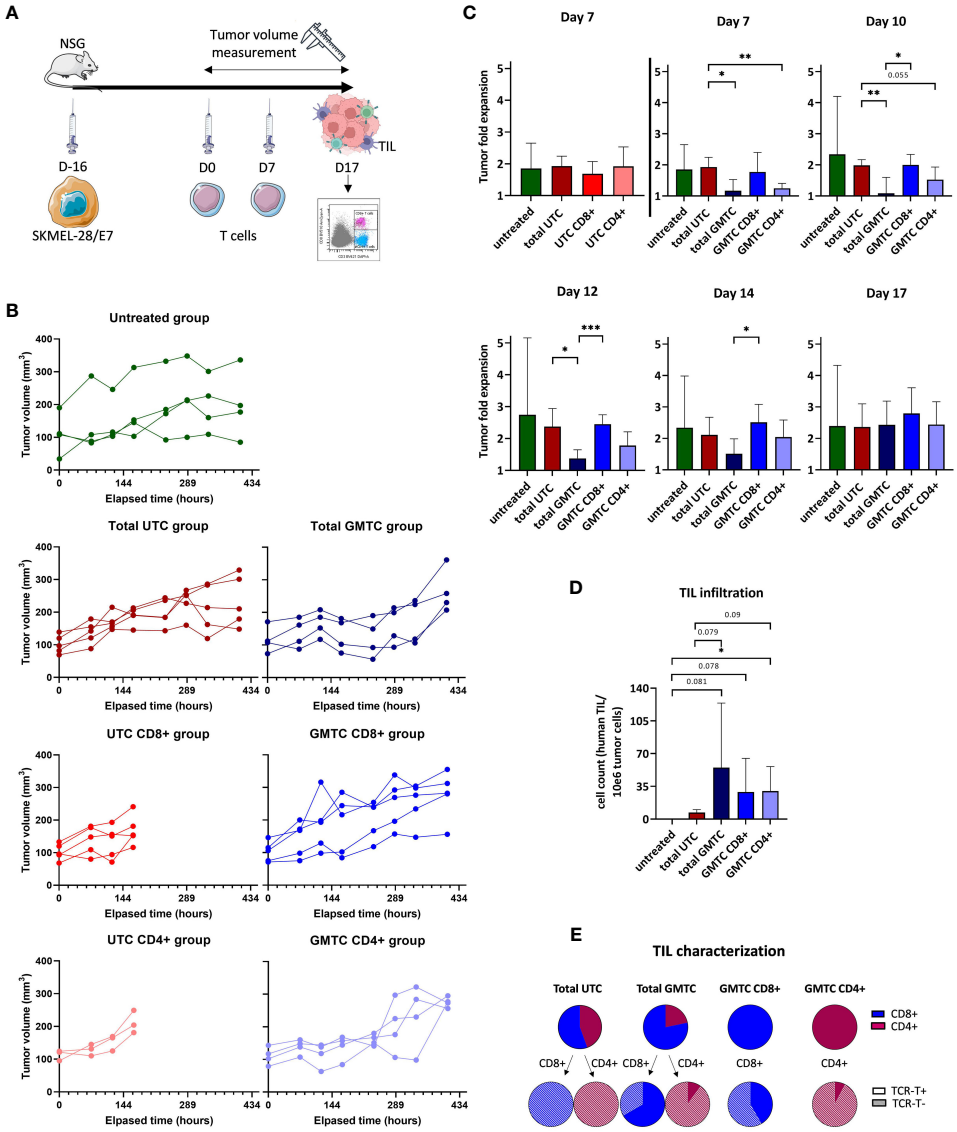

FIGURE 5
in vivo cytotoxic properties of CD4+ and CD8+ TCR-T cells evaluation **(A)** Experiment design. Figure adapted from images created with BioRender.com. and Servier Medical ART. **(B)** Tumor volume measurement for each mouse (green: untreated group, dark blue: total GMTC group, medium blue: CD8+ GMTC, light blue: CD4+ GMTC, dark red: total UTC, medium red: CD8+ UTC, light red: CD4+ UTC), at day 7, 10, 12, 14 and 17. **(C)** Tumor fold expansion for each mice group (mean+/-SD) (green: untreated group, dark blue: total GMTC group, medium blue: CD8+ GMTC, light blue: CD4+ GMTC, dark red: total UTC, medium red: CD8+ UTC, light red: CD4+ UTC), at day 7, 10, 12, 14, 17; two-tailed unpaired t-test, *: p< 0.05, **: p< 0.01 and ***: p< 0.001. **(D)** Number of human TIL/10^6 tumor cell count for each mice group (mean+/-SD) (green: untreated group, dark blue: total GMTC group, medium blue: CD8+ GMTC, light blue: CD4+ GMTC, dark red: total UTC, medium red: CD8+ UTC, light red: CD4+ UTC); one-tailed unpaired t-test, *: p< 0.05. **(E)** TIL phenotypic characterization regarding CD4 (dark pink) or CD8 (blue) co-receptor and transgenic TCR expression or not (full and hatched part of pie charts).

the *ex vivo* T cell culture process favors Th1 CD4+ CTX T cell expansion rather than Treg expansion, possibly because of IL-2 bioavailability (9, 26). We confirm that culturing CD4+ T cells in the presence of IL-2 after initial activation is likely to induce strong CD107a expression and a cytotoxic phenotypic profile (10, 27) after a rechallenge-mimicking antigen exposure. We notice that these IL-2 exposed cell cytotoxic capacities seem to be mediated by the secretory Perforin/granzymes pathway, rather than by the death receptors pathway, as shown by the presence of Granzyme B/Perforin/CD107a and the absence of FasL and TRAIL in these CD4+ T cells. This associated cytotoxic phenotypic pattern is globally consistent with the one described at the mRNA level by Liang et al. (22). Thus, MART-1/HLA-A2 TCR-T CD4+ cells are able to transcribe gene coding for Granzyme B, Perforin, CD107a, SLAMF7, OX40, 4-1BB after antigen exposure; nevertheless, contrary to our present study, authors showed elements in accordance with an implication of both granule-dependent and independent killing pathways. Our data involving IL-2 or IL-7 and IL-15 supplemented cultured CD4+ T cells show similar results in terms of degranulation capacities and cytotoxic phenotypic profile. This element points out that IL-2 exposure is not the only way to favor the development of cytotoxic CD4+ T cells in *ex vivo* cultures.

Nevertheless, we demonstrate a lower intensity of degranulation marker expression by CTX CD4+ T cells compared to their CTX CD8+ counterparts. These data are consistent with those obtained by Schober and colleagues (23), showing a faster decrease of Granzyme B secretion from CD4+ TCR-T compared to CD8+ TCR-T when reducing the E:T ratio. Then, in clinical settings, relatively less potent intrinsic cytotoxic capacities are likely to be expected from CTX CD4+ T cells. Nevertheless, any changes in the T cell *ex vivo* expansion step in a setting of ACT should be carefully evaluated regarding the CD4+ T cell cytotoxic status. Overall, we demonstrated that MHC II-restricted HPV16-E7$_{70\text{-}89}$ GMTC CD4+ T cells display a cytolytic phenotype, thus confirming the studies of Kyte et al. (18), and that this phenotype is translated into cytotoxic function. This cytotoxicity potential is objectivated by *in vitro* target-specific killing as well as *in vivo* tumor control in mice. The *in vivo* experimentation, involving immunocompromised NSG mice and xenogeneic T cell graft, displays a valuable result regarding the differential capacity of CD4+, CD8+ and total TCR-T to control tumor growth. Indeed, a more durable response is obtained after total TCR-T injection. This result is consistent with the idea of a cooperation between CTX and helper T cell subsets to efficiently eradicate target cells. In the present model, CD4+ TCR-T are able to control tumor growth to a lesser extent, whereas CD8+ TCR-T are not. We hypothesize that CD4+ transgenic T cells, which acquired CTX properties during the *ex vivo* culture (even if their cytotoxic capacity is less intense than their CD8+ counterparts in terms of degranulation), have the capacity to supply both required cytotoxic and help features, contrary to CD8+ T cells which probably only exert cytotoxic function (34). Notably, we observe a discrepancy between *in vitro* and *in vivo* cytotoxicity assays regarding CD8+ TCR-T; these T cells are able to eliminate a cognate peptide-pulsed BLCL target cell line *in vitro*, but not the SKMEL-28 cell line *in vivo*, and to a lesser extent *in vitro*. We can assume that the lower HLA-DRB1*04 surface expression level displayed by the SKMEL-28 cell line compared to BLCL's has an impact on TCR II/CD8+ mismatched T cells antigen recognition capacity, especially in a lack of help context. Another explanation can rely on the target cell line model, which can be sensitive to differential lytic pathways. Reverse settings, involving mismatched CD4+/TCR I TCR-T, have already been studied by Schober et al. (23) and Frankel et al. (24). In Schober's study, CD4+ T cells display cytotoxic activity against cognate Ewing sarcoma target cells, both *in vitro* and *in vivo*, even if less efficiently compared to their matched-CD8+ TCR-T counterparts. Our study is in line with these results regarding the MHC/co-receptor match, even if the MHC context and the MHC/co-receptor mismatch are different and these features can influence the capacity of CD4+ and CD8+ TCR-T to eradicate tumor cells. Thus, the mismatch between MHC restriction and co-receptor expression could inherently limit for part the T cell functionalities. Interestingly, in Schober's article, the *ex vivo* culture duration positively influences CD4+ T cell cytotoxic capacities. This issue could be addressed in our settings, even if positioned in a translational context. In Frankel's work relying on tyrosinase expressing-melanoma models, unsorted, CD4+ and CD8 + TCR-T cells exert cytotoxic activity against cognate target tumor cell line, both *in vitro* and *in vivo*. All three subsets are able to induce a tumoral regression in mice at a similar level. In this setting, the mismatch between MHC restriction and co-receptor expression has no influence on tumor control, highlighting the difficulty of extrapolating previously described results in the TCR-T setting, obtained with a different study model. Furthermore, our study establishes that both CD8+ and CD4+ TCR-T cells are able to infiltrate the tumor and persist for part of them, even after tumor escape. TIL persistence could be reinforced for a potentially longer impact on the anti-tumoral immune response. Indeed, herein, TCR-T cells are expanded *ex vivo* in the presence of IL-2, which is known to induce more differentiated T cells. Replacing IL-2 with other cytokines such as IL-7 and IL-15 is likely to induce less differentiated T cells, retaining self-renewing potential in culture (31). Interestingly, we show that a fraction of TCR-T TIL does not express the transgenic TCR at the time of mice sacrifice. This lack of expression remains to be unraveled. Some hypothesis rely on a TCR-T expression loss during the *in vivo* experiment process or on a selective persistence of a minority ΔCD19-negative contaminating T cell subset.

Thereby, the existence and cytolytic activity of CTX CD4+ and CD8+ TCR-T, appropriately matched or not with the MHC expression, are assessed in this study and supply additional data to the existing literature. Miscommitment and/or MHC-mismatch seem to represent a weak limitation to T cell cytotoxicity in some models, without challenging TCR-T approaches and the different effector T cell subset role. At this stage, we can first expect simultaneous targeting of cytolytic and cognate helper fates against a given TAA through the transduction of TCR-T, either in an MHC I or MHC II context.

Certainly, MHC I is quite uniformly expressed by tumor cells, even if the loss of its expression is well known to be a cancer cell immune escape mechanism, while a great majority of tumor cells do not express MHC II, except in some hematologic malignancies or melanoma tumor cells. Thus, it could remain difficult for MHC II-restricted CD8+ or CD4+ T cells to be able to directly target a majority of cancer cells. Nevertheless, an indirect CD4+ T cells killing mechanism, implying IFN-γ secretion and tumoricidal macrophages, has already been reviewed and could represent the way for MHC II-restricted T cells to eliminate tumor cells, without any MHC I-restricted CD8+ T cells involvement (35). The same beneficial involvement could be expected for cytotoxic CD4+ T cells in the setting of antitumor CAR-T cells, because of the lack of MHC restriction involvement. A follow-up study of a CAR-T cell clinical trial (36) relates the *in vivo* persistence of cytotoxic characteristics-bearing CD4+ CAR-T cell clones more than 10 years after infusion. This tremendous persistence is associated with durable anti-tumor activity and patient long-term survival. Moreover, according to Yang et al. (37) in a mouse CAR-T cell setting, CTX CD4+ T cells remain insensitive to endogenous TCR engagement, contrary to CD8+ T cells which are prone to exhaustion after endogenous TCR triggering; these points are in favor of some expected CTX CD4+ T cell beneficial effect in this ACT context. Despite these CTX CD4+ TCR-T potential beneficial properties, the presence of these cells in ACT products should be considered with caution. Indeed, studies from Malek Abrahimians et al. (38) show the existence of CD4+ T cells able to acquire apoptosis-inducing properties on antigen-

presenting cells and CD4+ MHC II expressing cells after cognate recognition of natural antigens and the opportunity of inhibiting these T cells to improve diabetes syndrome in a NOD mouse model. In this setting, CTX CD4+ T cells should be considered as a regulatory subset, potentially dysregulated in auto-immune diseases. However, these hypothetical deleterious effects, mediated by CTX CD4+ TCR-T within ACT products, should be mitigated by several observations. First, it has been known for a long time that dendritic cells are able to resist CTL lysis through an upregulation of Serpin Serine Protease Inhibitor 6 expression (39). Second, a recent study by Boulch et al. (40) showed that CAR-T cells-mediated-target-lysis is partly due to a cooperation with host immune cells.

So, we can secondly conclude that potential benefits associated with the presence of tumor-specific TCR-armed CTX CD4+ are now preclinically demonstrated. However, CTX CD4+ related deleterious effects could concomitantly occur. This issue should be taken into account when designing and developing a TCR-T-based ACT procedure, in the cancer treatment setting. Today, CD4+ and CD8+ TCR-T bulk injection is the more common approach reported in the clinical literature and relies on a global evaluation of specific anti-tumoral activity. According to present knowledge, the ideal composition of TCR-T in terms of CTX CD4+ and CD8+ T cell presence and ratio remains questionable and is likely to differ according to either the MHC context or evaluated tumor model, regarding efficiency indicators. Regardless of the engineered T cell-mediated approach, interactions between tumor-reactive modified T cells and other host immune cells related to toxicity-mediated impacts need to be carefully evaluated in clinical settings.

Data availability statement

The raw data supporting the conclusions of this article will be made available by the authors, without undue reservation.

Ethics statement

The studies involving humans were approved by CODECOH (collection agreement number AC-2020-4129). The studies were conducted in accordance with the local legislation and institutional requirements. The participants provided their written informed consent to participate in this study. The animal study was approved by Ministry of Agriculture (number 2021-004-OA12PR). The study was conducted in accordance with the local legislation and institutional requirements.

Author contributions

PM-L designed the study, performed the experimental work, analyzed the data and wrote the manuscript. AK and CM reviewed and corrected the manuscript. OA, YG were involved in the management of the research work. JG supervised the work. All authors contributed to the article and approved the submitted version.

Funding

The author(s) declare that financial support was received for the research, authorship, and/or publication of this article. The work was founded by grants from the foundation “Ligue contre le cancer” (no grant number, call for proposals 2018 CCIR Est) and the MiMedI consortium (grant no. DOS0060162/00). Substantial support was also brought by research institutions INSERM, EFS and University of Franche-Comté.

Acknowledgments

Authors address special thanks to Dr. Caroline Laheurte and Eléonore Gravelin, manager and technician of the Biomonitoring platform, respectively, for assistance regarding the acquisition and analysis of data through the CytoFLEX LX flow cytometer. Dr Aurélie Baguet is thanked too for furnishing the HPV16-E7-encoding vector. The animal facility staff is deeply thanked for mice care and technical assistance.

Conflict of interest

The authors declare that the research was conducted in the absence of any commercial or financial relationships that could be construed as a potential conflict of interest.

Publisher’s note

All claims expressed in this article are solely those of the authors and do not necessarily represent those of their affiliated organizations, or those of the publisher, the editors and the reviewers. Any product that may be evaluated in this article, or claim that may be made by its manufacturer, is not guaranteed or endorsed by the publisher.

Supplementary material

The Supplementary Material for this article can be found online at: https://www.frontiersin.org/articles/10.3389/fimmu.2024.1202017/full#supplementary-material

SUPPLEMENTARY FIGURE 1
In vivo cytotoxicity assay-designed cellular tools validation. **(A-C)** Characterization of SKMEL-28 as a target cell line. **(A)** HLA-DR expression: comparison of SKMEL-28 cell line and BLCL. The light grey peak and dark grey peak represent unstained and HLA-DR-stained cell line, respectively. Ratio of fluorescence intensity between the two peaks (RFI) is plotted on each graph. **(B)** Untransduced and transduced T cells are co-cultured with 1:1 SKMEL-28 cells, pulsed or not with the HPV16-E7$_{70-89}$ peptide, then evaluated for IFN-γ secretion (CD4+ and CD8+ T cell subsets). **(C)** HPV16-E7 validation expression of transfected SKMEL-28 cells by Western Blotting. **(D, F)** Characterization of effector GMTC subsets batch *in vitro* cytotoxicity. **(D)** Representation of residual alive CFSE labelled-target cells [pulsed or not BLCL (black and medium grey bars) and pulsed or not SKMEL-28 cell line (dark and light grey bars)] after co-culture with effector T cells (total, CD8+ and CD4+

GMTC) at an effector:target ratio of 1:1. Specific target lysis = (Number of alive targets/Number of seeded targets) x 100. **(E)** Representation of residual alive CFSE labelled-target cells [pulsed BLCL (left) or SKMEL-28 cell line (right)] after coculture with effector T cells [total (circle), CD8+ (square) and CD4+ (triangle) GMTC] at an effector:target ratio of 1:1 and 1:5. Specific target lysis = (Number of alive targets/Number of seeded targets) x 100.

References

1. Yang JC, Rosenberg SA. Adoptive T-cell therapy for cancer. In: *Advances in Immunology*. Amsterdam, Netherlands: Elsevier (2016). p. 279–94.

2. Baulu E, Gardet C, Chuvin N, Depil S. TCR-engineered T cell therapy in solid tumors: State of the art and perspectives. *Sci Adv*. (2023) 9:eadf3700. doi: 10.1126/sciadv.adf3700

3. Morgan RA, Dudley ME, Wunderlich JR, Hughes MS, Sherry RM, Royal RE, et al. Cancer regression in patients after transfer of genetically engineered lymphocytes. *Science* (2006) 314(5796):126–9. doi: 10.1126/science.1129003

4. Fournier C, Martin F, Zitvogel L, Kroemer G, Galluzzi L, Apetoh L. Trial Watch: Adoptively transferred cells for anticancer immunotherapy. *Onco Immunol*. (2017) 6: e1363139. doi: 10.1080/2162402X.2017.1363139

5. Oppermans N, Kueberuwa G, Hawkins RE, Bridgeman JS. Transgenic T-cell receptor immunotherapy for cancer: building on clinical success. *Ther Adv Vaccines Immunother*. (2020) 8:251513552093350. doi: 10.1177/2515135520933509

6. Lu YC, Parker LL, Lu T, Zheng Z, Toomey MA, White DE, et al. Treatment of patients with metastatic cancer using a major histocompatibility complex class II–restricted T-cell receptor targeting the cancer germline antigen MAGE-A3. *J Clin Oncol*. (2017) 35:3322–9. doi: 10.1200/JCO.2017.74.5463

7. D'Angelo SP, Melchiori L, Merchant MS, Bernstein D, Glod J, Kaplan R, et al. Antitumor activity associated with prolonged persistence of adoptively transferred NY-ESO-1 c259T cells in synovial sarcoma. *Cancer Discovery*. (2018) 8:944–57. doi: 10.1158/2159-8290.CD-17-1417

8. Doran SL, Stevanović S, Adhikary S, Gartner JJ, Jia L, Kwong MLM, et al. T-cell receptor gene therapy for human papillomavirus–associated epithelial cancers: A first-in-human, phase I/II study. *J Clin Oncol*. (2019) 37:2759–68. doi: 10.1200/JCO.18.02424

9. Śledzińska A, Vila de Mucha M, Bergerhoff K, Hotblack A, Demane DF, Ghorani E, et al. Regulatory T cells restrain interleukin-2- and blimp-1-dependent acquisition of cytotoxic function by CD4+ T cells. *Immunity*. (2020) 52:151–166.e6. doi: 10.1016/j.immuni.2019.12.007

10. Oh DY, Fong L. Cytotoxic CD4+ T cells in cancer: Expanding the immune effector toolbox. *Immunity*. (2021) 54:2701–11. doi: 10.1016/j.immuni.2021.11.015

11. Pearce EL, Shedlock DJ, Shen H. Functional characterization of MHC class II-restricted $CD8^+$ $CD4^-$ and $CD8^-$ $CD4^-$ T cell responses to infection in $CD4^{-/-}$ mice. *J Immunol*. (2004) 173:2494–9. doi: 10.4049/jimmunol.173.4.2494

12. Ranasinghe S, Lamothe PA, Soghoian DZ, Kazer SW, Cole MB, Shalek AK, et al. Antiviral CD8+ T cells restricted by human leukocyte antigen class II exist during natural HIV infection and exhibit clonal expansion. *Immunity*. (2016) 45:917–30. doi: 10.1016/j.immuni.2016.09.015

13. Migueles SA, Connors M. Class II-restricted CD8s: new lessons violate old paradigms. *Immunity*. (2016) 45:712–4. doi: 10.1016/j.immuni.2016.10.004

14. Nyanhete TE, Frisbee AL, Bradley T, Faison WJ, Robins E, Payne T, et al. HLA class II-Restricted CD8+ T cells in HIV-1 Virus Controllers. *Sci Rep*. (2019) 9:10165. doi: 10.1038/s41598-019-46462-8

15. Nishimura MI, Avichezer D, Custer MC, Lee CS, Chen C. Tumor infiltrating lymphocyte. *Cancer Res*. (1999) 59:6230–8.

16. Ranheim EA, Tarbell KV, Krogsgaard M, Mallet-Designe V, Teyton L, McDevitt HO, et al. Selection of aberrant class II restricted $CD8^+$ T cells in NOD mice expressing a glutamic acid decarboxylase (GAD)65-specific T cell receptor transgene. *Autoimmunity*. (2004) 37:555–67. doi: 10.1080/08916930400020545

17. Mercier-Letondal P, Marton C, Deschamps M, Ferrand C, Vauchy C, Chenut C, et al. Isolation and characterization of an HLA-DRB1*04-restricted HPV16-E7 T cell receptor for cancer immunotherapy. *Hum Gene Ther*. (2018) 29:1202–12. doi: 10.1089/hum.2018.091

18. Kyte JA, Gaudernack G, Faane A, Lislerud K, Inderberg EM, Brunsvig P, et al. T-helper cell receptors from long-term survivors after telomerase cancer vaccination for use in adoptive cell therapy. *OncoImmunol*. (2016) 5:e1249090. doi: 10.1080/2162402X.2016.1249090

19. Dillard P, Köksal H, Maggadottir SM, Winge-Main A, Pollmann S, Menard M, et al. Targeting telomerase with an HLA class II-restricted TCR for cancer immunotherapy. *Mol Ther*. (2021) 29:1199–213. doi: 10.1016/j.ymthe.2020.11.019

20. Chhabra A, Yang L, Wang P, Comin-Anduix B, Das R, Chakraborty NG, et al. $CD4^+$ $CD25^-$ T cells transduced to express MHC class I-restricted epitope-specific TCR synthesize th1 cytokines and exhibit MHC class I-restricted cytolytic effector function in a human melanoma model. *J Immunol*. (2008) 181:1063–70. doi: 10.4049/jimmunol.181.2.1063

21. Quezada SA, Simpson TR, Peggs KS, Merghoub T, Vider J, Fan X, et al. Tumor-reactive CD4+ T cells develop cytotoxic activity and eradicate large established melanoma after transfer into lymphopenic hosts. *J Exp Med*. (2010) 207:637–50. doi: 10.1084/jem.20091918

22. Liang Y, Xu Q, Liu S, Li J, Wang F, Li Z, et al. Single-cell transcriptomics reveals killing mechanisms of antitumor cytotoxic CD4+ TCR-T cells. *Front Immunol*. (2022) 13:939940. doi: 10.3389/fimmu.2022.939940

23. Schober SJ, Thiede M, Gassmann H, Prexler C, Xue B, Schirmer D, et al. MHC class I-restricted TCR-transgenic CD4+ T cells against STEAP1 mediate local tumor control of ewing sarcoma in vivo. *Cells*. (2020) 9:1581. doi: 10.3390/cells9071581

24. Frankel TL, Burns WR, Peng PD, Yu Z, Chinnasamy D, Wargo JA, et al. Both CD4 and CD8 T cells mediate equally effective *in vivo* tumor treatment when engineered with a highly avid TCR targeting tyrosinase. *J Immunol*. (2010) 184:5988–98. doi: 10.4049/jimmunol.1000189

25. Frentsch M, Stark R, Matzmohr N, Meier S, Durlanik S, Schulz AR, et al. CD40L expression permits CD8+ T cells to execute immunologic helper functions. *Blood*. (2013) 122:405–12. doi: 10.1182/blood-2013-02-483586

26. Juno JA, van Bockel D, Kent SJ, Kelleher AD, Zaunders JJ, Munier CML. Cytotoxic CD4 T cells—Friend or foe during viral infection? *Front Immunol*. (2017) 8:19. doi: 10.3389/fimmu.2017.00019/full

27. Cachot A, Bilous M, Liu YC, Li X, Saillard M, Cenerenti M, et al. Tumor-specific cytolytic CD4 T cells mediate immunity against human cancer. *Sci Adv*. (2021) 7: eabe3348. doi: 10.1126/sciadv.abe3348

28. Sauce D, Bodinier M, Garin M, Petracca B, Tonnelier N, Duperrier A, et al. Retrovirus-mediated gene transfer in primary T lymphocytes impairs their anti–Epstein-Barr virus potential through both culture-dependent and selection process–dependent mechanisms. *Blood*. (2002) 99:1165–73. doi: 10.1182/blood.V99.4.1165

29. Chen J, Qiu S, Li W, Wang K, Zhang Y, Yang H, et al. Tuning charge density of chimeric antigen receptor optimizes tonic signaling and CAR-T cell fitness. *Cell Res*. (2023) 33:341–54. doi: 10.1038/s41422-023-00789-0

30. Schmueck-Henneresse M, Omer B, Shum T, Tashiro H, Mamonkin M, Lapteva N, et al. Comprehensive approach for identifying the T cell subset origin of CD3 and CD28 antibody–activated chimeric antigen receptor–modified T cells. *J Immunol*. (2017) 199:348–62. doi: 10.4049/jimmunol.1601494

31. Marton C, Mercier-Letondal P, Loyon R, Adotévi O, Borg C, Galaine J, et al. Homeostatic cytokines tune naivety and stemness of cord blood-derived transgenic T cells. *Cancer Gene Ther*. (2022) 29:961–72. doi: 10.1038/s41417-021-00395-5

32. Oladepo DK, Idigbe EO, Audu RA, Inyang US, Imade GE, Philip AO, et al. Establishment of reference values of CD4 and CD8 lymphocyte subsets in healthy Nigerian adults. *Clin Vaccine Immunol CVI*. (2009) 16:1374–7. doi: 10.1128/CVI.00378-08

33. Weber EW, Parker KR, Sotillo E, Lynn RC, Anbunathan H, Lattin J, et al. Transient rest restores functionality in exhausted CAR-T cells through epigenetic remodeling. *Science*. (2021) 372:eaba1786. doi: 10.1126/science.aba1786

34. Castro A, Zanetti M, Carter H. Neoantigen controversies. *Annu Rev BioMed Data Sci*. (2021) 4:227–53. doi: 10.1146/annurev-biodatasci-092820-112713

35. Haabeth OAW, Tveita AA, Fauskanger M, Schjesvold F, Lorvik KB, Hofgaard PO, et al. How do CD4+ T cells detect and eliminate tumor cells that either lack or express MHC class II molecules? *Front Immunol*. (2014) 5:174. doi: 10.3389/fimmu.2014.00174/abstract

36. Melenhorst JJ, Chen GM, Wang M, Porter DL, Chen C, Collins MA, et al. Decade-long leukaemia remissions with persistence of CD4+ CAR T cells. *Nature*. (2022) 602:503–9. doi: 10.1038/s41586-021-04390-6

37. Yang Y, Kohler ME, Chien CD, Sauter CT, Jacoby E, Yan C, et al. TCR engagement negatively affects CD8 but not CD4 CAR T cell expansion and leukemic clearance. *Sci Transl Med*. (2017) 9:eaag1209. doi: 10.1126/scitranslmed.aag1209

38. Malek Abrahimians E, Vander Elst L, Carlier VA, Saint-Remy JM. Thioreductase-containing epitopes inhibit the development of type 1 diabetes in the NOD mouse model. *Front Immunol*. (2016) 7:67. doi: 10.3389/fimmu.2016.00067

39. Medema JP, Schuurhuis DH, Rea D, van Tongeren J, de Jong J, Bres SA, et al. Expression of the serpin serine protease inhibitor 6 protects dendritic cells from cytotoxic T lymphocyte–induced apoptosis: differential modulation by T helper type 1 and type 2 cells. *J Exp Med*. (2001) 194(5):657–67. doi: 10.1084/jem.194.5.657

40. Boulch M, Cazaux M, Loe-Mie Y, Thibaut R, Corre B, Lemaître F, et al. A cross-talk between CAR T cell subsets and the tumor microenvironment is essential for sustained cytotoxic activity. *Sci Immunol*. (2021) 6:eabd4344. doi: 10.1126/sciimmunol.abd4344

Frontiers in Immunology

Explores novel approaches and diagnoses to treat immune disorders.

The official journal of the International Union of Immunological Societies (IUIS) and the most cited in its field, leading the way for research across basic, translational and clinical immunology.

Discover the latest Research Topics

See more →

Frontiers

Avenue du Tribunal-Fédéral 34
1005 Lausanne, Switzerland
frontiersin.org

Contact us

+41 (0)21 510 17 00
frontiersin.org/about/contact